Junnarkar, Mahesh R.

PICOSECOND AND STEADY STATE SPECTROSCOPY OF THE WURTZITE SEMIMAGNETIC SEMICONDUCTOR CADMIUM(1-X)MANGANESE(X)SELENIUM

City University of New York PH.D. 1986

PLEASE NOTE:

In all cases this material has been filmed in the best possible way from the available copy. Problems encountered with this document have been identified here with a check mark __✓__.

1. Glossy photographs or pages _____
2. Colored illustrations, paper or print _____
3. Photographs with dark background _____
4. Illustrations are poor copy _____
5. Pages with black marks, not original copy __✓__
6. Print shows through as there is text on both sides of page _____
7. Indistinct, broken or small print on several pages __✓__
8. Print exceeds margin requirements _____
9. Tightly bound copy with print lost in spine _____
10. Computer printout pages with indistinct print __✓__
11. Page(s) _____ lacking when material received, and not available from school or author.
12. Page(s) _____ seem to be missing in numbering only as text follows.
13. Two pages numbered _____. Text follows.
14. Curling and wrinkled pages _____
15. Dissertation contains pages with print at a slant, filmed as received __✓__
16. Other _____

_____

_____

University
Microfilms
International

PICOSECOND AND STEADY STATE SPECTROSCOPY OF THE WURTZITE SEMIMAGNETIC SEMICONDUCTOR $Cd_{1-x}Mn_xSe$.

By

Mahesh R. Junnarkar

A dissertation submitted to the Graduate Faculty in Physics in partial fulfilment of the requirements for the degree of Doctor of Philosophy, the City University of New York.

1986

This manuscript has been read and accepted for the Graduate Faculty in Physics in satisfaction of the dissertation requirement for the degree of Doctor of Philosophy.

3/26/86
Date

Robert R Alfano
Chair of Examining Committee

3/26/86
Date

Executive Officer

Prof. Fred H. Pollak BCNY

Prof. H. Z. Cummins CCNY

Dr. G. Lampel CNRS Lab,France

Supervisory Committee

The City University of New York.

Abstract

PICOSECOND AND STEADY STATE SPECTROSCOPY OF THE WURTZITE SEMIMAGNETIC SEMICONDUCTOR $Cd_{1-x}Mn_xSe$

by

Mahesh R. Junnarkar

Advisor: Professor Robert R. Alfano

The kinetics of a non-equilibrium photogenerated electron-hole plasma in CdSe is investigated using picosecond time resolved spectroscopy at room temperature. Based on the fact that the polar optical phonon emission rate is reduced due to screening by the high density of e-h plasma, the remaining dominant mechanism for hot carrier cooling is the non-polar optical phonon emission even though CdSe is a highly polar semiconductor. Rapid plasma expansion has been proposed as a possible explanation for much lower estimated carrier densities on the grounds of the observed larger spatial width of the photoluminescence relative to the laser spatial width, moderate change of Auger recombination rate with the excitation fluence, the absence of an observed change in the Fermi level with increased excitation intensity and earlier formation of excitons after the picosecond pulse (5 psec) excitation at a low temperature (12K). Large values of the diffusion c-

onstant are explained in terms of a screened electron-phonon interaction.

Picosecond time resolved spin relaxation kinetics of high density free carriers is investigated at low temperatures in CdSe (x=0) and in the dilute semimagnetic semiconductor $Cd_{1-x}Mn_xSe$ for x=0.05 and 0.10. The fast spin relaxation observed in CdSe results from a mechanism associated with the noncentrosymmetric character of the band structure for this material. The spin relaxation times are < 20 psec in $Cd_{1-x}Mn_xSe$ and are consistent with spin flip Raman scattering measurements. The increase in spin relaxation rate relative to CdSe is explained in terms of the spin exchange between the carriers and the magnetic spin sites.

Using steady state photoluminescence from $Cd_{1-x}Mn_xSe$ ($0 \leq x \leq 0.86$), we were able to measure the optical deformation potentials of the conduction band (0.5×10^9 eV/cm) and valence band (0.24×10^9 eV/cm) in CdSe. The temperature dependent additional bound excitonic binding energy was attributed to the formation of a bound magnetic polaron (h-BMP) at low temperature. The h-BMP formation times are ~ 340 psec in $Cd_{0.95}Mn_{0.05}Se$ and ~90 psec in $Cd_{0.9}Mn_{0.1}Se$. These times corresponding to the formation of the BMP from the bound excitons which themselves are formed ~ 185 psec after the picosecond excitation pulse.

This thesis is dedicated to

'Mami and **Mama'**

whose sacrifice introduced me

to higher education.

ACKNOWLEDGEMENTS

I take this as an opportunity to 'time capsule' and express my sincere gratitude to my wife, Pruthvi, and family. Without their encouragement and sacrifice, I would not have been able to complete this work. I am greatly indebted to Shree Saibaba for spiritual guidance and teaching me to hope for a solution to every problem. My research advisor, Professor Robert R. Alfano, has been not only an excellent teacher but an elder brother to me, who not only applauded my achievements but sympathized with my failures. I would also thank my extremely friendly colleagues, at the Institute for Ultrafast Spectroscopy and Lasers of City College of New York, for giving me help and advice. I thank Dr. Arya and Dr. A. Roy for helpful discussions. I must thank the faculty at CCNY, who taught me physics. My extensive discussions with Dr. Nathan Ockman provided me an opportunity for deeper understanding of semiconductor physics. The financial support for the entire project was provided by the National Science Foundation under grant No. DMR-840-4932 and by Air Force Office of Scientific Research under contract No. AFSOR-850013. I would like to acknowledge the technical support of Hamamatsu Corporation. The samples provided by Professor J. Furdyna of Purdue University were invaluable.

It is my pleasure to thank the Physics workshop for their prompt and skillful preparation of various mechanical components. My thesis could not have been finished on time without the help of Mr. Yuri Budansky in providing skillful drawings and Ms. Rina Herrera in typing. I must thank Ms. Megan Gibbs for providing secretarial service.

On top of this I consider myself being very fortunate for having an opportunity to experience and be part of the physics community. I not only learned physics but a lot about life in general. Ironically, I also learned how little I know !

TABLE OF CONTENTS

CHAPTER III

'Photogenerated High Density Electron-Hole Plasma Energy Relaxation and Experimental Evidence for Rapid Expansion of the Electron-Hole Plasma in CdSe.'

CHAPTER IV

'High Density Photogenerated Free Carrier Spin Relaxation Processes in the Wurtzite Semiconductors: CdSe and Semimagnetic Semiconductors $Cd_{1-x}Mn_xSe$.'

LIST OF TABLES

Chapter III

LIST OF FIGURES

Chapter IV

Chapter V

CHAPTER 1

1.1 INTRODUCTION

In this thesis I have examined energy relaxation processes of a high density electron-hole plasma generated by an intense picosecond laser pulse in CdSe, as well as the kinetics of electron spin relaxation in wurtzite dilute semimagnetic semiconductor (DMS) $Cd_{1-x}Mn_xSe$. The purpose of this research is six fold: First, to experimentaly demonstrate the rapid diffusion of photogenerated carriers in CdSe (assumed also in CdMnSe) from the photoexcited region at both room and low temperatures. Second, to show the role of partially screened non polar optical phonon emission in the cooling of high density hot carriers and in rapid diffusion of these carriers. Third, to investigate spin relaxation mechanisms in semimagnetic semiconductors $Cd_{1-x}Mn_xSe$. Fourth, to demonstrate the use of steady state luminescence from $Cd_{1-x}Mn_xSe$ in evaluating conduction and valence band deformation potentials seperately. Fifth, to study the exchange interactions between bound exciton and the Mn^{2+} spins. And sixth, to measure additional localization rates provided by these exchange interactions. The thesis has been divided into five chapters. This introductory chapter contains an overview of the known energy and spin relaxation processes in semiconductors. Experimental details are described in chapter 2. The subsequent chapters are research chapters which are inter related

but deal with different aspects of the physics of semimagnetic semiconductors. The major effort in Chapter 3 is to point out the rapid diffusion of free carriers which limits the carrier density produced in the photo excited region. The lower densities of free carriers makes the spin relaxation rate discussed in Chapter 4 smaller and independent of the excitation photon fluence. Another consequence of fast diffusion is the earlier formation of excitons and bound magnetic polarons (BMP) in DMS, which is discussed in Chapter 5.

I have tried to make the research chapters self contained. It is the objective of this chapter to fill in the gaps and give the reader a broader perspective prior to reading the research material that follows.

Photogeneration and thermalization of carriers in semiconductors envolve a variety of basic physical concepts. Such a dynamical system provides a laboratory to test these concepts. The incident photon energy is absorbed either by electron-hole pair creation or by free carrier excitation. Initially, with a few carriers present, the former process dominates, so that near the semiconductor surface photon absorption rate $g = P(1-R)/\delta\hbar\omega_\ell$, where P is the incident laser power per unit area, R is the reflectivity of the sample, $\hbar\omega_\ell$ is the photon energy, and δ is the absorption length. The primary chanels for energy redistribution are carrier-carrier collisions and plasmon production. The carriers thermalize

typically within 10^{-14} sec to a psuedotemperature and are under quasi-equilibrium. These hot carriers then transfer their excess energy to the lattice through phonon emission.

The loss of excess energy of hot carriers has been studied extensively in GaAs[1,2,3]. The development of picosecond time resolved spectroscopy has made these investigations possible although the mechanisms of the relaxation process have been known[4] for decades. Several workers using various picosecond resolution techniques studied the electron energy loss in the early stages of excitation in GaAs. They concluded that for low excitation levels, generating photo carrier densities less than $10^{18}/cm^3$, the electron gas cools to within 100 K of the lattice temperature in 2-4 picoseconds. This time corresponds to an optical phonon emission time of 0.1 psec. Leheny and co-workers[2] in 1979 confirmed the previous results at low carrier densities, but in addition found a modest five fold decrease in the energy loss rate at a carrier density of $10^{18}/cm^3$. This change was attributed to the screening of the electron-phonon interaction. Later Yoffa[5] calculated the effect of carrier screening on the energy loss rate in both Si and GaAs. Almost at the same time Van Driel[6] (1979) postulated that sufficient optical phonons are created during the cooling process to raise the phonon temperature. This should inhibit the cooling process due to equilibrium between phonons and the partially cooled electron gas (phonon bottle neck). This model was devel-

oped to explain the data obtained by Smirl[7] et al and Elci[8] et al for picosecond optical transmission in germanium.

A study of radiative recombination of free carriers in CdSe by Shah et al[9] in 1974 using steady state spectroscopy revealed that the hot carrier temperature could be as high as 140K at the highest excitation intensity of $4x10^6$ W/cm^2, although the lattice temperature was 2K. They quantitatively explained the electron heating in terms of unscreened polar optical scattering. Their observed departure from the usual logarithmic dependence on excitation intensity was explained assuming existance of a critical density. If the carrier density exceeds this limit, it would cause the optical phonon temperature to approach the carrier temperature. This diminishes the efficiency of the polar optical phonon scattering as a loss mechanism. However, this explanation needs a carrier life time of 30 psec, contrary to our direct experimental measurement of the lifetime of 460 psec at room temperature. If this is taken into account the estimated critical density would be $> 2x10^{19}/cm^3$ instead of $2x10^{18}/cm^3$. Most of the work done[10,11,12,13] with the transient spectroscopy (10 psec) on CdSe corresponds to e-h plasma of density $< 10^{19}/cm^3$ and is related to the condensation of e-h plasma into exciton gas and molecules or low density ($\sim 10^{18}/cm^3$) e-h plasma.

The optical phonon emission by hot carriers being the dominant mechanism for energy relaxation[4,14], I will first review the

different scattering processes which are mainly the non-polar (optical deformation) and polar optical electron-phonon interaction. Potential fluctuations within the lattice due to phonons (in the otherwise periodic potential) can scatter hot electrons. The change in the carrier energy is related to the local dialation[4,15] as,

$$H' = D''.\Delta \qquad (1.1.1)$$

where D'' is a constant and Δ is the dialation. This is specifically true if the semiconductor is non-polar since in the Eq.(1.1.1) electrostatic contribution is neglected. In the presence of high density e-h plasma the electrostatic contribution is negligible and the electron-phonon scattering is predominantly due to the deformation potential. The scattering rate for optical phonon emission can be calculated in a similar manner[4] as for acoustical phonon emission.

$$\frac{1}{\tau} = \left(\frac{m_e V}{2\pi\hbar^3 k}\right)\left[\int_{k-k\left(1+\frac{\hbar\omega_o}{E}\right)^{0.5}}^{k+k\left(1+\frac{\hbar\omega_o}{E}\right)^{0.5}} |\langle \vec{k}+\vec{q}|H'|\vec{k}\rangle|^2 q\,dq\right.$$

$$+ \int_{k-k(1-\frac{\hbar\omega_o}{E})^{0.5}}^{k+k(1-\frac{\hbar\omega_o}{E})^{0.5}} |\langle \vec{k}-\vec{q}|H'|\vec{k}\rangle|^2 q dq] \qquad (1.1.2)$$

The integration limits comes from the optical phonon dispersion relation. E is the kinetic energy of carriers. $\vec{q}$ and $\vec{k}$ are the phonon and electron wave vectors, respectively. The absolute square of the nonpolar optical matrix element[4] is written as,

$$\langle \vec{k}\pm\vec{q}|H'|\vec{k}\rangle|^2 = D''^2(\frac{K^2\hbar}{2V\rho\omega_o})\left[N_q + \frac{1}{2} + \frac{\delta N_q}{2}\right]$$

or

$$= D'^2(\frac{\hbar}{2V\rho\omega_o})\left[N_q + \frac{1}{2} + \frac{\delta N_q}{2}\right] \qquad (1.1.3)$$

where $D''K = D'$ and K is the reciprocal lattice vector.

In polar semiconductors the optical deformation potential scattering becomes negligible at very low carrier densities ($<10^{16}/cm^3$) as the polar interactions are unscreened and dominating. However, at high carrier densities the long range Coloumb interaction between carriers and ions weakens. The electrostatic potential in the presence of dielectric polarization field can be written as[15],

$$\Phi(x) = -4\pi iF(\sum)(\frac{1}{q})(b_q e^{i\vec{q}.\vec{x}} - b_q{}^{\dagger} e^{-i\vec{q}.\vec{x}}) \qquad (1.1.4)$$

where b_q and $b_q{}^{\dagger}$ are Boson operators for phonons. F is a constant and is determined from the second order purturbation theory using phonon wave function with zero dispersion. This contribution accounts for the difference between $e^2/\varepsilon_o r$ and e^2/ε_∞, where the dielectric constant ε_o includes electronic and ionic polarizibilities, and ε_∞ includes only the electronic contribution.

$$\frac{1}{\varepsilon_o} = \frac{1}{\varepsilon_\infty} - \frac{8\pi F^2}{\omega_o} \qquad (1.1.5)$$

Using the first order purturbation theory one obtains,

$$|\langle \vec{k} - \vec{q}|H = e\Phi|\vec{k}\rangle|^2 = \frac{(4\pi eF)^2}{q^2} \qquad (1.1.6)$$

The phonon emission rate can be calculated using Eq.(1.1.2). So far screening effects due to the presence of high density electron-hole plasma are neglected. In other words the dielectric constant is taken to be purely electronic and ionic (see Eq. 1.1.6). A more accurate treatment by Yoffa et al[5] consists of calculating carrier excitation spectrum as the phonon emission rate is related. The rate of emission for phonons (wavevector q, frequency ω) is given by the golden rule to be,

$$R_{q,\omega} = \left(\frac{2\pi}{\hbar}\right)\left(\sum_{ij}\right)\left(\sum_{k\sigma}\right)\left|V^{ij}_{\vec{k}+\vec{q},\vec{k}}\right|^2 f^{i}_{\vec{k}+\vec{q},\sigma}\left(1-f^{j}_{\vec{k},\sigma}\right)$$

$$X\delta\left[\hbar\omega-\left(E^{j}_{\vec{k}+\vec{q}}-E^{j}_{\vec{k}}\right)\right] \qquad (1.1.7)$$

where $V^{ij}_{\vec{k}+\vec{q},\vec{k}}$ is the unscreened matrix element for the transition of an electron from a state $(\vec{k}+\vec{q})_i$ to a state $(\vec{k})_j$ via phonon emission. $f^{i}_{\vec{k}\sigma}$ stands for occupation probability of a state in the i^{th} valley with a momentum $\vec{k}$ and spin σ. Note that the screening effects are entirely included in ϵ, the total dielectric constant. It has been shown by Yoffa et al[5] that,

$$Im\left[\frac{1}{\epsilon(\vec{q},\omega)}\right] = \left(\frac{1}{\epsilon_o}\right)\left(\sum_{ij}\right)\left[Z_{ij}(\hbar\omega_{pi})^2\left(\frac{m_j}{m_i}\right)^{0.5}\left(\frac{\hbar\Gamma_{ij}(\hbar\omega)^2}{E_{\vec{q}}}\right)\right]X$$

$$X\left[Z^2_{ij}(\hbar\omega_{pi})^4\left(\frac{m_j}{m_i}\right)\left(\frac{\hbar\omega}{E_{\vec{q}}}\right)^2+(\hbar\Gamma_{ij})^2(\hbar\omega)^2\right] X\ \delta_{\vec{q},\vec{q}_{Oij}} \qquad (1.1.8)$$

where $\Omega_{ij}(\vec{q}_{Oij}) = \omega$. Using above equations,

$$R_{\vec{q},\omega} = \Omega\left(\exp\ -\frac{\beta\hbar\omega}{\pi he^3\epsilon_o{}^3}\right)\left(\sum_{ij}\right)\left|V^{ij}_{q}\right|^2 Z_{ij}(\hbar\omega_{pi})^2\left[\frac{m_j{}^{1.5}}{(m_i)^{0}}\cdot{}^{5}\right]\delta_{\vec{q},\vec{q}_{o}ij}$$

$$\left[\hbar\Gamma_{ij}\left[1\ +\ \frac{Z^2_{ij}(\hbar\omega_{pi})^4 m_j}{(\hbar\Gamma_{ij})^2 E_{\vec{q}}{}^2 m_i}\right]\right]^{-1} \qquad (1.1.9)$$

By recognizing $(\hbar\omega_{pi})^2 \sim N_i$, where N_i is the density of carriers in valleys i. The critical value of N_i for the onset of screening (or dramatic reduction in $R_{\vec{q},\omega}$) is

$$(N_{ic})_{ij} = \left[\frac{\epsilon_o(\hbar\Gamma_{ij})^2 q^2 O_{ij}}{8\pi e^2 Z_{ij}}\right]\left(\frac{m_i}{m_j}\right)^{1.5} . \qquad (1.1.10)$$

As expected, large wavevector transitions are more difficult to screen. The details of the above calculations are found in ref.5. The theory holds true despite the explicit nature of $|V_{\vec{q}}^{ij}|$ i.e. polar or non-polar. The relevence of this work to my experimental condition is discussed in detail in Chapter 3.

In my present work however, I find theoretically that the screening is more dominant in CdSe than in GaAs and forbids polar optical phonon emission. But the phonon emission through the non-polar optical deformation potential scattering should survive to play the role of the dominant energy relaxation mechanism. The critical density for the onset of the screening in CdSe is much lower than GaAs ($\sim 10^{17}/cm^3$). The data suggests against the phonon bottle neck mechanism. It is also observed that within the excitation fluence of my experiments the carrier density remains less than $2x10^{19}/cm^3$. This I have attributed to the fast diffusion of the carriers from the photo excited region. This process would play an important role in terms of energy relaxation and spin

relaxation processes. The screening of the electron-phonon interactions also explains rapid carrier diffusion. I have not separately investigated the energy relaxation of free carriers for the dilute semimagnetic semiconductors (DMS) $Cd_{1-x}Mn_xSe$ ($x \neq 0$). For small Mn concentrations the energy relaxation process should not differ from the one discussed for CdSe($x = 0$) unless the optical deformation potential is strongly affected by the presence of Mn in the lattice. In dilute semimagnetic semiconductors (DMS) emission of magnons is one of the energy relaxation processes but is insignificant on a picosecond time scale.

I have studied spin alignment and spin relaxation of photogenerated carriers in $Cd_{1-x}Mn_xSe$. The spin alignment of photo excited carriers can be demonstrated[14] in terms of transitions that occur between the atomic type of energy levels (symmetry) near the center of the Brillouin zone (k=0). This is almost universal in all direct gap materials including $Cd_{1-x}Mn_xSe$($x < 0.3$). The conduction, heavy hole (Γ_9 valence in CdSe), light hole (Γ_7 valence in CdSe), and split off valence bands are represented by their total angular quantum numbers and total magnetic quantum numbers, $| C, {}^1/_2 \pm {}^1/_2 \rangle$, $| V_{hh}, {}^3/_2 \pm {}^3/_2 \rangle$, $| V_{lh}, {}^3/_2 \pm {}^1/_2 \rangle$, and $| \Delta, {}^1/_2 \pm {}^1/_2 \rangle$, respectively. The different transitions (see Fig. 4.6.1) from the valence bands to the conduction band are as follows:

$$\langle C, {}^1/_2, \pm {}^1/_2 | \vec{P} | V_{hh}, {}^3/_2, \pm {}^3/_2 \rangle = \frac{P}{\sqrt{2}} (\hat{i} \pm \hat{j}) \quad (1.1.11)$$

$$\langle C, {}^1/_2, \pm {}^1/_2 | \vec{P} | V_{hh}, {}^3/_2, \mp {}^3/_2 \rangle = 0 \quad (1.1.12)$$

$$\langle C, {}^1/_2, \pm {}^1/_2 | \vec{P} | V_{lh}, {}^3/_2, \pm {}^1/_2 \rangle = \frac{\sqrt{2}}{\sqrt{3}} P\hat{k} \quad (1.1.13)$$

$$\langle C, {}^1/_2, \pm {}^1/_2 | \vec{P} | V_{lh}, {}^3/_2, \mp {}^1/_2 \rangle = \frac{1}{\sqrt{6}} P (\hat{i} \mp \hat{j}) \quad (1.1.14)$$

$$\langle C, {}^1/_2, \pm {}^1/_2 | \vec{P} | \Delta, {}^1/_2, \pm {}^1/_2 \rangle = - (\frac{1}{\sqrt{3}}) P\hat{k} \quad (1.1.15)$$

$$\langle C, {}^1/_2, \pm {}^1/_2 | \vec{P} | \Delta, {}^1/_2 \mp {}^1/_2 \rangle = (\frac{1}{\sqrt{3}}) P (\hat{i} \mp \hat{j}) \quad (1.1.16)$$

The electric dipole transition probabilities ($\sim |\vec{P} \cdot \hat{E}|^2$) for right circularly polarized light ($\hat{E} \sim (\hat{i} + \hat{j})$) with photon energy $\overline{E_g} < h\nu < E_g + \Delta$ are as follows (see appendix):

Initial State		**Final State**	**Probability of transition**
$\lvert V_{hh}, {}^3/_2, - {}^3/_2 \rangle$	$\rightarrow$	$\lvert C, {}^1/_2, - {}^1/_2 \rangle$	$\sim 2P^2$
$\lvert V_{\ell h}, {}^3/_2, - {}^1/_2 \rangle$	$\rightarrow$	$\lvert C, {}^1/_2, + {}^1/_2 \rangle$	$\sim 2/3P^2$

This means using one photon excitation, one can create a population ratio of spins ↑ : ↓ = 1:3. It will be discussed in Chapter 4 that this ratio decreases for electrons generated away from the center of the Brillouin zone. Now for circularly polarized light with photon energy $1/2E_g < h\nu < 1/2(E_g + \Delta)$ which is propagating in the direction of the electron wave vector $\vec{k}$, the only non vanishing matrix elements for two photon absorption are $\langle V_{hh}, {}^3/_2, -{}^3/_2 | P^2 | C, {}^1/_2, + {}^1/_2 \rangle$ (right handed polarization) or $\langle V_{hh}, {}^3/_2, {}^3/_2 | P^2 | C, {}^1/_2 - {}^1/_2 \rangle$ (left handed polarization). This is because as expected, two units of angular momentum are required to be absorbed. This fact suggests a ratio of spins ↑ : ↓ = 1:0 (or 0:1). If the angle $(\hat{k},\hat{x})$ ($\hat{x}$ is the direction of light) is different from 0 or π the electrons can be scattered into states with both spin orientations and the spin alignment is no longer[16] 100%. Also for electrons created away from the center of the Brillouin zone, the percentage could be reduced as discussed in Chapter 4.

There are four mechanisms, proposed[17] so far, to account for the fast relaxation of spin alignment of the conduction band electrons in semiconductors. Contributions of these mechanisms depends on the carrier density and temperature. The most applicable mechanism, which was originally proposed by D'yakonov and Perel'[18,19] for GaAs (zinc blende crystal structure) is dicussed in Chapter 4. This case of spin relaxation arises because of the lifting of the Kramer's degeneracy for conduction states with k ≠

0. The splitting can be viewed as due to a pseudomagnetic field which is activated when the carrier undergoes a collision in which its momentum is reversed. Since, the original direction of the momentum provides a quantization axis for the electron spin, if a collision occurs with a change from this direction, it would cause the spin projection to change its sign. Of course this is true only if the precession frequency is low compared to the collision frequency and the spin cannot adjust itself to the new direction. Thus, the spin relaxation rate inversely depends on the collision rate. The spin relaxation rate can be expressed in terms of the precession frequency $\omega(E)$ and collision time $\tau(E)$ as,

$$\frac{1}{T_s(E)} \sim \omega^2(E)\ \tau(E)\ . \qquad (1.1.17)$$

The precession frequency is related to the non centrosymmetric contribution[20] ($\sim k$) to the band energy for wurtzite (and $\sim k^3$ for zinc blende), and in general is written as,

$$\omega^2(E) \sim \left(\frac{E}{E_g}\right). \qquad (1.1.18)$$

This mechanism is described in detail in Chapter 4.

Another relaxation mechanism, known as the Elliot and Yafet mechanism[21,22], arises due to the spin-orbit coupling which makes

the conduction band states a mixture of the two spin states and not pure spin states. This results in a finite probability that, during a scattering event the electron can have its spin as well as its momentum changed. The spin relaxation rate[17] will be the momentum scattering rate times the probability that the event reverses the spin,

$$\frac{1}{T_s(E)} \sim \frac{|M_{k'+},\ k-|^2}{|M_{k'+},\ k+|^2} \frac{1}{\tau_c(E)}, \tag{1.1.19}$$

where $|M_{k'+},\ k-|$ and $|M_{k'+},\ k+|$ are the matrix elements for spin flip and spin unchanged transitions with a momentum change $\hat{k} \rightarrow \hat{k}'$, respectively. For screened ionized impurity scattering, the rate is given by,

$$\frac{1}{T_s(E)} = \frac{32}{27} \left(1 - \frac{m_e}{m_o}\right)^2 \left(\frac{1 + \frac{1}{2}\eta}{1 + \frac{2}{37}\eta}\right)^2 \left(\frac{\eta}{1+\eta}\right)^2 \left(\frac{E}{E_g}\right)^2 \frac{1}{\tau}. \tag{1.1.20}$$

Where $\eta = \Delta/E_g$. For CdSe $\Delta = 0.4$ eV and $E_g = 1.8$ eV.
Thus, the spin relaxation rate is of the order of,

$$\frac{1}{T_s} \sim 0.03 \left(\frac{E}{E_g}\right)^2 \frac{1}{\tau} \sim 4\times10^{-5} \frac{1}{\tau}. \tag{1.1.21}$$

For energy values ($E \sim E_F$) in our experiments of 72 meV, corres-

ponding to carrier densities of ~ $5 \times 10^{18}/cm^3$, and collision time τ ~ 10^{-14} sec, the spin relaxation time is ~ 225 psec.

The third mechanism of electron spin relaxation is due to the spin exchange of electrons and holes in the crystal. This mechanism was first proposed by Bir, Aronov and Pikus[23] in 1975. In this mechanism electronic spin alignment is reduced due to collisions with holes. The spin relaxation rate is expressed in terms of experimentally measured parameters as,

$$\frac{1}{T_S(E)} = N_h \left(\frac{(5\pi)^{1/2}}{8}\right) \frac{\Delta_{x,1s}}{E_{x,1s}} \; a_{x,1s})^2 \left(\frac{2E}{\mu}\right)^{1/2}. \qquad (1.1.22)$$

where $E_{x,1s}$, $\Delta_{x,1s}$, $a_{x,1s}$ and μ are exciton binding energy, 1s exciton spliting (between triplet and quintuplet), 1s exciton Bohr radius and 1s exciton reduced mass, respectively. In CdSe these values are 17 meV, 0.1 meV, 40 Å, and 0.1 m_o, respectively. In our experiment the photogenerated hole density and electron Fermi energy are $5 \times 10^{18}/cm^3$ and 72 meV, respectively. Thus the spin relaxation time in this case is ~ 3 nsec.

The most recently proposed spin relaxation mechanism is that of Kleinman and Miller[24] in which, a virtual recombination of an electron-hole pair produces a virtual photon. This virtual photon could then be reabsorbed producing a new electron-hole pair in which the spin of the electron may be flipped.

This mechanism provides for a nonvanishing relaxation rate at zero temperature, quite unlike any other mechanism that has been proposed. In the degenerate hole case, the spin relaxation time is predicted to be independent of hole concentration. Thus,

$$\frac{1}{T_s} = \frac{1}{\tau_o} \text{ for } k_B T \ll \mu_h \qquad (1.1.23)$$

$$= \frac{1}{\tau_o} \frac{N_h}{4} \left(\frac{2\pi^2}{(m_e+m_h)k_B T}\right)^{3/2} \text{ for } kT \gg \mu_h \ ,$$

where μ_h is the hole Fermi energy, and

$$\frac{1}{\tau_o} = \left(\frac{22}{9}\right) (e^2|P|^2 n E_g)/(m_o^2 h^2 c^3) \ .$$

In CdSe $E_g = 1.8$, $|P^2|m_o \sim 13$ eV, $m_e = 0.13 m_o$ and $n = 2.6$, where $|P|$ is the interband matrix element of the momentum operator and n is the refractive index. These parameters would give us $\tau_o \sim 2$ nsec. These mechanisms cannot explain the short spin relaxation times measured in CdSe. In $Cd_{1-x}Mn_xSe$ an additional spin relaxation mechanism occurs due to the strong spin exchange[25] interaction whose magnitude depends on x and is comparable to the D-P process for $x \sim 0.1$. This mechanism is described in Chapter 4.

The last research chapter deals primarily with the effect of Mn^{2+} isoelectronically replacing Cd^{2+} cations in the wurtzite lat-

tice. This replacement shows a non magnetic rigid band gap shift[26] and a small magnetic shift of the exciton energy state termed "bound magnetic polaron" (BMP)[27]. For $x > 0.3$, I have observed luminescence primarily associated with the photoexcited M_n^{2+} ions and valence bands. The most striking feature of this luminescence is that its peak position shifts with x, contrary to that observed in $Cd_{1-x}Mn_xTe$ system. In $Cd_{1-x}Mn_xTe$, an almost zero shift[28] is observed over a wide range of x ($x > 0.4$). I have calculated the deformation potential for conduction and valence band separately[29] by combining the luminescence data and lattice constant (using x-ray) data. The above model takes into account only the differences in the deformation potentials due to alloying, and totally neglects covalent bonding and ionicity contibutions. This approach may not be accurate enough for evaluating values of deformation potentials. However, this model leads to values of deformation potential close to the given in references (chapter III and IV). The measurements of BMP energies for various x and the effect of clustering[30] of Mn^{2+} ions on BMP energies is investigated in Chapter 5.

1.2 REFERENCES

1. R. F. Leheny, J. Shah, R. L. Fork, C. V. Shank, and A. Migus, Sol. Stat. Comm. 31, 809 (1979).

2. D. Von der Linde and R. Lambrich, Phys. Rev. Lett. 42, 1090 (1979).

3. D. Von der Linde, J. Kuhl, and H. Klingenberg, Phys. Rev. Lett. 44, 1505 (1980).

4. E. Conwell, Solid State Phys. Suppl. 9 (1967).

5. E. J. Yoffa, Phys. Rev. 23B, 1909(1981).

6. H. M. Van Driel, Phys. Rev. 19B, 5928 (1979).

7. A. L. Smirl, J. R. Lindle, and S.C. Moss, Phys. Rev. 18B, 5489 (1978).

8. A. Elci, A. L. Smirl, C. Y. Leung, and M. O. Scully, Sol. Stat. Electr. 21, 151 (1978).

9. J. Shah, Phys.Rev.B, 9, 562 (1974).

10. Masato Hayashi, Hiroshi Saito and Shigeo Shionoya, Sol. State Comm. 24, 833 (1977).

11. Yuzo Yoshikuni, Hiroshi Saito and Shigeo Shionoya, Sol. State Comm. 32, 665 (1979).

12. J. Collet, M. Pugnet, A. Cornet, M. Brousseau, B.S. Razbirin, and G.V. Miknailov, Phys. Stat. sol.(b) 103, 367 (1981).

13. H. Yoshida, Hiroshi Saito, and Shigeo Shionoya J. Phys. soc. Japan, 50, 881 (1981).

14. 'Semiconductors probed by Ultrafast Laser Spectroscopy Vol.2'Edited by, R. R. Alfano (Academic Press, 1985), p.199.

15. C. Kittel 'Quantum Theory of Solids, 1967,p.138.

16. E. L. Ivchenko, Sov. Phys. Sol. State, 14, 2942 (1972).

17. G. Fishman and G. Lampel, Phys. Rev. 16B, 820 (1977).

18. M. I. D'yakonov and V. I. Perel', Sov. Phys. JETP 33, 1053 (1971).[Zh. Eksp. Teor. Fiz. 60, 1954 (1971).]

19. R. J. Seymour, M. R. Junnarkar, and R. R. Alfano, Phys. Rev. 24B, 3623 (1981).

20. A. D. Margulis and VI. A. Margulis, Sov. Phys. Semicond., 18, 305 (1984).

21. R. J. Elliot, Phys. Rev. 96, 266 (1954).

22. Y. Yafet, in Solid State Physics, edited by F. Seitz and D. Turnbull (Academic, New York, 1963) Vol.14, p. 1-98.

23. G. L. Bir, A. G. Aronov, and G. E. Pikus, Sov. Phys. JETP, 42, 705 (1975)[Zh. Eksp. Teor. Fiz. 69,1382 (1975)].

24. D. A. Kleinman and R. C. Miller, Phys. Rev. Lett. 46, 68 (1981).

25. D. Heiman, Appl. Phys. Lett. 42, 775 (1983).

26. J. Stankiewicz, Phys. Rev. 27B, 3631 (1983).

27. T. Dietl and J. Spalek, Phys. Rev. 28B, 1548 (1983).

28. M. P. Vecchi, W. Giriat, and L. Videla, Appl. Phys. Lett. 38, 99 (1981).

29. M. Grynberg, Int. Conf. on Semicond. Phys. 7^{th} Proc., Paris 1964 V.1, by Hulin M. (Academic Press 1964) p. 135.

30. T. Giebultowicz, W. Minor, H. Kepa, and J. Ginter, J. Mag. and Mag. Materials, 30, 215 (1982).

CHAPTER II

2.1 PICOSECOND EXPERIMENTAL SETUP

For picosecond time resolved and time integrated luminescence measurements, a mode-locked[1] Nd^{3+}: glass laser was used. In this laser medium (Nd^{3+}:glass), the spectral width of the gain profile is due to inhomogeneous broadening and its FWHM is 30 cm^{-1}. The laser medium is in the form of a rod with its ends cut at Brewster's angle for 1064 nm emission. The rod is pumped optically by discharging a bank of capacitor (~ 3 kV) through a helical water cooled halogen lamp. This laser is operated only in the pulse mode at a maximum rate of one shot every two minutes. The various longitudinal modes determined by the round trip time ($2\ell/c$ ~ 6 nsec) within the laser cavity and limited by the gain profile $G(\omega)$ can be phase locked using a saturable absorbing medium. For this laser it was done by using a dye, "Kodak 9860", dissolved in 1,1' dichloroethane. This passive mode locking of the longitudinal modes generates a train of ~ 100 pulses separated from each other by a round trip time (~ 6 nsec) with each pulse ~ 6 psec duration at 1064 nm. The train of pulses leaks out of the cavity from a 50% transparent mirror at the end of the cavity, then enters a pulse selector (see Fig. 2.1.1).

The pulse selection[2] is accomplished by applying a high voltage pulse to a Pockels cell which is placed between crossed polarizers. When the voltage is applied to the Pockels cell, one-half wave retardation is induced by the electro-optic effect. This rotates the plane of the polarization by 90° so that the pulse is transmitted through the second polarizer and along the main optical path of the laser. The voltage pulse is generated and timed by a short transmission line terminated at one end by a high impedence current limiting resistor (10 megohms) connected to a high voltage power supply (15.8 KV for the Nd^{+3}:glass laser, which corresponds to twice the one half wave retardation for 1064 nm). The other end of the short transmission line is terminated at a high pressure (100 psi) laser triggered spark gap[3]. The length of this transmission line is adjusted so that when it is discharged into a matched impedance load, it will produce a voltage pulse (5 nsec wide) whose duration is less than the time between the pulses. When there isn't any voltage on the Pockels cell the train of laser pulses is deflected out of the main optical path by a Glan-Thompson prism which is the second of the two crossed polarizers. This train is focussed into the spark gap where one of the pulses initiates an avalanche breakdown which allows the charge that has been stored in the short transmission line to discharge into another transmission line whose length is adjusted so that the voltage pulse arrives at the Pockels cell shortly before another

pulse from the laser train. This voltage pulse then induces a retardation as previously described. The Pockels cell is connected to another long (20 nsec) transmission line which is terminated into a matched resistive load (50 ohms) to prevent reflections which would otherwise partially reopen the Pockels cell. The effect of this arrangement is to select a single pulse from the mode-locked train of pulses. Figure 2.1.2 shows the pulses propagating along the two possible optical paths. Figure 2.1.2a is the mode-locked train of pulses with a single pulse selected out of the train. This oscilloscope trace is from a photodiode placed behind the spark gap.

After the pulse leaves the single pulse selector it is amplified by passing it through two Nd^{+3}:glass rods. The flashlamps that excite the amplifying Nd^{+3}:glass rods are triggered simultaneously with the laser oscillator flashlamp via common electrical pulses so that the maximum gain in the amplifier is available when the pulse arrives at the amplifier. This timing is relatively easy since the amplifier gain follows the flashlamp intensity which has a broad peak 1 millisecond wide. For the Nd^{+3}:phosphate glass amplifiers we use, the total amplification is approximately a factor of 30. After leaving the amplifier the laser pulse is directed into a Potassium Dihydrogen Phosphate (KDP) second harmonic generator crystal[4]. This converts about 10% of the incident 1060 nm radiation to 530 nm radiation. The 1060 nm infrared radi-

ation is either removed with a colored glass filter (Corning 1-75) leaving a pulse of green light (530 nm) or the 530 nm pulse is blocked with a Corning 7-69 filter leaving the 1064 nm pulse to continue along the optical path .

A small portion of the pulse is reflected out of the optical path with an uncoated glass slide and directed onto a silicon photodiode. The electrical pulse output of the silicon photodiode is used as the trigger signal for a streak camera. The output of the silicon photodiode is directed to a variable delay line where various transmission lines can be switched in and out of the electrical circuit. This provides for various delays (adjustable in 250 picosecond steps) to be added to the arrival time of the photodiode output at the streak camera. It is necessary to easily adjust the timing of the triggering since different streak rates have different times between the trigger pulse arrival and the start of the camera streak (intrinsic delay). Furthermore, over the course of an experiment the intrinsic delay for a given streak rate will slowly change by 1 to 2 nanoseconds.

The light pulse continues beyond the photodiode beam splitter and then enters an optical delay line (typically 30 nanoseconds) consisting of either a series of mirrors or a White cell (which provides for multiple reflections from a pair of concave mirrors). Long focal length lenses are introduced as needed in the optical path to recollimate the beam. Before being focussed onto the

sample, part of the pulse is again split off by another beam splitter and directed onto a vacuum photodiode to provide a measure of the energy of each excitation pulse. A third beam splitter provides a small-amplitude pulse which is directed onto the slit of the streak camera. This marker prepulse enables an accurate determination of the time of the excitation. This is done by adjusting the length of the optical path of the prepulse so that it arrives 100 picoseconds before an undelayed luminescence signal would arrive. The actual delay for a particular experiment is calibrated by measuring the delay between the prepulse and the scattered excitation from the sample.

The pulse is then focussed onto the sample (maximum energy is 400 μJ in a 1.35 mm diameter spot size at 530 nm or 1.2 mJ in a 1.9 mm diameter spot size at 1064 nm) after being attenuated by neutral density filters as necessary. The resulting luminescence is collected and collimated by a lens and then passed through appropriate color and bandpass dielectric filters to remove the excitation radiation and select the appropriate spectral region of the luminescence for that particular experiment. The collimated and spectrally filtered luminescence is then refocused onto the streak camera slit (or spectrometer slit).

2.2 STREAK CAMERA

A streak camera[5] with over all resolution of 12 psec was used in the time resolved luminescence experiments. Figure 2.2.1 shows the basic operating principle of a streak camera. The device relies on conversion of time information into spatial information. Photons striking the photocathode of the streak tube produce emission of electrons in proportion to the incident light intensity. The electrons are then accelerated into the streak tube via an accelerating mesh and are electrostatically swept at a known rate over a known distance, converting temporal information into spatial information. These electrons then strike a microchannel plate capable of producing electron multiplication through secondary emission. The secondary electrons released at different times (in relation to the incident electrons) impinge upon a phosphor screen forming the streak image.

The photocathode of the streak tube (N895) is a multialkali with a UV glass faceplate. It has a spectral response similar to but slightly better than an S-20 surface and a useful diameter of 5mm, which under magnification of about 3 yields an effective diameter of 15mm at the output phosphor screen. It uses a P-11 phosphor, which under 3kV electron bombardment produces about 50 photons/electron. The multichannel plate (MCP) has a center-to-center distance of 14μm and an open area ratio of 60 percent. At its maximum rate of applied voltage (900V), the MCP gain reaches a

value of about 10^4. In the streak mode, a 1.5kV acceleration mesh over a distance of 3mm extracts photoelectrons from the photocathode. The applied deflecting voltage is 2kV p-p, and a central 1kV linear portion deflects the photoelectrons at variable speeds of 15, 7.5, 3, and 1.5mm/ns. The deflection sweep circuitry requires a minimum triggering voltage of 2V into 50 ohms. After triggering, the typical time delay to initiate a streak is about 11ns at the fastest sweep rate.

The SIT vidicon camera, which has an S-20 photocathode, monitors the streak image on the phosphor screen. The video signal is analyzed by a microcomputer model C1098 Temporalanalyzer (TA)(manufactured by Hamamatsu, Inc.). The TA microcomputer converts image information from analog to digital and corrects for dark current and sensitivity variations in the vidicon. It integrates and outputs the video intensity along each horizontal scanning line or a portion of it for different window settings.

To calibrate the time axis and intensity linearity of the combined system in the streak mode, a single 6ps, 530nm laser pulse is passed through a pair of etalon mirrors of transmission coefficient T (for each mirror) and separated by an air spacing of d. The calibrating pulses produced in this manner make up a train of pulses separated in time by $\Delta\tau = 2d/c$, where c is the velocity of light. The intensity profile of the train is a decreasing exponential with each subsequent peak reduced by $(1 - T)^2$. For each

round trip of the pulse between mirrors, a light pulse of intensity $I_k = I_o(1 - T)^{2k}$ is produced, for k = 0, 1, 2,,,n.- Since

$$I_k/I_{k+1} = 1/(1 - T)^2 = \text{constant},$$

the envelope formed by the peaks of the pulses follows a single exponential decay given by

$$I = I_0 \exp\left(\frac{t}{\Delta\tau}\ell n\ (1 - T)^2\right),$$

where the time between peaks is $t = k\Delta\tau$. The peaks are used to calibrate the time axis and correct for the intensity variations. The sweep rate per channel $\Delta T/\Delta X$ versus the channel number X is used to calibrate the time base of the streak camera where ΔX is the number of channels between peaks and $\Delta\tau$ is fixed for a given etalon mirror spacing. Figure 2.2.2a shows a typical calibration curve. This is also used to calibrate the intensity axis for the time sweep. Figure 2.2.2b shows a still frame video of the streak image of the C979 streak camera TD system with $\Delta\tau$ = 30ps and a streak speed of 15mm/ns. The graphic representation of that streak image as it appears on a TV monitor is shown in Figure 2.2.2c. The data acquired is then corrected for intensity and the non linearity of the streak rate (Appendix). The specific modifications for energy relaxation and spin relaxation are described in Chapter 3 and 4.

The streak camera can also be operated in the focus mode or non streak mode by switching off the sweep generator and applying an appropriate voltage across the deflection plate so that the

electronic image of the input slit is brought into the center of the field. This mode was extremely useful not only for alignment but also for spatially resolved studies of fast diffusion. This specific use has been described in Chapter 3.

2.3 TIME INTEGRATED SPECTRAL MEASUREMENT

For time integrated spectra measurements, I used a 1/4-m Spex spectrometer in place of the streak camera with an OMA II SIT (silicon intensified target) detector at the exit port. By removing the exit slit it was possible to measure the spectrum at every laser shot. The calibration, i.e., channel vs. wavelength was obtained by using 4 wavelengths almost evenly distributed over the spectral region. These wavelengths were selected by using precalibrated narrow band interference filters and a white light source at the sample site. The known wavelengths and their position as a function of channel number gave us the calibration. The photocathode used in the SIT tube has an extended S-20 (multialkali) spectral response. The spectral response curve was generated in the computer and used for correcting data. The other corrections involved are pixel position response (geometric response), cut off filter transmission (used for blocking excitation pulse from entering the spectrometer), and thermal background. The pixel response curve (Fig. 2.3.1) was obtained by removing the SIT camera from the spectrometer and illuminating the photocathode with a weak light

source through a good quality frosted glass for uniform illumination. It can be easily seen from figure 2.3.1 that the centered pixels receive more light than the ones situated at the edge. The cut off filter transmission was obtained by using a white light source at the sample site and then recording the spectrum through the spectrometer with and without the filter in front of the spectrometer. The ratio of the recorded intensities at each pixel corresponds to the transmission coefficient at a particular wavelength. The background was obtained before every spectrum by halting the lasing in the oscillator cavity yet allowing the flashlamps of the oscillator and amplifiers to fire as usual. This allowed us to incorporate any stray light from the flashlamps in the total background which could be subtracted channel by channel from the recorded data. All these corrections were done using the OMA (II) microprocessor and the corrected data was transferred to a Digital 11-03 computer.

2.4 STEADY STATE SPECTRAL MEASUREMENTS

An argon ion laser was used to excite the samples with 488 or 476 nm wavelength. The typical power densities used in the experiment were in the range of 10-100 W/cm^2. The samples were mounted on a cold finger in an optical helium dewar. The sample temperature was measured within ± 2K using a silicon diode. The excitation beam was chopped at 900 Hz. The photoluminescence was

collected and imaged into a double Spex 1/2m spectrometer with automatic wavelength sweep. For detection a RCA 7265 photomultiplier tube (S-20) and a PAR lock-in-amplifier tuned to 900 Hz was used (see Fig 2.4.1).

2.5 REFERENCES

1. A. J. DeMaria, D. A. Stetser and W. H. Gleen, J. Sceince, 156, 1557 (1967).

2. D. Von der Linde, O. Bernecker, and W. Kaiser, Opt. Comm. 2, 149 (1970).

3. W. K. Pendleton and A. H. Guenther, Rev. Sci. Instr. 36, 1546 (1965).

4. P. A. Franken, A. E. Hill, C. W. Peters and G. Weinreich, Phys. Rev. Lett. 7, 118 (1961).

5. D. J. Bradley, J. F. Higgins and M. H. Key, Appl. Phys. Lett., 16, 53 (1970).

2.6 FIGURE CAPTIONS

2.1.1 The Nd:glass laser system, single pulse selector, delay optics, and luminescence detection unit (here steak camera) are desplayed in block diagram. The details are discribed in the text.

2.1.2 The Operation of a spark gap triggered single pulse selector. The trace of a pulse train output on textronics 519 oscilloscope. The "hole" in the train corresponds to single pulse selected out from the train.

2.2.1 Basic streak camera operation.

2.2.2 Top corresponds to a calibration curve used in streak rate non-linearity correction for time axis and time resolved luminescence intensity. The bottom corresponds to etalon output of a single pulse input monitored by vidio system (left) and integrated output vs. vertical time axis (right).

2.3.1 Vidicon (OMA II) channel response, its photocathode spectral response, spectrometer grating response, and the transmission curve for 3-67 corning filter are displayed in the relevent spectral region.

2.4.1 Steady state luminescence setup.

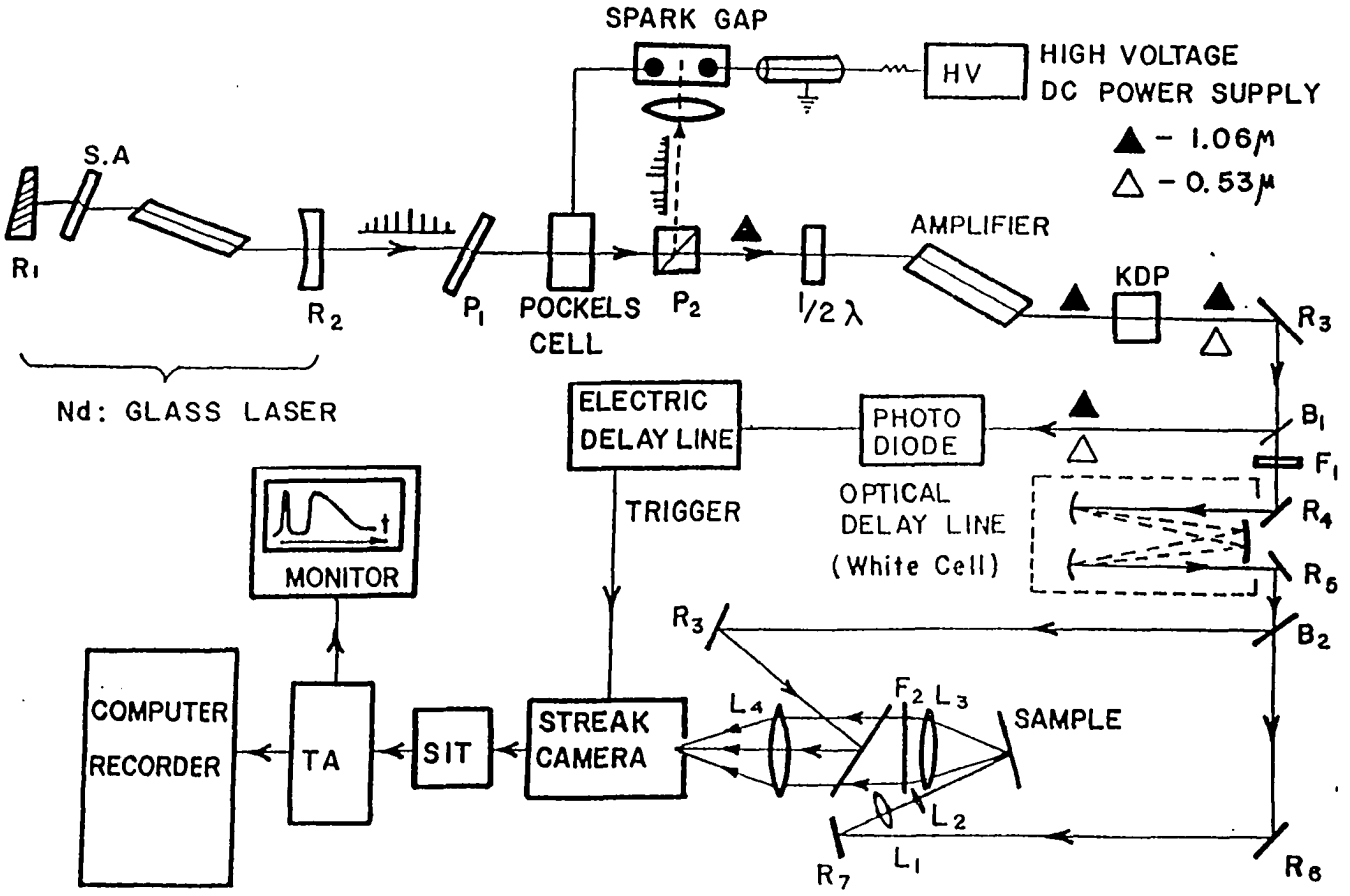

FIGURE **2.1.1**

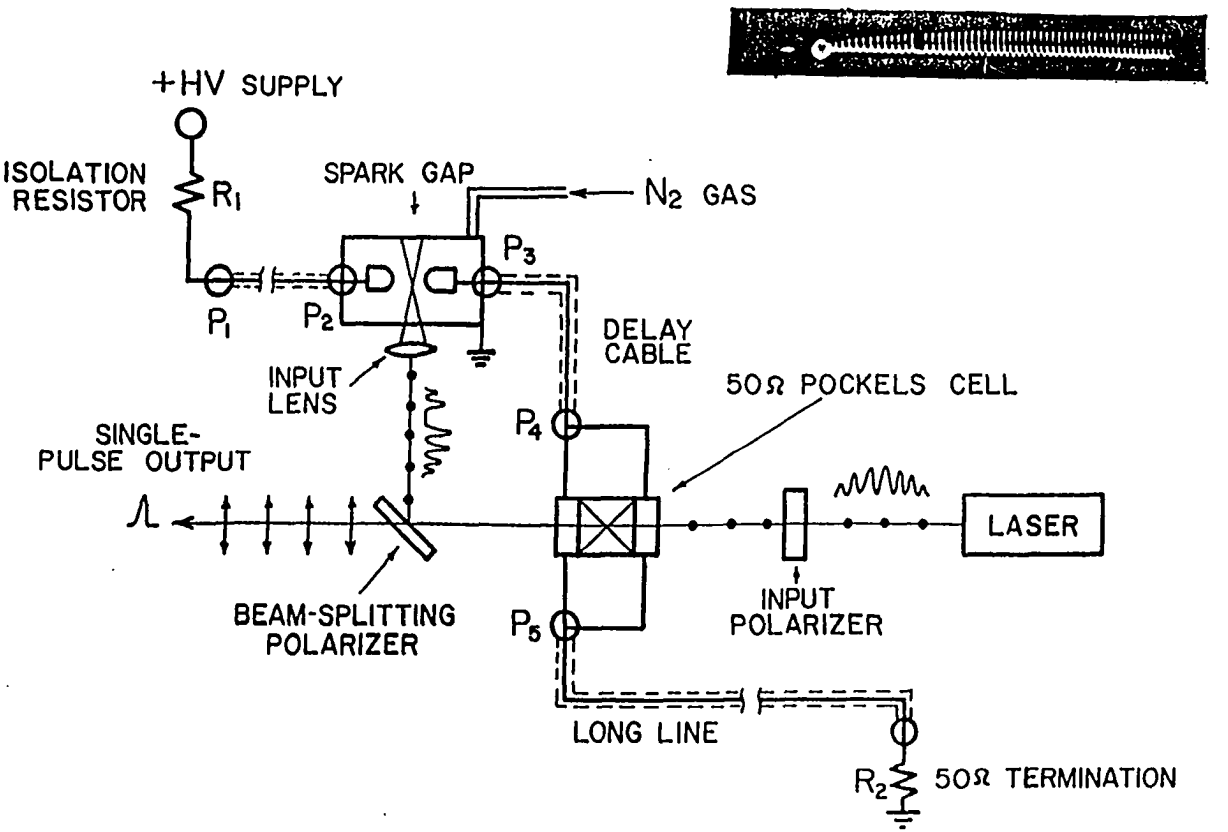

FIGURE **2.1.2**

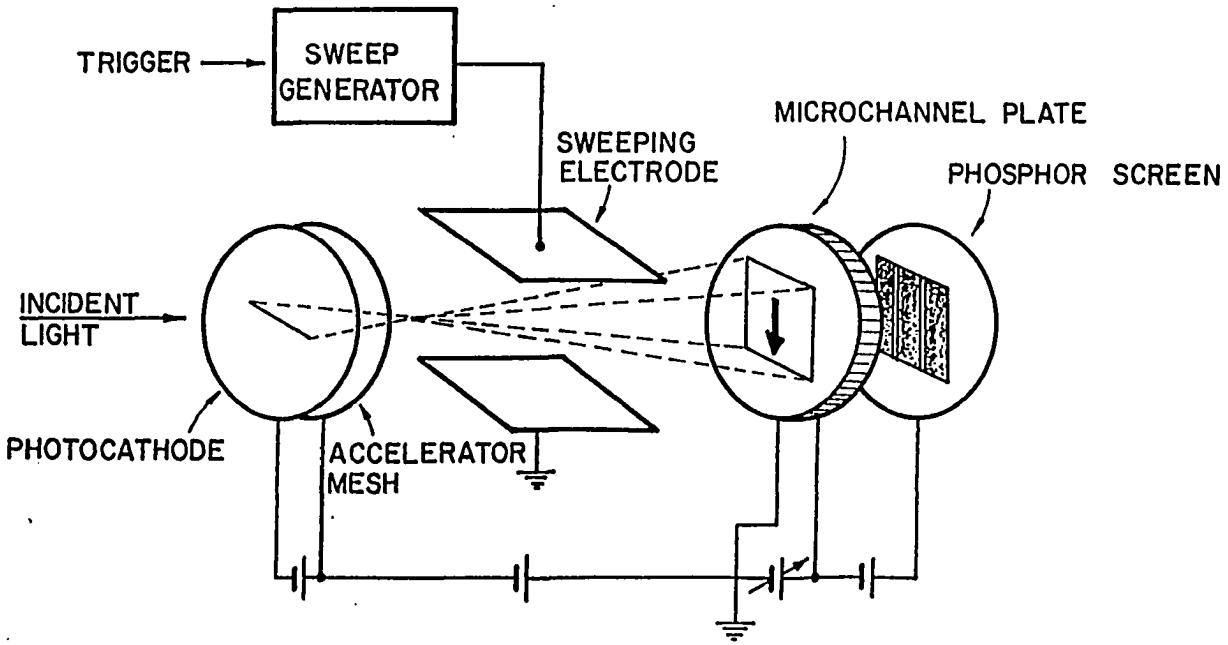

FIGURE **2.2.1**

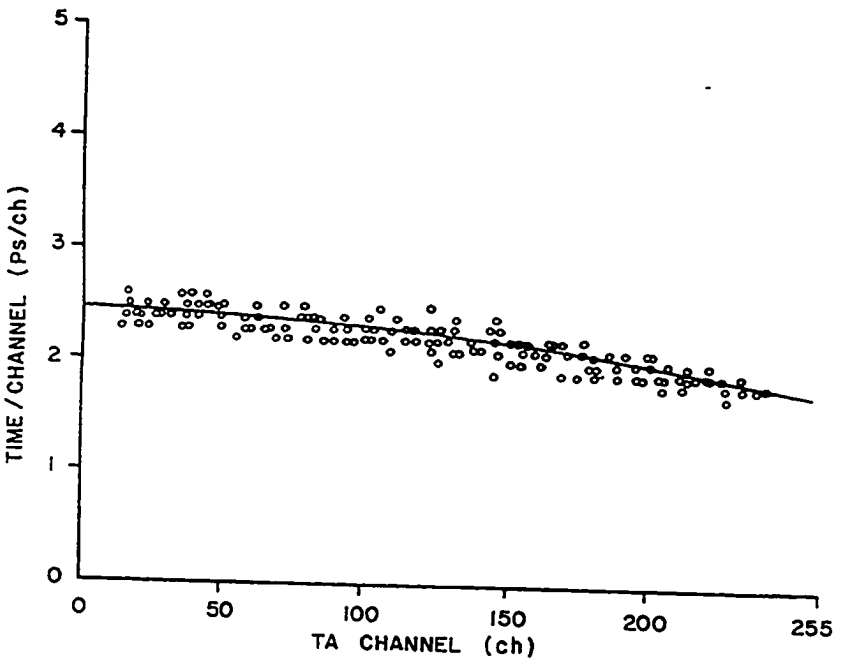

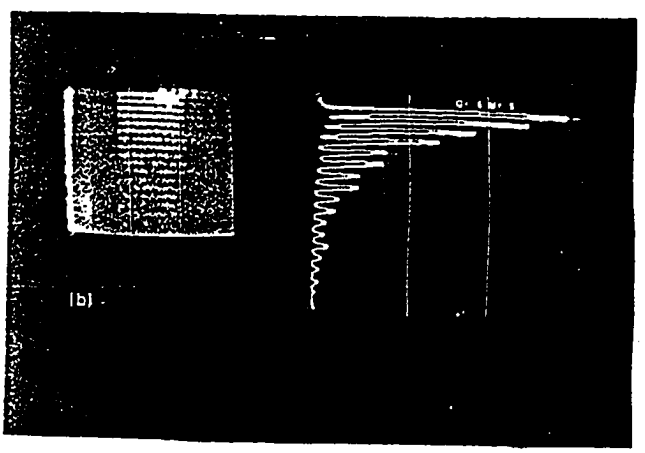

FIGURE **2.2.2**

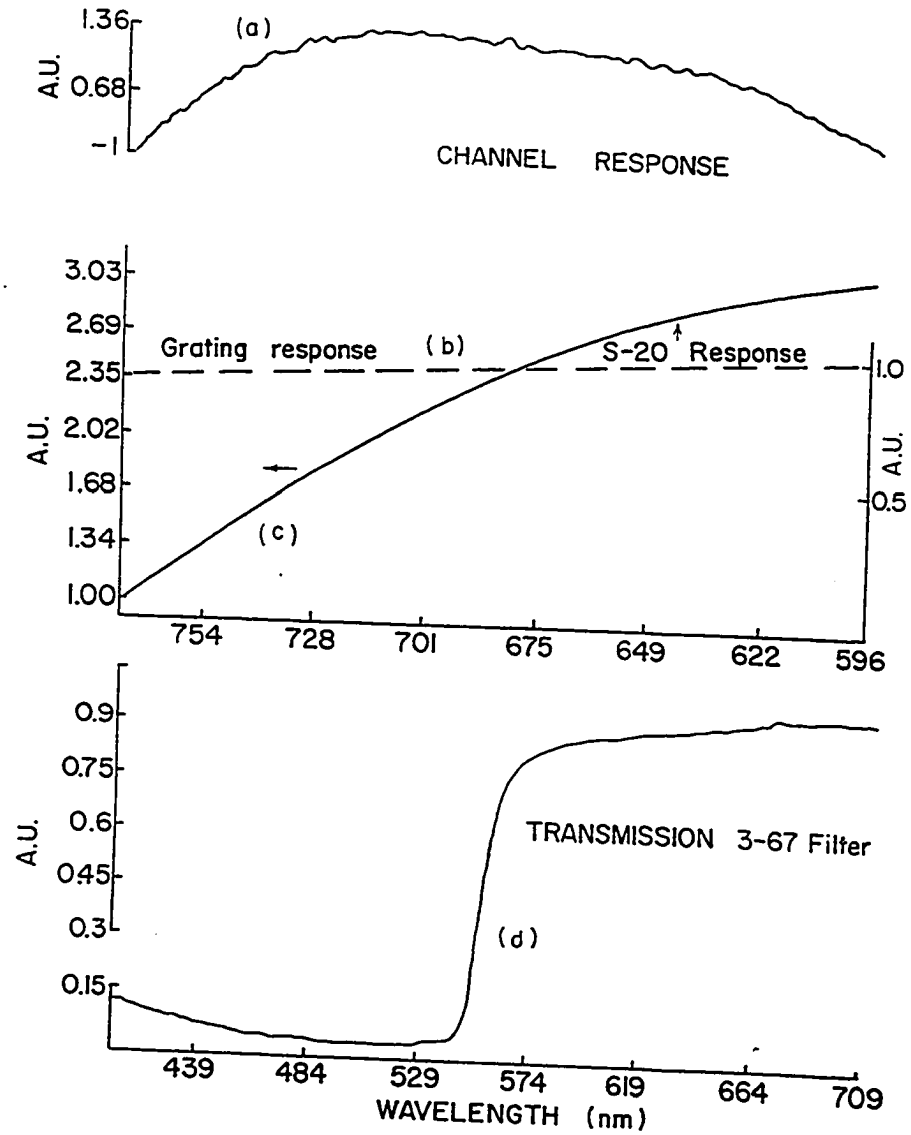

FIGURE **2.3.1**

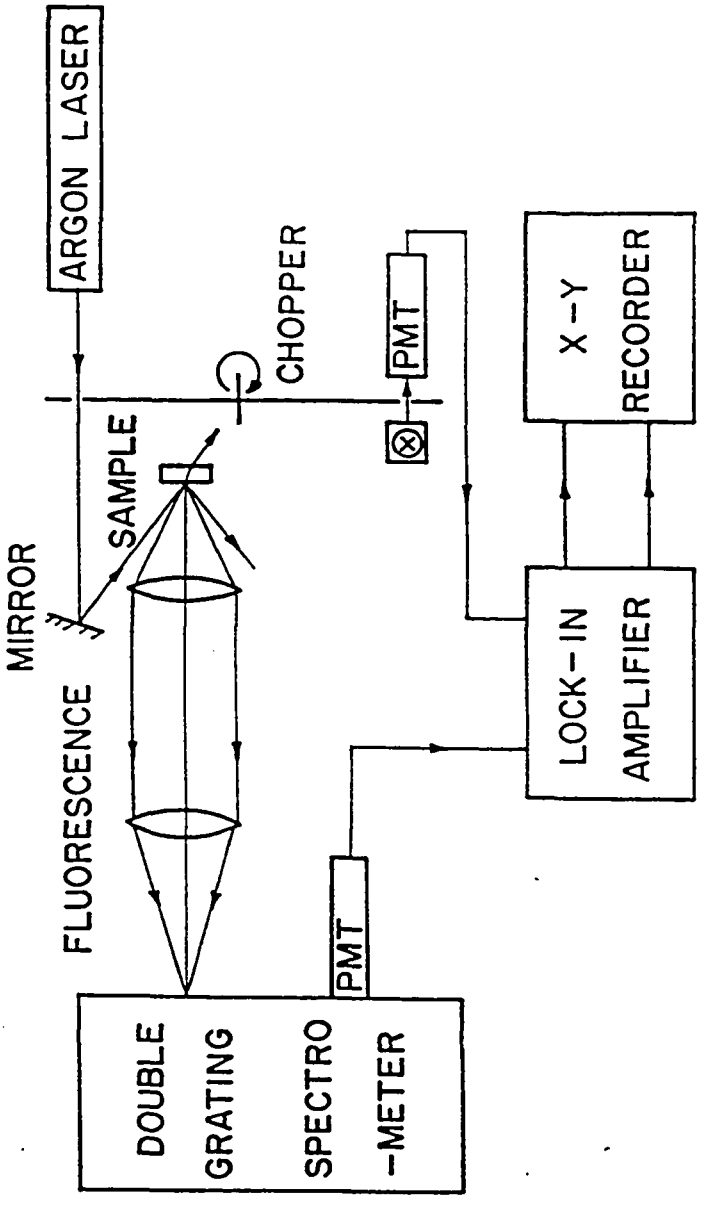

FIGURE 2.4.1

CHAPTER III

Photogenerated High Density Electron-Hole Plasma Energy Relaxation and Experimental Evidence For Rapid Expansion of the Electron - Hole Plasma in CdSe.

3.1 INTRODUCTION

Photogeneration of an electron-hole (e-h) plasma in semiconductors has been known[1,2,3] for many years. Probing this plasma in time provides valuable information on both the non-equilibrium and equilibrium states in terms of the interaction among elementary excitations with the environment, mainly the lattice. The knowledge obtained from these studies are relevant to laser annealing processes in semiconductors. The carriers created from the absorption of a laser photon at energy $\hbar\omega_\ell$ ($\hbar\omega_\ell > E_g$), where E_g is the bandgap, are hot having a pseudotemperature given by[4] $T_i \approx 1/3(\hbar\omega_\ell - E_g)/k_B$. Due to carrier-carrier scattering ($\sim 10^{-14}$ sec) it is assumed that the electron and hole system each have the same temperature. In our experiment, with CdSe and $\hbar\omega_\ell = 2.34$ eV, the carrier pseudotemperature is $\sim$ 2560K. The primary channels for energy relaxation of these hot carriers are carrier-carrier scattering, plasmon production and phonon emission. Of these processes, all but phonon emission primarily involve the redistri-

bution of the carrier energy among the electrons and holes with negligible amounts of energy transferred to the lattice. In a semiconductor, the optical phonon energy is typically ~ 25 meV, while the acoustical phonon energy is much smaller. Therefore, the energy relaxation process is dominated by optical phonon emission as long as the carrier kinetic energy is larger than the optical phonon energy. The rest of the kinetic energy is dissipated as acoustical phonons. An excellent review of these processes is given by E.J. Yoffa[5] and B.R. Nag[6]. Generally, the energy relaxation rates are carrier density dependent. For a hot electron (hole) having excess kinetic energy E, the energy loss rate/carrier due to collisions with the N other electrons (holes) is given by[7],

$$\frac{dE}{dt} = -\frac{4\pi N e^2}{\varepsilon_o^2 \sqrt{2 m_e E}} \quad , \tag{3.1.1}$$

where e and m_e are the electron (hole) charge and effective mass, and ε_o is the bulk dielectric constant. This N dependent energy relaxation rate causes rapid thermalization of photogenerated carriers within ~ 10^{-14} sec. The plasmon frequency is dependent on carrier density[5] ($\omega_p \sim \sqrt{N}$). The energy relaxation process involving LO phonons can be effectively screened at high carrier densities and this subject will be discussed later. The first steady state experimental observation of carrier heating in CdSe

was reported by Shah[2] et al in 1974 at an estimated photogenerated carrier density of 2x $10^{18}/cm^3$. Free e-h plasma expansion has been observed in CdSe at 4K by Cornet et al[8]. Their observation by analyzing spectra emitted from different photoexcited regions showed that the velocities are two orders of magnitude greater than the thermodynamic equilibrium diffusion velocity. However, they did not observe any plasma expansion at room temperature. They reasoned that the absence of large number of thermal phonons at low temperature made it possible to observe this expansion only at low temperatures. Combescot et al[9] have calculated diffusion velocities at T = 0K, using an hydrodynamic model. The velocities suggested by this model are ~ 10^8 cm/sec. It is also possible to calculate the velocities by considering[8,10] the pressure developed when the e-h plasma density is above the e-h liquid density (5.4x $10^{17}/cm^3$). The large pressure generated causes rapid diffusion of free carriers. The pressure is given by, $p = N(\partial F/\partial d\ln(n))|_{T,N'}$, where N' is the total number of e-h pairs, N is the carrier density and, F is the free energy per pair. The plasma expansion has also been observed in GaAs[11] and in $GaAs_{1-x}P_x$[12] at 2K. Forchel et al[13] have pointed out the significant effect of carrier drift velocities on the transmission and emission spectra of a rapidly diffusing non-equilibrium e-h plasma in semiconductors. These examples indicate that the presence of fast diffusion and the consequent reduction in carrier density can play an important role in various

energy relaxation processes.

The purpose of our research is two fold: to experimentally demonstrate the rapid diffusion of photogenerated carriers in CdSe from the photoexcitation region at both room and low temperatures and to show the role of partially screened non polar optical phonon emission in the cooling of high density hot carriers and in the rapid diffusion of these carriers.

3.2 BACKGROUND

a)Electron-phonon interaction and carrier temperature relaxation

It has been shown by Yoffa[14] that the electron (hole)-lattice (polar and non-polar) interaction which results in emission of LO phonons could be effectively screened for carrier densities greater than the critical density N_c, which is a characteristic of a particular semiconductor. In direct gap polar semiconductors like CdSe or GaAs the intravalley polar transitions are dominant in terms of hot carrier energy relaxation at low carrier densities ($N < N_c$). A typical scattering rate[5,14] in this situation is 1×10^{11} eV/sec. The critical density associated with such transitions (polar and non-polar) is given by,

$$N_c = \left(\frac{\varepsilon_0 \hbar q^3}{8\pi e^2}\right)\left(\frac{1}{\sqrt{\beta m_e}}\right) . \qquad (3.2.1)$$

In CdSe this equation can be simplified to $N_c = 1.5\times10^{-4}\sqrt{T_e}q^3$, where q is the phonon wave vector and $\beta = 1/k_B T_e$ where T_e is the carrier temperature. In polar semiconductors, the polar electron-phonon interaction is governed by matrix element[15,16] $V \sim 1/q$. Thus, the phonons with large q do not participate much in the interaction. Considering a parabolic conduction band in a semiconductor, one would like to see a range of q's of phonons emitted during the energy relaxation process via LO phonon emission. The figure (3.2.1) shows the relaxation of a hot electron via intravalley LO phonon emission. The minimum phonon wavevector that can couple two conduction band states occurs when the direction of the electron wave vector is unchanged. The maximum wavevector is created when the electron momentum direction is reversed. The values of q_{min} and q_{max} are weakly dependent on the initial electron energy and can be calculated from the band structure. Without screening the created phonons are not evenly distributed[17] between q_{min} and q_{max} because of the inverse q^2 factor in the Frolich interaction. The values of q_{min} and q_{max} are calculated at the point of excitation in the E-k band structure diagram.

For a semiconductor with bandgap E_g and laser photon energy $\hbar\omega$, the initial kinetic energy of electrons before thermalization is given by,

$$E_e = (\hbar\omega - E_g)\left(\frac{m_h}{m_h+m_e}\right) \qquad (3.2.2)$$

where m_e and m_h are the effective masses of electrons and holes, respectively. Since the electrons and holes are assumed to be in thermal equilibrium $T_e = T_h$ (e-e and e-h scattering time ~ 10^{-14} sec), the initial e-h plasma temperature during the laser pulse (width ~ 5psec) will be,

$$T_i = \left(\frac{1}{3k_B}\right)(\hbar\omega_\ell - E_g) \text{ and } E_i = \left(\frac{3}{2}\right)k_B T_i \qquad (3.2.3)$$

It can be easily shown that the minimum and maximum q values for LO-phonon energy δ is given by,

$$q_{min} = (\sqrt{2m_e})(\sqrt{E_i} - \sqrt{E_i-\delta})\left(\frac{1}{\hbar}\right) \qquad (3.2.4)$$

and

$$q_{max} = (\sqrt{2m_e})(\sqrt{E_i}+\sqrt{E_i-\delta})\left(\frac{1}{\hbar}\right) \qquad (3.2.5)$$

for the conduction band, respectively. Similarly, values can be

obtained for the valence band. Using Eq.s (3.2.3), (3.2.4), and (3.2.6), for CdSe with the values $0.13m_o$, 2.34 eV, 1.71 eV, and 26 meV of the electron effective mass, excitation laser photon energy, band gap and LO phonon energy, the carrier temperature is T_i = 2560K, E_i = 0.32 eV, q_{min} ~ 4.6×10^5 cm^{-1} and q_{max} ~ 2.2×10^7 cm^{-1}.

From Eq. (3.2.1) the critical density N_c corresponding to q_{min} is $7\times10^{14}/cm^3$, while the critical density corresponding to q_{max} is $8\times10^{19}/cm^3$. These values should only be used as a guideline since the q_{max} decreases with time during the energy relaxation process and hence the corresponding N_c will decrease with time. However, it is possible to calculate N_c if the carrier temperature is experimentally known.

In order to calculate the density of photogenerated carriers produced by a laser pulse, we should first consider the density of states[18] at the point of excitation. For a parabolic band the number of energy states per unit volume between the interval E and E+dE is given by,

$$N(E)dE = \left(\frac{1}{2\pi^2\hbar^3}\right)(2m_e)^{\left(\frac{3}{2}\right)}(\sqrt{E})dE \qquad (3.2.6)$$

Since the laser photon spectral width and band warping is 20 meV, dE = 20 meV and E_e = 0.489 eV. Thus, $N(E)dE = 1.3\times10^{19}/cm^3$. The

total density of states integrated from 0 up to E_i is $7x10^{19}/cm^3$. The e-e scattering time[5] τ_{e-e} is ~ 10^{-14} sec and the pulse width is 5 psec. The total carrier density could be as high as $6.5x10^{21}/cm^3$, if we take into account all the indirect valleys (equivalents of X and L). Because the scattering time out of the states being 10^{-14} sec is faster than the pump duration of 5 psec, the conduction state could be occupied and emptied 500 times ($5x10^{-12}/10^{-14}$) during the laser pulse. Most of the zinc blende type semiconductors like GaAs or CdTe have indirect L and X valleys with an indirect bandgap ≈ E_g + 0.3 eV. The local symmetry of the wurtzite crystal structure is very similar to zinc blende. It is reasonable to assume the existence of indirect valleys. As far as the electron (hole)-phonon interaction is concerned the total carrier density, irrespective of valleys, plays a role in the screening of this interaction. With our range of photon fluence $7x10^{16}$ (I_F)-$2x10^{15}$ ($1/33I_F$) photon/cm^2, a range of carrier densities $3x10^{21}$ - $8.5x10^{19}/cm^3$ can be estimated if one uses a reflectivity coefficient (refractive index ~ 2.6)[19] R = 0.2 and an absorption coefficient[20] α = $5x10^4$ cm^{-1}(for one photon absorption) in the expression,

$$N = (1-R).I.\alpha \quad /cm^3 \qquad (3.2.7)$$

This expression does not take into account any diffusion during the laser pulse duration nor any recombination. In this case the esti-

mated carrier density range of $3x10^{21}$ - $8.5x10^{19}/cm^3$ is below the saturation limit of $6.5x10^{21}/cm^3$.

The phonon emission rate per carrier can be written as[14],

$$\nu = \frac{\nu_o}{1 + (\frac{N}{N_c})^2} \qquad (3.2.8)$$

ν_o is the unscreened phonon emission rate and incorporates the Frolich interaction term ($1/q^2$) for polar interaction and is independent of q for non polar interaction. The phonon emission rate depends on the carrier density and can be estimated from the delay time of band edge luminescence. It can be seen that the q_{min} polar phonon emission is completely screened for a carrier density in the range $3x10^{21}$-$8.5x10^{19}/cm^3$ ($N_c \sim 1x10^{15}/cm^3$). But a q_{max} for phonon emission can not be screened until the carrier density reaches a value above $8x10^{19}/cm^3$. However, the $1/q^2$ dependence for the polar emission probability (incorporated in ν_o) decreases the emission rate by a factor of ~1370 over unscreened q_{min} phonon emission. The net effect is that all the intravalley polar LO phonon emission processes are screened and can not contribute to the hot carrier energy relaxation mechanism for $N > 10^{15}/cm^3$ on the picosecond time scale. The phonon emission frequencies for polar and non polar interactions for q_{min} and q_{max} are plotted

with the carrier density N in Fig.(3.2.2). The emission frequencies show a dramatic reduction for carrier densities exceeding the respective critical densities N_c.

Since, the polar phonon emission are most likely screened, the next dominant mechanism for energy relaxation of hot conduction electrons (valence holes) is due to LO phonon emission via nonpolar optical phonon scattering. This process is also known as optical deformation potential scattering[16]. In the case of nonpolar interactions, the optical phonon emission does not in general depend on the phonon wave vector. The non polar optical matrix element has been shown[16] to be almost independent of q with a small higher order dependence on the wave vector of the phonon. This type of scattering is similar to acoustical phonon scattering except that a fixed quantaum of energy $\hbar\omega_o$ (or δ)(LO phonon energy) is emitted for all q's.

The theory developed by Yoffa[14] for electron-optical phonon screening holds equally for polar and non polar phonons in terms of the critical carrier density calculation (Eq.(3.2.1)). Thus, non-polar phonon emission with wave vector q_{max}, and critical density $N_c = 8\times10^{19}/cm^3$, would dominate the energy relaxation process, while q_{min} emission is completely screened for the relevant carrier densities (10^{19}-$10^{21}/cm^3$) in our experiments (Fig.(3.2.2)).

The average rate of change of carrier energy due to nonpolar optical interactions for a Maxwell-Boltzmann distribution of car-

riers at temperature T_e, is given by[16],

$$\frac{dE}{dt} = -\left(\frac{\sqrt{2}}{\sqrt{\pi}}\right)\left(\frac{D'^2(m_e)(\frac{3}{2})}{\pi\hbar^2\rho}\right)(\sqrt{k_BT_e})\beta(x_o,x_e) \qquad (3.2.9)$$

where,

$$\beta(x_o,x_e) = \left[\frac{\exp(x_o-x_e)-1}{\exp(x_o)-1}\right]\left(\frac{x_e}{2}\right)\exp\left(\frac{x_e}{2}\right)K_1\left(\frac{x_e}{2}\right) ,$$

$$x_o = \frac{\delta}{k_BT_o},\ x_e = \frac{\delta}{k_BT_e},$$

T_o is the lattice temperature, K_1 is a Bessel function of the second kind ($K_1(x_e/2) \sim 2/x_e$ for small x_e), and D' is the conduction band deformation potential[16,21,22]. Eq.(3.2.9) gives $T_e(t)$ and the temperature relaxation rate of hot carriers.

b)Luminescence for high excitation

The photoexcited carriers (e-h) recombine during the process of thermalization. The recombination photoluminescence is characterized by carrier temperature, carrier density (Fermi energy) and the band gap of the semiconductor. This allows us to make a rea-

sonable estimate of the carrier density and carrier temperature T_e by studying either time resolved luminescence within different spectral bands (streak camera) or time resolved spectra (with time gate). An estimate of the average carrier density and temperature can be obtained from a time integrated spectrum within the dynamic range limited time interval (in our case, 100-800 psec to be explained later) of the detection system.

In semiconductors at ultra high photogenerated carrier densities, the third order non radiative band-to-band Auger mechanism[23] can dominate all other recombination processes such as radiative and surface recombination, and trapping at crystal defects. The cubic dependence[23] on carrier density in addition to the linear term arises from the three-body character of the Auger process, whereby an electron recombines with a hole, and the excess energy is transferred to another electron or a hole in the form of kinetic energy.

The equation for the time dependence of carrier density N(t) for Auger recombination of carriers is given by[23],

$$\frac{dN(t)}{dt} = - CN^3(t) - \frac{N(t)}{\tau} \qquad (3.2.10)$$

where C is the Auger recombination constant and τ is the total recombination lifetime of free carriers. For high density e-h plasma luminescence intensity $L(t) \sim N(t)P(t) \sim [N(t)]^2$. Hence, for

$B'/_2 = C$ and $2\tau' = \tau$, the Eq.(3.2.10) can be rewritten for the time dependence of luminescence intensities as,

$$\frac{dL(t)}{dt} = -B'[L(t)]^2 - \frac{L(t)}{\tau'} \quad , \qquad (3.2.11)$$

where τ' is the luminescence lifetime. The solution to Eq.(3.2.11) is given by,

$$L(t) = \frac{L(0)}{\left[(1 + L(0)\ B'\tau')\exp(\frac{t}{\tau'}) - L(0)B'\tau'\right]} \qquad (3.2.12)$$

The luminescence time resolved data can provide values (Appendix B7) of carrier density if the values of $1/2L(0)B'$ are obtained using Eq.(3.2.12) (see Fig. (3.5.12)) and if the Auger recombination constant is known ($N^2(0)\ C = B'/2L(0)$). It has been shown that the pure collision Auger process is almost negligible in comparison with the phonon-assisted Auger recombination over a wide temperature (>100 K) and for carriers with densities $\sim 10^{19}/cm^3$ on a psec scale. Takashima et al[24] have calculated the Auger recombination coefficient C for GaAs $\sim 10^{-29}$ cm^{-6} sec^{-1} taking into account screening of free carrier-phonon interactions. We have assumed $C \sim 1x\ 10^{-29} cm^{-6}$ sec^{-1} at 1000 K. We have used

this value of C to estimate the carrier density.

In direct gap semiconductors non-momentum conserving transitions[25] can connect states having different k-directions provided the emitted phonon has a large momentum but small energy. At high carrier temperature ~ 1000 K, the accoustical phonon emission rate is ~ 10^{10} eV/sec in CdSe (Eq.(3.6.4)). Hence, considering an upper limit for an acoustical phonon of 1 meV (and k ~ 10^{7} cm^{-1}) the corresponding phonon emission time is of the order of 0.1 psec. During the lifetime (~ 100 psec) of a free carrier, the acoustical phonon emission is highly probable and the luminescence spectra will correspond to non k selection transitions. In this case the luminescence intensities will depend on the electron and hole density of states separately. The emission arises from k rings at fixed energies ε_e and ε_h. This is in contrast to the conventional non k selection transition[25] which allows for large carrier energies requiring integration over $\varepsilon_e(\varepsilon_h)$. The large energy phonon emission probability is small compared to the small energy phonon. This type of momentum relaxed non k selection transition gives us the best theoretical fits.

In this case the emission spectrum $L(\varepsilon)$, taking into account the Fermi distribution of both electrons and holes, and the respective density of states is given by,

$$L(\varepsilon) = A\sqrt{\varepsilon_e}\sqrt{\varepsilon_h}/\{[e^{(\varepsilon_e - \mu_e)/k_B T_e} + 1][e^{(\varepsilon_h - \mu_h)/k_B T_e} + 1\} \quad (3.2.13)$$

where ε_e, ε_h are the free energies of electrons and holes, respectively, measured from the respective band edges; μ_e and μ_h are the Fermi energies for electrons and holes measured from the respective band edges; T_e is the common temperature assigned to the e-h plasma; and ε is the photoluminescence photon energy corresponding to an $(\varepsilon_e, \varepsilon_h)$ energy pair.

The expression given above (Eq. 3.2.13) is simplified further using the relationships,

$$\varepsilon = \varepsilon_e + \varepsilon_h + E_g \quad (3.2.14)$$

$$\varepsilon_e = \left(\frac{\varepsilon - E_g}{m_e + m_h}\right) m_h \quad (3.2.15)$$

$$\varepsilon_h = \left(\frac{\varepsilon - E_g}{m_e + m_h}\right) m_e \quad (3.2.16)$$

where m_e and m_h are the effective masses for electrons and holes. Furthermore,

$$\varepsilon_e = \frac{(\varepsilon - E_g)\mu}{m_e} \quad (3.2.17)$$

$$\varepsilon_h = \frac{(\varepsilon - E_g)\mu}{m_h} \qquad (3.2.18)$$

where μ is the reduced mass for electron and hole and

$$\frac{1}{\mu} = \frac{1}{m_e} + \frac{1}{m_h} \quad . \qquad (3.2.19)$$

Since the electron and hole density is the same ($N = n_e = n_h$) assuming all the preferential traps (n or p-type) are screened at the high e-h plasma density, the Fermi energies are related by:

$$\frac{\mu_e}{\mu_h} = \frac{m_h}{m_e}, \qquad (3.2.20)$$

where μ_e and μ_h are the Fermi energies for electrons and holes, respectively (and $N \sim [m_{e(h)}\mu_{e(h)}]^{3/2}$). Thus, $L(\varepsilon)$ can be written as,

$$L(\varepsilon) = A(\varepsilon - E_g)/[\exp((\varepsilon - E_g)\mu/m_e - \mu_e)/k_BT_e + 1]^{-1} \times [\exp((\varepsilon - E_g)\mu/m_h - \mu_h)/k_BT_e + 1]^{-1} \qquad (3.2.21)$$

By substituting Eq.(3.2.20) into Eq.(3.2.21), the luminescence spectrum can be experssed in terms of conduction electron parameters as,

$$L(\varepsilon) = A(\varepsilon - E_g)/[\exp((\varepsilon - E_g)\mu/m_e - \mu_e)/k_BT_e + 1]^{-1} \times$$

$$[\exp((\varepsilon - E_g)\mu/m_h - \mu_e m_e/m_h)/k_B T_e + 1]^{-1} \qquad (3.2.22)$$

The carrier density is estimated from curve fitting using the Fermi level energy parameter and carrier temperature parameter.

The carrier density is given by[23],

$$N = N_c' f_{1/2}(\eta) \qquad (3.2.23)$$

where $\eta = \mu_e/k_B T_e$ and

$N_c' = 4.831 \times 10^{15}(m_e/m_o)^{(3/2)} T_e^{(3/2)}$

$/cm^3$.

For a wide range of $\eta \geq 1$ it has been shown[23] within 3% error that,

$$f_{1/2}(\eta) = \left(\frac{4\eta(\frac{3}{2})}{3\pi(\frac{1}{2})}\right)\left[1 + \frac{\pi^2}{8\eta^2}\right]. \qquad (3.2.24)$$

where

$$f_{1/2}(\eta) = {}_0\int^{\infty}(\sqrt{(E/k_B T_e)}(dE/k_B T_e)/[1 + \exp(E - \eta)/k_B T_e] \qquad (3.2.25)$$

Using the known values of band gap of 1.71 eV (724 nm) at lattice

temperature (300K), the theoretical fits to the luminescence spectra for various excitation powers were obtained (Fig.(3.5.9) and (3.5.10)). The carrier temperature and Fermi level are used as variable parameters. The low energy edge of the luminescence spectra is sensitive to the choice of Fermi level values, while the high energy edge is sensitive to the choice of temperature values. The carrier density and T_e obtained from this analysis is an average within time interval 100 - 800 psec.

c) Hot and high density carrier diffusion

The photogenerated or electrically injected carriers diffuse into the bulk of a semiconductor even in the absence of an electric field due to their thermal velocities, band bending and intrinsic collisions. It has been pointed out by Yoffa[26] et al that at high photogeneration rates the laser energy given to the lattice within a characteristic depth is determined primarily by carrier diffusion.

The ambipolar diffusion constant D_o is given by[26],

$$D_o = \frac{2k_B T_e \tau_e \tau_h}{m_e \tau_h + m_h \tau_e} . \qquad (3.2.26)$$

where τ_e and τ_h are collision times and depend on carrier and lattice temperatures. For unscreened impurity scattering $\tau_{o_i} = \tau_{o_h}$ is

about 10^{-13} sec and for hot carrier temperature of 2000 K, D_{o_i} = 105 cm^2/sec. For unscreened non-polar optical phonon scattering τ_{o_p} is 2 $x10^{-12}$ sec (Eq.(3.2.9)) at T_e = 2000 K, yielding D_{o_p} = 2100 cm^2/sec.

The continuity equation which governs the carrier density in space (x) and time (t) for the one dimensional case in the absence of electric fields, for low carrier density and δ-function type photoexcitation is given by[27],

$$\frac{\partial N}{\partial t} = -\frac{N}{\tau} + D_o\left(\frac{\partial^2 N}{\partial x^2}\right) \qquad (3.2.27)$$

where τ is the total lifetime of a free carrier. The solution to the above equation is given by[27],

$$N(x,t) = \frac{N'}{(4\pi D_o t)^{(\frac{1}{2})}\left[\exp\left(-\frac{t}{\tau} - \frac{x^2}{4D_o t}\right)\right]} \qquad (3.2.28)$$

where $N' = N/\alpha$, assuming a small optical absorption depth ($\alpha \sim 5 \times 10^4$ cm^{-1}) and N is given by Eq.(3.2.7). During a typical delay time of ~ 30 psec observed in our experiments and a lifetime of 400 psec, the reduction in the carrier density is only by a factor of 10. In order to explain the observed (see sections 3.6.2a, 3.6.2b, 3.6.2c, and 3.6.2d) larger changes in the carrier density one needs a large diffusion constant which is at least $100D_o$.

Since the diffusion constant depends on a particular scattering mechanism via τ_e, one should take into account the screening effect on that scattering mechanism due to the presence of a high density e-h plasma.

The enhancement of the ambipolar diffusion constant D_o for large densities has been pointed out by Frigo et al[28]. Accordingly, the carrier diffusion at low temperature is dominated by impurity scattering. By treating the impurities as ionized centers whose Coloumb potential is screened by the carrier plasma, an effective diffusion coefficient can be determined[28] by using elementary kinetic theory and the Born approximation. For densities greater than Mott density N_m ($1\times10^{17}/cm^3$), this approach yields a density dependent diffusion coefficient[28],

$$D_i = D_{oi} (N/N_m)^{\alpha} \qquad (3.2.29)$$

where D_{oi} = 105 cm^2/sec (τ_{oi} for impurity scattering ~ 10^{-13} sec and T_e ~ 2000K) and α = 4/3 for ambipolar diffusion and full carrier screening. At high densities the potential is more effectively screened so that the carriers diffuse rapidly away from the surface. For the lower densities the impurities become more efficient scatterers and make the diffusion coefficient decrease with density.

At high carrier densities, as we have seen earlier (Eq.(3.2.8)), the LO phonon-carrier scattering time becomes longer:

$$\tau_p = \tau_{op}\left[1 + \left(\frac{N}{N_c}\right)^2\right] . \qquad (3.2.30)$$

Therefore using τ_p and Eq.(3.2.26), the phonon assisted carrier diffusion constant becomes:

$$D_p = D_{op}\left[1 + \left(\frac{N}{N_c}\right)^2\right] . \qquad (3.2.31)$$

The total diffusion constant due to impurity and phonon scattering is given by,

$$D_t = \frac{D_i D_p}{D_i + D_p}$$

$$= \frac{D_{oi}D_{op}\left(\frac{N}{N_m}\right)^{\alpha}\left[1 + \left(\frac{N}{N_c}\right)^2\right]}{\left[D_{oi}\left(\frac{N}{N_m}\right)^{\alpha} + D_{op}\left[1 + \left(\frac{N}{N_c}\right)^2\right]\right]} \qquad (3.2.32)$$

A plot of D_t vs. N is shown in Fig.(3.2.3) for D_{oi} = 105 cm^2/sec, D_{op} = 2100 cm^2/sec, T_e = 2000 K, τ_{i_o} = 10^{-13}sec, τ_{p_o} = 2×10^{-12} sec, N_m = $1\times10^{17}/cm^3$, and N_c = $8\times10^{19}/cm^3$. The salient features of the plot are, for N < $10^{19}/cm^3$, the diffusion constant increases

slowly, while for $N > 10^{19}/cm^3$, the diffusion constant increases rapidly and becomes extremely large. Thus, at very high densities the mean collision time becomes very large which removes the barrier for carrier expansion.

3.3 SAMPLES:

The samples used in this study were CdSe(1) with the c-axis perpendicular to the plane and CdSe(3) with the c-axis parallel to the plane. These samples were obtained from Cleveland Crystals. The crystals were of high resistivity and were grown by the vapor phase method and their surfaces were chemically etched.

3.4 EXPERIMENTAL METHODS

The samples: CdSe(1) and CdSe(3) were chosen to see if any difference would exist at room temperature in the e-h recombination kinetics[29] due to the participation of different valence bands. In the excitation process of CdSe(1), the holes are generated in the Γ_9(A) and Γ_7(B) valence bands. In CdSe(3), due to the orientation of the c-axis parallel to the excitation photon polarization, the holes are generated only in the Γ_7(B) valence band.

For the experiments at low temperature (12K), the sample was mounted on a cold finger, in an optical dewar, with a Si diode mounted behind it to measure the temperature. Otherwise, the samples were mounted on a glass plate for room temperature experi-

ments.

Photoexcited carriers were produced using a Nd:glass mode locked[30] laser. A single pulse of 1060 nm wavelength was selected using a spark gap and Pockel cell. The pulse width was about 5-6 psec. The pulse selected[30] at the 1060 nm wavelength was frequency doubled to 530 nm for one photon excitation experiments. For two photon excitation, the 1060 nm wavelength was selected. The pulse intensity was attenuated using calibrated neutral density filters. The maximum energy/pulse at 530 nm was 400 μJ with an excitation spot size of 1.35 mm diameter (photon fluence ~ 7×10^{16} photons/cm^2). The maximum energy/pulse at 1060 nm was 1200 μJ with an excitation spot size of 1.9 mm diameter (photon fluence ~ 2×10^{17} photons/cm^2).

For the time resolved luminescence study, the luminescence was collected, collimated and focussed onto a 50μ slit of a streak camera. The luminescence was selected in broad bands with combinations of filters (HOYA R68 passes 680 - 720 nm and the HOYA R64- DITRIC SHP680 combination passes 640-680 nm wavelengths). A prepulse was set (530 nm original pulse) by using a beam splitter, which would arrive at the streak camera about 110 psec prior to the beginning of luminescence. This was done in order to measure the delay times of the luminescence accurately. The total delay between the peak of the time resolved luminescence and the excitation pulse was calculated taking into account the optical path

length added to the excitation and to the luminescence path by the various combination of filters. The prepulse was also used as a marker for overlapping various data files for averaging (appendix B4). The data was stored in a Digital 11-03 computer and analyzed later (appendix B1).

The time integrated spectra was obtained using a 1/4 meter Spex spectrometer coupled to a vidicon intensified target (PAR OMA II). The grating used had 300 grooves/mm blazed at 500 nm. The spectral resolution of the system was 30Å. The spectra obtained were corrected for S-20 spectral response, pixel response, thermal background, and grating blaze, using the 1216 console (PAR OMA II) microprocessor of the system. The corrected data was then stored and transferred to a Digital 11-03 computer for analysis (appendix C1).

The time integrated spatial profiles of the laser pulse and luminescence were obtained using a streak camera in the focus mode with input slit removed. Each channel of the video system was calibrated (mm vs. channel #) by using an illuminated scale at the sample site.

Excitation laser intensities at 530 nm transmitted through neutral density filters OND, ND25, ND13, and ND3 filters correspond to excitation photon fluences I_F, $1/4I_F$, $1/8I_F$, and $1/33I_F$, respectively, where $I_F = 7 \times 10^{16}$ photons/cm^2. For the 1060 nm excitation wavelength, the transmission of ND25 is only 10%.

3.5 EXPERIMENTAL RESULTS

The rise times and decay times for the band edge luminescence (710 nm) were measured for both samples as a function of excitation fluence at room temperature. The formation time of the excitonic state at 12K and time integrated spectra were measured in order to get an estimate of the photogenerated carrier density as a function of excitation photon fluence. The spatial widths of the 710 nm luminescence were measured as a function of photon fluence to investigate transverse diffusion of carriers from the photo excited region. These various experimental results are summarized in the following sections.

a) Delay and decay time measurements:

The time resolved luminescence at various excitation fluences from CdSe(1) and CdSe(3) are displayed in Fig.s (3.5.1) and (3.5.2), respectively. These curves typically show a laser prepulse and luminescence rising rapidly (~ 20 psec) and decaying slowly (~ 230 psec) in time. The rise times (Figure 3.5.1: b, c, d, and e) were obtained (appendix B5) using the expression,

$$L(t) = A[\exp(-t/\tau') - \exp(-t/\tau'_r)] \qquad (3.5.1)$$

where τ' and τ'_r is the decay and rise time for the time resolved

luminescence, respectively. The curve 3.5.1(a) corresponds to the zero time, as it only shows the laser pulse (530 nm) scattered from the sample. The rise times measured for curves 3.5.1: (b), (c), (d), and (e) corresponding to CdSe(1) are 20 psec, 17 psec, 16 psec, and 13 psec, respectively. For the entire range of excitation fluence the decay times for 710 nm luminescence is ~ 230 psec. The delay times of the band edge luminescence (710 nm) for CdSe(1), under a range of photon fluence (I_F to 1/33 I_F), decreases from 46 psec to 27 psec. The total delay times and fluences are displayed in table (3.5.1). The delay times are corrected for the optical delay due to various filters in the path.

The rise times measured for curves 3.5.2: (b), (c), (d), and (e) corresponding to CdSe(3) are 18 psec, 19 psec, 17 psec, and 15 psec, respectively. In this case, the theoretical fitting is poor since the luminescence is assumed to be monomolecular in the extraction even though there is clearly a fast (35 psec) and a slow (230 psec) component. This behavior was seen for excitation polarizations both parallel and perpendicular to the c-axis (accessible by rotating the sample about the excitation axis and keeping the c-axis within the same plane). The rise times and delay times observed for CdSe(3) are similar to the ones observed in CdSe(1) (see table (3.5.1)). The rise times are of the order of ~ 20 psec while the delays are ~ 35 psec.

The luminescence maximum (dL(t)/dt = 0) occurs at a time $\Delta t'$ measured with respect to the arrival of the excitation pulse at the sample and is given by,

$$\Delta t' = \left[\frac{1}{\frac{1}{\tau'_r} - \frac{1}{\tau'}}\right] \ln\left(\frac{\tau'}{\tau'_r}\right) . \qquad (3.5.2)$$

For typical values of τ'_r = 20 psec and τ' = 230 psec, $\Delta t'$ = 53 psec. It is easy to measure $\Delta t'$ experimentally with high accuracy. The values of τ'_r obtained by curve fitting are sensitive to the fittings at large times, the starting point, and shape. Therefore, the delay times are a good measure of the average energy relaxation time Δt ($L(t) \sim [N(t)]^2$ and the luminescence maximum corresponds to the maximum carrier density $N(\Delta t)$ as $\Delta t = \Delta t'$) and should be taken as the average energy relaxation time measured experimentally.

b) Measurement of carrier temperature decay:

In order to measure carrier temperatures at different time intervals, the hot luminescence decay profiles (660 nm) and band edge luminescence decay profiles (710 nm) were obtained at various excitation fluences in CdSe(1) (Figs. (3.5.3) and (3.5.4)) and in CdSe(3) (Figs.(3.5.5), (3.5.6), (3.5.7), and (3.5.8)). The hot luminescence lifetimes are shorter than the band edge luminescence

which indicates rapid temperature changes at earlier times.

The method used to calculate the temperatures at different time intervals is described as follows. For a Maxwell-Boltzmann distribution of the photogenerated carriers one can evaluate the hot carrier energy relaxation rate from the ratio of hot luminescence to band edge luminescence intensities as a function of time. The inverse carrier temperature T_e at time t after the excitation pulse is given by,

$$\frac{1}{T_e(t)} = -\left[\frac{k_B}{E_{hot} - E_{BE}}\right]\left[\frac{R(t)}{R(t_\ell)}\right] + \frac{1}{T_\ell} \qquad (3.5.3)$$

where E_{hot} and E_{BE} are the hot and band edge luminescence photon energies (In our case, they correspond to 660 nm(1.875 eV) and 710 nm(1.743 eV), respectively); T_ℓ is measured from the time integrated spectra and corresponds to the lattice temperature within 100-700 psec; R(t) is the ratio of intensities of hot and band edge luminescence at time t; $R(t_\ell)$ is the corresponding ratio when the temperature T_ℓ is reached after 200 psec. Measurements of T_ℓ are discussed in the next section.

The curves 3.5.3(a) and 3.5.4(a) show the hot (660 nm), while the curves 3.5.3(b) and 3.5.4(b) show the band edge (710 nm) luminescence decay profiles for CdSe(1). The excitation and luminescence polarizations are perpendicular to the c axis. The tempera-

tures at 20 psec intervals (Fig. 3.5.3(c)) were obtained by a method described earlier. For the maximum excitation (I_F) the inital temperature of ~ 2200 K goes down to 1200 K within ~ 35 psec (^{1}/e time). For weak excitation (1/33 I_F), the cooling rate is smaller (1/e time~ 100 psec) and the initial temperature is ~ 700 K (Fig.(3.5.4)).

For CdSe(3), the temperature cooling times are smaller (rates are larger) for comparable excitation fluences as compared to CdSe(1). The curves 3.5.5(a), 3.5.6(a), 3.5.7(a), and 3.5.8(a) correspond to hot luminescence decay profiles for excitation fluences I_F, 1/4 I_F, 1/8 I_F, and 1/33 I_F, respectively. The curves 3.5.5(b), 3.5.6(b), 3.5.7(b), and 3.5.8(b) correspond to band edge luminescence for the same range of photon excitation fluence. The corresponding curves for temperatures vs. time in psec are shown in figures 3.5.5(c), 3.5.6(c), 3.5.7(c), and 3.5.8(c), respectively. The initial temperatures obtained for photon fluences I_F, 1/4 I_F, 1/8 I_F and 1/33 I_F are 2200 K, 1800 K, 1800 K and 1300 K, respectively. The temperature decay times are 30 psec, 35 psec, 35 psec, and 60 psec, respectively. The excitation polarization in this case was parallel to the c-axis, while the luminescence polarization was both parallel and perpendicular to the c axis. All the initial temperatures obtained correspond to times given in Table 3.5.1.

c) Measurement of time integrated spectra:

The time integrated spectra for CdSe(1) obtained at room temperature are shown in Fig.(3.5.9) for various photon fluences. The luminescence shows a high energy tail and an almost cut-off at low energy side. These measurements were made to obtain an average Fermi energy (hence carrier density) for a given excitation fluence. The carrier density is calculated to be ~ $5\times10^{18}/cm^3$ for the photon excitation fluence range I_F to 1/33 I_F (table (3.5.2)). The carrier temperature range for the time duration of 100-800 psec is estimated to be 600-400 K for the respective excitation fluences.

Similar results were obtained for CdSe(3) (see Fig.(3.5.10)). The carrier density in this case is ~ $7.5\times10^{18}/cm^3$ and the temperature range for the time duration (100-800 psec) is 800-500 K for the excitation fluence range I_F-1/33 I_F (table(3.5.3)).

d) Measurement of exciton formation time:

The free e-h plasma time resolved band edge photoluminescence from CdSe(3) at 12 K is displayed in Fig.(3.5.13a). The luminescence is delayed from the excitation pulse by ~ 20 psec at most. The lifetime corresponding to the decay ($^1/e$) is ~ 120 psec. The figure 3.5.13(b) correspond to excitonic luminescence (see discussion section c) at the lowest two photon excitation fluence. The peak of the lumincescence matches with the peak of the free

e-h luminescence peak in figure 3.5.13(a). The exciton peak, however, shifts to larger times with excitation (Fig.3.5.13b-d) and for the maximum two photon excitation it is delayed by 185 psec (Fig.16d). The free e-h plasma luminescence can not be observed due to the low quantum yield (lower by a factor of 250). A check for stimulated emission, by studying the luminescence intensity vs excitation fluence, confirmed its absence.

e) Measurement of luminescence spatial profiles:

In order to examine the existence of transverse diffusion of carriers, the luminescence spatial profiles at the samples (luminescence spot diameter) were measured. The laser spatial profile of a 530 nm pulse at the sample site is shown in figure 3.5.14(a) with FWHM of 1.35 mm. The band edge luminescence profile at the sample is about 2.19 mm wide (FWHM) for an excitation fluence of 1/33 I_F (Fig. 3.5.14(b) while for larger excitation at I_F the spot profile is still larger ~ 3.14 mm (Fig. 3.5.14(c)). The profiles observed were time integrated over a time period of 1 nsec (dynamic range limited time) on a streak camera in the focus mode.

3.6 DISCUSSION

In this section the delay times and the decay times will be analyzed to obtain the energy relaxation rates[5]. The decay kinetics will be analyzed in terms of Auger recombination[23,31] to esti-

mate the carrier density. The time integrated spectra is analyzed in terms of non-k selection allowed recombination to estimate the carrier density. The excitonic formation time is investigated in terms of the Mott criterion[28,32] and fast diffusion. The spatial profile broadening of the luminescence was interpreted in terms of fast diffusion. All the experiments at room temperature indicate that the maximum attainable density at the maximum of time resolved luminescence is $<2\times10^{19}/cm^3$ which will be discussed in detail in this section.

1)Hot carrier energy relaxation

The measured delay times are related to the screening of electron-phonon interactions. As we have discussed previously, the initial carrier temperature with our experimental condition (sample-CdSe and $h\omega$ = 2.34 eV) at t= 0 is 2560 K. This will be true irrespective of excitation fluences. The temperature of these photogenerated carriers reduces in time due to LO phonon emission. The temperature measured at the peak of the luminescence corresponds to the net cooling that occurs during the delay time of the luminescence. Since the cooling rate is a function of the carrier density produced at t= 0, the delay times are different at different excitation fluences. We attribute the large delay time at high excitation fluence to the reduction of LO phonon scattering via screening. As it is difficult to estimate the car-

rier density during the delay time due to fast diffusion of carriers, we use the delay time and the observed temperature at the peak of luminescence to estimate the average carrier density during the delay time.

The energy relaxation rate can be obtained from the temperature decay profile for times greater than the delay time for a given excitation fluence. This observed rate is compared with the theoretical rate. The difference if any is explained in terms of screening of the electron-phonon interaction by taking into account the carrier density (at time Δt) obtained using the Auger recombination kinetics and the critical density N_c at the temperature under consideration.

a)Screening of electron-phonon interaction and delay time

As a next step using energy loss rate Eq.(3.2.9), the theoretical values of Δt (delay time) will be calculated as follows. For T_e = 2560K (t = 0), $T_o \approx$ 300K, $D' = 0.6 \times 10^9$ eV/cm, ρ = 5.86 gm/cm^3, δ = 26 meV, and $m_e = 0.13 m_o$, we calculate,

$$\frac{dE}{dt} = 1.3 \times 10^{10} \text{ eV/sec at } t = 0.$$

After 46 psec (CdSe(1) Table 3.5.1), for maximum excitation fluence, the carrier temperature T_e is ~ 2100K (see Fig.3.5.3(c)). Hence, the energy relaxation rate is,

$$\frac{dE}{dt} = 1.2\times10^{10} \text{ eV/sec (at t = 46 psec).}$$

The average rate <dE/dt> during the luminescence delay time of 46 psec is ~ 1.25×10^{10} eV/sec. The total energy lost as the electrons cool from 2560K → 2100K is 0.06 eV. With the average rate 1.25×10^{10} eV/sec, the calculated electron (or luminescence) delay time Δt is 5 psec. This does not agree with the observed Δt of 46±5 psec (Table 3.5.1). The difference between Δt's we attribute to the screening of electron-phonon interaction since we have used the unscreened (larger) value to determine the average rate. Using Eq.(3.2.9) a 9 fold decrease is observed in phonon emission rate, giving $N/N_c = \sqrt{8}$. This corresponds to an average carrier density within 46 psec of $2\times 10^{20}/cm^3$ instead of $3\times10^{21}/cm^3$ obtained using Eq.(3.2.7). For 1/33 I_F excitation, the carrier temperature after 27 psec (CdSe(1), Table 3.5.1, and Fig. 3.5.4(c)) is 700K. The corresponding <dE/dt> is 1.1×10^{10} eV/sec and the calculated Δt is 21 psec compared to observed Δt of 27 psec. The carrier density obtained during 27 psec corresponds to $4\times 10^{19}/cm^3$(Eq.(3.2.9) and 1.3 fold reduction in phonon emission rate) instead of $8.5\times 10^{19}/cm^3$ (Eq.(3.2.7)).

These results clearly show the existence of screening of the electron-phonon interaction during the delay time of luminescence for high excitation fluence I_F and excitation fluence dependent

fast diffusion of carriers.

The results are similar for CdSe(3) except that the delay times (Table 3.5.1) and the temperatures (Fig. 3.5.5(c), 3.5.6(c), 3.5.7(c), and 3.5.8(c)) at time (Δt) are consistently larger for the comparable excitation fluences. This indicates more screening in CdSe(3) than in CdSe(1). This is related and consistent with the observed (discussed in the section 3.6c) smaller 'fast diffusion' in CdSe(3), making the average carrier density during Δt larger as compared to that in CdSe(1).

In our experiments the excitation spot size at the sample is $\sim$ 2.35mm, while the optical absorption length is $\sim$ 0.5μ. Thus, the longitudinal diffusion of carriers into the surface of the sample controls the carrier density in the photoexcited region due to maximum volume change along the excitation direction (longitudinal). In CdSe(1) the c-axis is coincident with the longitudinal direction, while in CdSe(3) the c-axis is perpendicular to the longitudinal direction. The lattice constant along the c-axis and perpendicular to the c-axis are $\sim$ 7$\mathring{A}$ and 4$\mathring{A}$, respectively making the mean collision time (unscreened) larger in the previous case as compared to the later. This fact qualitatively explains the larger diffusion constant in CdSe(1) making a smaller N(Δt) (by a factor of 2) compared to CdSe(3).

b)Screening of electron phonon interaction and temperature decay time

The temperature (or energy) relaxation rate obtained from Figs. (3.5.3c) is 0.3×10^{10} eV/sec, while the rate calculated using Eq.(3.2.9) is 0.9×10^{10} eV/sec at 1700K. This difference is due to the screening of the electron phonon interaction. For carriers having a temperature of 1700K (average temperature during 35 psec on the decay profile Fig.3.5.3c or $E_i \sim 0.21$ eV), one calculates using Eqs.(3.2.5) and (3.2.3) the critical density N_c to be $2 \times 10^{19}/cm^3$. The experimentally determined carrier density at the peak of the luminescence (Table 3.5.1) is $2 \times 10^{19}/cm^3$. At this density the phonon emission rate will be reduced by a factor of 2 i.e. 0.45×10^{10} eV/sec. This value is close to the observed value of 0.3×10^{10} eV/sec.

The temperature decay data (Fig.3.5.4(c)) obtained for $1/33 I_F$ excitation can not be analyzed in terms of Eq.(3.2.9) as the carriers are cooled to the lattice temperature ($\sim$ 400K) and the LO phonon emission process is no longer efficient. The data (Fig.s 3.5.5(c), 3.5.6(c), 3.5.7(c), and 3.5.8(c)) obtained for CdSe(3) also shows screening over the entire range of excitation fluences. This again indicates that the carrier densities are higher in CdSe(3) than in CdSe(1) due to 'less' fast diffusion as compared to CdSe(1).

The possibility of reduction in the cooling rate of hot photoexcited carriers due to phonon reabsorption can be eliminated on following grounds. If we assume a typical Debye heat capacitance[33] i.e. 25 $Jmol^{-1}K^{-1}$ for $T > \theta$, where θ is the Debye temperature (for CdSe ~ 315K), then for the maximum energy deposited of 400 μJ/pulse, we obtain a maximum lattice temperature rise of 150 K assuming a quantum efficiency of 10% (radiative life time ~ 2 nsec and observed lifetime of ~ 200 psec). In the above estimate, we assume that the phonons remain within the initial absorption depth ~ 10^{-4} cm. This is an over estimate as the phonon lifetime of ~ 5 psec has not been taken into account. Thus, carrier heating due to phonon absorption by the carriers is a negligible effect making the phonon bottleneck mechanism inefficient.

c)Estimates of effective diffusion constant:

The measured delay times and carrier densities (using Auger kinetics) can be used to estimate an effective diffusion constant D_t at different average photogenerated carrier densities during the delay times. The effective D_t is given by,

$$D_{t_{eff}} = \left(\frac{N}{\alpha N(\Delta t)}\right)^2 \left(\frac{1}{4\pi\Delta t}\right) \qquad (3.6.1)$$

where N is given by Eq.(3.2.7) and $N(\Delta t)$ is obtained from the Auger analysis which is listed in table 3.5.4 for various excitation flu-

ences. The values of Δt are listed in table 3.5.1 (CdSe 3). Thus, neglecting carrier recombination, the effective values of D_t obtained at the surface (x=0) are 2.2 $x10^4$, 2 $x10^3$, 5 $x10^2$, and 60 cm^3/sec for I_F, $1/4I_F$, $1/8I_F$, and $1/33I_F$ excitation fluences, respectively. Since, $N(\Delta t)$ depends on the Auger recombination constant C ($N(\Delta t) \sim 1/\sqrt{C}$) the effective D_t will depend on the choice of C. We have shown data of $D_{t_{eff}}$ for two values of C in Fig.(3.2.3). It is difficult to estimate C as the carrier temperature varies rapidly during Δt (Fig.3.5.3(c)). However, the data shows the same dependence for a large range of D_t at high carrier densities.

3.7 DIRECT EXPERIMENTAL EVIDENCES FOR FAST DIFFUSION

a) Time Integrated spectra:

From this study we were able to estimate directly average photogenerated carrier density and temperature at different excitation fluences. The moderate change in the estimated carrier density is due to rapid reduction in the carrier density within the thermalization period. At a maximum excitation intensity of $7x10^{16}$ photons/cm^2, the theoretical fit (appendix C2) to the time integrated luminescence spectra is not good Fig.3.5.9(a). The reason is because the temperature decay profile has two components at this high excitation fluences (see Fig.3.5.3(c) for CdSe(1) and 3.5.5(c) for CdSe(3)). Due to screening of the electron phonon interaction,

the high energy side of the time integrated spectra shows two components corresponding to these two temperature regimes. But for lower excitation intensities there is an excellent agreement between the theoretical fit and data for the parameters shown in Figs.3.5.9:(b) and 12(c). It should be noted here that the average electron temperature and the carrier density obtained are slightly larger for higher excitation power (see table 3.5.2).

For CdSe(3), the observed temperatures and carrier densities are higher than observed in CdSe(1) for the comparable excitation powers(see table 3.5.3). Since the dynamic range of sensitivity for our vidicon detection is from the maximum fluence I_F to the minimum $1/33I_F$ excitation and since the photoluminescence life time (1/e) is 230 psec, the integrated photoluminescence spectra obtained is an average over a maximum time duration of about 800 psec for full intensity and 500 psec for $1/8I_F$ excitation. The time resolved photoluminescence study shows that the hot carrier cooling occurs within 100 psec. Therefore, we can assume the carriers remain at a constant hot temperature for the next 100-800 psec. Thus, the temperature obtained from the theoretical fit of the time integrated photoluminescence is a good indicator of the average hot carrier temperature.

The entire photoexcitation fluence range I_F to $1/33I_F$ covered in the experiment has only a moderate effect on the final carrier temperature and average Fermi energy (average carrier density).

This observation strongly suggests longitudinal (bulk) fast diffusion of carriers away from the surface and from the photo excited region. The reasons, why the longitudinal and not the transverse (within the surface irrespective of the c-axis orientation) diffusion affects the carrier density, was discussed earlier. The carrier densities observed in CdSe(1) are less than the ones observed in CdSe(3). The only difference in the experimental condition between these samples is that the longitudinal diffusion occurs along the c-axis in CdSe(1) while, it is perpendicular to the c-axis in CdSe(3). This difference in the carrier densities suggests that diffusion along the c-axis is larger than along the perpendicular direction by a factor of 1.3.

The carrier densities measured by the time integrated spectra experiment are the average densities (over ~ 500 psec). Hence, if we correct them for the luminescence decay time of 230 psec, the carrier densities at the peak of the luminescence are 4.4×10^{19}, 5.3×10^{19}, and $3.4 \times 10^{19}/cm^3$ for I_F, 1/8 I_F, and 1/33 I_F excitation fluences, respectively. Similarly in CdSe(3) the initial carrier densities (max. of Lum.) are 6.3×10^{19}, 5.5×10^{19}, and $3.4 \times 10^{19}/cm^3$ for I_F, 1/4 I_F, and 1/8 I_F excitation fluences, respectively. These values of carrier densities are quite consistent with the ones obtained in the next section.

b) Auger recombination of carriers:

The time resolved band edge (710 nm) luminescence from CdSe(3) displays (Fig.(3.5.11)) a fast component of ~ 35 psec (τ_1) and a slow component of 230 psec (τ_2) which was fitted (appendix B6) by,

$$L(t) = A_1 \exp(-\frac{t}{\tau_1}) + A_2 \exp(-\frac{t}{\tau_2}) \qquad (3.7.1)$$

for t in psec. Such a double exponential analysis does not carry any physical meaning. We have analyzed the data with Eq.(3.7.1) just to rule out a possibility of intervalence band transition and relate the intensity dependence of A_1/A_2 to Auger recombination (Eq.(3.2.12) and Fig.(3.5.12)).The ratio A_1/A_2 for excitation intensities of I_F, $1/4I_F$, $1/8I_F$, and $1/33I_F$ are 0.45, 0.54, 0.075, and 0.003, respectively.

In this experiment the excitation photon polarization was set parallel (E || C) to the c-axis. The photoluminescence collected was not descriminated for polarization nor for the terminal valence band states Γ_9 and Γ_7 due to the choice of the broad band filter (R70) in front of the streak camera. In this geometry the holes are created only in the B-valence band at t=0. The fast component observed could arise from either to a fast scattering (say 35 psec) from Γ_7 (B-valence) band to Γ_9(A-valence) band or due to the Auger recombination[23] of carriers.

The possibility of hole scattering (Γ_9-Γ_7) is excluded for the five following reasons.

1. The initial (t=0) energy E_i^B of holes in B valence band is given by,

$$E_i^B = (\hbar\omega_1 - E_g)\ \frac{m_e}{m_h^B + m_e}\ , \qquad (3.7.2)$$

where $m_h^B = m_o$ is the effective mass of B (Γ_7) holes, $m_e = 0.13\ m_o$, and $E_g^B = E_g^A + 0.026 = 1.736$ eV ($\Delta_{cr} = 0.026$ eV). Thus, for 2.34 eV one photon excitation (530 nm) E_i^B is 70 meV. The total scattering of holes from B-valence to A-valence band is due to non polar LO phonon emission and to acoustical phonon emission.

The acoustical phonon scattering rate is given by[16],

$$\frac{dE}{dt} = -\ 8\sqrt{2}/(\pi^{(\frac{3}{2})})\ \frac{E_1^2 m^{(5/2)}}{\hbar^4 \rho}\ (kT_e)^{(\frac{3}{2})}(1-\frac{T_o}{T_e}) \qquad (3.7.3)$$

where $E_1 = 5.7$ eV is the acoustical deformation potential[16,21]. For $m = m_h^B$, $T_o = 300$K and $T_e = T_h = 2000$K, the estimated value is,

$$\langle \frac{dE}{dt} \rangle = 2.1 \times 10^{10}\ \text{eV/sec.}$$

Therefore, the total scattering time for emitting 100 meV energy from $\Gamma_7 \rightarrow \Gamma_9$ will occur in ~ 1 psec. This is contrary to the observed decay time of 35 psec.

One should note that Yoshida et al[29] had observed a scattering time of 35 psec for $\Gamma_7(B) \rightarrow \Gamma_9(A)$ hole scattering at 4K. The carrier density in their experiment was ~ $3 \times 10^{17}/cm^3$ and the carrier temperature T_e was low ~ 30 K. If one takes into account these facts, this should explain their measured scattering time of 35 psec within the frame work of non polar LO and acoustical phonon emission given above.

2. The B valence band holes are scattered into A-valence band. Since the luminescence of B and A valence band are observed simultaneously there should not be an added fast component to the luminescence decay.

3. The ratio of density of states of A-valence and B valence is given by,

$$\frac{N_A}{N_B} = \left(\frac{m_A}{m_B}\ \frac{E_i^A}{E_i^B}\right)^{(3/2)} \qquad (3.7.4)$$

Since m_A and m_B are 0.45 m_o and m_o, respectively and E_i^A = 140 meV

and E_i^B = 70 meV, therefore,

$$\frac{N_A}{N_B} = 0.85 \qquad (3.7.5)$$

Hence, the observed A_1/A_2 ratio should be ~ >1 compared to the observed ratio of <<1 (see Fig.(3.5.11).

4. The observed time resolved photoluminescence kinetics is intensity dependent.

5. For CdSe(3), if the excitation photon polarization is perpendicular to the c-axis (the c-axis is still in the plane) the same kinetics is observed. This is the most important observation since in this geometry of excitation both A and B bands are pumped and the scattering from B to A would be diminished. However, no fast component is observed in CdSe(1) for the same excitation polarization (the c-axis is perpendicular to the plane). These observations together support the strong Auger recombination[23] in CdSe(3) due to the presence of high carrier density (less diffusion) after the thermalization time of ~ 30 psec.

After excluding the above five possibilities, the Auger recombination[23] is considered to be responsible to the fast decay (Eq.(3.2.10),(3.2.11),and (3.2.12)).

The time resolved luminescence at various pump intensities (Fig.(3.5.12)) were analyzed using Eq.(3.2.12) and $C=1x10^{-29}$ $cm^{6}sec^{-1}$. In CdSe(1), we do not see the Auger recombination component (absence of fast component in Fig.(3.5.1)), even for the maximum photon fluence I_F. This suggests that the fast component is longer than the 460 psec (or rate < $1x10^{9}sec^{-1}$), the monomolecular lifetime of carriers. This indicates that for the whole excitation fluence range I_F to 1/33 I_F the carrier densities generated are less than $1x10^{19}/cm^3$. On the contrary, in CdSe(3), the observed Auger recombination (Fig.(3.5.12) fast coponent) indicates carrier densities > $1.0x10^{19}/cm^3$ (table IV) but < $2.0x10^{19}/cm^3$. The longitudinal fast diffusion, within 35 psec, away from the photoexcited surface could limit the initial carrier density in our experiment due to limited time resolution. In CdSe(1), the c-axis is perpendicular to the surface and in CdSe(3), the c-axis lies in the surface. Hence, we can conclude that the fast diffusion along the c-axis is greater than that along the perpendicular direction by a factor of 2.

c) Exciton formation from dense e-h plasma:

The exciton formation from a dense free e-h plasma occurs when the plasma density becomes equal to or less than the Mott density[28,32]. This can be used to estimate the initial free e-h plasma density.

The laser pulse, having a photon energy greater than the band gap, first creates a free electron hole pair which thermalizes and finally dissipates the excess energy to the lattice through LO and acoustical phonon emission. During the energy relaxation process, reduction in the carrier density occurs due to recombination and plasma expansion. Exciton formation occurs as a result of the Coloumb interaction between electrons and holes provided that the e-h plasma density is sufficiently low and lattice thermal energy is less than the exciton binding energy.

The criterion for this Mott transition which separates the conducting plasma state and the "insulating" excitonic state is that the carrier density should not be able to screen the coloumb interaction between the e-h pair. The Mott criterion[28,32] is written as,

$$N_m^{1/3} a_x \approx 0.2 \quad , \tag{3.7.6}$$

where a_x is the Bohr radius for an exciton and N_m is the number density of the e-h plasma. For CdSe, with $a_x \sim 40$ Å, this yields a Mott density of $N_m = 1 \times 10^{17}/cm^3$.

When the laser pulse photo-generates a carrier density $N > N_m$ there is a time delay between the onset of exciton formation and

the laser pulse. For the entire (intensity detection limited) one photon excitation fluence range the photogenerated carrier density $N >> N_m$. In order to overcome this difficulty two photon excitation was used. This method yielded a larger photoluminescence even though the carrier density was low. This is due to the larger penetration depth which reduces surface recombination compared to one photon excitation.

The carrier density for two photon absorption was calculated as follows[34],

$$\frac{dI(z)}{dz} = - [\alpha + \beta I(z)] I(z) \qquad (3.7.7)$$

where I(z) is the intensity of the laser in the sample at depth z measured from the incident surface, α is the one photon absorption coefficient ($\alpha \sim 0.18\ cm^{-1}$) at 1060 nm and β is the two photon absorption coefficient ($\beta \sim 0.03$ cm/MW) at 1060 nm. For the laser power > 1 GW/cm^2 (pulse), the one photon absorption at 1060 nm (Nd: glass laser fundamental wavelength) could be neglected in comparision to two photon absorption. In this case Eq.(3.7.7) reduces to,

$$\frac{1}{I(z)} = \frac{1}{I_o} + \beta z \qquad (3.7.8)$$

where I_o is the incident intensity at the surface (z=0). The reduction in intensity $\Delta I = (I_o - I)$ is,

$$\Delta I = \frac{\beta z I_o^2}{1 + \beta z I_o} \qquad (3.7.9)$$

As the luminescence observed emerges from a crystal depth of ~ 1μ (due to reabsorption near bandgap), we can calculate the average carrier density within 1μ of the surface assuming ΔI is converted into e-h plasma. For the maximum I_o of 7 GW/cm^2,

$$\Delta I = 144 \text{ MW/cm}^2.$$

For a pulse duration of 5 psec the maximum carrier density produced is 2×10^{19}/cm^3. For 10% attenuation of I_o with an ND25, ΔI = 1.44 MW/cm^2 and the carrier density is 2×10^{17}/cm^3.

For I_o excitation, the initial (t = 0) estimated carrier density is 2×10^{19}/cm^3 and the photoluminescence lifetime (Fig.3.5.13a) is ~ 120 psec. The time required for the density to go down by a factor 200 to reach the Mott density 1×10^{17}/cm^3 will be ~ 600 psec. Hence, the observed excitonic luminescence will be delayed in time to ~ 600 psec after the laser excitation pulse. This is outside the decay range and was not observed (Fig. 3.5.13(a)).

However, the experimentally observed time resolved excitonic peak occurs after 185 psec (i.e., the Mott density is reached after 185 psec) (see Fig.3.5.13(c)). This fact leads us to believe that the carrier density achieved after laser pulse with I_o excitation intensity is $\sim 5\times10^{17}/cm^3$ and not equal to the calculated value of $2\times10^{19}/cm^3$.

With 1/10 I_o excitation however, the excitons are formed almost instantly as the initial carrier density is about $2\times10^{17}/cm^3$. Experimentally one can see (fig.3.5.13(a)) that the free plasma peak with one photon excitation is separated from the prepulse by 105 psec while the excitonic peak is separated by 118 psec (Fig.3.5.13(b). The free plasma luminescence can not be observed along with the exciton luminescence because of the low quantum yield in the previous case (the exciton luminescence is strong compared to the free e-h plasma luminescence and is seperated by $\sim 50\text{Å}$ and cannot be discriminated by a broad band filter).

To account for the reduction of carrier density one needs a large diffusion constant. An effective diffusion coefficient $D_t = 4.2\times10^{4}$ cm^2/sec is estimated using Eq.(3.6.1), the initial density at t = 0 of $2\times10^{19}/cm^3$, and final density of $5\times10^{17}/cm^3$. Hence, the e-h plasma expands over a length of 40 μ after 30 psec (thermalization time of free e-h plasma) to yield a density of $5\times10^{17}/cm^3$.

d) Time integration spatial profile:

Using the streak camera in the focus mode we were able to measure the laser spatial profile and the luminescence spatial profile at the sample (CdSe(1)). The time integrated spatial profiles of the luminescence differ greatly in width (FWHM) as compared to the laser spatial profile. The photoluminescence profile was integrated over a time duration of 1 nsec (due to the dynamic range) and clearly shows a transverse diffusion of carriers within 1 nsec. The laser width was 1.35 mm while, the photoluminescnce width was ~ 2.19 mm (see Fig.(3.5.14)) at the sample. The estimate of the transverse velocity assuming that the luminescence is collected during 1 nsec, is $4x10^7$ cm/sec (velocity needed for plasma to expand through 0.42 mm in 1 nsec). The transverse diffusion does not contribute to the drastic reduction of carrier density within the thermalization time (~ 30 psec). This is due to the fact that the laser beam profile at the sample is focussed down to 1.35 mm diameter (2350 μ) as compared to the absorption depth for one photon absorption (2.34 eV) of 0.5 μ. However, it can easily be seen that in our experiments with the lower limit on the velocities of $4x10^7$cm/sec, the carriers initially generated within 0.5 μ will diffuse to 12μ within 30 psec (delay time). This reduces the density by a factor of 25. If the saturation of states is the reason for the observed broader luminescence profile instead of fast diffusion (the wings of the laser profile has

enough power to generate the same carrier density as at the center) i.e. 0.85 mm over the laser profile for $1/33I_F$ excitation, then the luminescence spatial profile would be 27 mm over the laser profile for I_F excitation. This is contrary to the observed increase of 1.79 mm (Fig.(3.5.14)).

3.8 CONCLUSION

Rapid diffusion of high density non equilibrium photogenerated carrier with diffusion constant largely exceeding the typical equilibrium values can account for moderate intensity dependenence of the Auger recombination of free carriers and of the carrier Fermi level in the time integrated spectra at room temperature. Such a rapid diffusion can also account for exciton formation at high excitation intensities and the increased photoluminescence spatial profile over that of the laser profile. We conclude that the maximum carrier density attainable by one photon excitation at room temperature is $\sim 1\times10^{19}/cm^3$ after 30 psec. This limit is further reduced to $5\times10^{17}/cm^3$ at low temperature and is due to the fast diffusion of carriers and not due to the saturation of absorbing states. Comparing the time resolved decay curves for CdSe(1) and CdSe(3), which shows absence of Auger recombination in the previous case, makes us believe that the diffusion velocities along the c-axis are greater than along the perpendicular direction by a factor of 2. This results in rapid diffusion within 30 psec reduc-

ing the initial carrier density in CdSe(1) more than in CdSe(3) with its c-axis parallel to the plane.

The possibility of reradiation and reabsorption is ruled out since such a process will shift the luminescence to the red (high energy tail will be absorbed more). The temperature cooling rate obtained from the time resolved, hot and band edge luminescence, would be faster yielding much lower temperatures after ~ 30 psec for high pump intensities. This is contrary to the observation. Such a mechanism is more important for ultrathin samples as compared to bulk. Also the luminescence from the samples was collected in a frontal geometry reducing the self absorption. In addition, this process will make lifetimes longer with increasing pump intensity in contrast to observation.

Within the theoretical frame work of screening of the electron-phonon interaction, we conclude from our experiments that the non polar optical phonon emission due to the optical deformation potential is the dominant energy relaxation mechanism. The rapid diffusion of carriers due to the screening of electron phonon interaction is an important phenomenon in limiting the photogenerated carriers and should be taken into account in refining the existing treatise of high density energy and spin relaxation[35].

3.9 REFERENCES

1. R. Ulbrich, Phys. Rev. 8, 5719 (1973).

2. J. Shah, Phys. Rev. B9, 562 (1974).

3. E. O. Gobel and O. Hildebrand, Phys. Stat. Sol. (b), 88, 645 (1978).

4. Since, $3/2K_BT_e + 3/2K_BT_h = 3/2K_B(T_e + T_h) = \Delta E$ and $T_e = T_h = T_i$, $3/2k_B(2T_i) = (\hbar\omega_\ell - E_g)$

5. E. J. Yoffa, Phys. Rev. B21, 2415 (1980).

6. B. R. Nag,'Semiconductors Probed by Ultrafast Laser Spectroscopy Vol.1' Edited by R. R. Alfano Academic Press,pa 3-43,1984.

7. C. J. Hearn, Proc. Phys. Soc. 86, 881 (1965).

8. A. Cornet, M. Pugnet, J. Collet, T. Amand and M. Brousseau, J. De Physique, C7, Suppliment 471 (1981).

9. M. Combescot, Solid State Comm., 30, 81(1979).

10. R. Zimmerman and M. Rosler, Phys. Stat.Sol.(b) 75, 633 (1976).

11. K. M. Romanek, H. Nather, J. Fischer and E. O. Gobel J. Lumin. 24/25, 585 (1981).

12. S. Modesti, L. G. Quaglino, A. Frova, J. L. Staehli and M. Guzzi, J. Lumin. 24/25, 581 (1981).

13. A. Forchel, H. Schweizer and G. Mahler, Phys. Rev. Lett. 51, 501 (1983).

14. E. J. Yoffa, Phys. Rev. B23, 1909 (1981).

15. H. Frohlich, Proc. Roy. Soc., A160, 230 (1937).

16. E. M. Conwell, 'High Field Transport in Semiconductors.' Academic press, (1967).

17. A. R. B. de Castro and R. S. Turtelli, Sol. Stat. Comm. 32, 819 (1979).

18. J. I. Pankove, 'Optical Processes in Semiconductors'. Dover, P.6(1975).

19. Cleveland Crystal Information Sheet. June 1980.

20. R. B. Parsons, R. B. Wardzynski and A. D. Yoffe, Proc. Roy. Soc. A262, 120 (1961).

21. M. Pugnet, J. Collet and A. Cornet, Sol. Stat. Comm. 38, 531 (1981).

22. M. R. Junnarkar, R. R. Alfano and J. Furdyna (to be published).

23. J. S. Blackmore, 'Semiconductor Statistics'. Pergamon press, page 214, (1962).

24. M. Takeshima, Phys. Rev. B23, 6625 (1981).

25. S. S. Yao and R. R. Alfano, Phys. Rev. B27, 1180 (1983).

26. E. J. Yoffa, Appl. Phys. Lett.36, 37(1980).

27. R. A. Smith, 'Semiconductors', Cambridge Univ. Press, (1961).

28. N. J. Frigo, H. Mahr and D. J. Erskine, IEEE J. Quant. Electr. QE-18, 192 (1982).

29. H. Yoshida, M. Saito and S. Shionoya, J. Phys. Soc. Japan, 50, 881 (1981).

30. P. Y. Lu, P. P. Ho and R. R. Alfano, J. Qunt. Electr. QE-15, 406 (1979).

31. A. Haug, Sol. Stat. Electr. 21, 1281 (1978).

32. N. Mott, Phil. Mag. 6, 287 (1961).

33. C. Kittel, 'Introduction to Solid State Physics', Wiley Eastern University Edition 5, p.136 (1977).

34. A. F. Stewart and M. Bass, Appl. Phys. Lett. 37, 1040 (1980).

35. M. R. Junnarkar, R. R. Alfano and J. Furdyna(to be published).

3.10 FIGURE CAPTIONS:

3.2.1. The parabolic band structure around k=0 is shown with initial energy ε_i (t=0). The phonon $\vec{q}$ vectors involved in one LO phonon emission are shown as $\vec{q}_{min}$ and $\vec{q}_{max}$.

3.2.2. Phonon emission frequencies for polar and non polar interactions and q_{min} and q_{max} are plotted as a function of carrier density. N_c's are the critical densities for polar and non polar phonon scattering.

3.2.3. Diffusion constant obtained by considering screened impurity and non polar phonon scattering of carriers are plotted as a function of carrier density. N_m and N_c are the critical densities for screened impurity and non polar optical phonon scattering. The carrier temperature and unscreened values of collision times are given in the figure. The ● and ▲ represent expeimental values for C = 1 $x10^{-29}cm^{-6}sec^{-1}$ and 1 $x10^{-28}cm^{-6}sec^{-1}$, respectively. □ represents diffusion constant obtained from exciton formation data.

3.5.1. The time resolved band edge photoluminescence at 710 nm from CdSe(1) for various excitation fluences are shown. The decay time for all the curves is 230 psec. The rise times for various curves are, (b) 20 psec; (c) 17 psec; (d) 16 psec; and (e) 13 psec, respectively. The curve (a) corresponds to the laser pulse scattered from the sample to provide time zero for accurate determination of delay times (see Eq.(3.5.1) for fits).

3.5.2. The time resolved band edge luminescence at 710 nm from CdSe(3) for various excitation fluences are shown. The rise times for various curves, are as follows: (b)18 psec; (c) 19 psec; (d) 17 psec; and (e) 15 psec, respectively. The curve (a) represents the laser pulse scattered from the sample to provide zero time for accurate determination of delays. The decay times were used only for convenience to obtain the rise times and have no physical significance (see Eq.(3.5.1) for fits).

3.5.3. The curves (a) and (b) represent hot (660 nm) and band edge (710 nm) luminescence from CdSe(1) at photon fluence I_F. The temperature decay profile is calculated using Eq.(3.5.3).

3.5.4. The curves (a) and (b) represent hot (660 nm) and band edge (710 nm) luminescence from CdSe(1) at photon fluence 1/33 I_F. The temperature decay profile is calculated using Eq.(3.5.3).

3.5.5. The curves (a) and (b) represent hot (660 nm) and band edge

(710) luminescence from CdSe(3) at photon fluence I_F. The temperature decay profile is obtained from Eq.(3.5.3).

3.5.6. The curves (a) and (b) correspond to hot (660 nm) and band edge (710 nm) luminescence from CdSe(3) at a photon fluence 1/4 I_F. The temperature decay profile is obtained from Eq.(3.5.3) is shown in the figure.

3.5.7. The curves (a) and (b) correspond to hot (660 nm) and band edge (710 nm) luminescence from CdSe(3) at a photon fluence 1/8 I_F. The temperature decay profile is obtained from Eq.(3.5.3).

3.5.8. The curves (a) and (b) represent hot (660 nm) and band edge (710 nm) luminescence from CdSe(3) at a photon fluence 1/33 I_F. The temperature decay profile is obtained from Eq.(3.5.3).

3.5.9. The time integrated photoluminescence spectra obtained for various excitation fluences (at 530 nm) in CdSe(1) are shown. The excitation fluence, carrier temperature T_e and carrier density N are indicated in the figures and were obtained by curve fitting (Eq.(3.2.22) for the parameters listed in the text.

3.5.10. The time integrated photoluminescence spectra obtained for various excitation fluences (at 530 nm) in CdSe(3) are shown. The excitation fluence, carrier temperature T_e and carrier density N are indicated in the figures. The continuous lines are theoretical fits (Eq.(3.2.22)).

3.5.11. The time resolved photoluminescence at 710 nm obtained from CdSe(3) at various photon fluences are shown. The continuous lines are double exponential fits (Eq.(3.7.1)) with time constants 35 psec and 230 psec. The ratios A_1/A_2 for the curves (a), (b), (c), and (d) are as shown in the figure.

3.5.12. The experimental data obtained under similar experimental conditions as that of figure (3.5.11) but with a maximum excitation fluence of $4I_F$. The continuous lines are fits to Eq.(3.2.12) with recombination rates shown in the figure using $C=1\times10^{-29}cm^{-6}sec^{-1}$.

3.5.13. Curve (a) represents free e-h plasma luminescence at 12 K from CdSe(3) obtained with 530 nm excitation. Curve (b) corresponds to exciton luminescence obtained with 2 photon excitation attenuated by 10% of the maximum used in curve (c). The exciton luminescence peak is (shown in curve (c)) delayed by 185 psec.

3.5.14 Curve (a) shows the laser spatial profile of 530 nm excitation. Curves (b) and (c) are the spatial profiles of 710 nm luminescence obtained over a period of 1 nsec after the pulse excitation. The FWHM of the profiles are shown in the figure.

3.11 TABLE CAPTIONS

3.5.1. The delays between the luminescence maximum and the excitation pulse at the samples are shown for CdSe(1) and CdSe(3) for various excitation fluences. These delays are corrected for the optical delays introduced by excitation and luminescence path filters.

3.5.2. The carrier temperatures and carrier densities obtained from theoretical fittings to the experimentally observed spectra are shown for CdSe(1) at various excitation fluences.

3.5.3. The carrier temperatures and carrier densities obtained from theoretical fittings to the experimentally observed spectra are shown for CdSe(3) at various excitation fluences.

3.5.4. The Auger recombination rates and carrier densities are obtained from fittings to the time resolved luminescence (Eq.(3.2.12)) at various excitation fluences.

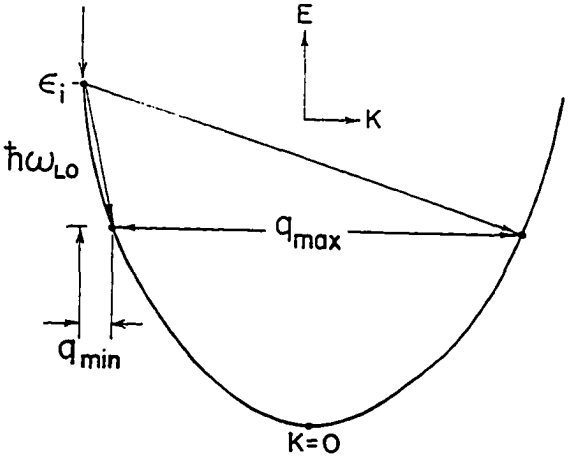

FIGURE 3.2.1

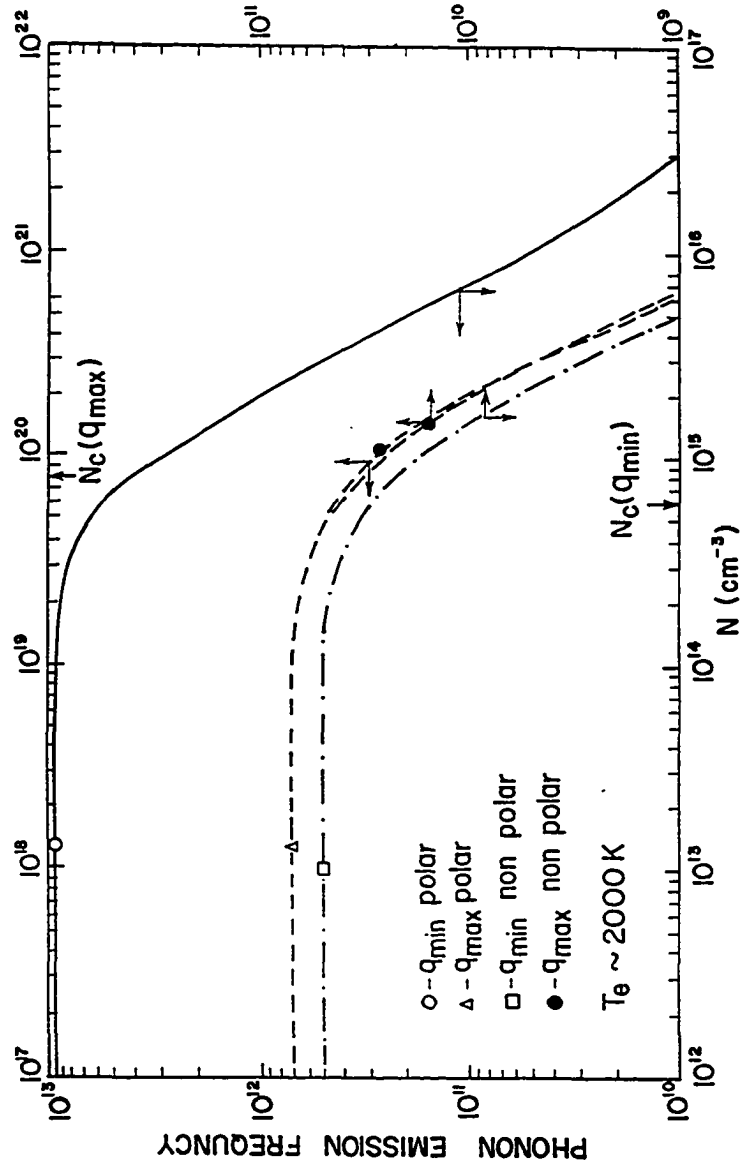

FIGURE 3.2.2

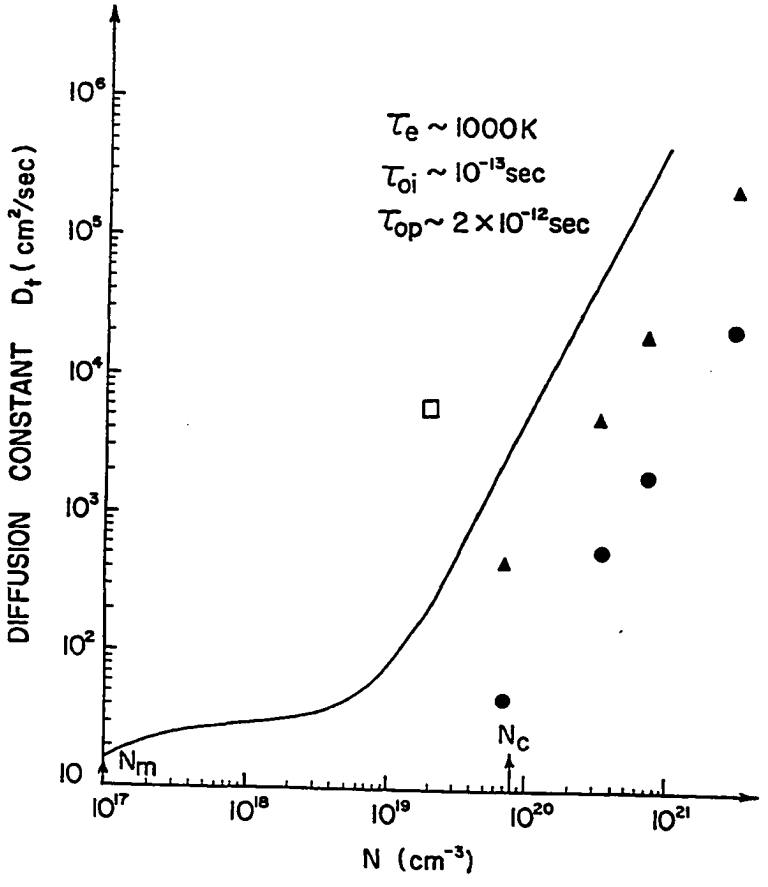

FIGURE 3.2.3

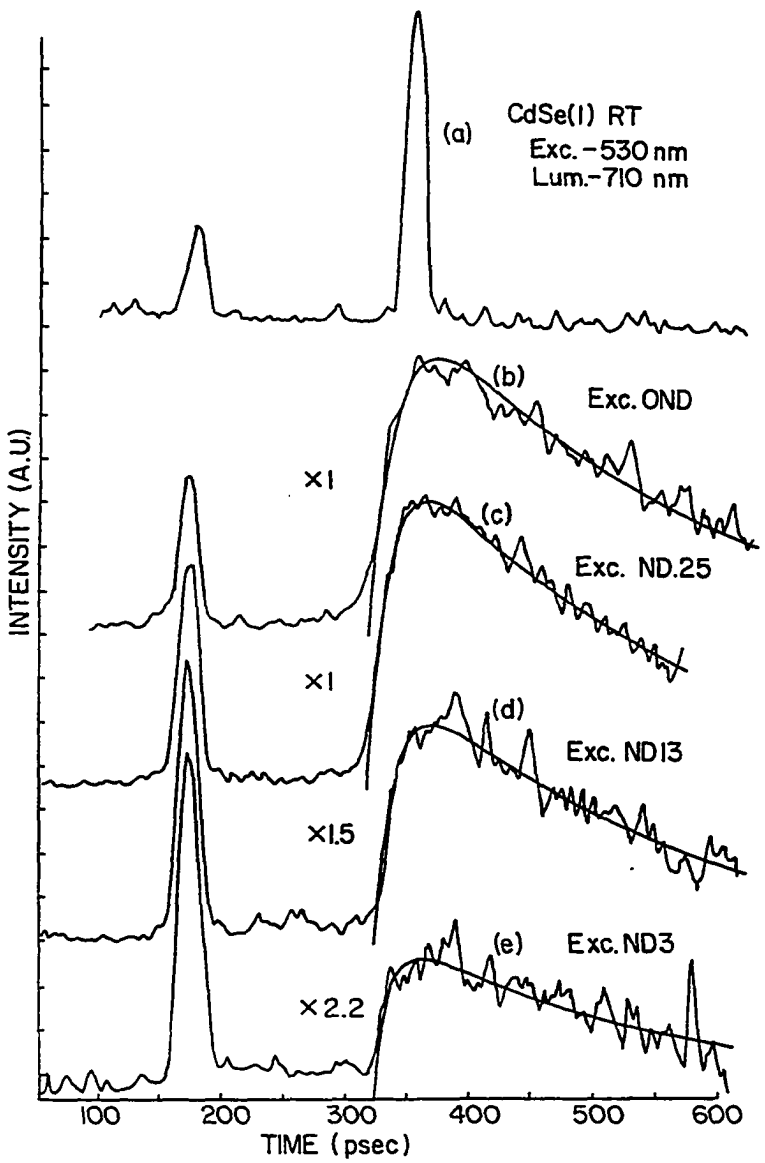

FIGURE 3.5.1

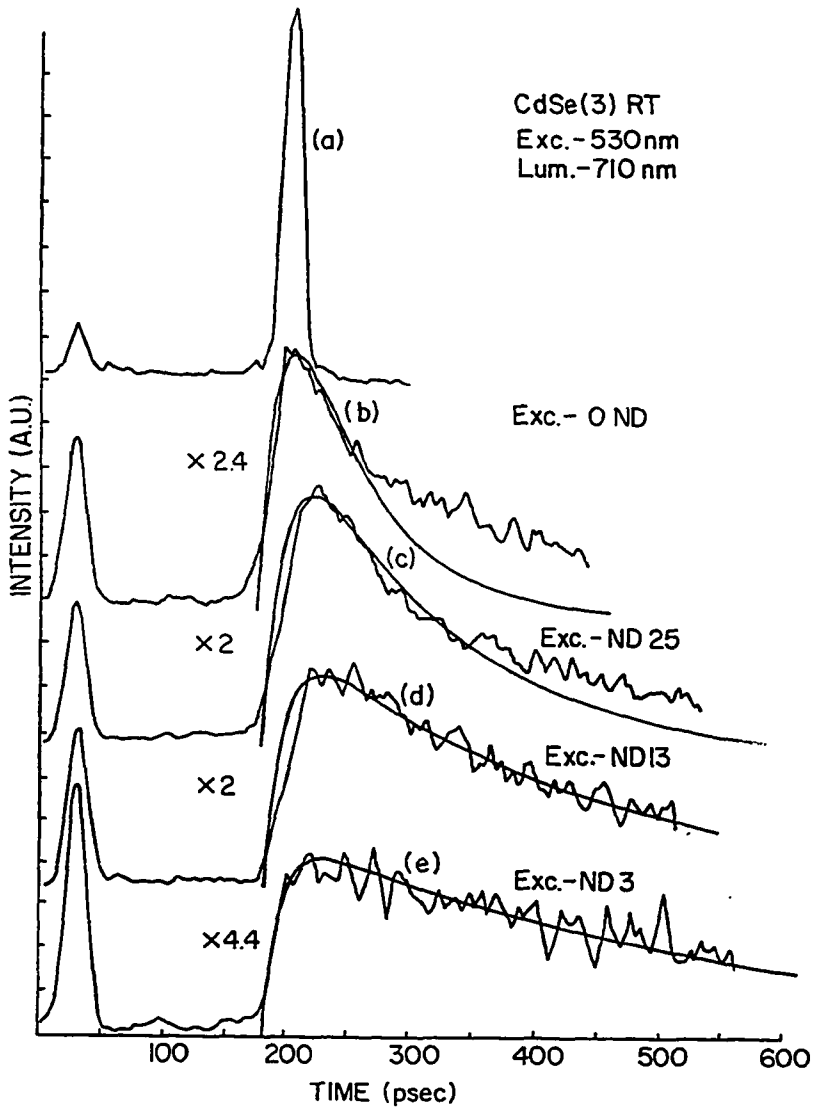

FIGURE 3.5.2

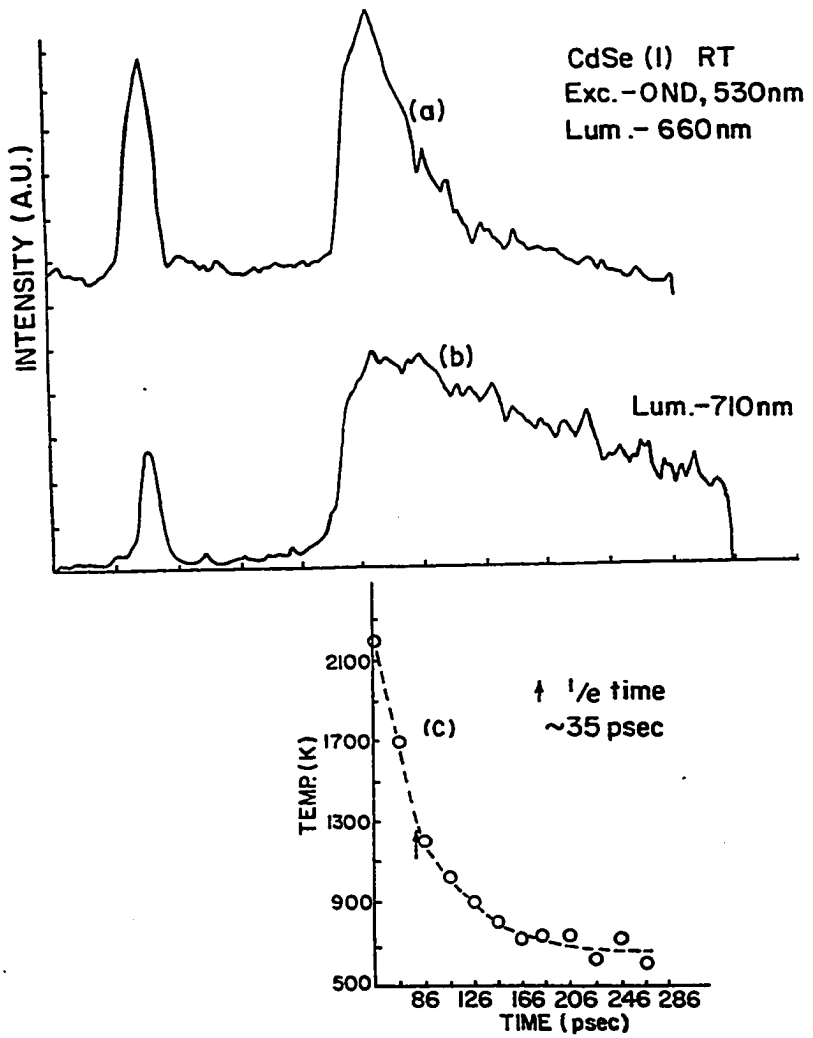

FIGURE 3.5.3

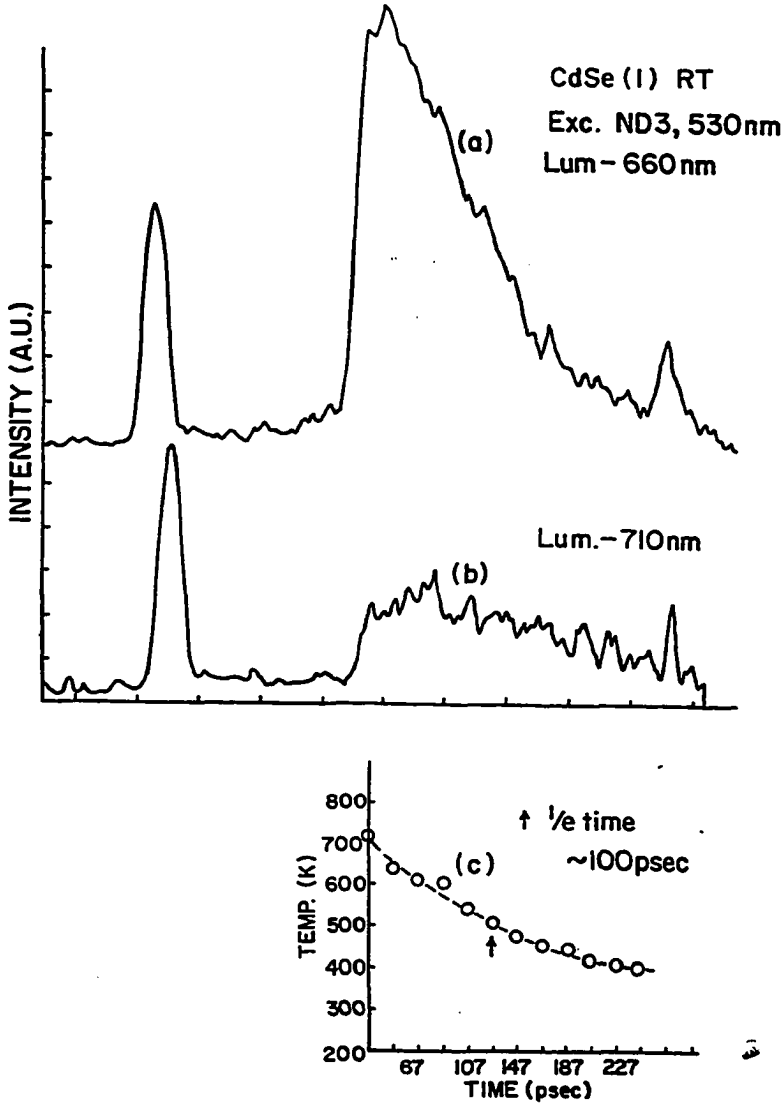

FIGURE 3.5.4

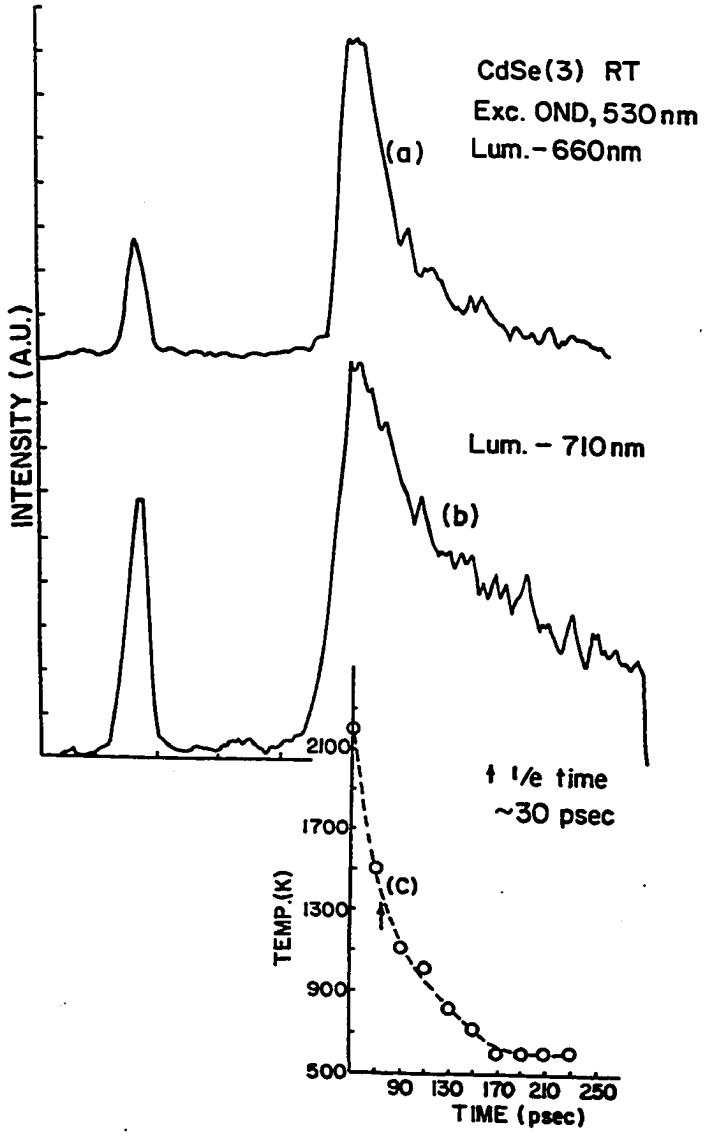

FIGURE 3.5.5

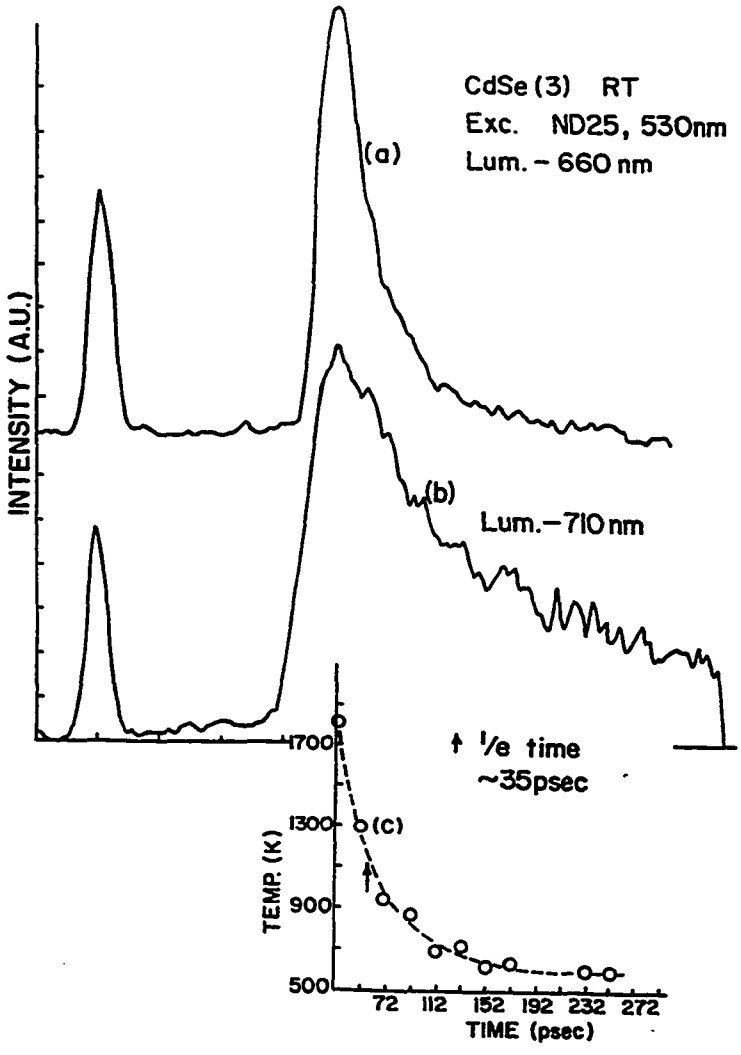

FIGURE 3.5.6

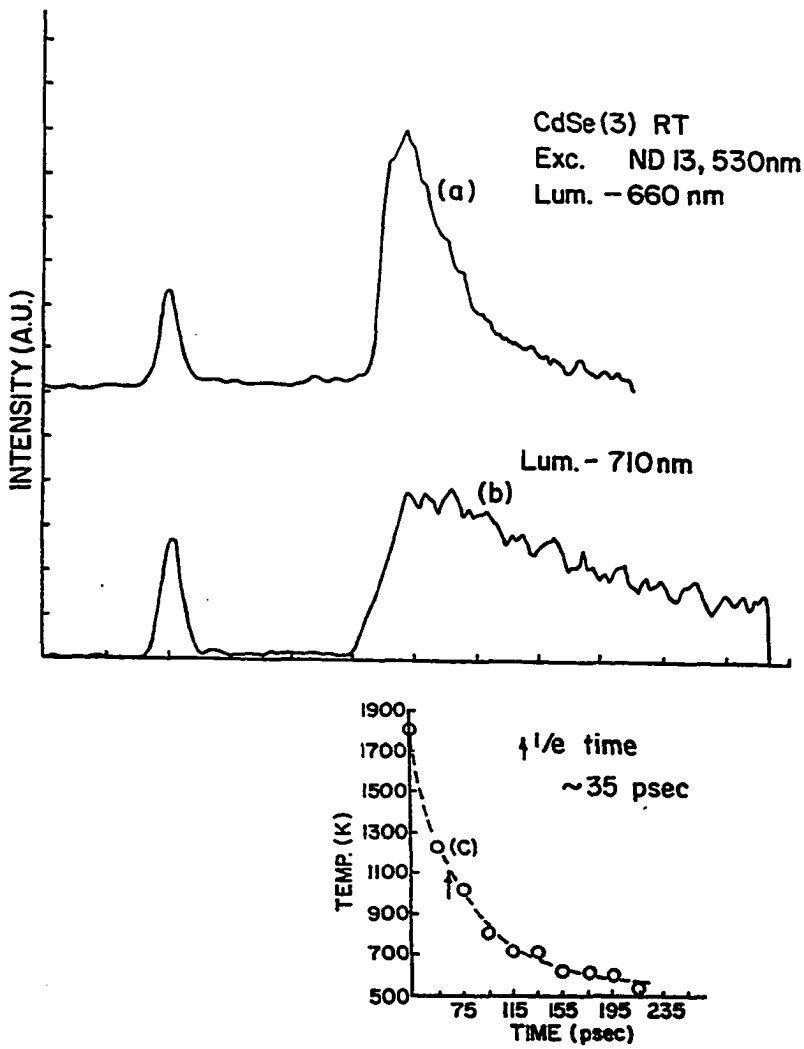

FIGURE 3.5.7

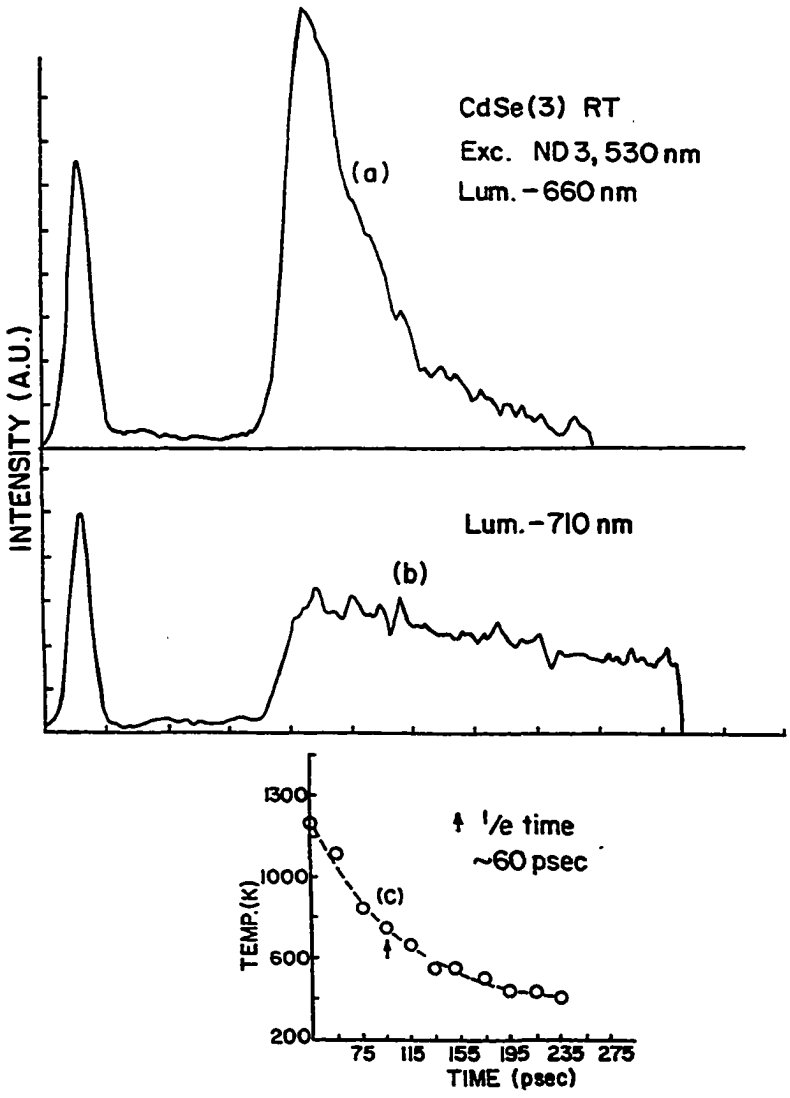

FIGURE 3.5.8

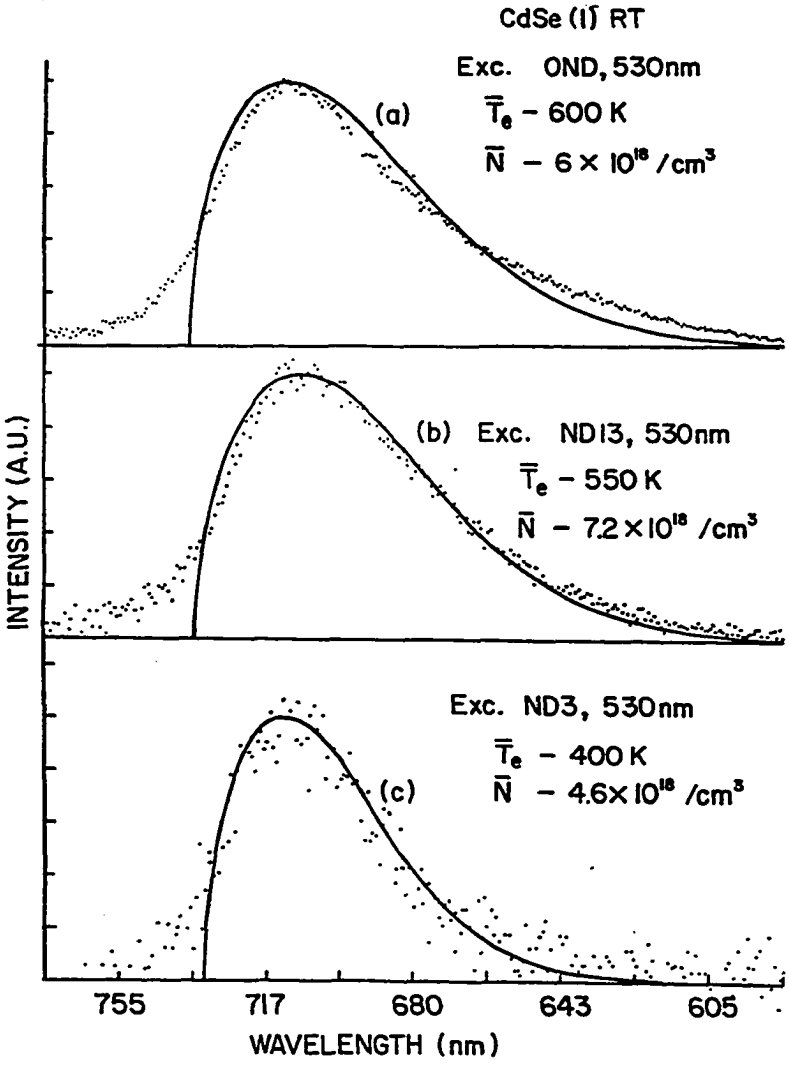

FIGURE 3.5.9

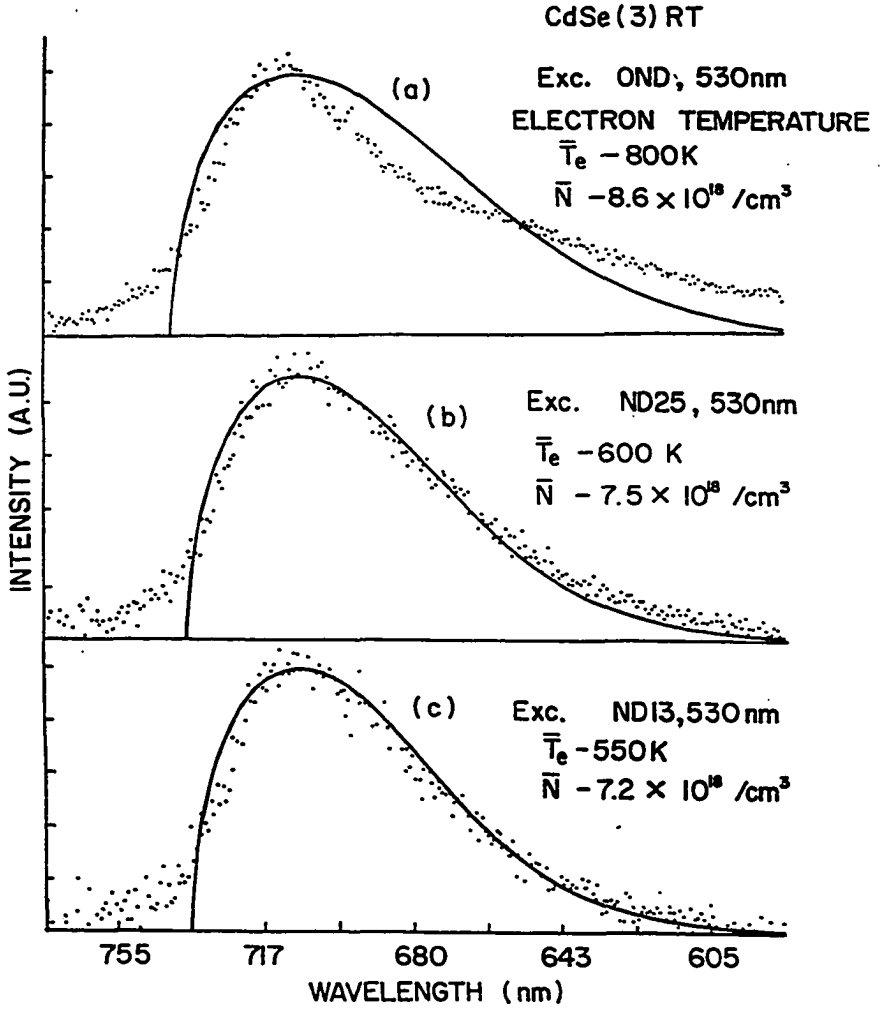

FIGURE 3.5.10

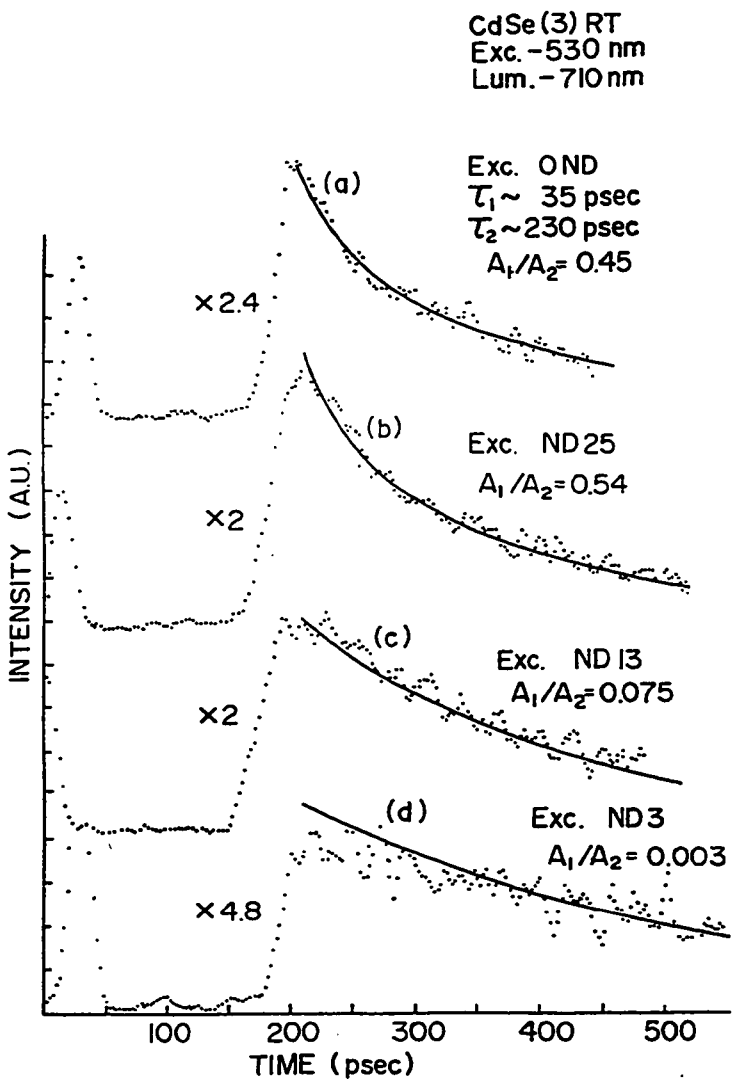

FIGURE 3.5.11

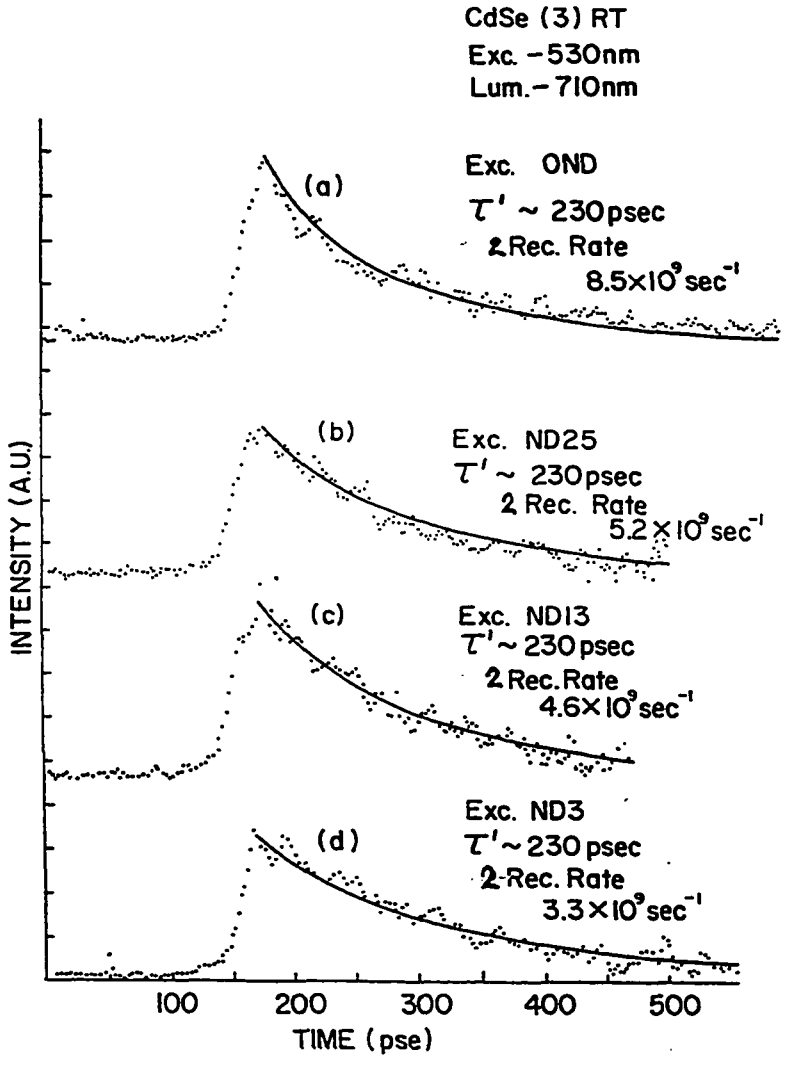

FIGURE 3.5.12

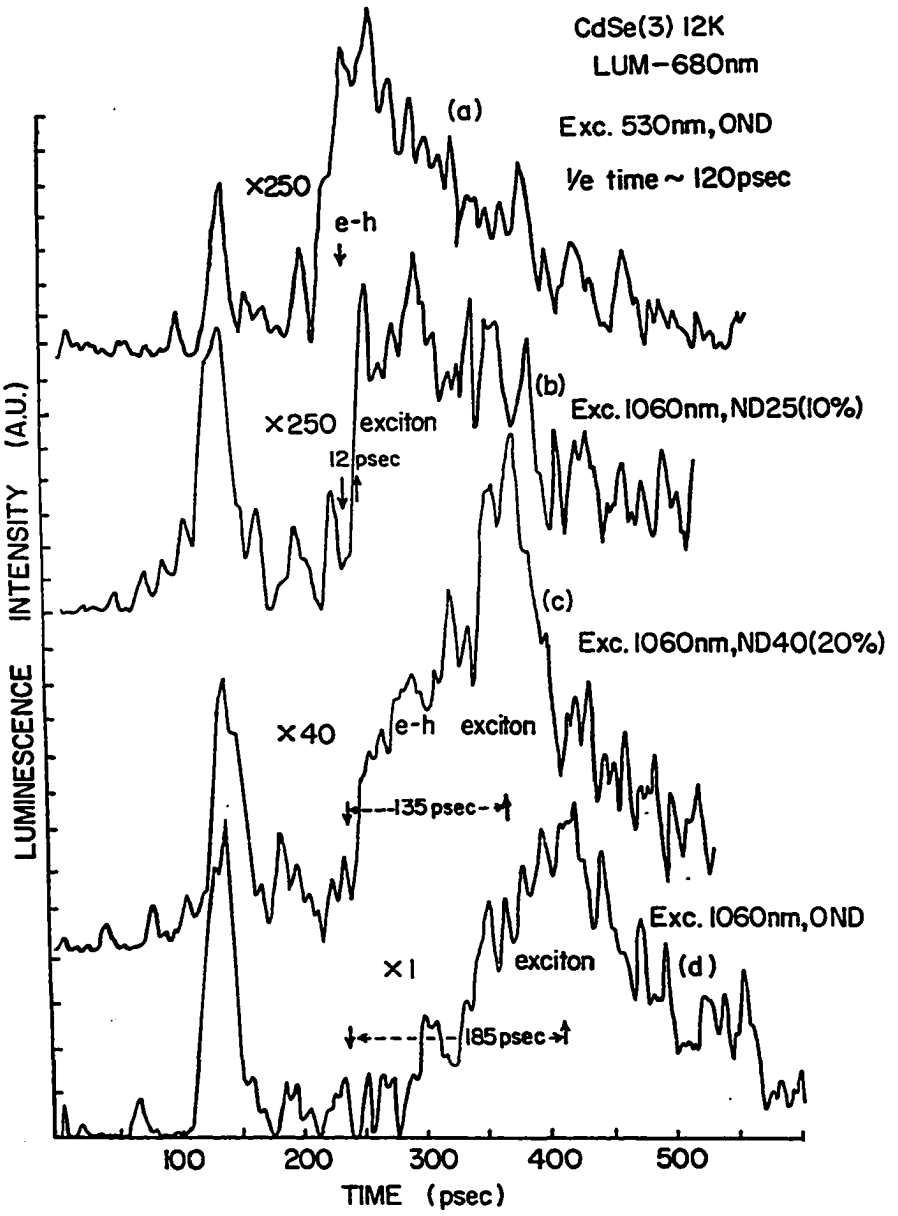

FIGURE 3.5.13

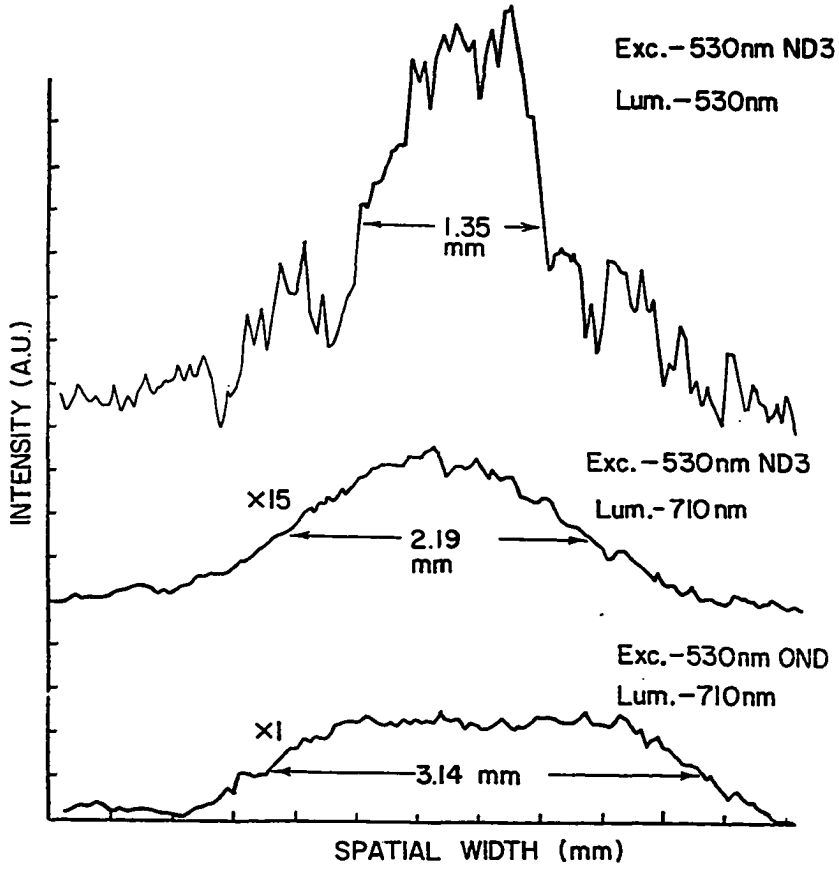

FIGURE 3.5.14

CdSe(1)		CdSe(3)	
Exc INTEN.	DELAY(psec)	Exc INTEN.	DELAY(psec)
I_F	46	I_F	50
$1/4\ I_F$	34	$1/4\ I_F$	32
$1/8\ I_F$	38	$1/8\ I_F$	35
$1/33 I_F$	27	$1/33 I_F$	35

TABLE 3.5.1

CdSe (I)

Exc. INTENSITY Photons/cm^2	CARRIER DENS. $\bar{N}$ (cm^{-3})	CARRIER TEMP. $\bar{T}e$ (K)
I_F	6.0×10^{18}	600
$1/8\ I_F$	7.2×10^{18}	550
$1/33\ I_F$	4.6×10^{18}	400

TABLE 3.5.2

CdSe (3)

Exc. INTENSITY Photons/cm^2	CARRIER DENS. $\bar{N}$ (cm^{-3})	CARRIER TEMP. $\bar{T}e$ (K)
I_F	8.6×10^{18}	800
$1/4\ I_F$	7.5×10^{18}	600
$1/8\ I_F$	4.6×10^{18}	550

TABLE 3.5.3

CdSe (3)

Exc. INTENSITY Photons/cm	Auger Rate sec^{-1}	CARRIER DENS. N cm^{-3}
I_F	4.5×10^{9}	2×10^{19}
$1/4\ I_F$	2.5×10^{9}	1.6×10^{19}
$1/8\ I_F$	2.5×10^{9}	1.5×10^{19}
$1/33\ I_F$	1.5×10^{9}	1.2×10^{19}

TABLE 3.5.4

CHAPTER IV

High Density Photogenerated Free Carrier Spin Relaxation Processes in Wurtzite Semiconductors: CdSe and Semimagnetic Semiconductor $Cd_{1-x}Mn_xSe$.

4.1 INTRODUCTION

An efficient source[1,2,3] of spin polarized electrons is of technological interest for high energy scattering, low energy electron diffraction, and atomic scattering. The generation of spin-oriented carriers in the conduction band by "polarized optical pumping" from heavy hole and light hole valence bands has been known[4,5] for over two decades. Measurements of the spin relaxation rates in semiconductors are important for understanding the basic physics behind carrier spin interaction and scattering mechanisms. The dipole allowed optical selection rules govern the maximum degree of spin polarization of carriers in semiconductors. In zinc-blende structures the optical transition from the valence bands Γ_8 to the conduction band Γ_6, shows that there are three times as many electrons excited to a state with spin antiparallel to the excitation photon angular momentum as compared with the spin parallel to it[6]. A similar situation arises for the semimagnetic semiconductor $Cd_{1-x}Mn_xSe$ ($0 \leq x < 0.5$) having a wurtzite lattice, even though the conduction band and valence bands are of

Γ_7 and Γ_9, Γ_7 group symmetry[7,8], respectively. The steady state spin polarization of the conduction electrons depends not only on the selection rules (or the symmetry of the crystal structure) but also on the relaxation mechanisms[6,9,10,11,12,13]. Various laboratories have investigated[13,14,15,16] the mechanisms of spin relaxation. Most of the work performed in this field has been confined to the study of GaAs with cubic symmetry, and the experimental techniques to obtain information on spin relaxation rates are indirect such as the Hanle effect[14,17], electron spin resonance[18], and spin flip Raman scattering[19,20]. Using a streak camera, we have previously made the first real time measurements[15,21] of the spin relaxation rates of high density photogenerated carriers in GaAs. Todate, no real time spin polarization kinetics have been studied in semimagnetic semiconductors.

Over the past three years, semimagnetic semiconductors have attracted a lot of attention because of their fascinating and useful[22] electronic, magnetic and optical properties i.e. large magneto-optic effect, large spin flip Raman shifts etc. These effects are due to the strong exchange interaction of carriers with the localized Mn^{2+} ions.

In this article, we continue our previous research[15,21] on spin relaxation mechanisms and direct our investgation to the transient spin effects in the II-VI wurtzite CdSe and the semimagnetic semiconductor: $Cd_{1-x}Mn_xSe$ for x = 0.05 and 0.1. These sam-

ples were chosen for spin relaxation experiments to investigate the spin exchange mechanism[22]. The experimental data is interpreted in terms of two spin relaxation mechanisms proposed by D'yakonov and Perel'[9]. The first mechanism of spin relaxation relates the relaxation rate to the noncentrosymmetric nature of the host crystal (CdSe), while the second mechanism addresses the effect of the exchange interaction between carrier spins and localized magnetic spins. Other mechanisms, particularly the one proposed by Elliot and Yafet[10,11] are discarded because of the ten fold slower kinetics.

4.2 BACKGROUND

The host crystal CdSe is a II-VI semiconductor with wurtzite crystal structure[7,8]. The valence bands consist of the A, B and C bands having Γ_9, Γ_7 and Γ_7 symmetry at k=0, respectively. The anisotropic crystal field in hexagonal crystals leads to lifting of the degeneracy at k=0 and to the splitting of the upper valence bands Γ_8 into subbands Γ_{9A} and Γ_{7B}. This is in contrast to the cubic crystals such as GaAs. The conduction band has Γ_7 symmetry having a direct band gap above Γ_{9A} of 1.84 eV at 4 °K. The energy splitting Γ_{9A}-Γ_{7B}, corresponding to the crystal field, is 26.3 meV and that of the split-off energy Γ_{7B}-Γ_{7C}, corresponding to the spin orbit interaction is 406 meV[7,8].

For single photon absorption, the selection rules are as follows: the transition from the Γ_{9A} valence band to the Γ_7 conduction band is allowed for light polarized $E \perp C$ (c-axis of symmetry), and transitions from the valence bands Γ_{7B}, Γ_{7C} to the Γ_7 conduction band are allowed for light polarized $E \perp C$ and $E \| C$. For the absorption with circularly polarized light propagating along the c-axis, the selection rules yield the same spin polarized carrier population ratio in the conduction band as for cubic crystals[7,8]. $Cd_{1-x}Mn_xSe$, within the range of Manganese atomic concentration $0 \leq x \leq 0.45$, has the wurtzite crystal structure. The selection rules are identical to those in the host CdSe lattice.

The spin polarization factor $\rho(t)$ is defined by,

$$\rho(t)=\frac{N\uparrow(t)-N\downarrow(t)}{N\uparrow(t)+N\downarrow(t)} \quad , \tag{4.2.1}$$

where $N\uparrow(t)$ and $N\downarrow(t)$ are the spin densities of electrons at time t with spin 1/2 and -1/2, respectively. The rate equations for the polarized carriers in terms of the total recombination lifetime τ and spin relaxation time T_s after a δ pulse excitation are given by,

$$\frac{dN\uparrow}{dt} = -\frac{N\uparrow}{\tau} - \frac{N\uparrow}{T_s} + \frac{N\downarrow}{T_s} \quad , \tag{4.2.2}$$

and

$$\frac{dN\downarrow}{dt} = -\frac{N\downarrow}{\tau} - \frac{N\downarrow}{T_s} + \frac{N\uparrow}{T_s} \quad . \tag{4.2.3}$$

The solution of these equations gives the time dependent polarization factor,

$$\rho(t) = \rho(0)e^{-t/(Ts/2)}, \tag{4.2.4}$$

where $\rho(0)$ is the selection rule allowed polarization factor. For one photon absorption[6] $\rho(0)$ turns out to be 50 %, while for two photon absorption[22] $\rho(0)$ is 100 %. Of course, these values are reduced from the maximum values because of band mixing. These effects will be discussed later in the theory section. If we assume that the holes depolarize very fast[23] ($\sim 10^{-13}$ sec), the luminescence polarization factor which is given by,

$$L(t)= \frac{\sigma+(t)-\sigma-(t)}{\sigma+(t)+\sigma-(t)} \quad , \tag{4.2.5}$$

is equal to $\rho(t)$. $\sigma^{+}(t)$ and $\sigma^{-}(t)$ are luminescence intensities for right and left circular polarization at time t.

The recombination lifetime is obtained by adding equations (4.2.2) and (4.2.3) as follows,

$$\frac{dN}{dt} = \frac{dN\uparrow}{dt} + \frac{dN\downarrow}{dt} \quad . \tag{4.2.6}$$

Hence,

$$N(t) = N(0)e^{-\frac{t}{\tau}} , \qquad (4.2.7)$$

where N(0) is the carrier density at t=0.

4.3 SAMPLES

The samples of CdSe (high resistivity and low resistivity) were acquired from Cleveland Crystals, Inc. All the samples used in this experiment have the c-axis perpendicular to the flat face ($\pm 2^{\circ}$).

The samples of $Cd_{1-x}Mn_xSe$ used were grown at Purdue University by the Bridgeman method. Both the samples (x=0.05 and 0.1) are background doped with In ($\sim 10^{16}/cm^3$). The sample geometry is similar to the CdSe crystals and was described earlier. The propagation vector K of the excitation photon is oriented parallel to the c-axis.

4.4 EXPERIMENTAL METHOD

Samples were mounted on a cold finger in a liquid He dewar with optical windows. The temperature was monitored using a Si diode. Photoexcited carriers were produced using a Nd:glass laser mode locked by Kodak A9860 dye dissolved in dichloroethane. Single pulse (6 psec) two photon excitation (λ =1060 nm) was

achieved using a spark gap and a Pockel cell for pulse selection from the mode locked train. The details of the time-resolved spin polarized photoluminescence setup and picosecond laser system have been described elsewhere[21,24]. The single photon excitation (λ= 530 nm) was carried out using second harmonic generation in KDP. Stokes-shifted stimulated Raman photon[25] excitation at 623 nm was achieved using a frequency-doubled pulse (530 nm) passing through ethanol.

The linearly polarized output of the laser system was circularly polarized (left or right) before excitation and the circularly polarized (left and right) luminescence from the sample was analysed using a broad band quarterwave plate. A Wollaston prism was placed in front of the entrance slit of a streak camera to spatially resolve the left and right circular polarization of the luminescence. A weak laser prepulse (530 nm) was directed into the entrance slit of the streak camera prior to the arrival of luminescence. This prepulse (see Figs.4.5.1, 4.5.2, 4.5.3, 4.5.4, 4.5.5, and 4.5.6) was used as a marker for overlapping various data files for averaging, adding, and subtracting. Thus, single shot kinetics for left and right circular polarization of the luminescence was investigated simultaneously. The electronic windows set on a video camera controlled by a microprocessor enabled us to record and store the data[26] in a minicomputer (appendix B1). The intensity and time axis of the measured temporal curves displayed

in Figs. (4.5.1), (4.5.2), (4.5.3), (4.5.4), (4.5.5) and (4.5.6) are corrected for the streak rate nonlinearity of the streak camera. The temporal resolution -laser pulse FWHM of the streak camera is 13 psec. This corresponds to total experimental time resolution. The luminescence band were selected using dielectric filters in front of the streak camera.

In order to measure $\rho(t)$, it is necessary to calibrate the intensity ratio between the two windows. Under the most ideal condition the windows are properly balanced and the ratio is equal to unity. In some cases this is not so, then the ratio was determined and used as a correction factor. To obtain this correction factor we used linearly polarized excitation. The luminescence from a sample in such a case would be equally circularly polarized ($I_{\sigma+} = I_{\sigma-}$), while the recorded data in the two windows would reflect the imbalance of the intensity response (appendix B2). Using this information, all the subsequent time resolved photoluminescence data for circularly polarized excitation was corrected for the different window sensitivity. Using equations (4.2.4) and (4.2.6) we deduced the values of $\rho(0)$, T_s and, τ.

4.5 EXPERIMENTAL RESULTS

1) CdSe

Experiments on CdSe were carried out at 77K. Fig.(4.5.1) shows spin polarized time resolved luminescence for one photon 530

nm and σ+ polarization pumping. The curves (a) and (b) in Fig.(4.5.1) correspond to σ+ and σ- polarization of the near band gap (680-700 nm) luminescence. The inset displays the polarization factor ρ(t) calculated from the data using equations (4.2.4) and (4.2.5) on an expanded time scale. The solid line is an exponential fit to the data with $\rho(0)=36\pm5$ % and $T_s=28\pm4$ psec. Fig.(4.5.2) displays spin polarized luminescence under similar experimental conditions for luminescence band 620-660 nm (hot luminescence). The polarization factor is $\rho(0)=44\pm5$ % and the spin relaxation time is $T_s=24\pm5$ psec. Fig.(4.5.3) describes band edge spin polarized luminescence for 623 nm excitation wavelength. The corresponding values of $\rho(0)$ and T_s are 48 ± 4 % and 30 ± 4 psec, respectively.

2) $Cd_{1-x}Mn_xSe$

Experiments on $Cd_{1-x}Mn_xSe$ were carried out at 30 K. The band gap in $Cd_{1-x}Mn_xSe$, as a function of x concentration, is given by[27] $E_g = 1.817+1.53x$ ev at a temperature of 30K. The band gaps for x=0.05 and 0.1 are 1.89 eV and 1.97 eV, respectively. Two photon excitation (1060 nm) was used to enhance the initial spin polarization. The photoluminescence for $Cd_{0.95}Mn_{0.05}Se$ was recorded with a narrow band filter centered at 660 nm, while a broad band filter (620-660 nm) was used for $Cd_{0.9}Mn_{0.1}Se$. The time resolved photoluminescence shows complex behavior (Fig.(4.5.4) and (4.5.5)). The second peak is delayed by about 100 psec after the first fast

decay in the sample with x=0.05. The second peak is delayed by ~50 psec in the case of x=0.1. It is observed that the first luminescence peak (time resolved) is spin polarized, while the second peak is unpolarized. The second peak rises slowly and decays slowly in either case. Nurmikko[28] et al have observed the exchange interaction induced red shift associated with BMP formation in their time resolved spectra. Their data suggest BMP formation time of ~ 400 psec in $Cd_{0.95}Mn_{0.05}Se$. Our result is consistant with Nurmikko et al[28] taking into account the formation time of bound exciton and BMP. The second peak is believed to be originated from the bound magnetic polaron formation (BMP) and disappears at high temperature (see Fig.(4.5.6)). A detail study will be dicussed in a future publication[29]. The values of $\rho(0)$ and T_s for the sample with x=0.05 are 18 ± 4 % and 16 psec, respectively (see Fig.(4.5.4)) and the displayed inset. The corresponding values for the sample with x = 0.1 are 28 ± 5 % and 20 psec, respectively (see Fig.(4.5.5)). Electron-hole recombination luminescence lifetimes derived from the first peak for x= 0.05 and 0.1 are about 20 psec in both samples.

4.6 THEORY

1. Spin Polarization:

For most III-V and II-VI semiconductors, the transitions between the valence bands and the conduction band are principally

the transitions between bands of $|P\rangle$ and $|S\rangle$ types. Spin orbit interaction makes $|P\rangle \rightarrow |3/2,\pm 3/2\rangle$ and $|3/2,\pm 1/2\rangle$, and $|S\rangle \rightarrow |1/2,\pm 1/2\rangle$. The values of $\langle P|P_z|S\rangle$ are practically the same for all semiconductors and depend weakly on K (vary by a factor of two over the extent of the Brillouin zone)[30,31,32]. Fig.4.6.1(a) displays the optical transitions for near band edge one photon absorption, and Fig.4.6.1(b) displays two photon transition. The relative transition probabilities are shown in Fig.(4.6.1). The relative probability ratio[33] for $\sigma+$ polarization absorption at 530 nm for A, B, and C valence bands to the conduction band is $\approx$ 3:1:2.

Using Kane's model for band structure in semiconductors, the spin polarization factor $\rho_1(0)$ for one photon absorption in terms of the band gap and excitation photon energy is given by[34],

$$\rho_1(0)=\frac{(\frac{1}{2})(3\sqrt{1+y'}+4y'-1)}{3\sqrt{1+y'}+1+2y'^2} \quad , \qquad (4.6.1)$$

where $\rho_1(0)$ denotes the spin polarization factor at t=0, $y'=E_g/\hbar\omega_1$, and ω_1 is the excitation frequency (see appendix A).

In the case of two photon absorption, the spin orientation factor $\rho_2(0)$ (neglecting the split off band contribution) is given by[34],

$$\rho_2(0)=\frac{19+\left[\frac{32y}{3}-\frac{2}{y}-\frac{4}{3}\right][1+y]^{(\frac{3}{2})}\left[\frac{3}{2}-y\right]^2}{30+\left[\frac{32y^2}{3}+\frac{3}{8y^2}\right][1+y]^{(\frac{3}{2})}\left[\frac{3}{2}-y\right]^2} \qquad (4.6.2)$$

where $\rho_2(0)$ denotes the spin polarization factor at t=0, $y = E_g/2\hbar\omega_1$, and ω_1 is the excitation frequency.

For one photon excitations at 530 nm and 623 nm in the case of CdSe with band gap of 1.81 eV (684 nm), the initial polarization factor is calculated to be 48 % and 50 %, respectively. This is in good agreement with experiment, since the measured values for $\rho_1(0)$ are 44 % and 48 %, respectively. The band gap of $Cd_{1-x}Mn_xSe$ for x = 0.05 is 1.89 eV. The calculated value of $\rho_2(0)$ is 63 %, which compares poorly with the experimental value of 18±5 %. Similarly for $Cd_{0.9}Mn_{0.1}Se$ with a band gap of 1.97 ev, the calculated and experimental values of $\rho_2(0)$ are 64 % and 28±5 %, respectively.

2. Spin Dephasing

a) D'yakonov and Perel' Spin Dephasing Mechanism :

The observed fast spin relaxation of free carriers in semiconductors with the wurtzite structure will be discussed within the framework of the theory proposed by D'yakonov and Perel'[6,9] and extended by Margulis et al[35]. This theory is applicable to both semiconductors i.e. CdSe and $Cd_{1-x}Mn_xSe$. In our previous work[15] on the spin relaxation mechanisms of high density photogen-

erated carriers in GaAs, we had observed that the spin relaxation is primarily due to the D'yakonov and Perel' mechanism.

According to D'yakonov and Perel'[6,9], a semiconductor without an inversion center has a spin relaxation mechanism whose role rapidly increases in effectiveness with increasing electron energy. This mechanism involves spin splitting of the conduction band proportional to the quasimomentum. This splitting is equivalent to an effective magnetic field acting on the spins, whose direction depends on the direction of the momentum. In a GaAs crystal which has zinc blende crystal symmetry, the lack of inversion symmetry contributes a k^3 term to the conduction band electronic Hamiltonian. In a similar way the Hamiltonian describing free carriers in a semiconductor with wurtzite crystal structure has the following form[35,36,37,38],

$$H = \frac{\hbar^2 k^2}{2m_e} + \gamma \hat{c}(\vec{\sigma} x \vec{k}) , \qquad (4.6.3)$$

where $\hat{c}$ is a unit vector parallel to c axis, γ is a constant describing the spin splitting of the conduction band at $k \neq 0$, and $\sigma(\sigma_x, \sigma_y, \sigma_z)$ are the Pauli spin matrices. The role of the second term can be seen as the $\vec{k}$ dependent effective magnetic field interacting with the carrier spins. Thus with every collision the effective magnetic field changes its direction, and the spin component changes its sign provided that the precession time is longer

than the collision time (slow precession and high collision rate).

Using equation (4.6.3) Margulis et al have shown that, for a strongly degenerate carrier distribution the spin relaxation rate is given by[35],

$$\frac{1}{T_s} = \frac{16}{3} \frac{\gamma^2 m_e \xi \langle\tau\rangle}{\hbar^4} , \qquad (4.6.4)$$

where ξ is the Fermi energy; $\langle\tau\rangle$ is the collision time; and m_e is the effective mass of the electron. For a highly degenerate carrier distribution the Fermi energy is expressed in terms of the carrier density N as,

$$\xi \sim \frac{\hbar^2((3\pi^2.N)^{(\frac{2}{3})})}{2m_e} . \qquad (4.6.5)$$

For the estimated carrier density of 5 $x10^{18}/cm^3$, ξ= 72 meV. The value of γ has been measured[38] (2.56 $x10^{-31}$ Joule-m) in CdS using spin flip Raman scattering. The upper limit on γ set by Hopfield[36,37] in the case of CdSe is of the order of (1-3)10^{-31}Joule-m. We have used the value of γ measured in CdS for our order of magnitude calculation.

Using $m_e = 0.13m_o$, $\gamma = 2.56\ x10^{-31}$ Joules.m, and a collision time $\langle\tau\rangle$ of 1 $x10^{-14}$ sec, the expression for the spin relaxation rate

reduces to,

$$\frac{1}{T_s} = 6.67 \times 10^{11} \xi \ , \qquad (4.6.6)$$

where the Fermi energy ξ is in eV. This implies that the spin relaxation time is 21 psec, for a carrier concentration of 5 $x10^{18}/cm^3$ (ξ = 0.072 eV), which is is quite close to the measured values of ~ 26 psec. The calculated spin relaxation times for estimated carrier densities of 2 $x10^{18}/cm^3$ and 8 $x10^{18}/cm^3$ are 38 psec and 15 psec, respectively.

The temperature of the lattice does not play any significant role as long as the carriers are highly degenerate. This is due to the averaging of spin relaxation rate over a Fermi thermal distribution. We have observed almost no spin relaxation dependence on laser excitation intensities. To account for this, we believe a rapid diffusion[39,40] of carriers from the photoexcited region takes place during the laser pulse making the carrier concentration 5 $x10^{18}/cm^3$ independent of excitation power within the excitation fluence (4.25 $x10^{27}$-1.29 $x10^{26}/cm^2sec$). It is difficult to estimate the exact carrier concentration. The following experimental observations support this conclusion: Excitons are formed earlier than predicted by the Mott criterion and free e-h plasma, no shift in the Fermi level[40,41] as a function of excitation power was

evident from the time integrated luminescence spectra observed under high excitation laser pulses, and no appreciable change in the Auger recombination rate[40,42,43] ($\sim N^2$) was observed at various excitation fluences. From time resolved carrier temperature study[40] made at room temperature, the carrier temperature T_e is established to be < 1000 K within 30 psec. Furthermore, at 77 K the carriers will cool much more rapidly. Hence, the criteria for a degenerate thermal distribution i.e. $\xi/K_B T_e > 1$ at ξ = 72 meV is justified.

b) **Spin-localized spin exchange dephasing mechanism :**

Ultrafast spin relaxation and the initial small spin alignment in $Cd_{1-x}Mn_xSe$ is an indication of rapid spin exchange of carrier spins with Mn^{2+} localized spins of S=5/2. In wide gap semimagnetic semiconductors the splitting of the conduction band is given by[44],

$$\Delta E_c(H,T) = N_o . \alpha . x \langle S_z \rangle , \qquad (4.6.7)$$

where $N_o \alpha$ (200 mev) is the exchange parameter between the conduction s and Mn^{2+} $3d^5$ states; x is the mole fraction of Mn atoms; and $\langle S_z \rangle$ is the mean spin component along the external magnetic field. At very low temperatures x is replaced by $\tilde{x}$ in order to account for an antiferromagnetic interaction[45,46] between Mn^{2+}

ions. This will be ignored here as the temperatures are greater than $T_{AF} \approx 3K$. Heiman et al have observed[46] a zero field spin flip Stokes energy of 1 mev (x = 0.1) for of lattice temperatures (1.9 - 28 K). The zero field spin flip energy for x=0.05 is 0.5 mev[44]. These values can be used for the exchange energy between free electron and Mn^{2+} ions, even though these spin flip measurements are typically for donor bound electrons. This implies that an electron is scattered by a Mn^{2+} ion with net statistical spin of $\langle S_z \rangle = 0.05$ instead of 5/2. Assuming a spin field dependence given by,

$$\langle S_z(r) \rangle = (\frac{5}{2}) \exp -(\frac{r}{a'})^2 \qquad (4.6.8)$$

due to a localized electronic spin of strength 5/2, where a' is the radius of the ion and r is the distance measured from the center of the ion, we have calculated the distance at which the $\langle S_z \rangle$ = 0.05. Assuming a Mn^{2+} ionic radius[47] of 1.0 $\mathring{A}$, the estimated statistical distance measured from a Mn^{2+} ion, for spin flip scattering is 1.88 $\mathring{A}$("a"). With these specified numbers in mind we can apply the theory of D'yakonov and Perel'[48] for optical orientation in a system of donor bound electrons and lattice nuclei in semiconductors. They have calculated the effective magnetic field due to the hyperfine interaction between localized electronic spins and lattice nuclei as,

$$H_c = (\mu_o \tilde{g})^{-1} \Omega_o \left(\sum_{n=1}^{\infty} \right) \left(|\psi(r_n)|^2 A_{HFN} S_n \right) \quad , \qquad (4.6.9)$$

where μ_o is the Bohr magneton; $\tilde{g}$ is the effective g-factor; Ω_o is the volume of the unit cell; A_{AFN} is the hyperfine interaction coefficient; S_n is the nuclear spin of n-th nucleus; and $\psi(r_n)$ is the wave function of donor bound electrons at the n-th nucleus. The wave function for the localized electronic state takes the form $\psi(r) = 1/\sqrt{(\pi a^3)} e^{-r/a}$. The theory could be modified for exchange interaction. The mean square effective field is then given by[48],

$$\langle H_c^2 \rangle = \left(\frac{25\pi}{128} \right) . \left(\frac{x N_o a^3}{(\mu_o \tilde{g})^2} \right) . \Delta^2_{ex} \quad , \qquad (4.6.10)$$

for S = 5/2, where xN_o is the Mn^{2+} ionic concentration (N_o is the cation density in CdSe), and Δ_{ex} is the exchange energy. For a 10 % Mn^{2+} concentration xN_o is $\approx 1.8 \times 10^{21}/cm^3$ for a unit volume of 369 ($Å^3$) with wurtzite lattice parameters of b=4.3 Å and c=7 Å.

This theory is applicable to free electron exchange interaction provided "a" is identified as the interaction distance parameter. The precession frequency is given by,

$$\omega_c = \frac{\mu_o \tilde{g} \sqrt{\langle H_c^2 \rangle}}{\hbar} \quad , \tag{4.6.11}$$

and the spin relaxation rate is given by,

$$\frac{1}{T_s} = \left(\frac{1}{9}\right) \omega_c^2 \tau_c \quad , \tag{4.6.12}$$

where τ_c is the collision time for electron-Mn^{2+} ion small angle scattering[9,14].

The effective $\tilde{g}$ value derived from the mean field theory is expressed[46] in terms of Mn^{2+} concentration as,

$$\tilde{g} = g + \frac{35.x.\alpha.N_o}{12K(T+T_{AF})} g_{Mn} \tag{4.6.13}$$

where $g^* = 0.5$ is for free carriers in n-CdSe; T_{AF} is the temperature corresponding to antiferromagnetic interaction; and $g_{Mn} = 2.0$ for Mn^{2+} ions. $N_o = 1.8 \times 10^{22}/cm^3$ is the cation density in CdSe. Lattice heating is negligible and at 30K the values of effective $\tilde{g}$ for x=0.05 and 0.1 are 1.6 and 47.2, respectively.

The estimate of collision time of free electrons with magnetic ions requires a value of mean free path. It has been pointed out that for a Born approximation calculation[46] with $\alpha N_o \sim 0.2$ ev the mean free path is given by,

$$\lambda \approx (\frac{1}{x})(\frac{m_o}{m})^2 10^{-6} \quad , \qquad (4.6.14)$$

where λ is expressed in cm. For a Mn concentration of 10 % (x=0.1) the mean free path is calculated to be 6 $x10^{-4}$ cm. Assuming a Fermi velocity of 4.5 $x10^{7}$ cm/sec corresponding to the Fermi energy of 72 meV, one calculates a collision time of ~ 14 psec. Hence, from equations (4.6.7),(4.6.8) and (4.6.9), we find the mean magnetic field, the precession frequency and the spin relaxation time to be 976 gauss, 1.4 $x10^{11}$/sec and 21.6 psec, respectively. In the case for the x = 0.05 CdMnSe sample these numbers are 220 gauss, 4.8 $x10^{10}$/sec and 90 psec, respectively.

Using the equations (4.6.6), (4.6.7), (4.6.9), (4.6.10) and (4.6.11) and taking into account the spin relaxation mechanisms of the host crystal (CdSe) and the localized Mn^{2+} ions, the theoretical total spin relaxation rate (for ξ=72 meV) (Fig. 4.6.2) is given by,

$$\frac{1}{T_s} = 1.08\ x10^{12}(x^2) + 4.75\ x10^{10} \qquad (4.6.15)$$

in sec^{-1}.

The total spin relaxation times calculated are 17 and 20 psec for x=0.1 and 0.05, respectively. These values are in reasonable agreement with our measurements.

4.7 DISCUSSION

a) CdSe (host crystal x=0)

The spin polarization factors and spin relaxation times for CdSe measured for various luminescence bands with different one photon excitation energies are in excellent agreement with theory.

For GaAs the valence bands $|3/2,\pm3/2\rangle$ and $|3/2,\pm1/2\rangle$ are degenerate at the center of Brillouin zone, this results in the luminescence polarization factor of $\approx$ 25% (for a selection rule allowed spin polarization factor of $\approx$50%). In CdSe, the valence band degeneracy is removed by crystal field splitting Δ_{cr} $\approx$26 meV at k=0. At our excitation levels the hole Fermi level is about 24 meV, which allows only the $|3/2,\pm3/2\rangle$ (A valence) band holes to participate in the luminescence process. The B and C band are occupied by electrons. In this case the luminescence polarization factor is the same as the free carrier spin polarization factor because the $|3/2,\pm1/2\rangle$ band does not participate in the recombination.

The luminescence bands selected for 530nm excitation are in the 620 - 660nm and 680 - 700nm wavelength regions. The luminescence band for 630nm excitation in our experiment is 15 meV above the bottom of conduction band with a luminescence region of 680 - 700nm. The difference between these pulse excitation conditions is that the split - off valence band Γ_7 is pumped by 530nm excitation, while for 630nm excitations it is precluded due to the energy

difference. The near bandedge (15 meV above bandgap) spin polarization factor is defined to be ρ_{BE}.

The polarization factor ρ, measured near the excitation energies, for 530nm and 630nm excitation are 44±5 % and 48±4 % (as shown in Fig.4.5.2 and 4.5.3), respectively. This agrees well with the theoretical values of 48% and 50%, respectively. To qualitatively understand the relationship between these ρ's, the effect of the split off valence band (Γ_7) has been neglected for 530nm excitation. This is a reasonable assumption because the density of states is about a factor of 10 smaller for Γ_7 than for the Γ_9 valence band. This generates fewer carriers in the conduction band edge due to the transition from the Γ_7 valence band. The effect of this transition is to depolarize the spin alignment of the conduction band edge electrons due to the nature of the selection rules[33]. This effect is less than 3%, and contributes to the observed band edge 680 - 700nm (15 meV above the band gap) spin polarization factor $\rho_{BE}(0)$ of 36±5 % observed under 530nm one photon excitation (Fig. 4.5.1). The observed hot electron polarization factor of 44±5 % (Fig.4.5.2) is somewhat larger than the band edge electron spin polarization factor. This observation is consistent with the split off valance band transition argument given above, although the difference is larger than expected. The observed delay time between the hot and band edge luminescence is ≈ 6 psec for 530nm excitation and less than 3 psec for 630nm exci-

tation. This can explain the lower value of $\rho_{BE}(0)$ if we allow for the spin relaxation ($\rho_{BE}(0) = \rho(0)\exp(-2t/T_s)$) during 6 psec with a spin relaxation lifetime of 30 psec. This result is consistent with 623nm (1.986 ev) excitation, as the observed value for $\rho_{BE}(0)$ of 48% is larger than 530nm excitation $\rho_{BE}(0)$ value of 36%. The spin relaxation times obtained in the hot luminescence region (620 - 660nm) and the band edge region (680 - 700nm) are 25±5 psec and 28±5 psec, respectively for 530nm excitation. The hot carriers have 15LO phonon excess energy compared to the band edge carriers. This means that the electron - LO phonon scattering additional channel is available for the hot electron energy relaxation and for spin relaxation. Since experimentally we do not find any significant difference between the spin relaxation times for different carrier energies we conclude that the LO phonon emission does not play a major role in the spin relaxation process. The measurements of spin polarization factors are also in agreement with the above conclusion as the LO phonon emission time is $\sim 10^{-12}$ sec compared to e-e or e-h collision times of $\sim 10^{-14}$ sec.

The measured value of spin relaxation time ($\approx$ 25 psec) is in good agreement with theory (21 psec). The theoretical spin relaxation times are sensitive to the exact knowledge of values of γ and Fermi level ξ. The spin relaxation times are a little longer for near edge carrier ($\approx$30 psec) compared to near excitation carriers (25 psec). This is expected as the mechanism is

effective for large k. Spin relaxation times and initial polarization factors are the same for the high resistivity (10^6 ohm-cm) and low resistivity (12 ohm-cm) samples, which indicates that the electron-Se vacancy scattering rate is significantly smaller as compared to electron-hole or electron-electron scattering rates ($\tau_c \sim 10^{-14}$ sec). The observed band edge luminescence ($\sigma+ + \sigma-$) shows two component decay (Fig.4.5.1), whereas the spin polarization $(\sigma+ - \sigma-)/(\sigma+ + \sigma-)$ is observed only in the fast component. The recombination luminescence lifetimes (fast component) are short ≈ 45 psec in the low resistivity sample (n-type) as compared to ≈ 70 psec in a high resistivity sample. This fast component is essentially due to Auger recombination. The difference in the lifetimes is a measure of hole capture rate at the hole capture centers existing in low resistivity samples (only n-type CdSe could be grown). However, the observed spin relaxation times are about the same in the high and low resistivity samples due to the lattice inherent DP mechanism. Conduction electron Raman spin flip measurements in CdS gives[19] an estimate of 10^{-11} sec for the spin relaxation time. Which should be of the order of magnitude expected for CdSe because of similarity in crystal structure. The very fact that experimentally we observe ~ 50% luminescence polarization at t=0, justifies the assumption that even in CdSe(x=0), the valence holes depolarize within 10^{-13} sec. Warnock[23] et al have observed this fast spin relaxation of holes in $Cd_{1-x}Mn_xSe$ (x

= 0.05 and x = 0.1) for above bandgap excitation.

b) $Cd_{1-x}Mn_xSe$ (x=0.05 and 0.1)

The observed values of the two photon spin polarization factor $\rho_2(0)$ of 20% for $Cd_{0.95}Mn_{0.05}Se$ and 28% for $Cd_{0.9}Mn_{0.1}Se$ are not consistent with the theoretical values of 63% and 64%, respectively (see table 4.7.1). This is believed to be due to the existance of Mn^{2+} excited states[49,50] (^4G) in the conduction band. Angle-resolved ultraviolet photoemission spectroscopy[51] studies had clearly indicated strong hybridization of Mn^{2+} d levels with p-like states in the valence band. In such a case, the optical transition is from a mixed ($p-\Gamma_6^1$) valence band to a mixed ($s-{}^4A_1, {}^4E, {}^4T_1$ and, ${}^4T_2$) conduction band. These mixed levels may play an important role in reducing the polarization factor $\rho_2(0)$ by modifying the selection rules. The theoretical agreement of spin relaxation times in $Cd_{1-x}Mn_xSe$ is subject to our approximation in the calculations of the collision distance, a, and scattering time, τ_c. However, in the case of $Cd_{1-x}Mn_xSe$ samples, a confirming trend of shorter spin relaxation time with increasing x has been established through our experiments, although the exact relationship between T_s and x has not been well established (see Eq. (4.6.15) and Fig.4.6.2). It is necessary to measure high concentration samples with higher temporal resolution in order to obtain the exact dependence of spin relaxation time on magnetic concen-

tration.

The free carrier luminescence (first peak) is polarized and BMP luminescence (second peak) shows almost zero polarization. This is consistent with Warnock[23] et al (steady state $\rho \sim 1\%$), which is due to fast relaxation of free carriers (e-h) within 30 psec for above bandgap excitation. Therefore, they observed the near zero polarization of BMP. It is known[48] that the spin state of the nuclei changes due to the exchange interaction with the spin polarized electrons. Since, the spin exchange time involved is $\sim 10^{-6}$ sec, this can not influence the spin relaxation rate of free carriers during the lifetime of the free carriers (40 psec). Thus, the observed increase in spin relaxation time (20 psec in $Cd_{0.9}Mn_{0.1}Se$ vs. 16 psec in $Cd_{0.95}Mn_{0.05}Se$) is not due to the transfer of angular momentum from Mn^{2+} spins to carrier spin system. Raman spin flip scattering (RSFS) line widths is an indirect measure of spin dephasing times. For $Cd_{1-x}Mn_xSe$, data on conduction electron Raman spin flip scattering time is not available. For localized bound states (i.e. BMP) the Raman spin flip line width broadening is partly due to large inhomogeneities of the environment. Hence, the observed line width of ~ 8 cm^{-1} (1 mev for x=0.1)[46] is enhanced and should not be taken to calculate the spin relaxation time. This will give an under estimate $< 10^{-12}$ sec. Taking this factor into account, we believe our direct measurements are more accurate than the dephasing time established by the

RSFS measurements.

The observed spin relaxation times in $Cd_{1-x}Mn_xSe$ could be explained in terms of D'yakonov and Perel' mechanisms since other spin relaxation mechanisms i.e. Elliot-Yafet[10,11], Bir-Aronov-Pikus[12] and Kleinman-Miller[13] virtual photon mechanisms are at least one order of magnitude slower. Since, the different mechanisms depend on the levels of carrier density and temperature, a large range of excitation powers is needed to understand and quantitatively describe which spin relaxation process dominates in $Cd_{1-x}Mn_xSe$. Our present single shot laser system precludes a density dependence study due to a lack of good signal to noise ratio at low excitation.

4.8 REFERENCES

1. R.L. Bell, 'Negative Electron Affinity Devices' (Claredon, Oxford 1973).

2. D.I. Pierce, R.J. Celotta, G.C. Wang, W.N. Unerti, A. Galejs, G.E. Kuyatt and S.R. Mielezareck, Rev. Sci. Instrum. 51 (1980).

3. M.Erninyam and G. Lampel, XIth International Conference on the Physics of Electronics and Atomic collions. (Kyoto, Japan. 1979).

4. G. Lampel, Phy. Rev. Lett. 20, 491 (1968).

5. R.R. Parsons, Phy. Rev. Lett. 23, 1152 (1969).

6. M.I. D'yakonov and V.I. Perel', Sov. Phys. JETP 33, 1053 (1971).

7. Donald Long, 'Energy bands in semiconductors', chapt.7 (1968).

8. J.L. Birman, Phys. Rev. Lett. 2, 157(1959), J. Phys. Chem. Solids 8, 35 (1959), Phys. Rev. 114, 1490 (1959).

9. M.I. D'yakonov and Perel', Sov. Phys. Solid state, 13, 3023 (1972)

10. R.J. Elliott, Phys. Rev. 96,266 (1954).

11. Y. Yafet, in Solid State Physics, edited by F. Seitz and D. Turnbull (Acadamic, New York, 1963), vol. 14, pp1-98.

12. G.L. Bir, A.G. Aronov, and G.E. Pikus, Sov. Phys. JETP 42, 705 (1976).

13. D.A. Kleinman and R.C. Miller, Phys. Rev. Lett. 46, 68 (1981).

14. G. Fishman and G. Lampel, Phy. Rev. B16, 820 (1977).

15. R.J. Seymour, M.R. Junnarkar and R.R. Alfano, Phy. Rev. B24, 3623 (1981).

16. A.H. Clark and R.D. Burnham, D.J. Chadi and R.M. White, Sol. State. Comm. 20, 385 (1976).

17. V.B. Vekua, R.I. Dzhioev, B.P. Zakharchenya, V.G. Fleisher, Sov. Phys. Semicond. 10, 210 (1976).

18. G. Lampel, Proceedings of the 12th International Conference on the Physics of Semiconductors edited by M.H. Pilkuhn (Teubner, Stuttgart 1974) P.743.

19. P.A. Fleury and J.F. Scott, Phy. Rev. B3, 1979 (1971).

20. J.F. Scott, T.C. Damen, and P.A. Fleury, Phy. Rev. B6, 3856 (1972).

21. R.J. Seymour and R.R. Alfano, Appl. Phys. Lett. 37, 231 (1980).

22. J.K. Furdyna, J. Appl. Physics 53, 7637 (1982).

23. J. Warnock, R. N. Kershaw, D. Ridgley, K. Dwight, A. Wold, and R. R. Galazka, Sol. State Comm. 54, 215(1985).

24. P.Y. Lu, P.P. Ho and R.R. Alfano, J. Quant. Electronics QE-15, 406 (1979).

25. N. Bloembergen, American J. of Phys., 35, 989 (1967).

26. R.J. Seymour thesis ' Electron Spin and Energy Relaxation in highly excited GaAs. ' (unpublished) New York University, (1981).

27. J. Stankiewicz, Phy. Rev. B27, 3631 (1983).

28. J.H. Harris and A.V. Nurmikko, Phys. Rev. Lett. 51,1472(1983). Also see C.A. Huber and A.V. Nurmikko Sol.State Comm. 48, 675 (1983).

29. M.R. Junnarkar, R.R. Alfano, and J. Furdyna (to be published)

30. M. Cardona, J. Phys. Chem. Sol. 24, 1543 (1963).

31. M. Cohen and T.K. Bergstresser, Phy. Rev. 141, 789 (1966).

32. M. Cardona and G. Harbeeke, Phy. Rev. A137, 1467 (1965).

33. 'Semiconductors probed by Ultrafast Laser Spectroscopy. Vol. 2' edited by, R.R. Alfano (Acadamic Press, 1985), p.199.

34. E.L. Ivchenko, Sov. Phy. Solid State 14, 2942 (1972). Also see Appendix 'Picosecond and Steady State Spectroscopy of Wurtzite Semimagnetic Semiconductor $Cd_{1-x}Mn_xSe$.' Thesis by M.R. Junnarkar (unpublished) City University of New York (1986).

35. A.D. Margulis and VI.A. Margulis, Sov. Phys. Semicond. 18, 305 (1984).

36. J.J. Hopfield, J. Appl. Phys. 32, 2277 (1961).

37. G.D. Mahan and J.J. Hopfield, Phy. Rev. 135, A428 (1964).

38. R. Romestain, S. Geschwind and G. Devlin, Phy. Rev. Lett. 39, 1583 (1977).

39. N.J. Frigo, H. Mahr and David J. Erskine, J. Quantum Electronics, 18, 192 (1982). Comm.41, 657 (1982).

40. M.R. Junnarkar and R.R. Alfano (to be published).

41. J.I. Pankove, Optical Processes in Semiconductors, Dover Pub. page 129, (1971).

42. J.S. Blakemore, Semicondutor Statistics (Pergammon, New York, 1962) p.214.

43. D.H. Auston and C.V. Shank and P. LeFur, Phys. Rev. Lett. 35, 1022 (1975).

44. M. Nawrocki, R. Planel and G. Fishman, Phys. Rev. Lett. 46, 735 (1981).

45. D. Heiman, Appl. Phy. Lett. 42, 775 (1983).

46. D. Heiman, P.A. Wolff and J. Warnock, Phy. Rev. B27, 4848 (1983).

47. A. Beiser, Perspectives of Modern Physics, Mc Graw - Hill, 1969, p.424.

48. M.I. D'yakonov and V J Perel', Sov. Phys. JETP 38, 177 (1974).

49. M.P. Vecchi, W. Giriat and L. Videla, Appl. Phys. Lett. 38, 99 (1981).

50. R.Y. Tao, M.M. Moriwaki, W.M. Becker and R.R. Galazka, J.

Appl. Phys. 53, 3772 (1982).

51. P.Oelhafen, M.P. Vecchi, J.L. Freeouf and V.L. Moruzzi, Solid. state comm. 44, 1547(1982).

4.9 FIGURE CAPTIONS

4.5.1. The curves (a) and (b) represent photoluminescence from CdSe correspondingto σ+ and σ- polarizations. The excitation wavelength and polarization are 530 nm and σ+, respectively. The luminescence corresponds to the 680 - 700 nm spectral region (band edge) at 77K. The inset is experimental data on a expanded time scale for polarization factor ρ(t). The solid line is an exponential fit with $\rho(0) = 0.36$ and $T_s = 28$ psec.

4.5.2. The curves (a) and (b) represent photoluminescence with σ+ and σ- polarization. The excitation wavelength and polarization are 530 nm and σ+, respectively. The luminescence wavelength region is between 620 - 660 nm. The inset shows the theoretical fit corresponding to $\rho(0) = 0.44$ and $T_s = 24$ psec.

4.5.3. The curves (a) and (b) corresponds to σ+ and σ- polarization with excitation wavelength of 630 nm. The excitation polarization is σ+. The luminescence corresponds to 680-700 nm spectral region at 77K. The inset shows the theoretical fit corresponding to a single exponential with $\rho(0) = 0.48$ and $T_s = 30$ psec.

4.5.4. The curves (a) and (b) represent spin polarized photoluminescence from $Cd_{0.95}Mn_{0.05}Se$ at 30K. The σ+ and σ- luminescence corresponds to two photon excitation at 1060 nm and σ+ polarization. The spectral band of the luminescence is 660 ±10 nm. The inset curve fitting parameters are $\rho(0) = 0.2$ and $T_s = 16$ psec.

4.5.5. The curves (a) and (b) represent spin polarized photoluminescence from $Cd_{0.9}Mn_{0.1}Se$ at 30K. The σ+ and σ- luminescence corresponds to two photon excitation at 1060 nm and σ+ polarization. The spectral band is 620 - 660 nm. The inset curve fitting parameters are $\rho(0) = 0.28$ and $T_s = 20$ psec.

4.5.6. The unpolarized time resolved band edge luminescence for a) $x = 0.05$, 4K, b) $x = 0.05$, 77K, c) $x = 0.1$, 4K, and d) $x = 0.1$, 77K.

4.6.1. Figure (a) shows one photon transitions from valence bands A, B, C, to the conduction band for a wurtzite semiconductor. The relative transition probabilities are shown. The spin densities involve addition of various transitions with weighted density of states. In (b) the simple two photon absorption model is shown.

The two photon absorption predicts 100% spin polarization unless band mixing is taken into account. The straight arrows correspond to absorption while wiggled arrows show photoluminescence.

4.6.2. The dotted line corresponds to the theoretical expression $1/T_S = Ax^2 + B$. Where $1/B$ is the spin relaxation time of carriers in host CdSe. The values of A and B are as in Eq.(20). The o are the experimental points.

4.10 TABLE CAPTION

4.7.1 The experimental condition (excitation wavelength, temperature, and luminescence band), measured values of ρ_o and T_S, and theoretical values of ρ_o and T_S are tabulated for $Cd_{1-x}Mn_xSe$.

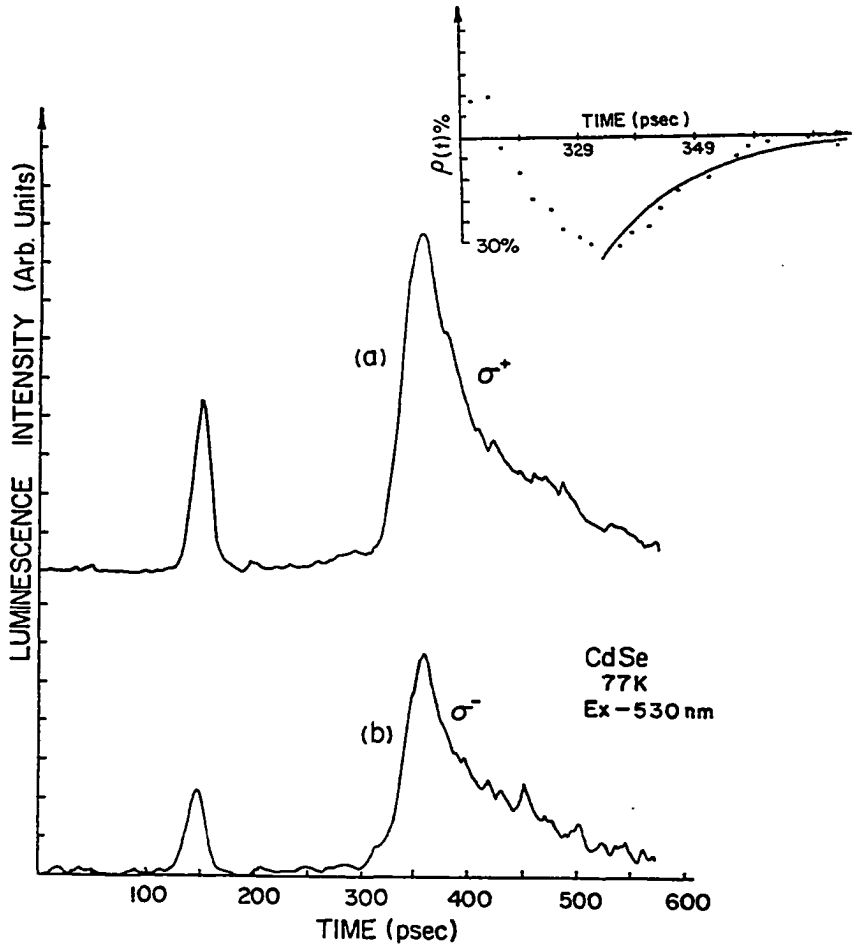

FIGURE 4.5.1

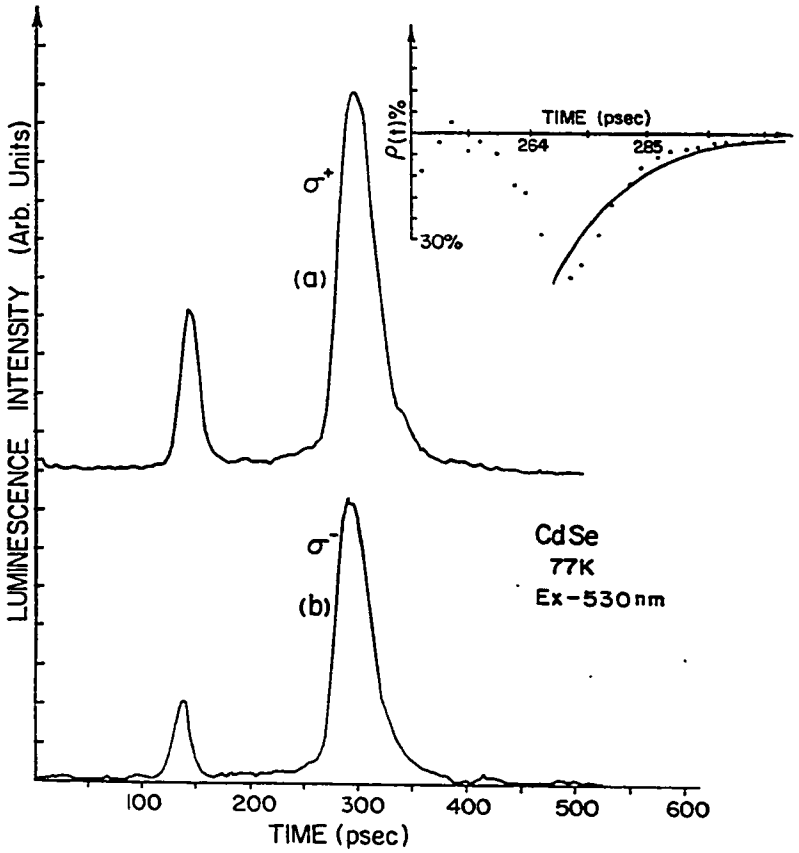

FIGURE 4.5.2

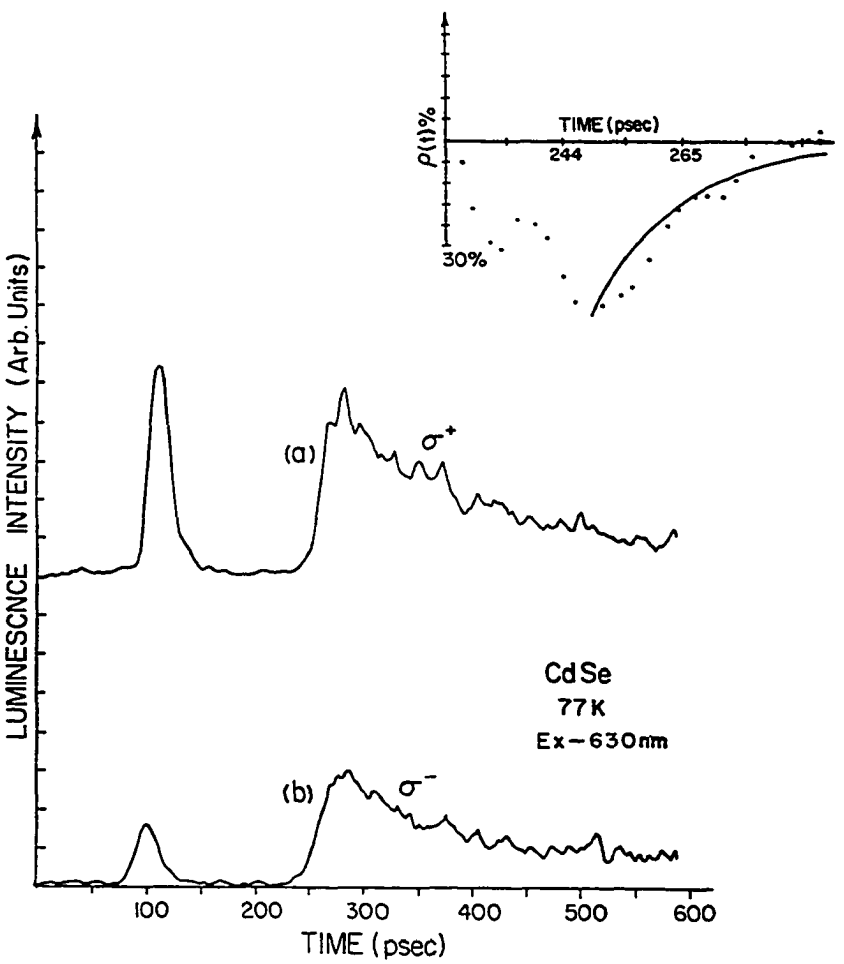

FIGURE 4.5.3

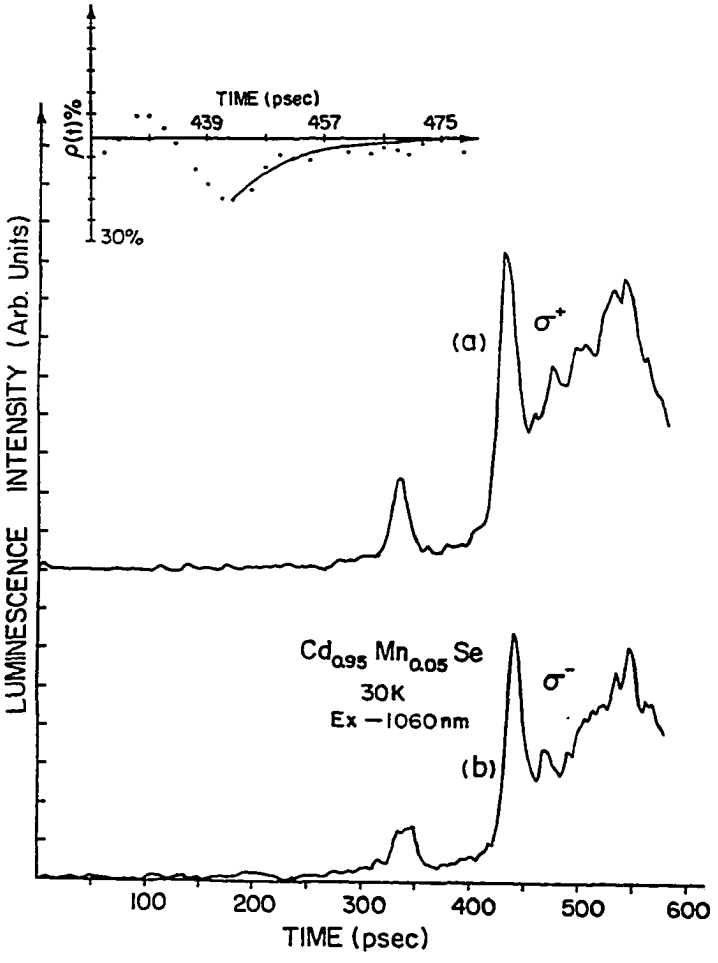

FIGURE 4.5.4

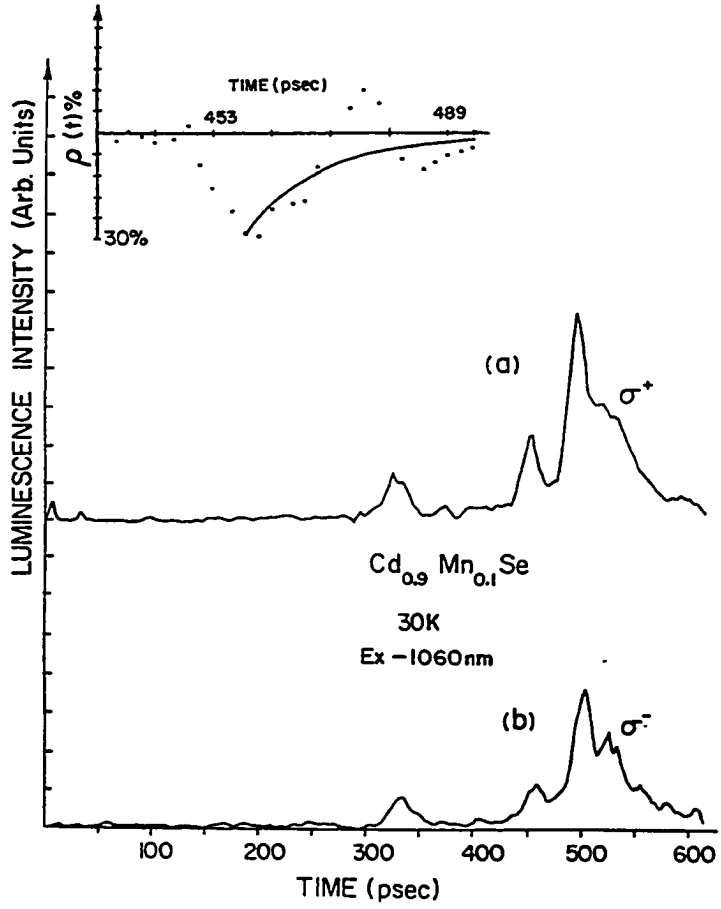

FIGURE 4.5.5

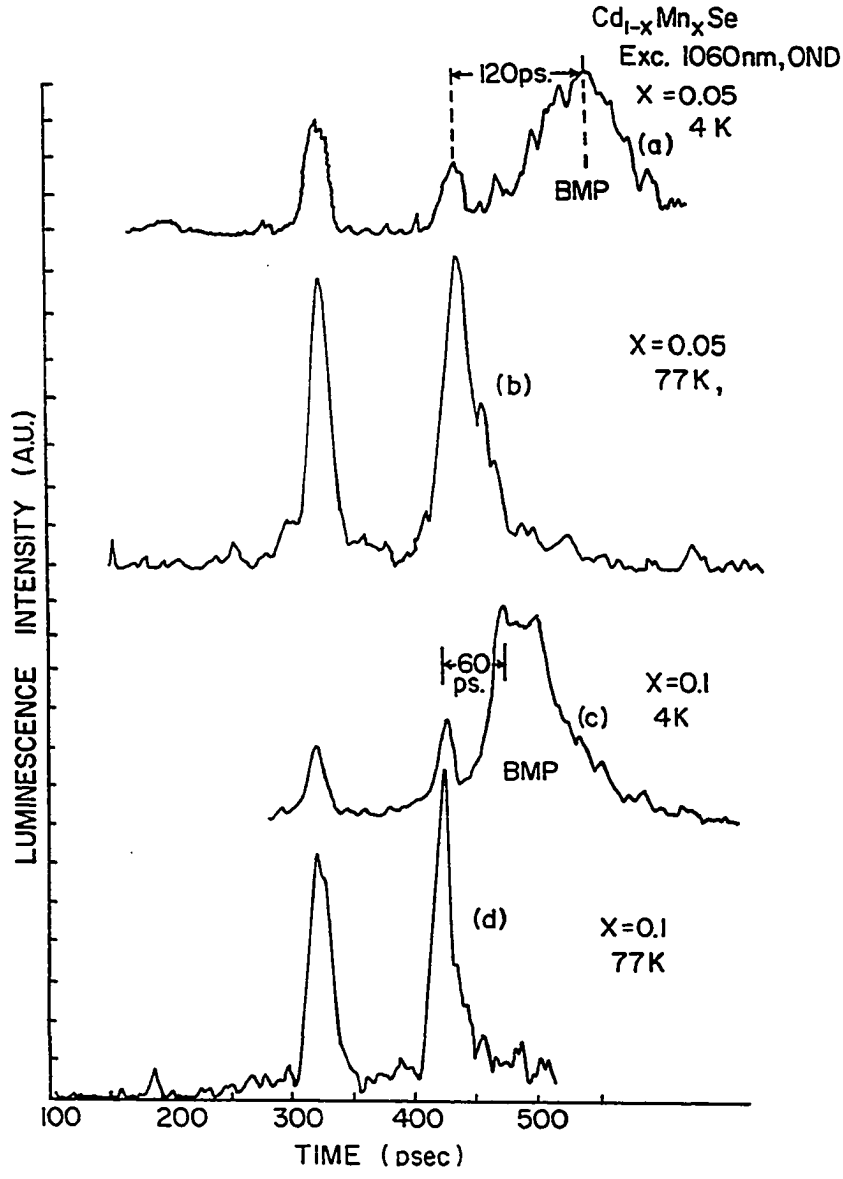

FIGURE 4.5.6

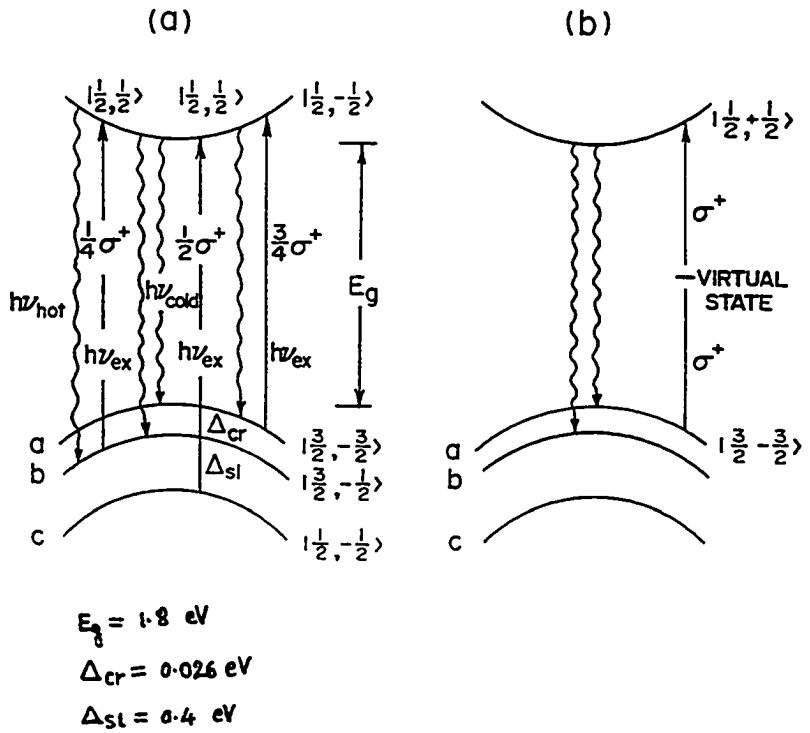

FIGURE 4.6.1

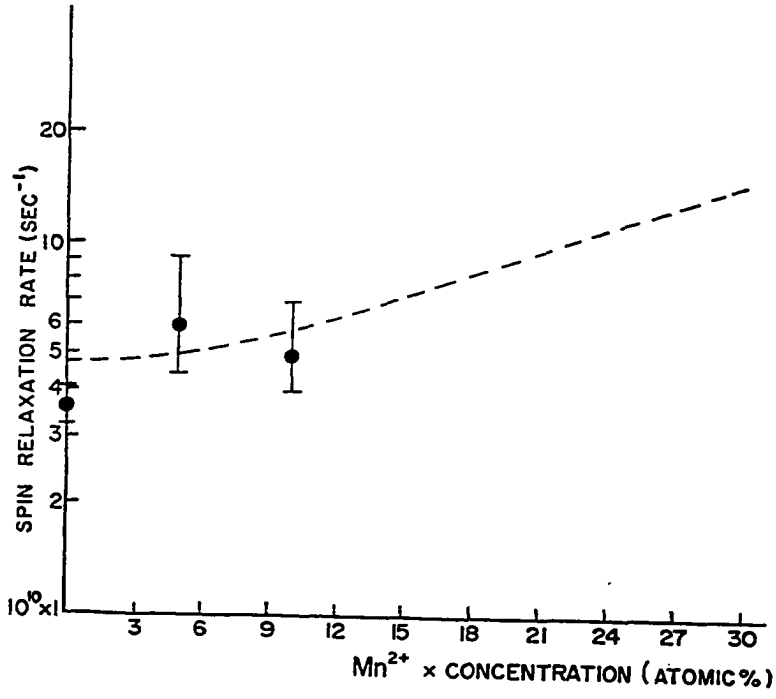

FIGURE 4.6.2

EXPERIMENTAL CONDITIONS and MEASUREMENTS					THEORETICAL VALUES	
SAMPLE	ρ_0(%)	Ts (psec)	EXCITATION WAVELENGTH (nm)	PHOTO LUMINESCENCE WAVELENGTH (nm)	ρ_0(%)	Ts (psec)
CdSe X=0 (77K)	44±5	24±5	530	620 - 660	48	21
	36±5	28±5	530	680 - 700	32	21
	48±4	30±4	630	680 - 700	50	21
$Cd_{0.95}Mn_{0.05}Se$ (30K)	18±4	16±5	1060	660 ± 10	63	20
$Cd_{0.9}Mn_{0.1}Se$ (30K)	28±5	20±5	1060	620 - 660	64	17

TABLE 4.7.1

CHAPTER V

Influence of Mn^{2+} Ions on Bound States of Carriers in Wurtzite Semimagnetic Semiconductors $Cd_{1-x}Mn_xSe$.

5.1 INTRODUCTION

Over the past three years semimagnetic semiconductors like $Hg_{1-x}Mn_xTe$, $Cd_{1-x}Mn_xTe$ and $Cd_{1-x}Mn_xSe$, have gained a lot of attention[1,2] because of their fascinating and useful properties. Most of these properties evolve around the large magneto-optic effect[1,2] due to strong exchange interactions between spins of the localized electrons and the band electrons. The interactions affect the energy band and impurity level parameters of these semiconductors. The band parameters[1] can be varied over a wide range by changing the Mn concentration and the external magnetic field. In principle, a semiconductor in which some of the lattice constituent atoms (cations) are replaced by magnetic ions, can be regarded as a dilute semimagnetic semiconductor (DMS). The crystal structure, as well as the mechanical, optical and electrical properties of DMS are qualitatively similar to their non-magnetic "parent" compounds; that is, $Cd_{1-x}Mn_xTe$ resembles CdTe in many respects. In DMS the substitutional Mn^{2+} ions are generally considered to be randomly distributed in the lattice although there is evidence for strong deviations from a random statistical distribution. The half filled $3d^5$ shell of the Mn^{2+} ion is highly local-

ized at the ion site, and contains five electrons with aligned spins, giving each individual ion a magnetic moment[3] of five Bohr magnetons (S=5/2). The interaction among these localized spins are interesting in their own right, giving insight into the behavior of a disordered magnetic system. Most of the knowledge[1,2] of the magnetic properties of DMS comes from specific heat, low-field magnetic susceptibility, high-field magnetization, neutron scattering, and electron paramagnetic resonance (EPR) studies. Optical measurements unlike the previously mentioned ones probe the local environment rather than that of the bulk and reveal interactions between the carriers and the Mn^{2+} ions.

Recently, we have determined[4] the effect on spin relaxation rates of free carriers due to the exchange interaction. It seems reasonable to assume that within a free carrier lifetime of ≈ 40 psec, a carrier undergoes one or two collisions with a high probability of spin exchange. This situation is different compared to an e-h pair in an excitonic state which encloses within its orbit a large number of Mn^{2+} ions. Due to the long lifetime (> 1 nsec) of this bound state, the carriers slowly digs in an attractive potential well for itself. The final state is more localized in nature and is known as a bound magnetic polaron[5,6,7] (BMP). The luminescence observed from this state reveals the exchange energy contribution to the binding energy, changes in the binding energy due to antiferromagnetic interaction among the enclosed Mn^{2+} ions and

also the non magnetic bandgap shifts.

In this article, the effects of Mn^{2+} ions on the bound state of carriers using steady state and picosecond time resolved spectroscopy are presented. Using steady state luminescence from $Cd_{1-x}Mn_xSe$ samples within the range $0 \leq x \leq 0.86$, we have measured bandgap changes as a function of Mn concentration. Combined with the x-ray lattice constant data[8], we are able to deduce the individual conduction and valence band deformation potentials[9,10,11]. In doing so, we demonstrate the importance of the localized nature of the Mn^{2+} ion excited state[12,13] ^4G in determining the individual contribution of the deformation potentials of the conduction and valence bands to the bandgap.

The temperature dependence of the luminescence peak position for a given $Cd_{1-x}Mn_xSe$ sample was studied. Using the CdSe luminescence peak as a reference position, we are able to obtain bound magnetic polaron energies after taking into account the temperature and x dependence of the bandgaps. In this analysis it was also assumed that the binding energies of the exciton state prior to taking into account any exchange energy does not depend on x. The BMP radius was obtained using the theory developed by Spalek et al[5] and the smaller radii for BMP's in large x samples ($x > 0.3$) are interpreted as due to the BMP localized on one of the Mn^{2+} ions. This BMP is termed as BMP-II. This is contrary to the ordinary type BMP(-I), which is localized on a donor site in small

x (< 0.3) samples. The temperature dependence of the BMP luminescence peak position and intensity shows an anomaly around ~60 K. This anomaly is explained in terms of the Neel' temperature behavior of the antiferromagnetic interaction[14,15,16] among Mn^{2+} ions. From the picosecond time resolved luminescence data, we have deduced BMP formation times. Furthermore, the two BMP regimes (x >0.3 and x <0.3) show different temporal behavior.

5.2 BACKGROUND

Similar to many ternary semiconductors[17] like, the bandgap of $Cd_{1-x}Mn_xSe$ increases linearly[18] with x. Low-field electroreflectance (ER) data on $Cd_{1-x}Mn_xSe$ in the energy range 1.2-2.7 eV for various temperatures and compositions reveal transitions from the top valence band (split by the hexagonal crystal field and spin-orbit coupling) to the conduction band. The ER study for a temperature range of 4-300 K and composition range of $0 \leq x \leq 0.45$ have shown this linear behavior.

The bandgap varies[18] as,

$$E_g = 1.829 + 1.63x \qquad \text{at 4 K,} \qquad (5.2.1)$$

$$E_g = 1.807 + 1.32x \qquad \text{at 77 K,} \qquad (5.2.2)$$

and

$$E_g = 1.725 + 1.16x \qquad \text{at } 300 \text{ K} \qquad (5.3.3)$$

in eV.

These bandgap dependences on x and temperature have been used in our analysis of BMP binding energies obtained from the observed dependence of luminescence peak position on x and temperature. Since the ER techniques[19] (pressure modulation) are sensitive to the pressure sensitive states, it reveals the fundamental band edge due to the relatively large deformation potential of the conduction band. Thus, a Mn^{2+} level with a small crystal field parameter D_q could easily go undetected in an ER measurement. However, in a luminescence experiment it is possible (for $x > 0.3$) to observe a transition from the excited Mn^{2+} level to the valence band.

In directgap semiconductors the photoluminescence peak is observed at about $\sim E_g + 1/2k_BT_e$ eV for high temperatures and above bandgap excitation, where T_e is the free carrier temperature. At low temperatures free carriers form free and bound excitons. In these circumstances the luminescence peak will be at $\sim E_g - E_x$ and $E_g - E_b$, where E_x and E_b are the binding energies of the free excitons and bound excitons, respectively. For dilute semimagnetic semiconductors further complications arise because of the temperature and concentration dependent red shift[20,21] of these excitons

due to the exchange interaction between the electrons(e) and holes(h) with Mn^{2+} spins. Experimentally, it has been observed that for a Mn concentration of 40% in $Cd_{1-x}Mn_xSe$ the band gap energy of 2.2 eV (4K) is equal to the Mn^{2+} first excited state $^4T_1$.

The large changes in the band gap of mixed semiconductors are related to the change in the crystal lattice parameter. In the case of CdMnSe, the atomic radii of Mn, Cd and Se are 1.30 Å, 1.56 Å, and 1.17 Å, respectively. When Mn ($4S^2$ states) becomes an isoelectronic substituent for Cd ($5S^2$ states), the lattice parameter becomes smaller with increases in x. This can be viewed as host crystal CdSe being under x dependent hydrostatic pressure. For the wurtzite structure of $Cd_{1-x}Mn_xSe$ the lattice parameters are found to vary[8] as,

$$a = 4.049 - 0.12x \text{ Å} \qquad (5.2.4)$$

and

$$c = 6.629 - 0.193x \text{ Å} \qquad (5.2.5)$$

We have used this x-ray data in evaluating deformation potentials in the conduction and valence bands. The average lattice parameter change Δa is $= 0.15x$ Å.

5.3 MATERIAL

The single crystals of $Cd_{1-x}Mn_xSe$ ($0.045 < x < 0.42$) were grown using the Bridgman method at Purdue University. The composition of the samples was checked by atomic-absorption (Schwazkopf Microanalytical Laboratory, Inc). All of the samples used in the experiment are A-plate with the c-axis parallel to the linear polarization of the excitation beam. The samples of CdSe were grown by Cleveland Crystal, Inc.

5.4 METHODS

a) **Steady State Photoluminescence:**

An argon ion laser was used to excite the samples at either 488 nm or 477 nm wavelengths. The typical power densities used in the experiment were in the range of 10-100W/cm^2. The excitation beam was chopped at 900 Hz. The samples were mounted on a cold finger in an optical helium dewar. The sample temperature was measured within ±2 K using a silicon diode. The photoluminescence was collected and imaged into a double Spex-1/2m spectrometer and detected by a RCA-7265 photomultiplier tube (S-20) and a PAR lock-in-amplifier tuned to 900 Hz.

b) **Time Resolved Photoluminescence:**

The photoexcited carriers were produced using a Nd:glass laser mode locked by Kodak A9860 dye dissolved in dichloroethane.

Single pulse (6 psec) two-photon excitation (λ=1060 nm) was achieved using a spark gap and Pockel cell for pulse selection[22] from the mode locked train. Single photon excitation (λ= 530 nm) was achieved using second harmonic generation in KDP. The photoluminescence was collected and focused onto the entrance slit (50μ) of a streak camera for time resolved photoluminescence studies. An attenuated laser pulse (530 nm) was directed into the entrance slit of the streak camera prior to the arrival of luminescence. The prepulse was used as a marker for overlapping various data files for averaging and finding the start of luminescence after the excitation pulse. The electronic window set on the video camera controlled by a microprocessor enabled us to record and store (appendix B1) the data in a minicomputer. The over all streak camera resolution was 13 psec. All the time resolved data were corrected for nonlinearity of the streak rate using computer software (appendix).

5.5 EXPERIMENTAL RESULTS:

In the steady state luminescence measurements we typically observed a narrow peak at higher energy and a broad peak on the low energy side of the spectra (Figs.5.5.1 and 5.5.2). These two bands will be termed hereafter as the yellow emission and red emission. The yellow luminescence have been attributed to bound magnetic polaron emission and also could be associated approxi-

mately (± 30 mev) to the bandedge emission for x <0.3. This is because of linear dependence of bandgap (see for example Eq.(5.2.1)) and also of the binding energy (see Eq.(5.6.21)) of BMP on x. Using the x dependence of steady state yellow luminescence peak position, the optical deformation potential for conduction and valence bands were estimated. The temperature dependence of the yellow luminescence has been used in obtaining the BMP energies for various samples. The red luminescence has not been found to be relevent to the band structure. The time resolved measurements of yellow luminescence were used in obtaining BMP formation time. The time resolved measurement for red luminescence can not be interpreted in terms of any mechanism.

a) Yellow Luminescence:

Fig.(5.5.3) and (5.5.4) summarize the steady state luminescence spectra for different x and at 4K. The temperature dependence of the luminescence peaks are summarized in Figs.(5.5.3), (5.5.4), (5.5.5), (5.5.6), and (5.5.7). The yellow emission for CdSe is due to donor bound excitons and its peak position monotonically shifts towards the red at a rate of -2×10^{-4} eV/K (Fig. 5.5.3(a)). The intensity of the peak also decreases at a rather slow rate with temperature. The intensity at 200K is 35% of the intensity at 4K (Fig. 5.5.4(a)). The temperature dependence of the peak position of the luminescence for the sample with x=0.045 is almost

identical (Fig. 5.5.3(b)) to CdSe (x=0). In this case the rate of the shift is -2.7×10^{-4} eV/K. However, the observed intensity decreased faster with the increase in temperature (Fig. 5.5.4(b)). The intensity at 200K is 10% of the intensity at 4K. For a larger x (i.e. x=0.092), the general trend of the shift (Fig. 5.5.3(c)) of the luminescence peak (-2.4×10^{-4} eV/K) is the same as discussed earlier except for the peak position whose shift within the temperature range of 35-55K is unusual. Even the intensity decreases (Fig. 5.5.4(c)) rapidly compared to previously discussed samples of x=0 and 0.045. The intensity decreased to 5% at 80K from its maximum value at 4K. Within the temperature range of 50-55K the intensity increases with increase in the temperature. For the x=0.3 sample the peak position within the temperature range of 4-65K shows a non-monotonic behavior (Fig. 5.5.3(d)) but for $T \geq 65K$ the peak position shifts towards lower energy at a rate of -5.3×10^{-4} eV/K which is considerably larger than for samples with x=0, 0.045 and 0.092. For x = 0.3, the peak intensity also shows a nonmonotonic behavior (Fig. 5.5.4(d)) for the temperature range of 4-65K. The peak position and the intensity is maximum at 65K. For the sample with x=0.36, the peak position of the luminescence shifts towards lower energy (red shift) for the temperature range of 4-110K (Fig. 5.5.5(a)). Within the 110-130K range the peak position is constant at ~ 2.164 eV. For temperatures > 130K the peak shifts linearly with a slope of -5×10^{-4} eV/K (Fig. 5.5.5(a)). The

intensity also decreases (Fig. 5.5.5(b)) at 200K to 8% of its maximum value at 5K. But the decrease is rapid up to 70K and slower at higher temperature. The same temperature behavior of the peak position and intensity of the luminescence is shown (Fig. 5.5.6(a) and 5.5.6(b)) by the sample with x = 0.42. However, the abnormal features are more distinct than for the sample with x=0.36. Here, the peak shifts towards the low energy up to 65K. For the range of temperature 65-110K the shift is oscillatory with temperature. For temperature > 110 K the peak position shifts at a rate of -5.4×10^{-4} eV/K. The intensity decreases with temperature and becomes 6% of the maximum (at 4K) at 180K. The intensity shows a cusp at 80K. The sample with x=0.86 shows complex temperature behavior whose features are very distinctly shown in Figs. 5.5.7(a) and 5.5.7(b). It is interesting to note that the intensity increases for the range 110K-200K.

b) Red Luminescence:

We have observed in addition to BMP (yellow) luminescence an emission around 1.8 ev (see Figs. 5.5.1 and 5.5.2) for all samples of $Cd_{1-x}Mn_xSe$ ($0.045 \leq x \leq 0.86$). This emission is weak in the case of samples with x=0.045 and x=0.092. The luminescence for x=0.045 with its peak position at 1.75 eV, does not change with temperature (±5mev). The intensity of this luminescence decreases slowly to 10% of the peak intensity (15K) around 80K. There is no

abnormal behavior within the range of 4-80K. On the contrary, the sample with x=0.092 shows a structure (Fig. 5.5.8(a)) at 60K both in the dependence of the peak position (~1.8 ev) and intensity (Fig. 5.5.9(a)) on temperature of the luminescence. The same features with more prominence are observed in the sample with x=0.3. In this case the peak position (~ 1.91 ev) (Fig. 5.5.8(b)) and intensity shows an abnormal temperature dependence (Fig. 5.5.9(b)) at 60K. Similar features are present in the samples with x=0.36 and 0.42. The sample with x=0.86 shows much more complex behavior in which the peak position (Fig. 5.5.8(c)) shifts towards higher energy and the intensity (Fig. 5.5.9(c)) of the peak shows a change in the temperature dependence at ~70K. The ratio of the luminescence intensities with polarization perpendicular to the c-axis to that parallel to the c-axis i.e. $I_{\perp}$ /$I_{\parallel}$ is plotted in Fig.(5.5.10). It is clear that for samples with $0 \leq x < 0.1$ the ratio monotonically decreases, while for $0.42 \geq x \geq 0.36$ it is almost the same (~ 2). It is very interesting to note that the ratio is less than 1 for x=0.86. This indicates that the valence band symmetry involved is mixed rather than Γ_9 and Γ_7 as is the case in CdSe.

c) Time Resolved Yellow Luminescence

Time resolved kinetics have been measured for yellow luminescence in five samples with different x and low temperatures ~ 10K.

(1) CdSe(x=0)

The time resolved luminescence (1.8 eV) corresponding to free e-h plasma shows, when excited with a 530 nm pulse, a simple exponential decay profile with a 1/e time of ~ 120 psec and a rise time of ~ 20 psec (Fig. 5.5.11(a)). There is no change in the decay profile even for a reduction of the excitation intensity by a factor of 30. With the maximum two photon excitation I_o (~ 2×10^{17} photons/cm^2), the luminescence peak is shifted by 185 psec as measured from the start of one photon excitation (Fig. 5.5.11(b)). For a reduction in the intensity by a factor of 4 the delay is reduced to 100 psec. By reducing the excitation intensity by a factor of 10, the delay becomes negligible (Fig. 5.5.11(c)).

(2) $Cd_{0.95}Mn_{0.05}Se$

The time resolved luminescence at 4K shows an instantaneous peak with lifetime ~ 20 psec, which is followed by a delayed peak (Fig. 5.5.12(c)). The delayed peak occurs after 124 psec for the maximum two photon excitation and is absent for one photon excitation. The delayed peak disappears for $1/10 I_o$ two photon excitation fluence. The delayed peak also disappears at 77K (Fig. 5.5.12(d)).

(3) $Cd_{0.9}Mn_{0.1}Se$

The characteristics of the time resolved luminescence are similar to the one observed in the sample with x = 0.05 except that the delay of the second peak is ~ 60 psec (Fig. 5.5.13(c)).

The delayed peak also disappears at 77K (Fig. 5.5.13(d)).

(4) $Cd_{0.64}Mn_{0.36}Se$

The luminescence peak is delayed by 80 psec at the maximum two photon excitation fluence (I_o)(Fig. 5.5.14(a)). At $1/5I_o$ excitation fluence, the rise time is ~ 150 psec (Fig. 5.5.14(b)), and for $1/10I_o$, the rise time is ~ 200 psec (Fig. 5.5.14(c)).

(5) $Cd_{0.58}Mn_{0.42}Se$

The luminescence delay with intensity of excitation is entirely different than the ones observed in samples with $0 \leq x \leq 0.1$. For maximum excitation intensity the luminescence maximum ocurs within 30 psec (Fig. 5.5.15(d)) and the delay increases as the excitation intensity of the two photon excitation is decreased by a factor of 10 (Fig. 5.5.15(b)). The maximum delay is 100 psec. The one photon excitation shows a similar rise time (Fig. 5.5.15(a)) as in the maximum two photon excitation. However, the luminescence lifetime is longer (100 psec) than one observed in two photon excitation (20 psec).

d) Time Resolved Red Luminescence

The red luminescence observed for x=0.045 shows no structure and has a lifetime (1/e) of 20 psec over the temperature range 4-77 K (Figs. 5.5.12(a) and 5.5.12(b)). On the contrary, the sample

with x=0.092 shows a second peak separated by 30 psec from the first one (Figs. 5.5.13(a) and 5.5.13(b)). For samples x=0.42 and 0.36 (x>0.3) the red luminescence shows a very different decay profile. In this case, the luminescence shows a risetime of ~ 200 psec and a decay time of 1.2 nsec (Fig. 5.5.16).

5.6 DISCUSSION

In wurtzite CdMnSe the arrangement[23] of the atoms up to and including next nearest neighbors is identical to that of a zinc-blende crystal such as CdMnTe. In each case, the Mn^{2+} ion is situated at a lattice site with a tetrahedral arrangement of the nearest neighbors. Because of the similarity of the arrangement for these DMS, any difference observed in properties which are influenced by a short range interaction between the Mn^{2+} and the local environment, can be attributed to the different chalcogen occupying the nearest neighbor site. In zincblende structures the kinetic and potential energy contribution to the deformation potential for valence bands are of opposite sign[24] and the net deformation potential is small, hence the maximum of the valence band energy does not change significantly with contraction. Here, we must point out that the temperature dependence of the valence and conduction bands are different. This is primarily because of the fact that the temperature dependence includes a Debye-Waller-factor (DWF) and a volume term. The volume term contribution is

atleast 10% smaller than the DWF term. Hence, in this case the conduction band temperature coefficient is insignificant compared to the valence band temperature coefficient[25,26].

The temperature dependence[27,28] of the photoluminescence peak of $Cd_{1-x}Mn_xTe$ for $x < 0.4$ and for $x > 0.4$ are essentially the same ($\sim 4 \times 10^{-4}$ eV/K) even though in the former ($x < 0.4$) the transition involved is band-band, while in the latter ($x > 0.4$) it is from a Mn^{2+} excited ionic state to the p-d hybridized[29] valence state. This is consistent, since the valence state is the main contributor and the ionic state has little effect due to the temperature dependence of the crystal field parameter D_q. As a matter of fact the crystal field parameter D_q decreases with temperature due to an increase in the lattice constant[30,31], which in turn would increase the energy difference for the transition.

The essential difference observed between the $Cd_{1-x}Mn_xTe$ and $Cd_{1-x}Mn_xSe$ photoluminescence (PL) peak position dependence on x is summarized as follows. The PL peak position is essentially independent[13] of x for $x > 0.4$ in $Cd_{1-x}Mn_xTe$ at a given temperature, while our data for $Cd_{1-x}Mn_xSe$ shows that there is a break point at x=0.3 after which the PL peak increases towards higher energy less rapidly ($\sim$ 0.4 eV/x) as compared to that for $x < 0.3$ (1.2 eV/x)(Fig.5.6.1). We believe this difference is due to the difference in the crystal symmetry of these mixed crystal and not due to the different anions (Te and Se). The bandgap temperature coeffi-

cients[25] of ZnSe and ZnTe, both of which have zincblende symmetry, are -5.1×10^{-4} eV/ K and -5.5×10^{-4}eV/K, respectively. These results, together those from other examples[25] like GaSb and InSb both of which are zincblende, shows that for a given crystal symmetry the crystals with different anions show similar bandgap temperature dependences (including the volume contribution). Hence, in spite of the fact that the anions (Te and Se) are different, the x dependence of the PL peak in $Cd_{1-x}Mn_xSe$ for $x > 0.3$ is due to the valence band shift (in addition to the expected conduction band shift) which is probably related to the different crystal symmetry.

a) Deformation potential

In order to analyze our data, we first review the stress work of Grynberg[10] on CdSe. According to their data the absorption edge does not shift by stress when $\hat{E} \parallel \hat{C}$ and $\hat{P} \perp \hat{C}$ or $\hat{P} \parallel \hat{C}$. They did not observed any shift when $\hat{E} \perp \hat{C}$ and $\hat{P} \perp \hat{C}$ ($\hat{E}$, $\hat{P}$, and $\hat{C}$ are unit vectors along absorption photon polarization, uniaxial stress, and the c- axis, respectively). However, a considerable shift of the absorption edge was observed when $\hat{E} \perp \hat{C}$ and $\hat{P} \parallel \hat{C}$. The observed shift of the absorption edge is given by, $\phi = 4\times10^{-6}$ eV/Kg/cm^2. Knowing the value of ϕ, and using the theory developed by Pikus[11], one can obtain deformation potentials for the conduction and valence bands as follows.

The energy shift relations of conduction, Γ_9 valence and Γ_7 valence bands as a function of various stress component is given by[10],

$$E_c = E_c^{\circ} + D_1 \varepsilon_{11} + D_2 \varepsilon_L, \tag{5.6.1}$$

$$E_{\Gamma_9} = E_{\Gamma_9}^{\circ} + \delta_1 + \delta_2 \tag{5.6.2}$$

and

$$E_{\Gamma_7} = E_{\Gamma_7}^{\circ} + \delta_1 + \gamma\delta_2 \tag{5.6.3}$$

where E_c°, $E_{\Gamma_9}^{\circ}$, and $E_{\Gamma_7}^{\circ}$ are the band energies before stress is applied and $\varepsilon_{11} = \varepsilon_{zz}$, $\varepsilon_L = \varepsilon_{xx} + \varepsilon_{yy}$, $\delta_1 = C_1 \varepsilon_{11} + C_2 \varepsilon_L$, $\delta_2 = C_3 \varepsilon_{11} + C_4 \varepsilon_L$. The D_1, D_2, C_1, C_2, C_3, and C_4 are the components of the deformation potential tensors for the conduction and valence bands, respectively.

The value of γ for the band model as presented by Thomas and Hopfield is given by[10,11],

$$\gamma = (\frac{1}{2})(1 - \frac{\Delta_1 - \Delta_2}{[(\Delta_1 - \Delta_2)^2 + 8\Delta_2^2](\frac{1}{2})}) \tag{5.6.4}$$

where Δ_1 - crystal field splitting, $3\Delta_2$ - spin orbit splitting, and γ for CdSe is 0.643.

The measurement of the energy gap, which gives us the change in the relative positions of the bands, shows that for $\hat{P} \perp \hat{C}$, $\hat{E} \parallel \hat{C}$ and $\hat{E} \perp \hat{C}$ the energy gap is constant. Thus,

$$D_1 \varepsilon_{11} + D_2 \varepsilon_L - [C_1 \varepsilon_{11} + C_2 \varepsilon_L + \gamma(C_3 \varepsilon_{11} + C_4 \varepsilon_L)] = 0 \quad (5.6.5)$$

$$D_1 \varepsilon_{11} + D_2 \varepsilon_L - [C_1 \varepsilon_{11} + C_2 \varepsilon_L + C_3 \varepsilon_{11} + C_4 \varepsilon_L] = 0 \quad (5.6.6)$$

and for $\hat{P}$ $\hat{C}$,

$$D_1 \varepsilon_{11}' + D_2 \varepsilon_L' - [C_1 \varepsilon_{11}' + C_2 \varepsilon_L' + \gamma(C_3 \varepsilon_{11}' + C_4 \varepsilon_L')] = 0 \quad (5.6.7)$$

$$D_1 \varepsilon_{11}' + D_2 \varepsilon_L' - [C_1 \varepsilon_{11}' + C_2 \varepsilon_L' + C_3 \varepsilon_{11}' + C_4 \varepsilon_L'] = \phi.P \quad (5.6.8)$$

where $\phi = dE_g/dP \big|_{\hat{P} \parallel \hat{C}} = 4.10^{-6}$ eV/Kg/cm^2

The deformation potential tensor can be evaluated using the stress tensor and the elastic modulii matrix for CdSe given by Berlincourt et al[32]. It now follows that $\varepsilon_{11} = PS_{13}$, $\varepsilon_L = P(S_{11} + S_{12})$, $\varepsilon_{11}' = PS_{33}$ and $\varepsilon_L' = 2PS_{13}$.

Solving these equations i.e. (5.6.5), (5.6.6), (5.6.7), and (5.6.8), the calculated deformation potentials are,

$$D_1 - C_1 = 2.17 \text{ eV},$$

$$D_2 - C_2 = -1.5 \text{ eV},$$

$$C_3 = 3.4 \text{ eV},$$

and

$$C_4 = -2.3 \text{ eV}. \qquad (5.6.9)$$

For hydrostatic pressure ($\varepsilon_{11} = \delta$ and $\varepsilon_L = 2\delta$), the equations ((5.6.1) and (5.6.2)) reduce to:

$$E_c = E_c^0 + (D_1 + 2D_2)\delta, \qquad (5.6.10)$$

$$E_{\Gamma_9} = E_{\Gamma_9} + (C_1 + 2C_2 + C_3 + 2C_4)\delta, \qquad (5.6.11)$$

$$= E_{\Gamma_9} + (D_1 + 2D_2 - 0.37)\delta, \qquad (5.6.12)$$

and

$$E_g(\delta) = E_g^0 + 0.37\delta. \qquad (5.6.13)$$

In our case the hydrostatic pressure is caused, as mentioned earlier, by the replacement of Cd by Mn in $Cd_{1-x}Mn_xSe$. We assume

that the mechanical properties do not change significantly with this substitution. We can correlate the stress dependence of the band gap of CdSe and our experimental observation of the band gap dependence of $Cd_{1-x}Mn_xSe$ on x as follows.

$$E_g(x) = E_g^{\circ} + 1.2x \qquad (5.6.14)$$

This is the approximate band gap dependence observed in Fig.(17) and by Stankiewicz[18] et al. The pressure caused by fractional Cd replacement, using Eq.(5.6.13) and Eq.(5.6.14), is given by,

$$\delta = 1.2/0.37x \ . \qquad (5.6.15)$$

Hence, Eq.(5.6.10) and (5.6.11) are rewritten as,

$$E_c = E_c^{\circ} + (D_1 + 2D_2)(3.2x) \qquad (5.6.16)$$

$$E_{\Gamma_9} = E_{\Gamma_9} + (D_1 + 2D_2 - 0.37)(3.2x) \qquad (5.6.17)$$

For $x > 0.3$, the luminescence observed corresponds to a Mn^{2+} excited state and the terminal valence band maximum. If the Mn^{2+} levels remain fix with respect to the vacuum level then the dependence of luminescence peak position on x can be related to the x-dependent shift of the valence band maximum. Thus, using

Eq.(5.6.17) and the experimental observation summarized in Fig.(5.6.1), we get,

$$3.2(D_1 + 2D_2 - 0.37) = -0.4 \text{ (slope\#2 = 0.411 eV/x)}$$

by taking into account the negative energy increase of the valence band with x. Thus, using Eq.(5.6.16) and (5.6.17), the deformation potentials of the conduction and valence bands are given by,

$D_1 + 2D_2 = 0.25$ eV/Kg/cm^2 and $D_1 + 2D_2 - 0.37 = -0.12$ eV/Kg/cm^2.

Hence,

$$E_c = E_c^{\circ} + 0.8x \qquad (5.6.18)$$

and

$$E_{\Gamma_9} = E_{\Gamma_9} - 0.38x \; . \qquad (5.6.19)$$

Since the stress involved is localized around the Mn atom the deformation potential obtained in this case is the optical deformation potential and not the acoustical one. Using Eq.s (5.2.4) and (5.2.5) which imply average lattice parameter change $\Delta a = 0.15x$ Å along with Eqs.(5.6.18) and (5.6.19), the values of conduction band and the valence band deformation potentials in conventional units of eV/cm are 0.5×10^9 eV/cm and 0.24×10^9 eV/cm, respectively. In the above analysis it is assumed that the role of Mn substitution is to generate local strain in the basic host crystal CdSe and the

values of deformation potentials are for $Cd_{1-x}Mn_xSe$ for $x \leq 0.5$. The optical deformation potential plays an important role in hot carrier energy relaxation via non polar optical phonon emission as the polar interaction gets screened at high carrier densities[33]. Thus, our photoluminescence technique brings out an important difference between the zincblende and wurtzite crystal structure in terms of a very small valence deformation potential in zinc blende semiconductors compared to those of wurtzite structure. The measured value of the optical deformation potential is in good agreement with the literature i.e. 10^9 eV/cm.

b) Bound magnetic polaron energies

The second part of the study consists of the determination of the PL peak position dependence on temperature for $0 \leq x \leq 0.86$. From this study bound magnetic polaron energies were determined for a wide range of temperature and Mn concentration. The temperature dependent shifts are of the order of 10 meV in addition to the rigid bandgap shift due to the Debye-Waller factor[25,26](DWF) term or phonon contribution. This study brings out the small but clear temperature and x dependent spin exchange interaction between the Mn^{2+} ions and the bound localized state of the electron-hole plasma. The exchange interaction is represented as a magnetic polaron by Gennes[7,34] and this concept was developed further by Kasuya et al[35] to explain the metal-insulator transi-

tion in Eu-rich EuO through the d-f exchange interaction. It has also been used by Dietl and Spalek[5,6] to explain physical properties, i.e. spin flip Raman scattering of bound carriers, due to the presence of bound magnetic polarons (BMP) in $Cd_{1-x}Mn_xSe$.

An extensive theoretical treatment of BMP in DMS has been discussed by many authors[5,6,36,37] and a large number of experiments in various DMS explain the spin flip Raman scattering (SFRS) experiments[36,37] involving donor bound electrons. Planel et al[37] have derived the following expression for the mean BMP exchange energy,

$$< E_{BMP} > = \frac{3E_p k_B T + E_p^2}{E_p + k_B T} , \qquad (5.6.20)$$

where polaron energy

$$E_p = \left[\frac{S(S+1)}{12} \right] (N_o \alpha)^2 \left(\frac{xS_o}{S}\right) (8\pi a^3 N_o)^{-1} (k_B(T + T_{AF}))^{-1} . \qquad (5.6.21)$$

In the above expression, S = 5/2 is the electron spin quantum number of Mn^{2+} ions, xS_o/S can be interpreted[37] as an effective concentration, $N_o = 1.8 \times 10^{22}/cm^3$ is the number of cations per unit volume, and $8\pi a^3 N_o$ is the effective number of cation sites lying within the spatial extent of the electron (hole) wave function. At low temperatures $< E > = E_p$, while at high temperatures it vanishes as $3E_p$ (polaron energy E_p itself is a function of tempera-

ture). The antiferromagnetic temperature T_{AF} reflects the Mn^{2+}-Mn^{2+} antiferromagnetic interaction. Although, the expression (Eq.(5.6.21)) is derived for donor bound electron exchange detected in SFRS, in our luminescence experiments we have to take into account the hole exchange energy to calculate the total exchange induced red shift. Since the exchange coeffient $N_o\beta$ for holes is greater than for electrons (i.e. $N_o\beta \approx 1.15$ eV and $N_o\alpha \approx 0.28$ eV)[36] the major contribution to the net exchange energy comes from hole of the bound exciton even though we are concerned with n-$Cd_{1-x}Mn_xSe$. In order to compare the experimentally determined values of BMP energies with theory one needs to know the values of $\tilde{x}$ and T_{AF} usually obtained from magnetization experiments. For $x = 0.1$, the values[36] of xS_o/S (= $\tilde{x}$) and T_{AF} are 0.04 and 3 K, respectively. While for $x = 0.3$, the values[38] of $\tilde{x}$ and T_{AF} are 0.06 and 14 K, respectively. Such a remarkable difference between x and $\tilde{x}$ for $x = 0.3$ is due to cluster formation in which the spins cancel out in pairing. In order to get theoretical fittings to the experimental data of BMP energy dependence on temperature, we have used values of $\tilde{x}$ and T_{AF}, corresponding to antiferromagnetic interactions, obtained by extrapolating values from the data[41] on $Cd_{1-x}Mn_xTe$. The best least square fit obtained for $\tilde{x}$ and T_{AF} for a wide range of x ($0 \leq x \leq 0.7$) is as follows,

$$\tilde{x} = \frac{x}{2.5}(0.13 - 0.42\log x) \qquad (5.6.22)$$

$$T_{AF} = (35.3)x^{0.9} \qquad (5.6.23)$$

The values of $\tilde{x}$ for x = 0.36, 0.42 and 0.86 are 0.081, 0.079 and 0.067, respectively. The values of T_{AF} are 14K, 16K and 30K, respectively. This extrapolation is necessary since magnetization data is unavailable for these samples. For x = 0.045[42], 0.092[36], and 0.3[38], the values of $\tilde{x}$ are 0.028, 0.04, and 0.075, respectively. For the respective x, the values of T_{AF} are 2.5K, 3.8K, and 14K.

In order to extract the BMP contributions from the total binding energy of an BMP-exciton, we first take the difference in the binding energies (BE) at 100K between $Cd_{1-x}Mn_xSe$ and CdSe assuming negligible magnetic contributions (our experiments are with zero magnetic field). This difference corresponds to the rigid band gap difference (deformation potential related) at 100K. The exciton binding energies which are almost the same for the samples would be cancelled out. A similar difference obtained at 4K (or any other lower temperature T) is subtracted to find the BMP energy at 4K (or T). For bandgaps which vary linearly with x and T this can be summarized as follows,

$$E_X(T) - E_X(100) = E_o(T) - E_o(100) + [(\partial E_o/\partial x)|_T - (\partial E_o/\partial x)|_{100}]x + \Delta_{BMP} \qquad (5.6.24)$$

for $0 \leq x \leq 0.1$ and $T < 100$ K.

$$\left(\frac{\partial E_o}{\partial x}\right)\Big|_T = \left(\frac{\partial E_o}{\partial x}\right)\Big|_{10} + \left[\left(\frac{\partial E_o}{\partial x}\right)\Big|_{10} - \left(\frac{\partial E_o}{\partial x}\right)\Big|_{100}\right]\left(\frac{1}{90}\right)(10 - T)$$

(5.6.25)

The parameters $\partial E_o/\partial x|_{10}$ and $\partial E_o/\partial x|_{100}$, in the above expression, are taken from the electroreflectance data of Stankiewicz et al[18] obtained at 10K and 100K assuming $\partial E_o/\partial x$ is a linear function[18] of temperature. Substituting $\partial E_o/\partial x|_{10}$ = 1.45 eV/x and $\partial E_o/\partial x|_{100}$ = 1.3 eV/x into Eq.(5.6.25), a simple expression for determining Δ_{BMP} from the experimentally determined luminescence peak position can be written as follows: From Eq.(5.6.24)

$$\Delta_{BMP} = [E_x(T) - E_x(100)] - [E_o(T) - E_o(100)] - \left[\left(\frac{\partial E_o}{\partial x}\right)\Big|_T - \left(\frac{\partial E_o}{\partial x}\right)\Big|_{100}\right]x$$

(5.6.26)

where $E_x(T)$ and $E_x(100)$ are the peak photoluminescence energies (Fig.(5.5.3)) for $Cd_{1-x}Mn_xSe$. $E_o(T)$ and $E_o(100)$ are the peak photoluminescence energies for CdSe (Fig.(5.5.3)) at temperatures T and 100K, respectively.

For x = 0.092, using $E_x(100)$ = 1.903 eV and $E_o(100)$ = 1.785 eV, Eq.(5.6.26) reduces to,

$$\Delta_{BMP} = E_x(T) - E_o(T) - 0.132 - 1.6\times10^{-4}(10 - T)\ eV \quad (5.6.27)$$

Substituting $E_x(T)$ and $E_o(T)$ obtained from Fig.(5.5.3) in Eq.(5.6.27), Δ_{BMP} values were obtained at different temperatures (see Fig.5.6.2).

For x = 0.045,

$$\Delta_{BMP} = E_x(T) - E_o(T) - 0.062 - 7.65\times10^{-5}(10 - T)\ eV \quad (5.6.28)$$

($E_x(100)$ = 1.839 eV see Fig.5.6.3)

In the case of the x = 0.3 sample, we assumed the magnetic effects disappear only at 170K (convenient data point) and not at 100K as previously assumed for low x samples.

$$\Delta_{BMP} = [E_x(T) - E_x(170)] - [E_o(T) - E_o(170)] - \left[\left(\frac{\partial E}{\partial x}\right)\Big|_T - \left(\frac{\partial E}{\partial x}\right)\Big|_{170}\right]x \quad (5.6.29)$$

$\partial E/\partial x|_{170}$ is calculated by using the temperature range 100 - 300K i.e. from the given slopes $\partial E/\partial x|_{100}$ and $\partial E/\partial x|_{300}$ by Stankiewicz et al[18]. The values of $\partial E/\partial x|_T$ for T < 100K are determined from the known values of $\partial E/\partial x|_{10}$ and $\partial E/\partial x|_{100}$, while for T > 100 they are determined from $\partial E/\partial x|_{100}$ and $\partial E/\partial x|_{300}$. This is necessary since

the assumption of a linear relationship between $\partial E/\partial x$'s at different T's is valid for a small range of temperatures.

Hence, for T < 100,

$$\left(\frac{\partial E}{\partial x}\right)\Big|_T - \left(\frac{\partial E}{\partial x}\right)\Big|_{170} = 0.20 + 1.70\times10^{-3}(10 - T) \text{ eV}$$

and

and for T ≥ 100,

$$\left(\frac{dE}{dx}\right)\Big|_T - \left(\frac{dE}{dx}\right)\Big|_{170} = 0.05 + 7.0\times10^{-4}(100 - T) \text{ eV}$$

Thus for T < 100,

$$\Delta_{BMP} = E_x(T) - E_o(T) - 0.408 - 5.1\times10^{-4}(10 - T) \text{ eV}$$

and for T > 100,

$$\Delta_{BMP} = E_x(T) - E_o(T) - 0.363 - 2.1\times10^{-4}(100 - T) \text{ eV}$$

$$(E_x(170) = 2.120 \text{ eV and } E_o(170) = 1.772 \text{ eV })$$

The theoretical fit is poor, since for x = 0.3 the Mn^{2+} excited state is close to the band edge (see Fig.5.6.2).

We would particularly like to emphasize that for x < 0.3 the bound exciton consist of an electron and hole with effective masses $0.13m_o$ and $0.45m_o$, respectively. Contrary to the previous case for x > 0.3 the exciton is formed from an excited electron on

a Mn^{2+} ion (^4G state) and a hole of the valence band as the Mn^{2+} ^4G level moves out of the conduction band and lies between the bandgap (see Fig. 5.6.2). The hole radius of the bound exciton for $x < 0.3$ is ≈ 30 A as in CdSe but it becomes smaller as x increases due to the increased exchange energy which adjusts the radius self consistently[37]. The luminescence peak (yellow) observed from samples with $x = 0.36$, 0.42 and 0.86 is associated with the magnetic exciton localized on Mn^{2+} ions. This exciton consist of an excited electron localized on the Mn^{2+} ion and a hole in the valence band. Since the electron is strongly localized on the Mn^{2+} ion, its effective mass is essentially m_o (and not $0.13m_o$ as for conduction band electrons), while the hole effective mass is $0.45m_o$. The Bohr radius associated with this configuration is 12.35A. In order to get the BMP contribution due to the exchange interaction of this exciton with the Mn^{2+} ions within its orbit, we can safely use the argument that the temperature dependence[25] of the band gap is derived from the energy changes of the valence band. We use the temperature coefficient of -7×10^{-4} eV/K as measured by Stankiewicz[18] for the band gap for $x > 0.3$. The BMP binding energy in this case is given by the difference between the bandgap energy and the observed luminescence peak energy. Thus,

$$\Delta_{BMP} = E_x(193) + 7\times10^{-4}(193 - T) - E_x(T) \quad \text{for} \quad x = 0.36 \tag{5.6.30}$$

(see Fig. 5.6.6)

$$= E_x(185) + 7x10^{-4}(185 - T) - E_x(T) \quad \text{for} \quad x = 0.42 \tag{5.6.31}$$

(see Fig. 5.6.7)

$$= E_x(245) + 7x10^{-4}(245 - T) - E_x(T) \quad \text{for} \quad x = 0.86 \tag{5.6.32}$$

(see Fig. 5.6.8)

in eV. The temperatures 193K, 185K and 245K for samples with x = 0.36, x= 0.42 and x = 0.86, respectively have been chosen sufficiently large for which the magnetic contribution is negligible.

Using the expressions for Δ_{BMP} (Eq.s (5.6.20) and (5.6.21)), The BMP radii for different x samples were obtained at 4K. These values for BMP radii for x = 0.045, 0.092, 0.3, 0.36, 0.42 and 0.86 are 30Å, 25Å, 15Å, 12Å, 12Å, and 12Å, respectively. The 12Å radius for x>0.3 is consistent with the Bohr radius for a bound electron and hole bound state with masses m_o and $0.45m_o$, respectively.

c) Antiferromagnetic interactions within a BMP

We have observed (Fig.(5.5.3) through (5.5.9)) the effect on the intensity and energy of the PL peak of the antiferromagnetic interaction between Mn^{2+}-Mn^{2+} ions within the BMP volume. The distribution of Mn^{2+} ions in the lattice can be completely random, or it can deviate from a statistical distribution[15]. Since there

are 12 cation nearest neighbors, one can expect for $x < 1/12$ (0.083) and a random distribution (good sample), that the Mn^{2+} ions are isolated from each other. This is one of the reasons that the antiferromagnetic interaction does not show a significant contribution ($T_{AF} \approx 0$ and $\bar{x} \sim x$) in our sample of x=0.045 (paramagnetic phase). But samples with large values of x contain certain numbers of pairs, triplets, and larger clusters. For $Cd_{1-x}Mn_xTe$ with a FCC lattice, a spin glass phase has been predicted[15] for $x > x_c$ ($x_c \approx 0.17$), where x_c is the percolation threshold. This spin glass phase due to short-range antiferromagnetic interaction is directly related to the frustration of the spins on a lattice which does not allow the simultaneous minimization of all exchange energies. A similar parallel can be drawn for $Cd_{1-x}Mn_xSe$ as the number of next nearest neighbors are the same as before. The spin glass (SG) and antiferromagnetic (AF) phases are identified by their magnetic susceptibility behavior as a function of temperature. For a typical AF phase, magnetic susceptibility is independent of temperature below the N'eel temperature (T_N) with low anisotropic magnetic field. SG phase magnetic susceptibilities show maxima near the freezing temperature (T_g). We would like to note that the T_g measured by Galazka et al for $Cd_{1-x}Mn_xTe$ in the range $0.4 < x < 0.6$ lies within 8-20 K, while the N'eel temperature obtained by fitting the Brillouin function to the experimental points gives $T_N = 49$ K even for x=0.3. The spin glass transition may go

unnoticed in luminescence experiments due to the small change in the magnetic succeptibility. Giebultowicz et al[39,40] carried out neutron scattering experiments on samples with $0.6 < x < 0.7$. The observed magnetic Bragg peaks were Lorentzian-shaped and not Guassian as is usually expected for true long range magnetic order. They[40] concluded that the spins of the randomly distributed Mn^{2+} ions are ordered in uncoupled (or weakly coupled) clusters which may be due to the distribution of the Mn atoms. The size of the clusters, which when deduced from the half width at half maximum, are of the order of a few lattice constants.

It is interesting to note that for the samples with x=0.36 and 0.42, the discrepancy between the theoretical and experimental points (see Figs. 5.6.6 and 5.6.7) is largest around 60K (~ 5 meV). This, we believe is due to the clusters of various sizes having a broad distribution of $\tilde{x}$ and T_{AF} contributing to the BMP energy. $\tilde{x}$ and T_{AF} may not be constant as assumed in magnetization experiment, and the Brillouin function theoretical analysis, and could be temperature dependent. The BMP energy as a function of temperature for x = 0.86 is very complex and additional experimental work is needed. Recently Spalek et al[3] determined the nearest neighbor exchange integral J_1 using magnetic susceptibility measurements. Accordingly, $2J_1/k_B$ is 21.2 ± 0.4 K, where k_B is the Boltzmann factor. Using this value we can determine the N'eel temperature for this incomplete antiferromagnetic phase. The Neel' tempera-

ture and J_1 are related as[16],

$$k_B T_N = 2/3\ S(S+1)(-zJ_1) \qquad (5.6.33)$$

where z is the number of nearest neighbors. For the smallest cluster involving a pair of Mn^{2+} ions, z = 1. Thus the N'eel temperature T_N for $0.3 < x < 0.45$ is ~ 62K.

This is the temperature around which we observe large discrepancies due to changes in $\bar{x}$ at T_N. At T_N, the antiferromagnetic coupling breaks down and two additional single Mn^{2+} electronic spins of 5/2 are made available per previously non contributing pair for hole-Mn^{2+} exchange interactions which is manifested as an observed increase in Δ_{BMP}.

d) Red luminescence

A broad band luminescence was observed at low temperature. The steady state luminescence peak positions of this band observed in various samples are shown in Fig.(5.6.1) at 4K. This luminescence band has been observed in many Mn substituted systems like ZnS: Mn, CdMnTe, etc. It has been suggested[31] that this band is to be due to the Jahn-Teller effect. It has been argued that in CdMnTe and CdMnSe distortion of the nearest neighbor tetrahedral co-ordination of the Mn^{2+} ion may occur as a result of a non uniform envoironment of the next nearest neighbors. Such a strain

purturbation, together with coupling with either an E or T_2 vibrational mode, may produce the two nonequivalent minima in configurational co-ordinate space. As a matter of fact, the yellow and red luminescence were assigned to the higher and lower-lying minimas of the configurational co-ordinate space, respectively. The excitation occurs in this case via a $^6A_1$ (valence hybridized) → $^4T_1$ transition, or from $^6A_1$ to higher Mn^{2+} $3d^5$ states i.e. $^4T_2$, $^4A_1$, ^4E etc. Fast relaxation into the higher lying minima of the $^4T_1$ state and also tunneling into the lower $^4T_1$ minima results yellow and red luminescence, respectively. This model requires Jahn-Teller distortion of the $^4T_1$ state by ~ 250 meV. This model[31] predicts a strong pair relationship between yellow and red luminescence which we have not observed except for the anomalous luminescence intensity dependence around 60K (Fig.(5.5.4) and Fig.(5.5.9)).

Another mechanism for red luminescence has been proposed[43,44] to be the radiationless resonant energy transfer from the primarily excited Mn^{2+} ions via several other Mn^{2+} ions to certain red emission centers. In this mechanism the two bands (yellow and red) should be dependent on each other but not as strongly as the one suggested by the previous mechanism[31]. The excitation spectra for both bands should be the same within the framework of either of the mechanisms. Even the temperature dependence of both bands should be related. However, the red emission centers may be more or less dependent on the sample quality. The Jahn-Teller distor-

tion of the first excited state ($^4T_1$) by 250 meV can not be produced by a non uniform crystal field environment[43]. - In the ZnMnS system, MnS_6 clusters i.e. octahedrally co-ordinated Mn^{2+} instead of the usual tetrahedrally co-ordinated Mn^{2+}, have been speculated. This is also applicable to clusters of $MnSe_6$. Such octahedral co-ordination of Mn^{2+} ions is possible in Mn clusters consisting of several Mn^{2+} ions with minimum distances which forms the red emission centers. The dependence of the intensity and peak position of the red luminescence on temperature around N'eel temperature (Figs. 5.5.8 and 5.5.9) indicates the probable origin of this luminescence i.e. from Mn clusters. The antiferromagnetic interaction could strongly affect the energy levels of these red centers. This would explain why the red emission is excited[31] only via resonance energy transfer from the yellow centers ($^4T_1$ excited state of Mn^{2+}). To fit such $MnSe_6$ clusters into the surrounding wurtzite-type lattice, intrinsic defects are necessary which reduce the symmetry of the lattice points. This will also make the red emission centers dependent on crystal growth condition as observed in ZnMnS and in CdMnSe. The ratio $I_\perp/I_{||}$ for red luminescence shown in Fig.(5.5.10) follows a similar dependence on x as for the yellow luminescence. Since the nature of the yellow luminescence itself is different for two regimes of x, it is possible that the origins of the red luminescence for $x < 0.3$ and for $x > 0.3$ are different. More experiments are required to understand

this emission.

e) Time resolved red luminescence

The decay kinetics of this luminescence band for $x < 0.3$ (Fig.5.5.12a and 5.5.13b) is remarkably different than that observed for $x > 0.3$ (Fig.5.5.16). The red luminescence model which assumes the presence of red centers due to $MnSe_6$ can not justify the longer rise times > 200 psec for $x = 0.42$ as compared to 20 psec in samples with $x = 0.05$ and $x = 0.9$. This is because the resonant non radiative transfer of the yellow luminescence photons to the red center will be rapid in large x samples. The Jahn-teller distortion model would partly explain the slow rise time (Fig.(5.5.16))of the red luminescence for $x > 0.3$. In this model the rise time corresponds to the scattering time for the electron from higher laying minima to the lower laying minima in the configuration space. At this stage it is difficult make a reasonable judgement about the nature of this luminescence from the time resolved data.

f) Bound Magnetic Polaron Formation

In a n-type semimagnetic semiconductor it is known that as the free exciton localizes at a neutral donor site with Mn^{2+} ions enclosed within its Bohr orbit, the initial (t=0) state comprised of n-BMP is transformed into h-BMP[*5]. This is always true for

CdMnSe since only n-type CdSe could be grown. The electron radius is smaller than the hole radius in a donor bound exciton. Hence, in the begining the exchange contributions to the BMP binding energy comes from electron exchange. The n-BMP and h-BMP states have binding energies of ~ 1meV and ~ 10meV, respectively, for a typical sample of $Cd_{0.9}Mn_{0.1}Se$. Thus, the n-BMP state can not be observed separately in a luminescence experiment (but can be measured in RSFS). The temperature dependent shifts we observed of the yellow emission in the steady state excitation experiments correspond indeed to the h-BMP as the n-BMP quantum yield is low (short lifetime). The second peak in our time resolved luminescence, is identified with the net formation time of the bound exciton- h-BMP. We can determine the formation time of the bound exciton from time resolved data on CdSe(x=0)(Fig. 5.5.11). To a first approximation, the total localization rate for forming the exciton-BMP complex comes from the couloumb field of a donor and free exciton and the exchange field of Mn^{2+} ions within the donor bound exciton radius. The measured total formation time (τ_r), the measured bound exciton formation time τ_{r-CdSe} and h-BMP formation time τ_{h-BMP} are related as,

$$\frac{1}{\tau_{h-BMP}} = \frac{1}{\tau_r} - \frac{1}{\tau_{r-CdSe}} \qquad (5.6.34)$$

τ_r is the total rise time of the 2nd peak (Fig.5.5.12c and 5.5.13c)

and τ_r-CdSe is the rise time of the bound exciton (Fig.5.5.11c). Bound exciton emission dominates the luminescence-spectrum in steady state and very low intensity excitation picosecond spectroscopy or towards longer times at high excitation intensity.

It has been observed that with the 530 nm (2nd harmonic) excitation, even at low power, the luminescence detected is due to the e-h plasma. This is because the carrier density generated is > $10^{19}/cm^3$. Hence, with the 120 psec lifetime of the luminescence, the carrier density does not reach a density of $1.0x10^{17}/cm^3$ (Mott density) required for exciton formation for at least 600 psec. On the contrary with our level of excitation power for two photon excitation (10% of the maximum) the band edge luminescence is almost entirely due to bound excitons from the beginning (~ t=0)(Fig. 5.5.11(b)). For the maximum fluence of two photon excitation, the free e-h plasma emission is weak and can not be detected along with high quantum yield exciton luminescence. The narrow band filters used are typically with bandwidth of 60 Å. The delayed luminescence peak corresponding to bound excitons is very distinct (Fig. 5.5.11(c)). Thus, by considering time zero as the time at which the peak of the free e-h plasma emission is maximum we deduce the bound exciton formation time of 185 psec for CdSe (x=0) at the maximum power density. Any deviation (Eq.(5.6.34)), i.e. reduced formation times in $Cd_{1-x}Mn_xSe$ (x # 0) will be considered as due to additional localization provided by

exchange interaction between hole and Mn^{2+} ion spins (h-BMP). Thus, the rise time of 120 psec of the 2nd peak (Fig. 5.5.12(c)) for x=0.045 yields a formation time $\tau_{h\text{-}BMP} \approx 340$ psec. In the case of the $Cd_{0.9}Mn_{0.1}Se$ sample the total rise time of 60 psec (Fig. 5.5.13(c)) yields a $\tau_{h\text{-}BMP}$ of 90 psec.

Harris and Nurmikko[46] measured the total formation time of ~ 400 psec for the final state i.e. h-BMP in $Cd_{0.9}Mn_{0.1}Se$. The Mn^{2+}-Mn^{2+} spin interaction is important and determines BMP formation time at low temperatures ($< T_{AF} = 3.8K$). Below T_{AF} the strong coupling within Mn^{2+} spins precludes exchange interaction with the hole spin making formation times longer. The extrapolated spin-spin dephasing time from data obtained by Oseroff et al[47] is ~ 100 psec. This represents a lower limit for the formation time of a BMP in $Cd_{0.9}Mn_{0.1}Se$. The observed BMP formation time by Harris et al[46] was obtained from the spectral shift of the exciton line with time. The BMP formation time of 90 psec obtained for $Cd_{0.9}Mn_{0.1}Se$ compare well within the other measurements of Harris et al[46] and Oseroff et al[47] which are 400 psec and 100 psec, respectively.

The BMP formation time to a first approximation, is inversely proportional to the h-BMP energies and is given by,

$$\tau_{BMP} = \frac{\tau_o[(T + T_{AF})a^3]}{\tilde{x}} \qquad (5.6.35)$$

where τ_o is a phenomenological constant. τ_o obtained from the experimental data for $Cd_{0.95}Mn_{0.05}Se$ is 5.42×10^{-5} psec/K/Å^3 using τ_{BMP} = 340 psec, $\bar{x}$ = 0.028, T_{AF} = 2.5K, and a = 30 Å. The BMP formation time obtained for $Cd_{0.9}Mn_{0.1}Se$ from Eq.(5.6.35) is 165 psec. The sample inhomogenieties, ferromagnetic domains etc. could play an important role in the formation time.

The nature of the transition involved in samples with $x > 0.3$ is different than for samples with $x < 0.3$. As mentioned earlier, in the previous case, with 2.34 eV photon excitation, the excitation and recombination is between the Mn^{2+} excited state and the p-d hybridized valence band. For the latter case the transition is between the conduction and valence band. The measured rise time of the second peak in this case ($x < 0.3$) is indirectly related to the formation of the h-BMP (type I). The time resolved luminescence from $Cd_{0.58}Mn_{0.42}Se$ shows a delay-rise time of 50 psec and a decay time of 30 psec at the maximum (I_o) two photon excitation. The luminescence peak gets delayed as the excitation power is lowered and for $1/10 I_o$ excitation fluence the peak is delayed by about ~ 100 psec. The time resolved luminescence behavior under 530 nm excitation is different. The delay time is negligible, while the decay time is 150 psec. Such temporal behavior under different excitation wavelength and intensities indicates that the luminescence observed at maximum two photon excitation is stimulated and at low excitation is mostly spontaneous. The bound

state between the electron localized on an excited Mn^{+2} ion with mass m_o and a hole from the valence band with effective mass $0.45m_o$ has a radius of 12 Å. This is also estimated by comparing Δ_{BMP} with the theoretical value given by Eq.(5.6.21) for samples with x = 0.36 and 0.42. The Mott density, which determines the the upper limit for the bound states/cm^3, would be $3x10^{18}/cm^3$. The absorption coefficients for CdMnSe are not known particularly for x > 0.3. It is expected to be much lower than for CdSe in which the measured two photon absorption coefficient β is 0.03 cm/MW and above bandgap one photon absorption coefficient is $4x10^4$ cm^{-1}. Taking these factors into account the maximum free hole density could be $10^{18}/cm^3$ instead of $2x10^{19}/cm^3$ as in CdSe or approximately in $Cd_{1-x}Mn_xSe$ for $x \leq 0.3$ (I_o = 7GW/cm^2). Hence, the exciton-BMP formation process should not be delayed as much as in $Cd_{0.95}Mn_{0.05}Se$ or $Cd_{0.9}Mn_{0.1}Se$ due to the minimal screening effects. The calculated BMP (type II) formation time for such a case (x = 0.36 and 0.42) would be ~ 20 psec using the relevant parameters and Eq.(5.6.35). This is much smaller than the measured value (from sponteneous emission Fig.5.5.14c and 5.5.15b) of 100 psec. More experiments are needed in the presence of a magnetic field to understand the role of exchange induced localization and other factors probably such as defects, domains etc.

5.7 CONCLUSION

From the steady state studies of the dependence of the luminescence peak position on the Mn concentration over a broad range ($0 \leq x \leq 0.86$), the optical deformation potentials were obtained for CdMnSe. The values of the conduction band and the valence band deformation potentials are 0.5×10^9 eV/cm and 0.24×10^9 eV/cm, respectively. The bound magnetic polaron energies were obtained for different Mn concentration samples as a function of temperature. From these studies it was concluded that there are two regimes of BMP which are distinguished from the other by radius or the effective electron mass. The BMP in low concentration samples ($x < 0.3$) consists of an electron ($0.13m_o$) and a hole ($0.45m_o$) localized at a donor. However, in high concentration samples ($x > 0.3$) the BMP consists of an electron (m_o) on an excited Mn^{2+} ion and a hole ($0.45m_o$). This causes a three fold reduction in the radius of the BMP in higher concentration samples. The antiferromagnetic interaction between Mn clusters within the Bohr radius of BMP could be observed in the form of changes in the luminescence intensity and peak position around $T_N \sim 60K$. In addition to the BMP luminescence (yellow) a separate luminescence band (red) is observed towards low energy. The source of this luminescence could be $MnSe_6$ clusters. The BMP formation times in $Cd_{0.95}Mn_{0.05}Se$ and $Cd_{0.9}Mn_{0.1}Se$ are 340 psec and 90 psec, respectively. The BMP formation times in $Cd_{0.64}Mn_{0.36}Se$ and

$Cd_{0.58}Mn_{0.42}Se$ are ~100 psec contrary to the estimated values of 20 psec. The BMP luminescence in these samples is stimulated at large two photon excitation fluences. The red luminescence time resolved measurements are inconclusive.

5.8 REFERENCES

1. J. Furdyna, J. Appl. Phys.,53, 7637 (1982).

2. J. A. Gaj, Proc. 15th Int.Conf.in Phy.of Semicond. Kyoto J. Phys. Soc. Japan, 49, 797 (1980)suppl.

3. J. Spalek, A. Lewicki, Z. Tarnawski, J.K. Furdyna, R.R. Galazka and Z. Obuszko (preprint).

4. M.R. Junnarkar, R.R. Alfano and J. Furdyna (to be published).

5. T. Dietl and J. Spalek, Phys. Rev. Lett.,48,3551 (1982).

6. T. Dietl and J. Spalek, Phys. Rev.B, 28, 1548 (1983).

7. A. Mauger, Phys. Rev. B, 27, 2308 (1983).

8. A. Pajaczkowska, Prog. Crystal Growth Charact.1, 289 (1978).

9. J. Bardeen, W. Shockley, Phys. Rev. 80, 72 (1950).

10. M. Grynberg, Proc. 7th Int.Conf. on semicond. Phys. Paris, V1 1964. Edited by Hulin, Academic Press 1964,P.135.

11. G.E. Pikus, Sov. Phys. Sol. state,6, 261 (1964).

12. M. Blume and R. Orbach, Phys. Rev. 127, 1587 (1962).

13. M.P. Vecchi, W. Giriat, and L.Videla, Appl. Phys. Lett. 38, 99 (1981)

14. Donald L. Decker and R. L. Wild, Phys. Rev.B, 4, 3425 (1971).

15. R.R. Galazka, Shoichi Nagata, P.H. Keesom, Phys. Rev. B, 22, 3344 (1980).

16. Takashi Ito, Kazuyoshi Ito, and Masahiro Oka, Jap. J. Appl. Phys., 17, 371 (1978).

17. R.J. Nelson and N. Holonyak, Jr., J. Phys. Chem. Solids, 37, 629 (1976).

18. J. Stankiewicz, Phys. Rev.B, 27, 3631 (1983).

19. M. Cardona, 'Modulation Spectroscopy', Spinger-verlag (1984).

20. C.A. Hubber, A.V. Nurmikko, M. Gaj, and A. Wold, Sol. State

Comm. 46, 41 (1983).

21. J. Warnock, R.N. Kershaw, D. Ridgley, K. Dwight, A. Wold and R.R. Galazka, Sol. State Comm. 54, 215 (1985).

22. P.Y. Lu, P.P. Ho and R.R. Alfano, J. Quantm. Electr. QE-15 406 (1979).

23. Donald Long, 'Energy Bands in Semiconductors', Interscience pubishers, 1968.

24. Gerard Martinez, 'Hand Book on Semoconductors'. V2, Edited by M.B. Balkanski, North-holland Publishing Company, 1980,P.181.

25. J. Camassel and D. Auvergne, Phys. Rev.B, 12, 3258 (1975).

26. Marvin L. Cohen and D.J. Chadi,'Hand Book on Semiconductors'.V2 Edited by M. Balkanski, North-Holland Publising Company 1980, P. 157.

27. J. Diouri, J.P. Lascaray, and R. Triboulet, Sol. State Comm. 42, 231 (1982).

28. E.I. Grancharova, J.P. Lascaray, J. Diouri, and J. Allegne, Phys. Stat. Sol.(b), 113, 503 (1982).

29. P. Oelhafen, M.P. Vecchi, J.L. Freeouf, and V.L. Moruzzi, Sol. State Comm., 44, 1547 (1982).

30. Y. Tanabe and S. Sugano, J. Phys. Soc. Japan,9, 753 (1954).

31. M.M. Moriwaki, Ph.D. Thesis, Purdue University 1983.

32. D. Berlincourt, H. Jaffe, L.R. Shiozawa, Phys. Rev. 129, 1009 (1963).

33. M.R. Junnarkar and R.R. Alfano (to be published).

34. P.C. de Gennes, Phys. Rev. 118, 141 (1960).

35. T. Kasuya, A. Yanase, T. Takeda, Sol. State Comm.,8, 1543 (1970).

36. D. Heiman, P.A. Wolff and J. Warnock, Phys. Rev. B, 27,4848 (1983)

37. R. Planel, Tran Hong Nhung, G. Fishman and M. Nawrocki, J. Physique, 45, 1071 (1984).

38. D. Heiman, Appl. Phys. Lett. 42, 775 (1985).

39. T. Giebultowicz, W. Minor, H. Kepa, J. Ginter and R.R. Galazka, J. Mag. Mag. Materials, 30, 2151 (1982).

40. T. Giebultowicz, W. Minor, B. Buras, B. Lebech, and R.R. Galazka, Physica Scripta 25, Dec1981.

41. J. A. Gaj, R. Planel and G. Fishman, Sol. State Comm., 29, 435 (1979).

42. M. Nawrocki, R. Planel and G. Fishman, Phys. Rev. Lett., 46, 735 (1981).

43. O. Goede and Dang Dinh Thong, Phys. Stat. Sol.(b), 124, 343 (1984).

44. Dang Dinh Thong, W. Heimbrodt, D. Hommel, and O. Goede, Phys. Stat. sol.(b), 81, 695 (1984).

45. J. Spalek, Phys. Rev. B, 32, Sept 1985.

46. J.H. Harris and A.V. Nurmikko, Phys. Rev. Lett. 51, 1472 (1983).

47. S.B. Oseroff, Phys. Rev.B, 25, 6584 (1982).

5.9 FIGURE CAPTIONS

5.5.1. Steady state luminescence spectra obtained at 4K with 488 nm excitation wavelength are shown with the luminescence peaks (yellow) marked in eV for various $Cd_{1-x}Mn_xSe$ samples, a) x = 0, b) x = 0.045, c) x = 0.092, and d) x = 0.3.

5.5.2. Steady state luminescence spectra obtained at 4K with 477 nm excitation wavelength are shown with the luminescence peaks (yellow) marked in eV for various $Cd_{1-x}Mn_xSe$ samples, a) x = 0.36, b) x = 0.42, and c) x = 0.86.

5.5.3. Steady state luminescence peak positions (yellow) obtained with 488 nm excitation wavelength are plotted as function of temperature for samples, a) x = 0, b) x = 0.045, c) x = 0.092, and d) x = 0.3. T_N is the N'eel temperature. The dashed lines drawn through the points are with the slopes, a) 2×10^{-4} eV/K, b) 2.7×10^{-4} eV/K, c) 2.4×10^{-4} eV/K, and d) 5.3×10^{-4} eV/K.

5.5.4. Steady state luminescence peak intensities (yellow) obtained with 488 nm excitation wavelength are plotted as a function of temperature for various samples, a) x = 0, b) x = 0.045, c) x = 0.092, and d) x = 0.3. T_N is the N'eel temperature. The lines drawn through the points are for visual guidance only.

5.5.5. Steady state luminescence peak positions and intensities obtained with 477 nm excitation are plotted as a function of temperature for x = 0.36. The straight line is of slope 5×10^{-4} eV/K. The dotted curve is for visual guidance only.

5.5.6. Steady state luminescence peak positions and intensities obtained with 477 nm excitation are plotted as a function of temperature for x = 0.42. The straight line is of slope 5.4×10^{-4} eV/K. The dotted line is for visual guidance only.

5.5.7. Steady state luminescence peak positions and intensities obtained with 477 nm excitation are plotted vs temperature for x = 0.86. The curves drawn through the points are for visual guidance only.

5.5.8. Steady state luminescence peak (red) positions are plotted vs temperature for samples, a) x = 0.092, b) x = 0.3, and c) x = 0.86. The lines drawn through the points are for visual guidance only. T_N is the N'eel temperature.

5.5.9. Steady state luminescence (red) intensities are plotted vs

temperature for samples, a) x = 0.092, b) x = 0.3, and c) x = 0.86. The curves drawn through the points are for visual guidance only. T_N is the N'eel temperature.

5.5.10. The ratios / for yellow and red luminescences obtained at 4K are plotted vs Mn concentration. The curves drawn through the points are for visual guidance only.

5.5.11. The time resolved band edge luminescence obtained at 12K for CdSe(3) are shown at different excitation wavelengths and intensities: a) 530nm, I_F; b) 1060 nm, $1/10I_o$; and c) 1060 nm, I_o.

5.5.12. The time resolved yellow and red luminescences obtained with 1060 nm excitation of the x= 0.045 sample are shown. The BMP is formed within 120 psec after pulse excitation.

5.5.13. The time resolved yellow and red luminescences obtained with 1060 nm excitation of the x = 0.092 sample are shown. The BMP is formed within 60 psec after pulse excitation.

5.5.14. The time resolved yellow luminescences obtained with 1060 nm excitation of the x= 0.36 sample at 4K are shown.

5.5.15. The time resolved yellow luminescences obtained with 530 and 1060 nm excitation of the x= 0.42 sample at 4K are shown.

5.5.16. Time resolved red luminescences obtained with 1060 nm excitation of the x= 0.42 sample at 4K are shown.

5.6.1. The steady state luminescence peak positions are plotted with Mn atomic concentration at 4K, 77K, and 185K. The straight line corresponds to the bandgap at 4K(Stankiewicz et al). The open circles correspond to the red luminescence peak positions at 4K.

5.6.2. The band structure variation model near Γ point for $Cd_{1-x}Mn_xTe$ (zinc blende) and $Cd_{1-x}Mn_xSe$ (wurtzite) with Mn^{2+} $3d^5$ level shown.

5.6.3. The BMP energies obtained using Eq.(35) are plotted vs temperature for x = 0.092. The continuous line represents Eq.(28) with the parameters shown in the figure.

5.6.4. The BMP energies obtained using Eq.(36) are plotted vs temperature for x = 0.045. The continuous line represents Eq.(28) with the parameters shown in the figure.

5.6.5. The BMP energies obtained using Eq.(37) are plotted vs

temperature for x = 0.3. The continuous line represents Eq.(28) with the parameters shown in the figure.

5.6.6. The BMP energies obtained using Eq.(38) are plotted vs temperature for x = 0.36. The continuous line represents Eq.(28) with parameters shown in the figure.

5.6.7. The BMP energies obtained using Eq.(39) are plotted vs temperature for x = 0.42. The continuous line represents Eq.(28) with the parameters shown in the figure.

5.6.8. The BMP energies obtained using Eq.(40) are plotted vs temperature for x = 0.86. The continuous line represents Eq.(28) with the parameters shown in the figure.

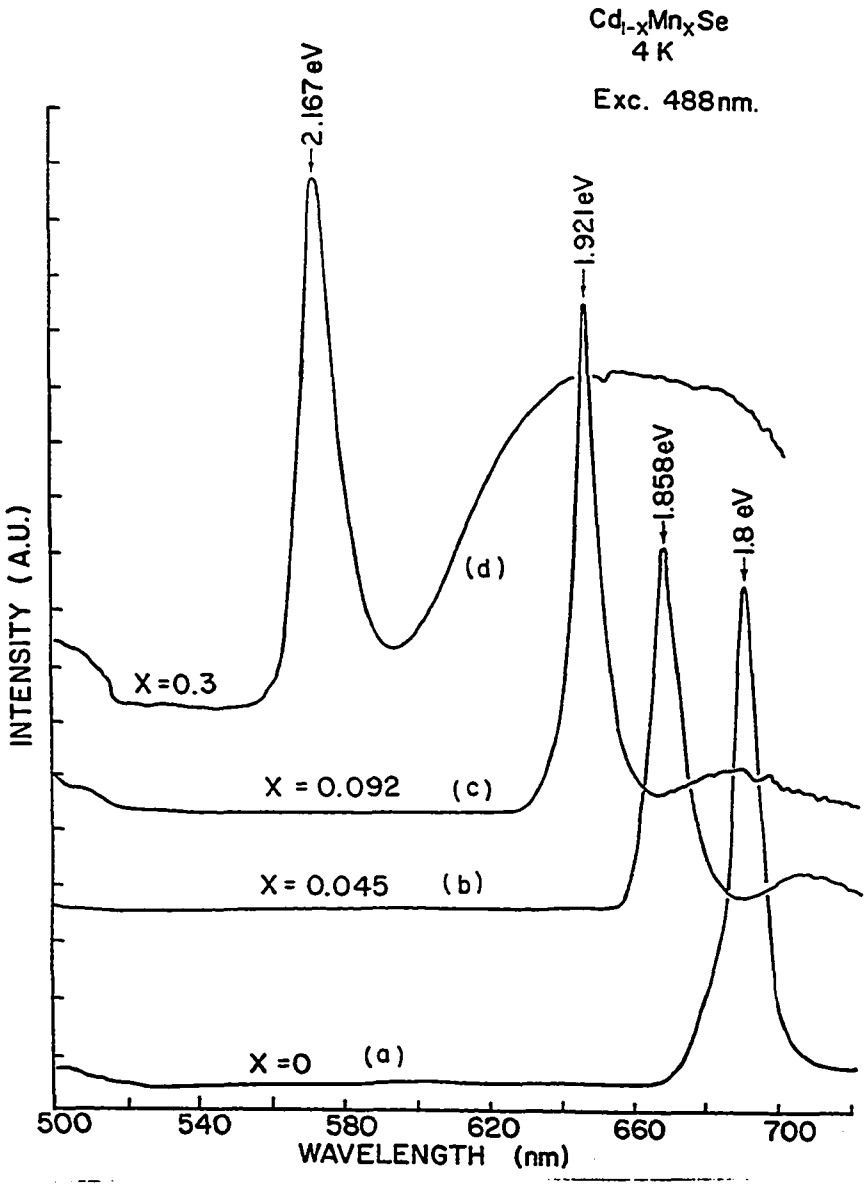

FIGURE 5.5.1

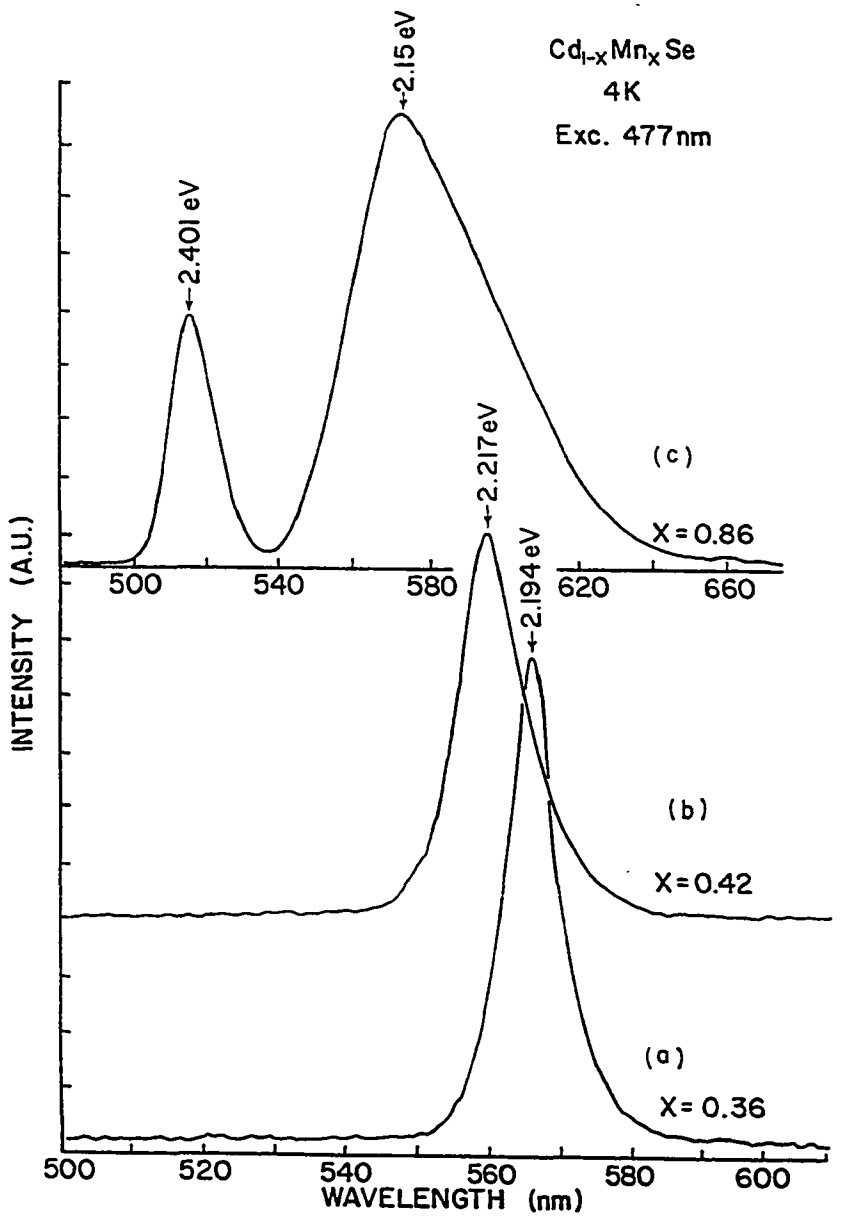

FIGURE 5.5.2

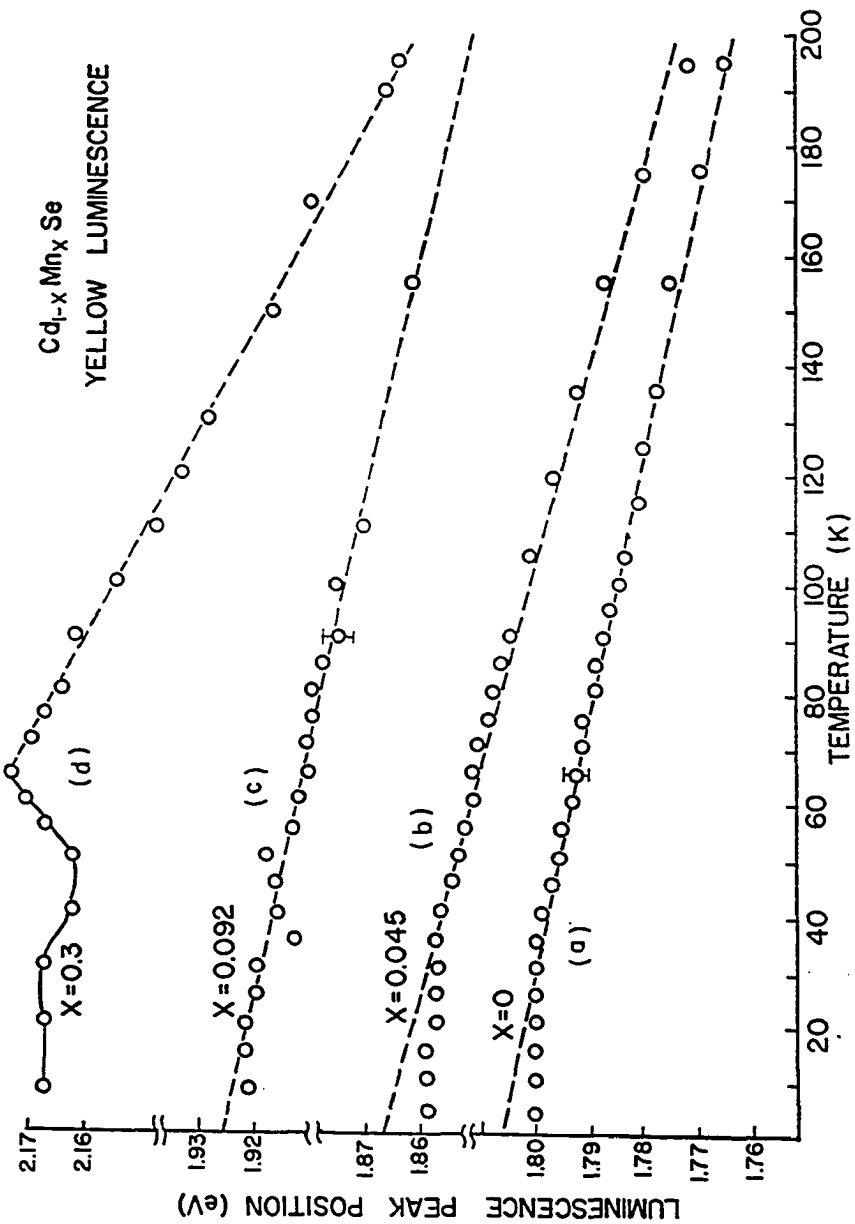

FIGURE 5.5.3

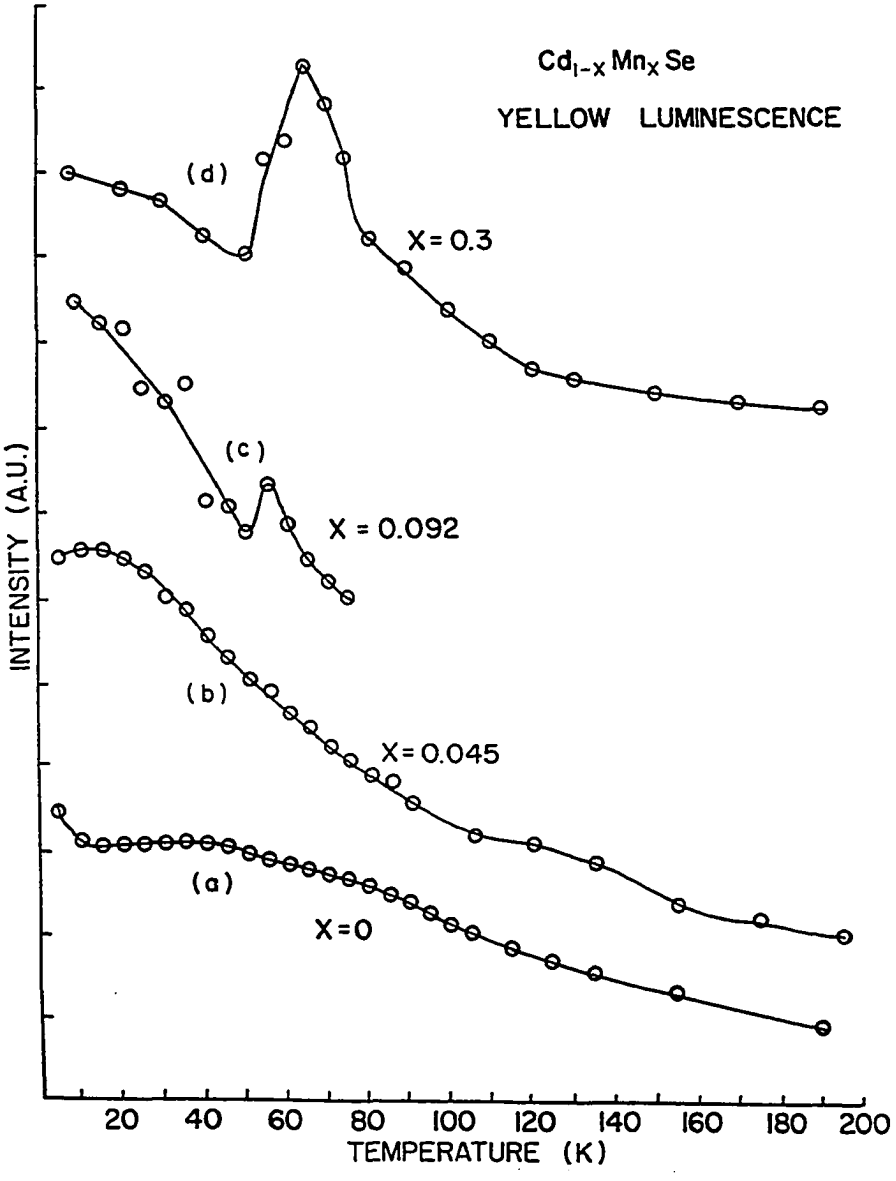

FIGURE 5.5.4

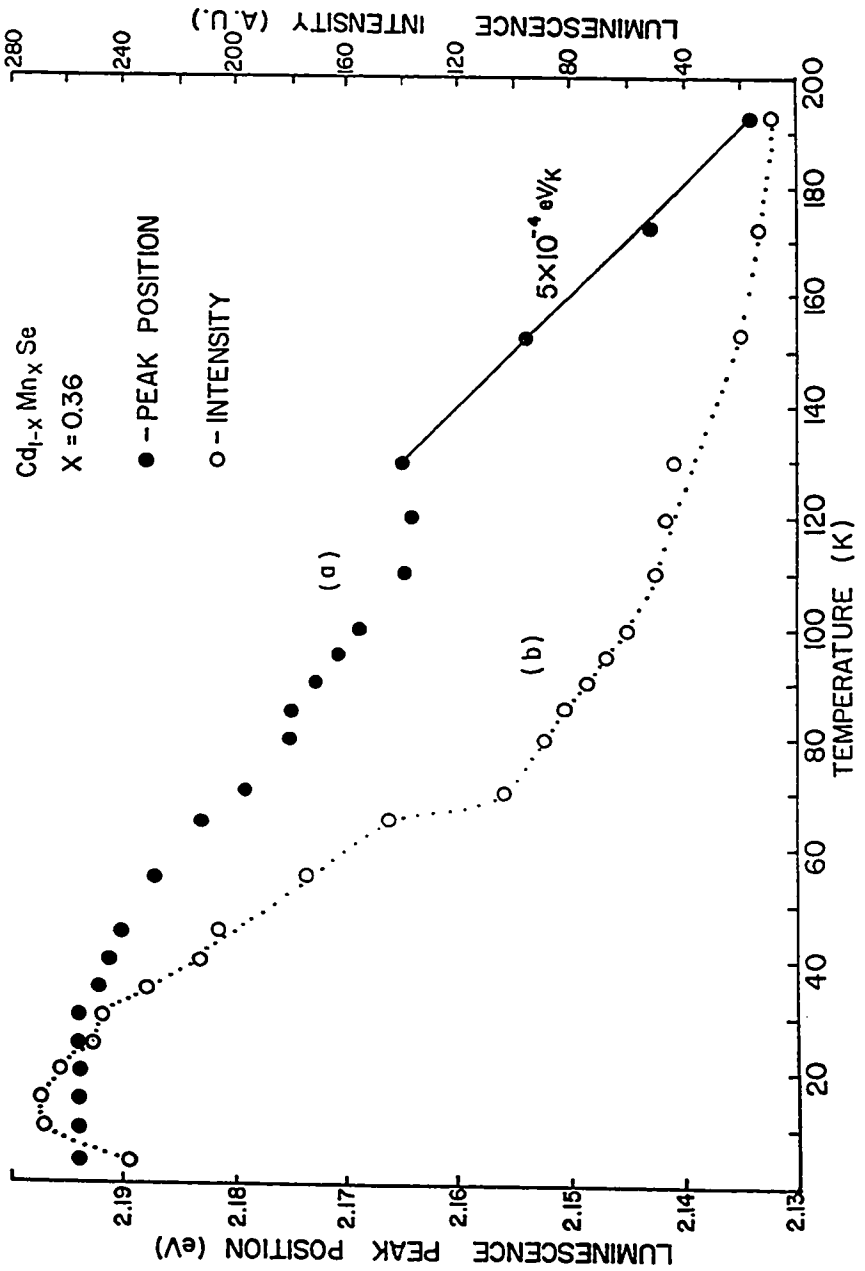

FIGURE 5.5.5

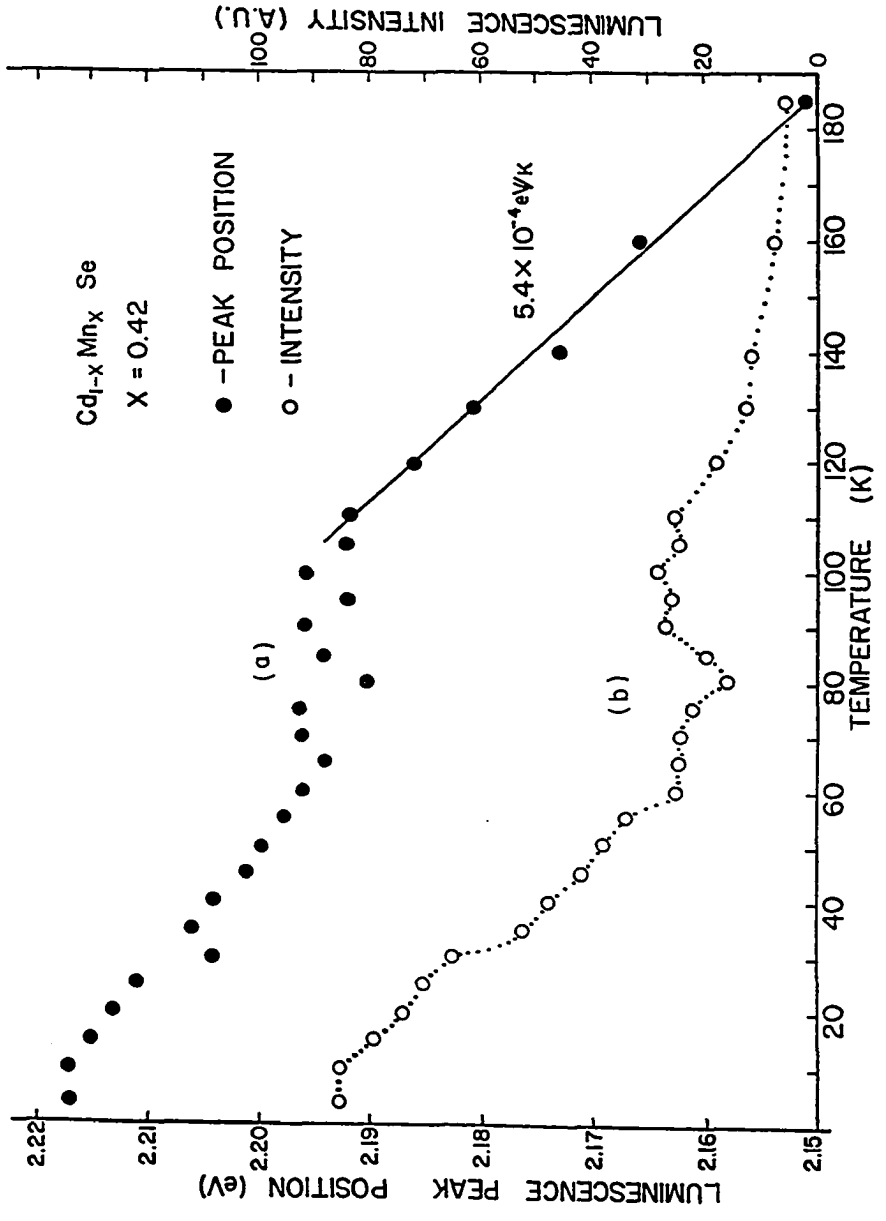

FIGURE 5.5.6

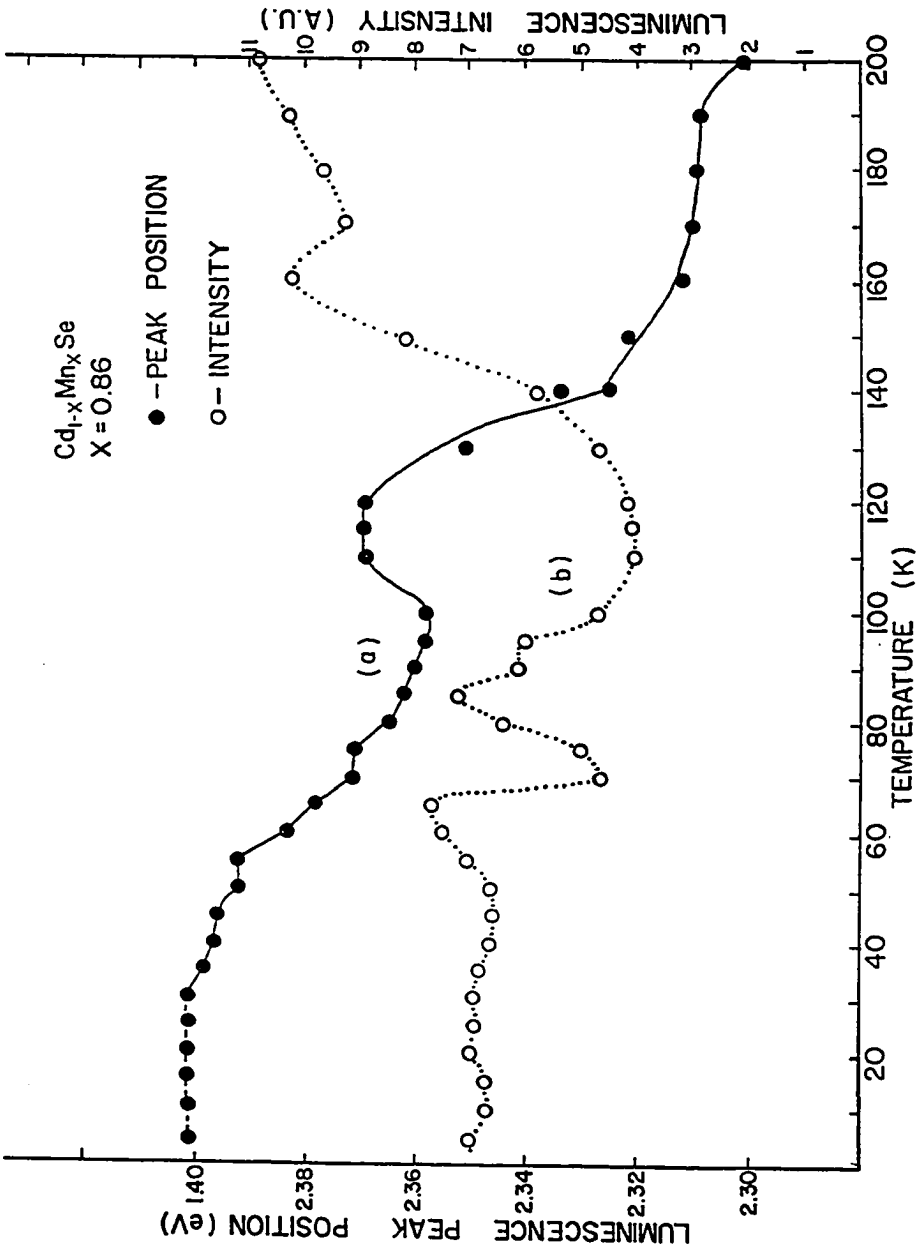

FIGURE 5.5.7

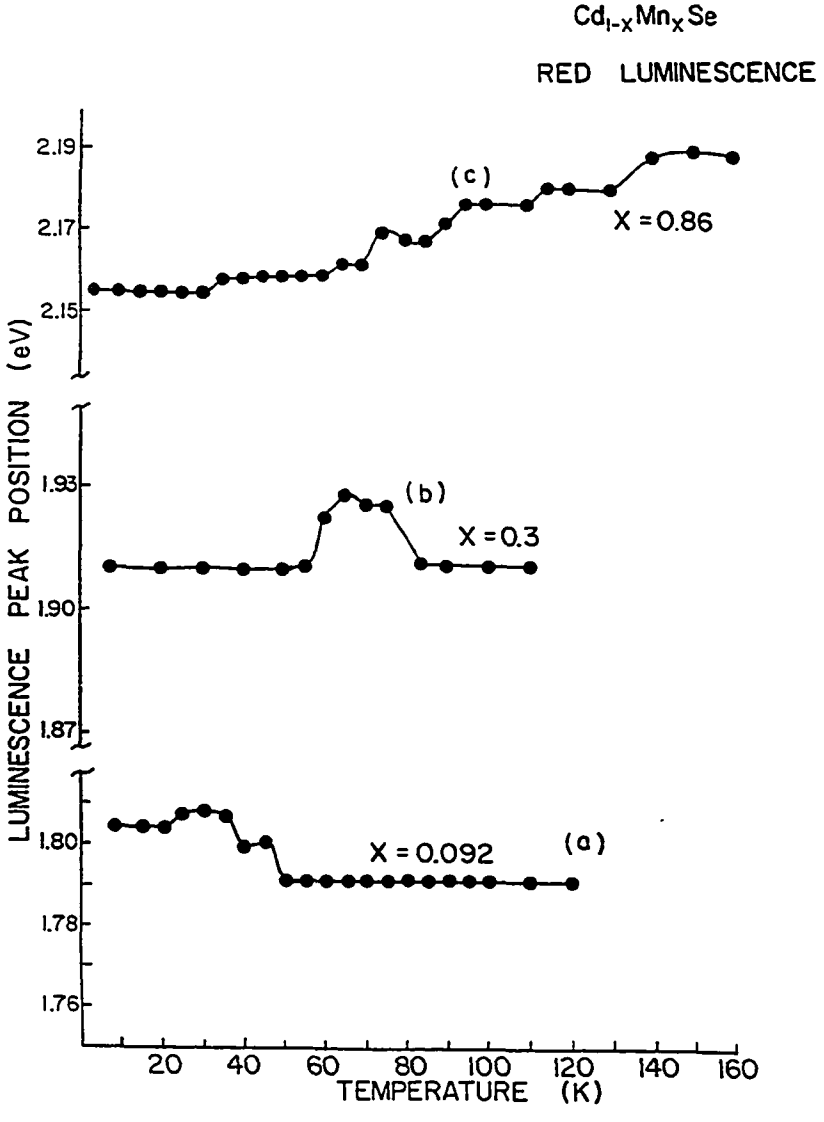

FIGURE 5.5.8

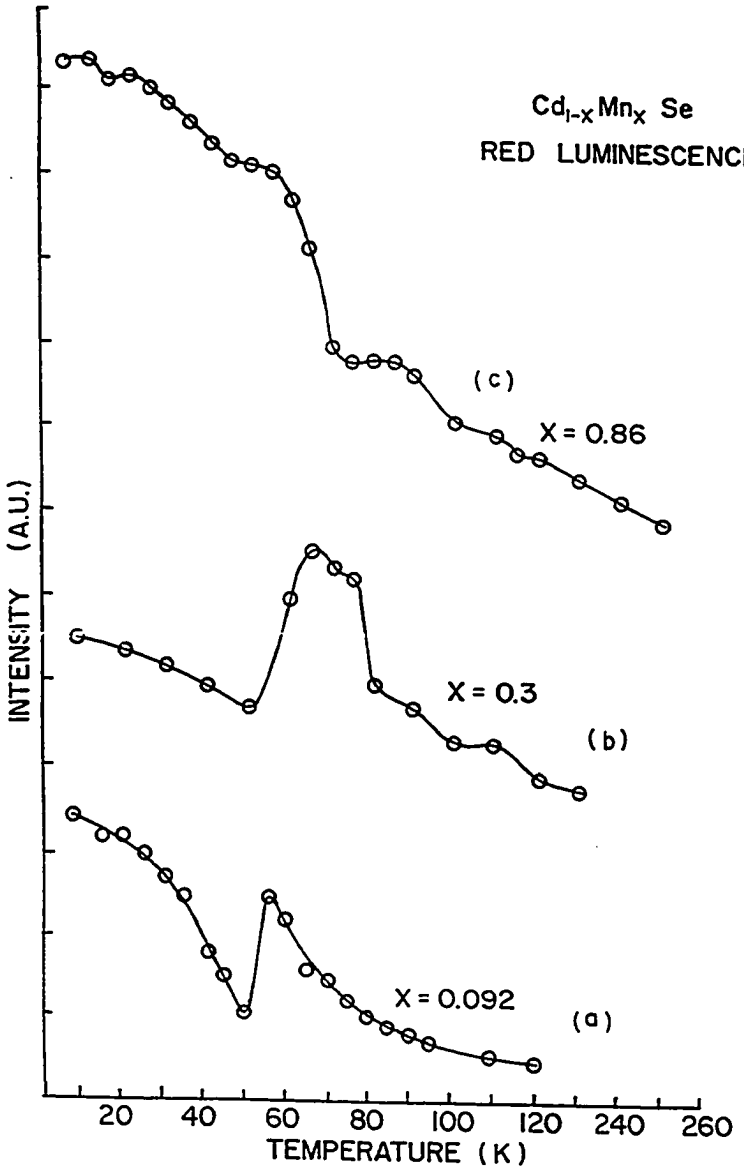

FIGURE 5.5.9

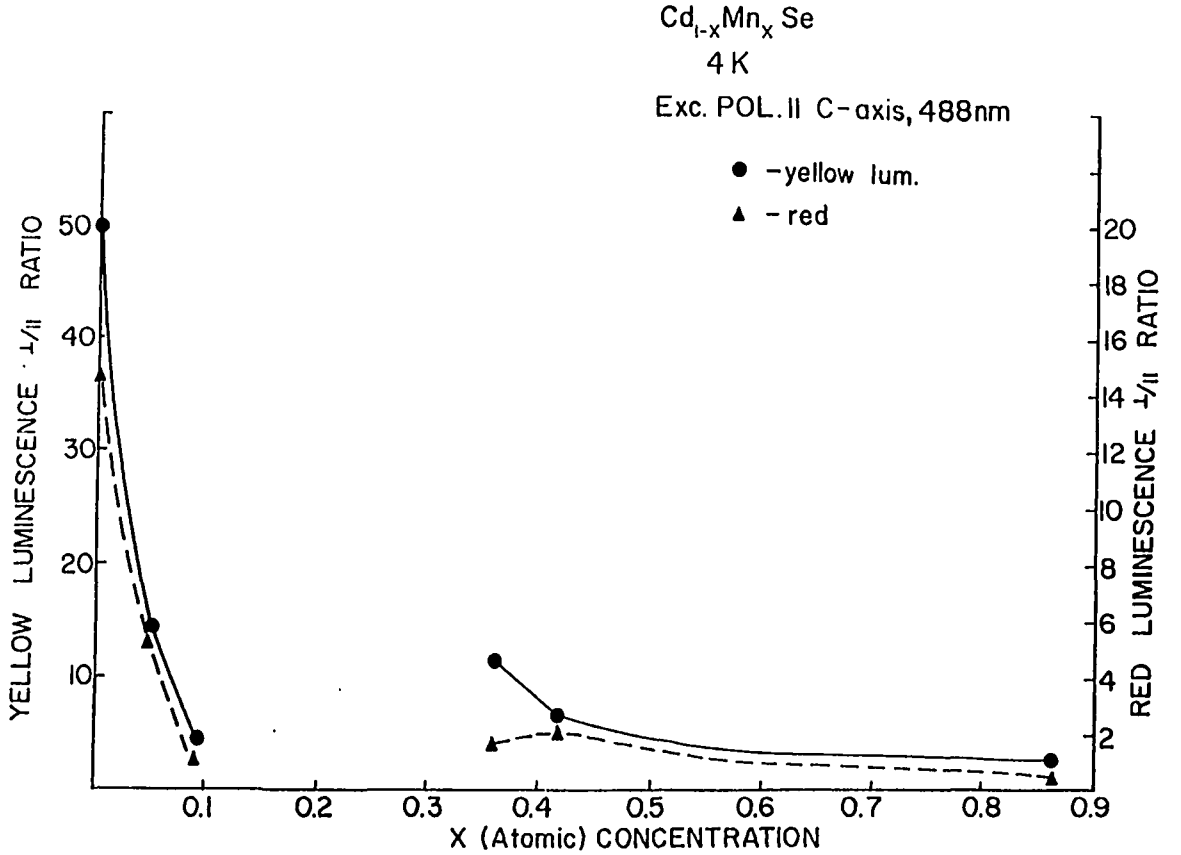

FIGURE 5.5.10

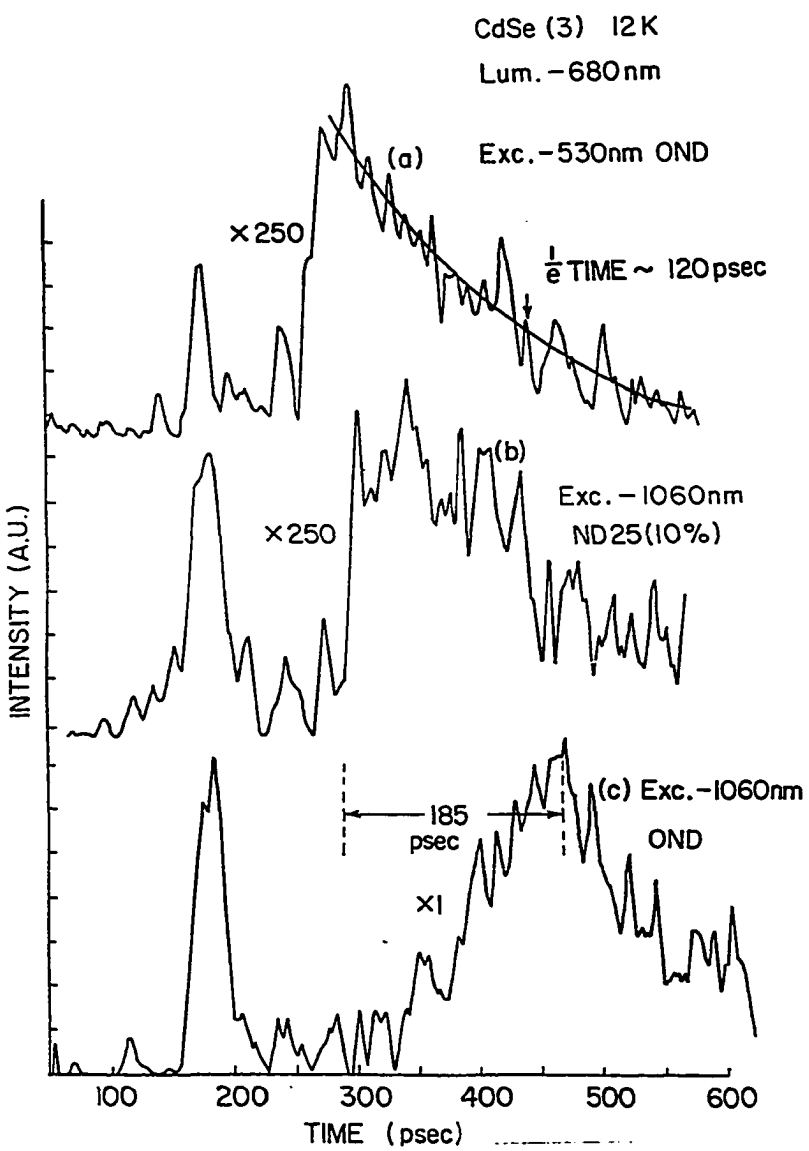

FIGURE 5.5.11

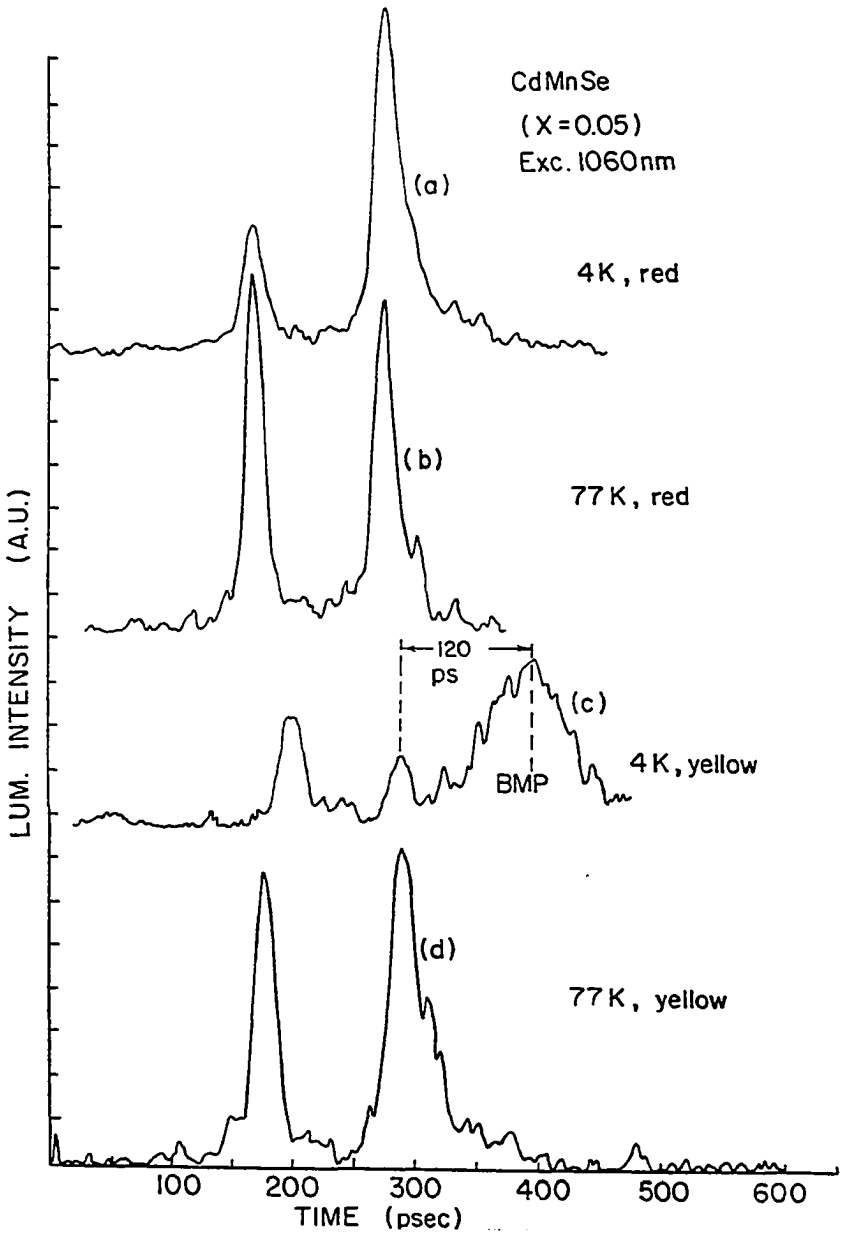

FIGURE 5.5.12

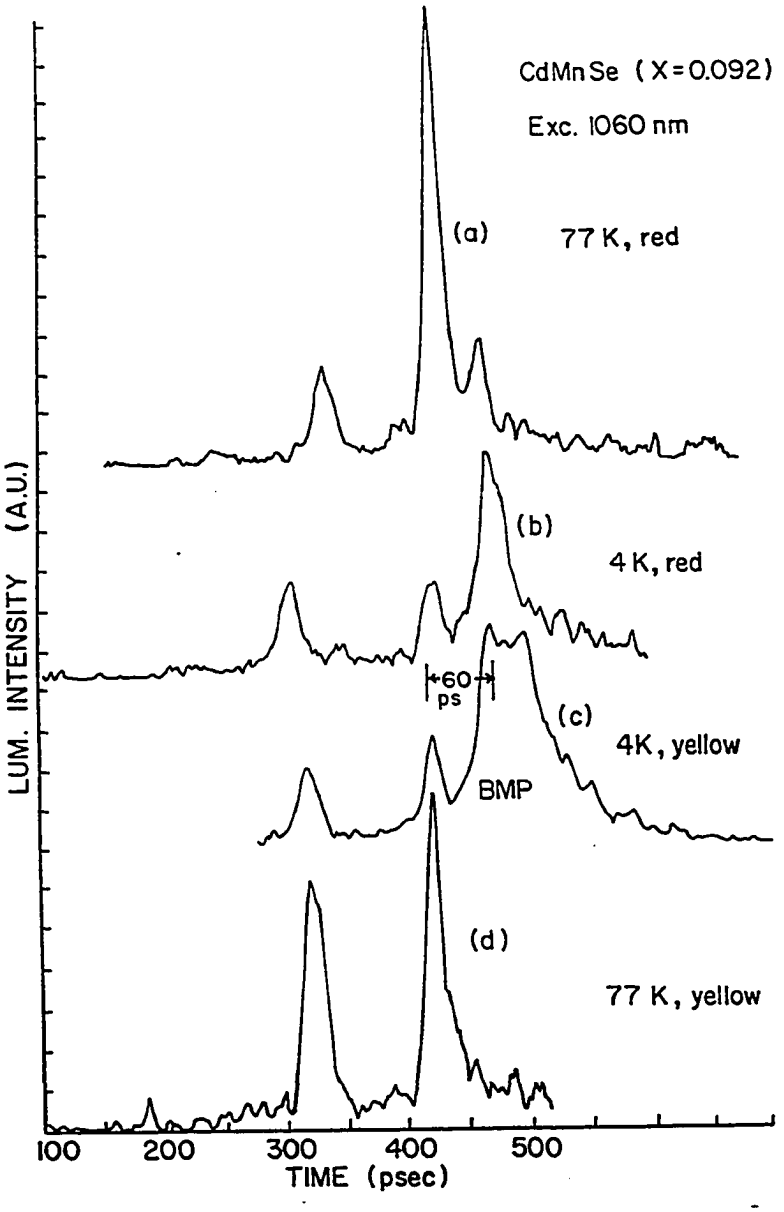

FIGURE 5.5.13

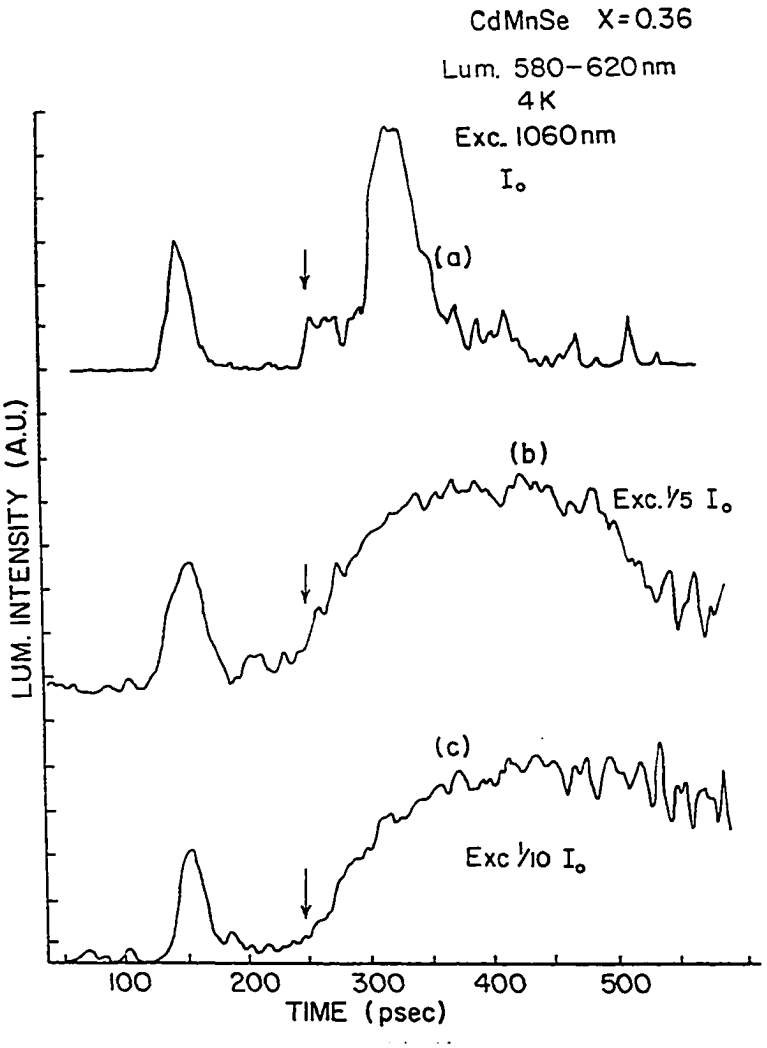

FIGURE 5.5.14

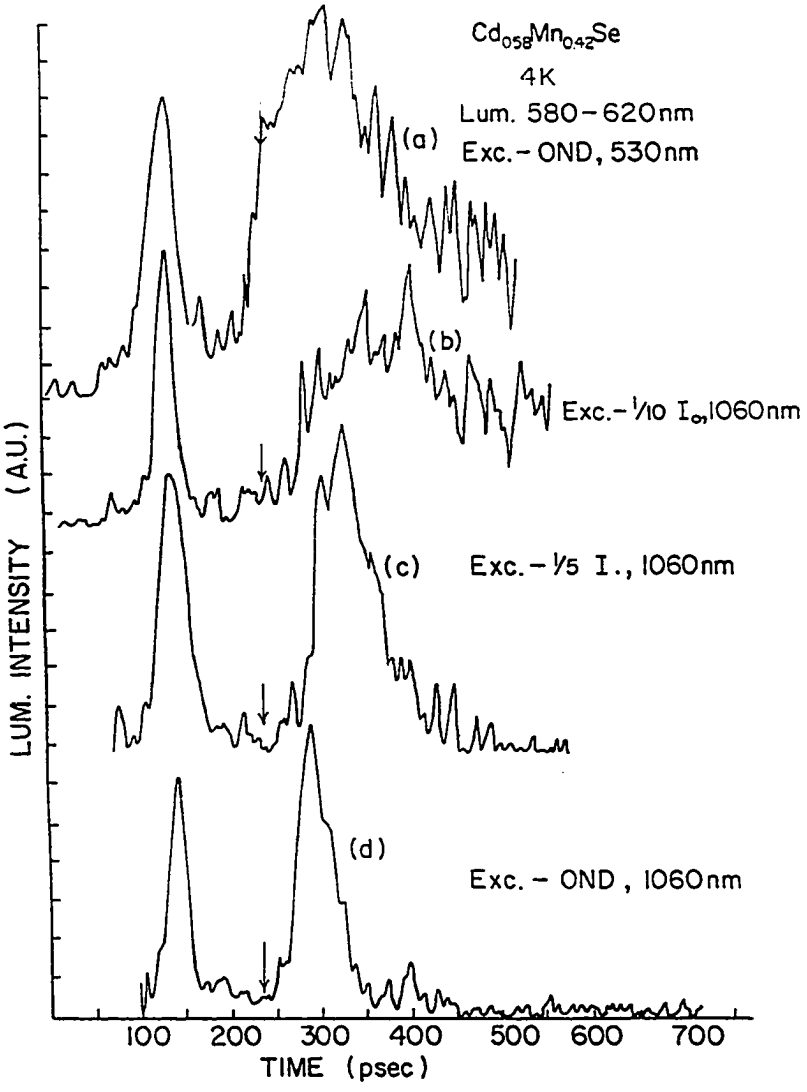

FIGURE 5.5.15

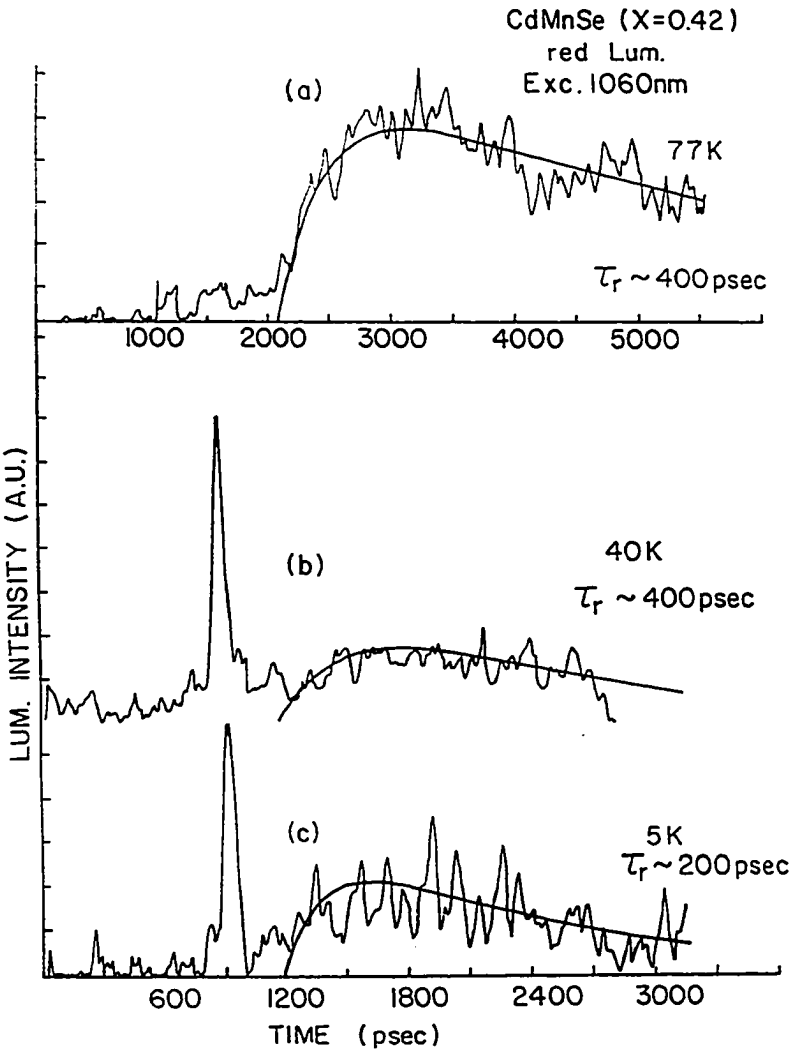

FIGURE 5.5.16

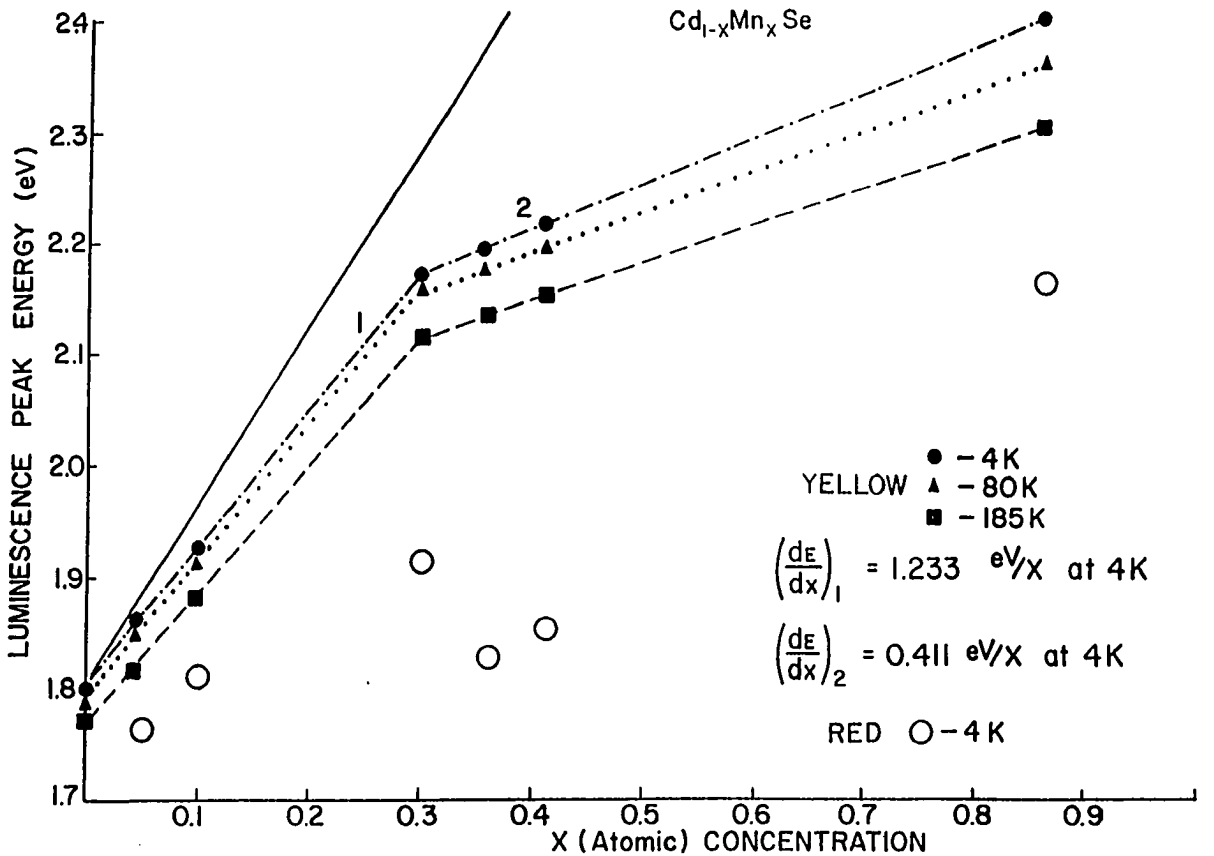

FIGURE 5.6.1

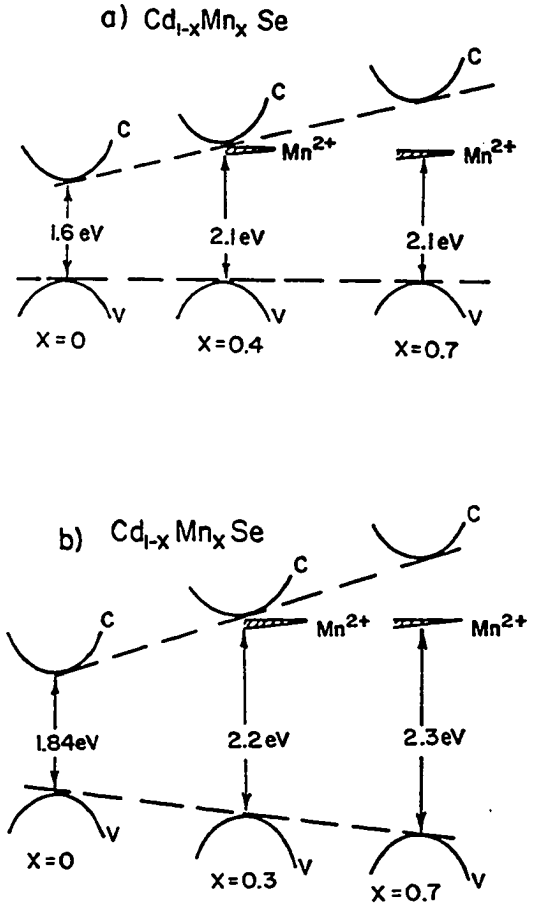

FIGURE 5.6.2

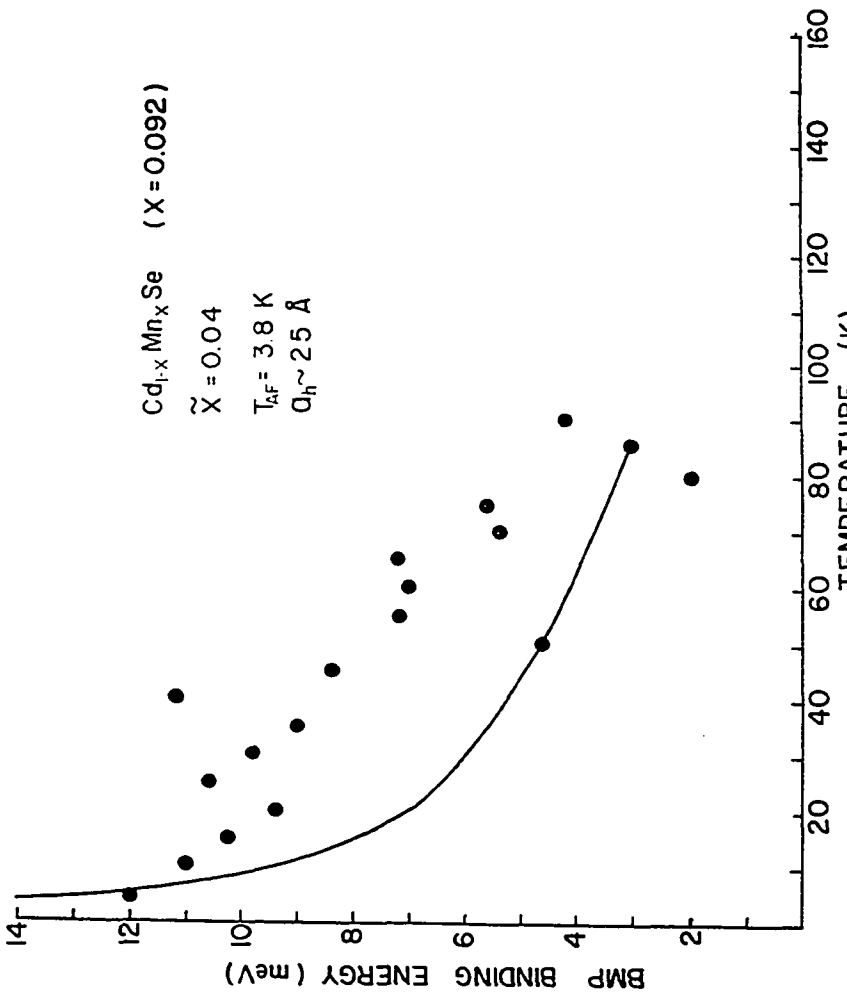

FIGURE 5.6.3

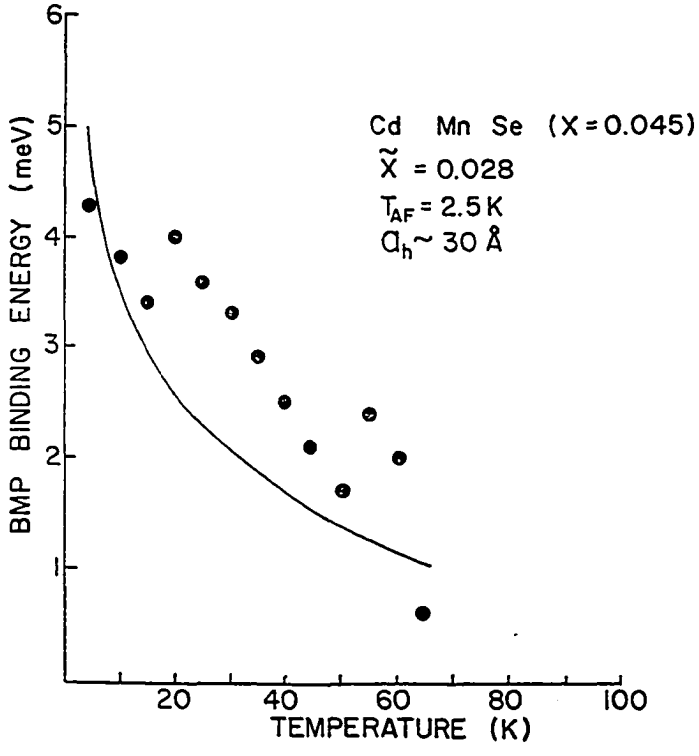

FIGURE 5.6.4

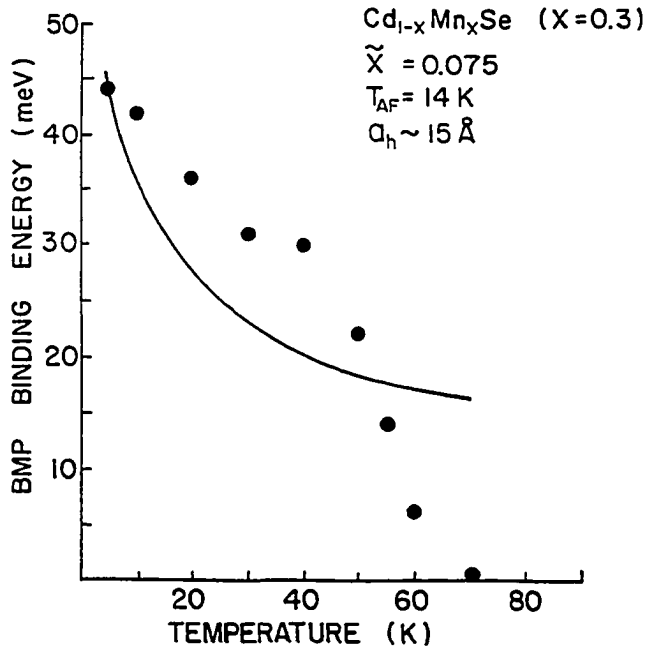

FIGURE 5.6.5

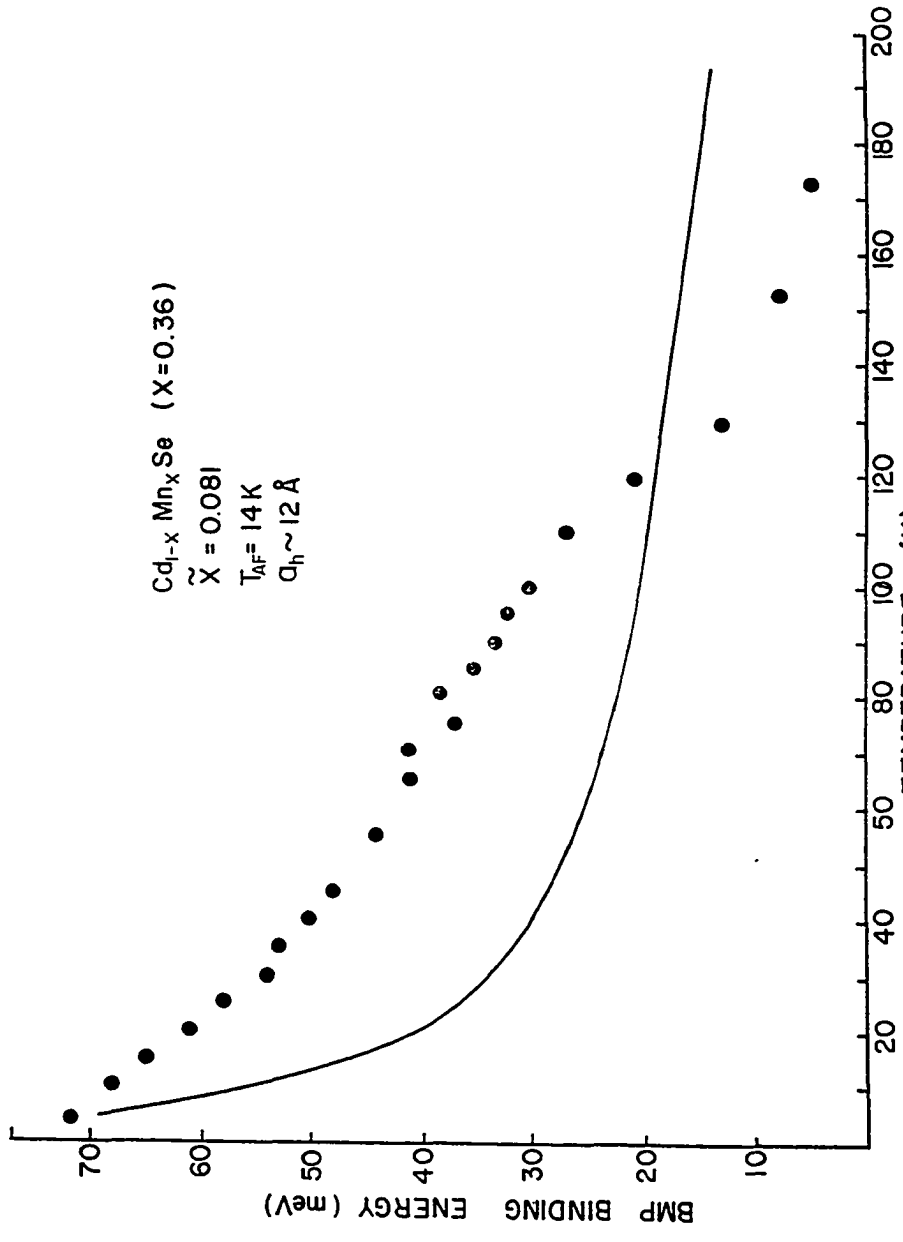

FIGURE 5.6.6

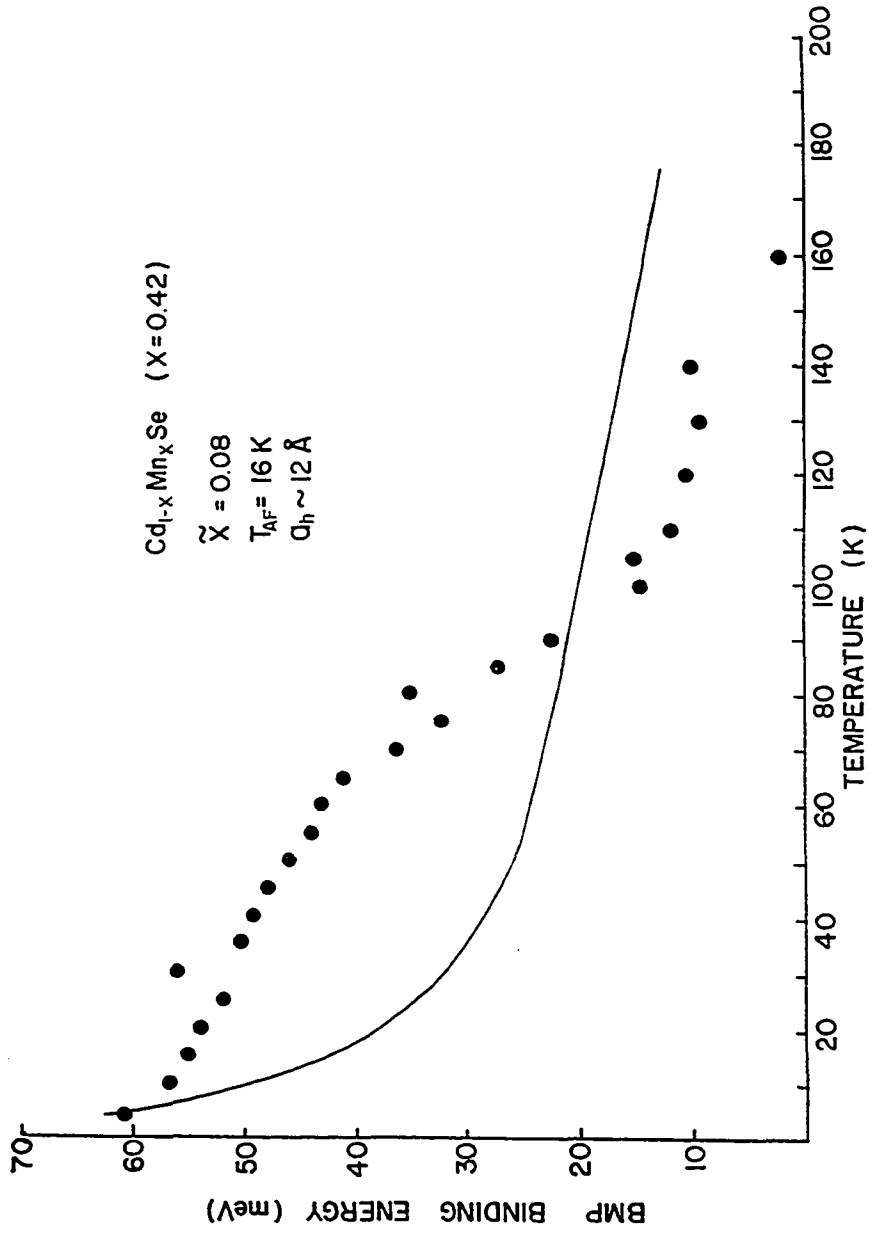

FIGURE 5.6.7

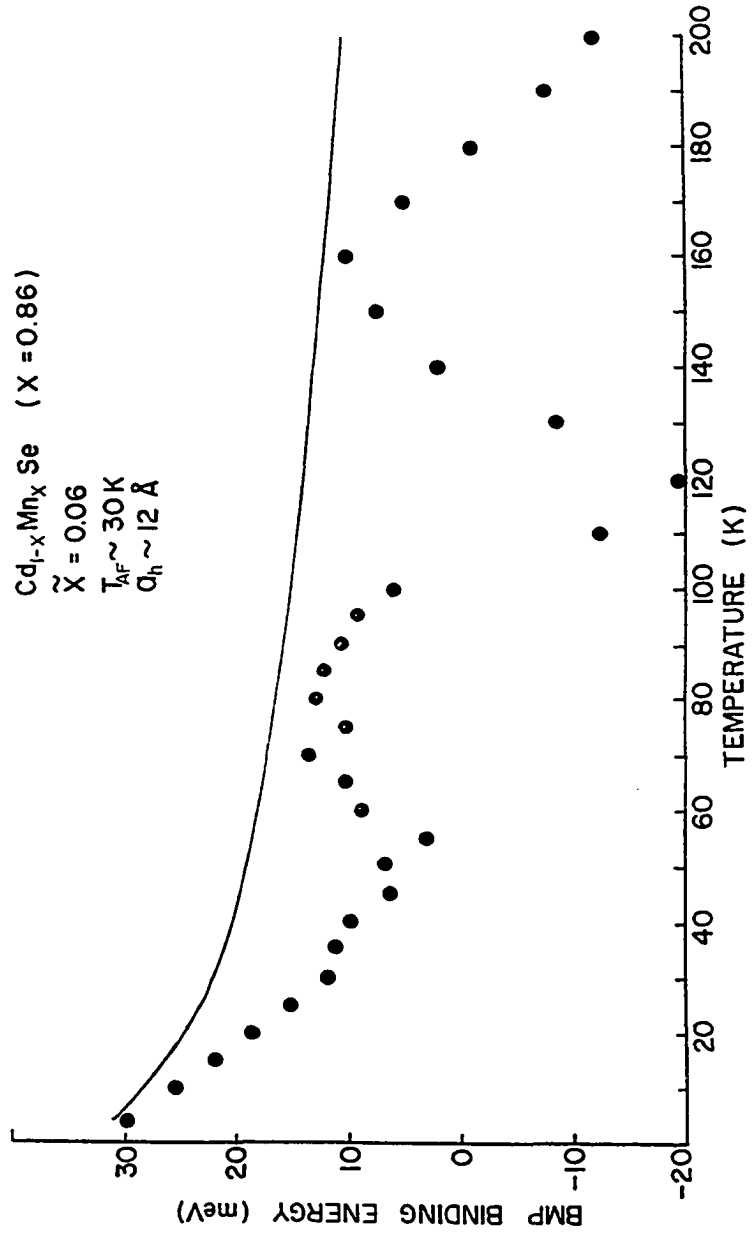

FIGURE 5.6.8

CHAPTER VI

CONCLUSIONS and FUTURE DIRECTIONS

In polar semiconductor CdSe, at photogenerated carrier densities > $10^{18}/cm^3$, the hot carrier energy relaxation is primarily due to non-polar optical phonons generated via optical deformation scattering. The phonons emitted are typically with wave vector $\sim 10^7$ $cm^{-1}(q_{max})$, since smaller q phonon emission proccesses become inefficient. This is primarily due to the critical carrier density N_c, which determines the onset of screening of the electron-phonon interactions for carrier densities exceeding N_c, is small for small q phonons. This screening mechanism also contributes to the rapid diffusion of carriers a for carrier density > $10^{19}/cm^3$. The maximum carrier density, ~30 psec (thermalization time) after an ultra-short laser pulse excitation, is $2x10^{19}/cm^3$ at room temperature and is ~ $5x10^{17}/cm^3$ at 12K. In order to examine the participation of "q_{max}" phonons, one should perform time resolved Raman scattering experiments with femtosecond (10^{-13} sec) resolution. Due to the parabolic nature of the conduction band, the Raman signal at different times will correspond to q_{max} of different magnitude. During the thermalization time, N_c also shifts from a larger value to a smaller value.

We find that in CdSe (x=0), the net spin alignment is best understood in terms of the band symmetry. The corresponding one photon spin alignment is 50% at t=0. However, this is not true for $Cd_{1-x}Mn_xSe$ (x#0) since the d like states of Mn^{2+} ions contribute to the conduction band for $x < 0.3$. The observed spin polarization factors are almost half the value calculated. Whether the d states really affect the spin alignment can be checked using samples of $x > 0.3$ and with the c-axis perpendicular to the surface. In these samples the d levels do not contribute to the conduction band and for the above bandgap excitation of free carriers the net spin alignment should be similar to CdSe.

The spin relaxation in CdSe at high carrier densities ($\sim 10^{18}/cm^3$) and low temperatures (< 100K) is due to the D'yakonov and Perel' mechanism. The spin relaxation times are ~ 30 psec. In $Cd_{1-x}Mn_xSe$, the spin relaxation is due to combination of the D-P and the spin exchange mechanism. We have observed spin relaxation times < 20 psec in $Cd_{0.9}Mn_{0.1}Se$ which is expected to be shorter for large x. Due to the lack of time resolution, we could not measure spin relaxation times for large x. It is necessary to make more measurements over a wide range of x.

We have measured optical deformation potentials for the conduction (0.5×10^9 eV/cm) and valence (0.24×10^9 eV/cm) bands separately. This was possible due to the presence of Mn^{2+} 3d levels within the forbidden bandgap for $x > 0.3$. We measured bound mag-

netic polaron (BMP) energies for various x and found that the antiferromagnetic interactions (Mn^{2+}-Mn^{2+}) strongly affects the BMP energies. The temperature dependence of the BMP luminescence and energy shows abnormalities around the N'eel temperature $T_N \sim 60K$ which we have attributed to the clusters. The BMP-I radii for $x < 0.3$ are $\sim 30\text{Å}$, while for $x > 0.3$ are $\sim 12\text{Å}$ (BMP-II). This is due to the different effective masses of the electrons involved, i.e. $m_e = 0.13m_o$ and $m_e = m_o$ for the former and later cases, respectively. The formation times of the BMP becomes shorter for large x ($0 < x < 0.3$). This is consistent with the steady state BMP energies since the large x provides more localization energies. For large x, the $\tilde{x}$ becomes independent of x. The BMP-II formation time for $x > 0.3$ may become constant. More time resolved spectral measurements are required to understand the effect of antiferromagnetic interaction on BMP. The red luminescence should be studied for well characterized samples incuding crystal growth conditions and under magnetic field to see the effect of antiferromagnetic interaction.

APPENDICES

A.1 ONE PHOTON SPIN ALIGNMENT EXCLUDING SPLIT-OFF VALENCE BAND

The right handed circularly polarized light adds one unit of angular momentum to the valence electron angular momentum during absorption. The final states are with angular momentum +1/2 or -1/2. Hence following transitions are possible (the dot product for all other matrix elements with electric field vector is zero):

Initial spin	+	Photon spin	=	Final spin
-3/2		1		-1/2
-1/2		1		+1/2

$$N(\uparrow) \sim |\langle C, {}^1/_2, +{}^1/_2|\vec{P}|V_{\ell h}, {}^3/_2, -{}^1/_2\rangle \cdot \hat{E}|^2$$

$$\sim |\frac{1}{\sqrt{6}} P(\hat{\imath} - \hat{\jmath})\ (\hat{\imath} + \hat{\jmath})|^2$$

$$\sim \frac{2}{3}P^2$$

$$N(\downarrow) \sim |\langle C, {}^1/_2, -{}^1/_2|\vec{P}|V_{hh}, {}^3/_2, -{}^3/_2\rangle \cdot \hat{E}|^2$$

$$\sim |\frac{1}{\sqrt{2}} P(\hat{\imath} - \hat{\jmath})\ (\hat{\imath} + \hat{\jmath})|^2$$

$\sim 2P^2$

The ratio $N(\uparrow):N(\downarrow)$ is 1:3. The polarization factor ρ is,

$$\rho = \frac{N(\uparrow) - N(\downarrow)}{N(\uparrow) + N(\downarrow)} = \frac{1}{2}.$$

A.2 ONE PHOTON SPIN ALIGNMENT INCLUDING SPLIT-OFF VALENCE BAND

Using the similar arguments as in A.1 we get,

$$N(\uparrow) \sim |\langle C, {}^1/_2, +{}^1/_2|\vec{P}|V_{\ell h}, {}^3/_2, -{}^1/_2\rangle\cdot\hat{E}|^2 + |\langle C, {}^1/_2, +{}^1/_2|\vec{P}|\Delta\ , {}^1/_2, -{}^1/_2\rangle\cdot\hat{E}|^2$$

$$\sim \frac{2}{3}P^2 + \frac{4}{3}P^2$$

$$\sim 2P^2$$

$$N(\downarrow) \sim |\langle C, {}^1/_2, -{}^1/_2|\vec{P}|V_{hh}, {}^3/_2, -{}^3/_2\rangle\cdot\hat{E}|^2$$

$$\sim 2P^2$$

The ratio $N(\uparrow):N(\downarrow)$ is 1:1 and the polarization factor is 0.

The more accutate treatment must include mixed states.

SPIN POLARIZATION BASED ON KANE BAND MODEL

Schrodinger Equation for an electron is given by,

$[P^2/2m + V(\vec{r})]\Psi(\vec{k},\vec{r}) = E\Psi(\vec{k},\vec{r})$

where P, $V(\vec{r})$ are momentum and ion core potential operators.

$\Psi(\vec{k},\vec{r}) = u_{\vec{k}}(\vec{r})e^{i\vec{k}.\vec{r}}$

$u_k(\vec{r})$ are Bloch wave functions.

$[(P^2/2m) + V(\vec{r}) + (\hbar/m)\vec{k}.\vec{P} + \hbar/4m^2c^2(\nabla V(\vec{r})x\vec{P}).\vec{\sigma}]u_k(\vec{r}) = E_k'u_{\vec{k}}(\vec{r})$

where $E_k' = E_k - \hbar^2/2m\ k^2$

Assume the solution of the equation,

$[P^2/2m + V]u_{ki} = E_iu_{ki}$,

is known i.e. u_{ki}'s form the basis. In III-V or II-VI material the coduction and valence bands are s and p type, respectively. Hence, using the basis functions $|iS\uparrow\rangle$, $|(X-iY)\uparrow/\sqrt{2}\rangle$, $|Z\downarrow\rangle$, $|(X+iY)\uparrow\rangle$, $|iS\uparrow\rangle$, $|-(X-iY)\downarrow/\sqrt{2}\rangle$, $|Z\uparrow\rangle$, $|(X-iY)\downarrow\rangle$ the 8X8 interaction matrix may be written as,

$$\begin{vmatrix} H & 0 \\ 0 & H \end{vmatrix}$$

This is due to two fold degeneracy of last four wave functions with the first four.

	$\|iS\downarrow\rangle$	$\|(X-iY)\uparrow/\sqrt{2}\rangle$	$\|Z\downarrow\rangle$	$\|(X+iY)\uparrow/\sqrt{2}\rangle$	
$\|iS\downarrow\rangle$	E_s	0	kP	0	
$\|(X-iY)\uparrow/\sqrt{2}\rangle$	0	$E_p-\Delta/3$	$\sqrt{2}\Delta/3$	0	= H
$\|Z\downarrow\rangle$	kP	$\sqrt{2}\Delta/3$	E_p	0	
$\|(X+iY)\uparrow/\sqrt{2}\rangle$	0	0	0	$E_p+\Delta/3$	

$P = -(i\hbar/m)\langle S|P_z|Z\rangle$

$\Delta = 3\hbar i/4m^2c^2\langle X|\partial V/\partial x P_y - \partial V/\partial y P_x|Y\rangle$

E_s and E_p are eigenvalues of the Hamiltonian $H_o = P^2/2m + V(r)$.

Eigenvalues of H are obtained as follows.

$$\det \begin{vmatrix} E_s & 0 & kP & 0 \\ 0 & E_p-\Delta/3-\lambda & \sqrt{2}/3\Delta & 0 \\ kP & \sqrt{2}/3\Delta & E_p & 0 \\ 0 & 0 & 0 & E_p+\Delta/3-\lambda \end{vmatrix} = 0$$

$(E_p + \Delta/3- \lambda)[(E_s - \lambda)(E_p - \Delta/3 - \lambda)(E_p-\lambda)-(E_s - \lambda)2/9\Delta^2 - (kP)^2(E_p - \Delta/3 -\lambda)] = 0$

For small values of k^2, the eigenvalues or energy bands are,

$$E_c = E_g + \hbar^2k^2/2m + P^2k^2/3(2/E_g + 1/(E_g+\Delta))$$

$$E_h = \hbar^2k^2/2m$$

$$E_l = \hbar^2k^2/2m - 2P^2k^2/3E_g$$

$$E_\Delta = -\Delta + \hbar^2k^2/2m - P^2k^2/(E_g+\Delta).$$

The wave functions for conduction, heavy hole, light hole and split-off valence bands are designated as c, V_h, V_l, and V_Δ, respectively (with respective spin coordinates too!).

$|C,1/2,1/2\rangle = A_c|iS\uparrow\rangle + B_c/\sqrt{2}|-(X+iY)\downarrow\rangle + C_c|Z\uparrow\rangle$

$|C,1/2,-1/2\rangle = A_c|iS\downarrow\rangle + B_c/\sqrt{2}|(X-iY)\uparrow\rangle + C_c|Z\downarrow\rangle$

$|V_h,3/2,3/2\rangle = 1/\sqrt{2}|(X+iY)\uparrow\rangle$

$|V_h,3/2,-3/2\rangle = 1/\sqrt{2}|(X-iY)\uparrow\rangle$

$|V_l,3/2,1/2\rangle = A_l|iS\uparrow\rangle + B_l/\sqrt{2}|-(X+iY)\downarrow\rangle + C_l|Z\uparrow\rangle$

$|V_l,3/2,-1/2\rangle = A_l|iS\downarrow\rangle + B_l/\sqrt{2}|(X-iY)\uparrow\rangle + C_l|Z\downarrow\rangle$

$|V_\Delta,1/2,1/2\rangle = A_s|iS\uparrow\rangle + B_s/\sqrt{2}|-(X+iY)\downarrow\rangle + C_s|Z\uparrow\rangle$

$|V_\Delta,1/2,1/2\rangle = A_s|iS\downarrow\rangle + B_s/\sqrt{2}|(X-iY)\uparrow\rangle + C_l|Z\downarrow\rangle$

$\hbar/m\langle S|\vec{P}|X\rangle = \hat{i}P$

$\hbar/m\langle S|\vec{P}|Y\rangle = \hat{j}P$

$\hbar/m\langle S|\vec{P}|Z\rangle = \hat{k}P$

All other matrix elements are equal to zero.

For the case of dipole interaction $(-\vec{A}.\vec{P})$ and right circular polarization (RCP) excitation, the probability of +1/2 spin transitions in conduction band is given by,

$|\langle C,1/2,1/2|P.A|V_h,3/2,3/2\rangle|^2 + |\langle C,1/2,1/2|P.A|V_h,3/2,-3/2\rangle|^2 +$

$|\langle C,1/2,1/2|P.A|V_l,3/2,1/2\rangle|^2 + |\langle C,1/2,1/2|P.A|V_l,3/2,-1/2\rangle|^2 +$

$|\langle C,1/2,1/2|P.A|V_\Delta,1/2,1/2\rangle|^2 + |\langle C,1/2,1/2|P.A|V_\Delta,1/2,-1/2\rangle|^2$

$=0 + 0 + 0 + (A_cB_l/\sqrt{2} - A_lB_c/\sqrt{2})^2 + (A_cB_s/\sqrt{2} - A_sB_c/\sqrt{2})^2$

The the probability of -1/2 spin transition in conduction band is given by,

$|\langle C,1/2,-1/2|P.A|V_h,3/2,3/2\rangle|^2 + |\langle C,1/2,-1/2|P.A|V_h,3/2,-3/2\rangle|^2 +$

$|\langle C,1/2,-1/2|P.A|V_\Delta,3/2,1/2\rangle|^2 + |\langle C,1/2,-1/2|P.A!V_l,3/2,-1/2\rangle|^2 +$

$|\langle C,1/2,-1/2|P.A|V_\Delta,1/2,1/2\rangle|^2 + |\langle C,1/2,-1/2|P.A|V_\Delta,1/2,-1/2\rangle|^2$

$0 + (A_c/\sqrt{2})^2 + 0 + 0 + 0$

Spin polarization $\rho = (n\uparrow - n\downarrow)/(n\uparrow + n\downarrow)$

$$= \frac{[(A_c B_\ell - A_\ell B_c)^2 - A_c^2]}{[(A_c B_\ell - A_\ell B_c)^2 + A_c^2]}$$

excluding split-off valence band.

For small k

$$A_c = kP[E_g + P^2k^2/3(2/E_g + 1/(E_g + \Delta)) + 2\Delta/3]/N$$

$$B_c = \sqrt{2}\Delta/3[P^2k^2/3(2/E_g + 1/(E_g + \Delta))]/N$$

$$B_\ell = \sqrt{2}\Delta/3[- 2P^2k^2/3E_g - E_g]/N$$

$$A_\ell = kP[-2P^2k^2/3E_g + 2/3\Delta]/N$$

$$A_s = kP[-\Delta-P^2k^2/3(E_g+\Delta)+2/3\Delta)/N$$

$$B_s = \sqrt{2}/3\Delta[-\Delta-P^2k^2/3(E_g+\Delta)-E_g]/N$$

where N is a normalizing factor equal to the square root of the sum of the squares of the numerators. For very small k,

$A_c = 1$, $B_c = C_c = 0$

$A_\ell = 0$, $B_\ell = 1/\sqrt{3}$, $C_\ell = \sqrt{2}/3$

and $\rho = -1/2$ as shown earlier in A.1.

The k's involved in spin ↑ and spin ↓ are different. Hence, k for the heavy hole and light hole should be calculated seperately.

$$\Delta E_e = \frac{\hbar^2k^2}{2m_e} = \frac{(h\omega - E_g)m_h}{m_e + m_h}$$

$$\Delta E_h = \frac{\hbar^2k^2}{2m_h} = \frac{(h\omega - E_g)m_e}{m_e + m_h}$$

Spin polarization including split-off valence band

$$\rho = \frac{[(A_c B_\ell - A_\ell B_c)^2 - A_c^2 + (A_c' B_s' - A_s' B_c')^2]}{[(A_c B_\ell - A_\ell B_c)^2 + (A_c' B_s' - A_s' B_c')^2 + A_c^2]}$$

'denotes split-off transition values as k would be different.

For large k, Δ can be neglected from the secular Eq.s.

The solutions to the secular Eq.s are,

$$E' = 0$$

and

$$E'(E'-E_g)(E'+\Delta) - k^2P^2(E'+2/3\Delta) = 0$$

Neglecting Δ, one obtains four solutions, i.e.

$$E_c = \hbar^2k^2/2m + [E_g + (E_g^2 + 4k^2P^2)^{1/2}]/2$$

$$E_{V_1} = \hbar^2k^2/2m$$

$$E_{V_2} = \hbar^2k^2/2m$$

$$E_{V_3} = \hbar^2k^2/2m + [E_g - (E_g^2 + 4k^2P^2)^{1/2}]/2$$

Hence,

$$A_c = kP[1/2(E_g + (E_g^2 + 4k^2P^2)^{1/2}) + 2/3\Delta)/N$$

$$B_c = \sqrt{2/3}\Delta[1/2(E_g + (E_g^2 + 4k^2P^2)^{1/2}) - E_g)/N$$

$$B_\ell = -\sqrt{2/3}\Delta E_g/N$$

$$A_\ell = kP(2/9\Delta)/N$$

k corresponding to 2.34 eV photon in CdSe with E_g = 1.8 eV and Δ = 0.4 eV,

$E_c - E_v = \hbar\omega = 1/2(E_g + \sqrt{(E_g^2 + 4k^2P^2)}$

for mP^2 = 13 eV, kP = 1.12 eV.

Neglecting Δ for large k transition in all valence band - conduction band transitions, the values of A_c, B_c, B_ℓ, A_ℓ, A_s, and B_s are aproximately 2.6, 0.15, -0.4, 0.3, 0.84, and 0, -respectively. Hence, the value of ρ calculated including split-off transition would be $\approx$ -0.35. In the above analysis I have neglected completely the k dependece of density of states. Since the split-off transition is additive to the contribution from various transitions to the ρ, the total ρ would be < -0.35 due to small density of states of the split-off valence band. This estimate is in good agreement with the references and measured values given in chapter IV.

All the following programs are written in programming language 'BASIC' under RT-11 operating system on Digital Minc 11-03 computer.

B.1 SPININ.BAS

This program collects 256 data points from Hamamatsu TA at 300 baud and stores the data along with information on temperature, TA gain, MCP gain, excitation wavelength and filters, luminescence path filters, slit width and streak rate etc.

```
100 REM THIS PROGRAM IS FOR ENTERING TWO WINDOW STREAK CAMERA DATA
110 REM      NO PROVISION IS MADE FOR ANY ON LINE ANALYSIS.
120 DIM A$(19)
130 DIM C(256),R(256)
140 PRINT "ENTER FIRST FOUR DIGITS OF FILE CODE"
150 LINPUT W$ \ W$="SY1:"+W$
160 U$="Y" \ Z$=""
170 PRINT "PRESS RETURN WHEN READY TO INPUT DATA"
180 INPUT T$
190 PRINT "START TA DIGITAL OUTPUT"
200 CIN(,A$(1),,1)
210 CIN(,A$(2),,1)
220 CIN(,A$(3),,1)
230 FOR I=1 TO 16
240 CIN(,A$(I+3),,1)
250 NEXT I
260 PRINT "DATA INPUT COMPLETE"
270 FOR I=3 TO 19
280 A$(I)=SEG$(A$(I),2,100)
290 PRINT A$(I)
300 NEXT I
310 PRINT "IS DATA TRANSFER GOOD? (Y OR N)"
320 LINPUT T$
330 IF T$<>U$ GO TO 170
340 C$=DAT$
350 PRINT "ENTER PICTURE NUMBER"
360 LINPUT D$
370 PRINT "ENTER WINDOW NUMBER"
380 LINPUT N$
390 PRINT "ENTER TA GAIN"
400 LINPUT M$
410 PRINT "OTHER INFO UNCHAGED? (Y OR N)" \ LINPUT T$ \ IF T$=U$ GO TO 570
420 PRINT "ENTER SAMPLE TEMP." \ LINPUT F$
430 PRINT "OTHER INFO UNCHAGED? (Y OR N)" \ LINPUT T$ \ IF T$=U$ GO TO 570
440 PRINT "ENTER EXCITATION WAVELENGTH AND FILTERS" \ LINPUT G$,H$
450 PRINT "OTHER INFO UNCHAGED? (Y OR N)" \ LINPUT T$ \ IF T$=U$ GO TO 570
460 PRINT "ENTER LUMINESCENT PATH FILTERS"
470 LINPUT O$
480 PRINT "OTHER INFO UNCHAGED? (Y OR N)" \ LINPUT T$ \ IF T$=U$ GO TO 570
490 PRINT "ENTER SAMPLE NAME"
500 LINPUT E$
510 PRINT "ENTER REFERENCE BEAM FILTERS"
520 LINPUT I$
530 PRINT "ENTER SLIT WIDTH AND STREAK CAMERA SPEED"
540 LINPUT J$,K$
550 PRINT "ENTER CHANNEL PLATE GAIN"
560 LINPUT L$
570 A$(1)=C$+" PICT$"+D$+" SAMPLE="+E$+" TEMP.="+F$+" WL="+G$+" ATTN. BY "
600 A$(1)=A$(1)+H$+" REF. FILTERS="+I$
610 A$(2)="SLIT="+J$+" STREAK SPEED="+K$+" CP GAIN="+L$+" TA GAIN="+M$
620 A$(2)=A$(2)+" WINDOW$"+N$+" FILTERS="+O$
630 PRINT A$(1)
640 PRINT A$(2)
650 PRINT "ENTER FILE NAME FOR THIS SHOT, LAST NAME WAS ",B$
660 INPUT B$
670 B$=W$+B$
680 OPEN B$ AS FILE #1
690 FOR I=1 TO 19
700 PRINT #1,A$(I)
710 NEXT I
720 CLOSE #1
730 PRINT "DO YOU WANT ANOTHER SHOT? (Y OR N)"
740 LINPUT T$
750 IF T$=U$ GO TO 170
760 END
```

B.2 SPINBL.BAS

This program gives the intensity ratio for two windows. The windows correspond to two orthogonal polarizations-but taken with single laser shot.

```
100 PRINT 'NAME OF THE FILE:   SPINBL'
110 PRINT 'THIS PRG. DETERMINES THE BALANCE OF TWO WINDOWS.'
120 PRINT 'YOU NEED TWO PERPENDICULAR FILES COR. TO SINGLE SHOT.'
130 DIM A$(19),B$(19)
140 DIM A(256),B(256),X(256),Y(256),L1(256),L2(256),R(256),S(256)
150 GOSUB 2000 \ REM LOAD THE STREAK CAMERA FILE
160 GOSUB 2100 \ REM LOAD THE PARALLEL FILE AND CORRECT IT
170 GOSUB 2200 \ REM LOAD THE PERPENDICULAR FILE AND CORRECT IT.
200 DISPLAY_CLEAR
210 REM ENTER REF CHANNEL PEAK, IF UNKNOWN THEN FIND IT.
220 REM
230 PRINT 'ENTER REF. CH.  FOR PARALLEL FILE, IF ? ENTER >256'
240 INPUT A2 \ IF A2>256 THEN  GOSUB 3000
250 PRINT 'ENTER REF. CH PEAK FOR PERPENDICULAR FILE, IF ? ENTER >256'
260 INPUT B2 \ IF B2>256 THEN  GOSUB 3100
270 FOR I=A2 TO 256
280 L1(A2-1)=0
290 X(I)=A(I)*S(I)
300 L1(I)=L1(I-1)+X(I)
310 NEXT I
320 FOR I=B2 TO 256
330 L2(B2-1)=0
340 Y(I)=B(I)*S(I)
350 L2(I)=L2(I-1)+Y(I)
360 NEXT I
370 R1=L1(256)/L2(256)
380 R2=1/R1
390 PRINT USING 'INTEGRATED INTENSITY W1 & W2###### ######',L1(256),L2(256)
400 PRINT USING 'R1 AND R2##.### ##.### ',R1,R2
500 PRINT 'DO YOU WANT ANOTHER FILE ?(Y OR N)'
600 LINPUT Q$ \ IF Q$='Y' THEN  GO TO 150
700 GO TO 10000
2000 REM THIS SUBROUTINE LOADS THE STREAK CAMERA RATE FILE.
2010 PRINT 'ENTER THE STREAK CAMERA RATE FILE.' \ LINPUT R$
2020 OPEN R$ AS FILE #1
2030 FOR I=1 TO 256 \ INPUT #1,R(I) \ NEXT I
2040 S(1)=R(1) \ FOR I=2 TO 256 \ S(I)=S(I-1)+R(I) \ NEXT I
2050 CLOSE #1 \ RETURN
2100 REM
2105 REM THIS SUBROUTINE LOADS THE PARALLEL FILE
2107 REM
2110 PRINT 'ENTER WINDOW 1 FILE NAME.' \ LINPUT A$ \ A$='SY1:'+A$
2115 PRINT 'ENTER WINDOW 2 FILE NAME' \ LINPUT B$ \ B$='SY1:'+B$
2120 OPEN A$ AS FILE #2 \ FOR I=1 TO 19 \ LINPUT #2,A$(I) \ NEXT I
2130 CLOSE #2 \ A1=POS(A$(2),'TA GAIN=',1) \ A0$=SEG$(A$(2),A1+8,A1+8)
2140 A(0)=VAL(A0$)
2150 FOR I=4 TO 19 \ FOR J=1 TO 16
2160 K=16*(I-4)+J \ C$=SEG$(A$(I),4*J-3,4*J-1) \ A(K)=VAL(C$)*R(1)/(A(0)*R(K))
2170 NEXT J \ NEXT I \ RETURN
2200 REM
2205 REM THIS SUBROUTINE LOADS THE PERPENDICULAR FILE
2207 REM
2220 OPEN B$ AS FILE #3 \ FOR I=1 TO 19 \ LINPUT #3,B$(I) \ NEXT I \ CLOSE #3
2230 A1=POS(B$(2),'TA GAIN=',1) \ A0$=SEG$(B$(2),A1+8,A1+8) \ B(0)=VAL(A0$)


2250 C$=SEG$(B$(I),4*J-3,4*J-1) \ B(K)=VAL(C$)*R(1)/(B(0)*R(K))
2260 NEXT J \ NEXT I \ RETURN
3000 REM THIS SUBROUTINE FINDS THE REFERENCE CHANNEL PEAK
3010 GRAPH('S',256,,A(1))
3020 PRINT 'MOVE CURSOR UNTIL IT IS ON THE REFERENCE CHANNEL '
3030 A2=75 \ FIND_POINT(A2,A3)
3040 A2=INT(A2) \ PRINT USING 'PAR. FILE REFERENCE  IS ###',A2 \ RETURN
3100 REM THIS SUBROUTINE FINDS THE REFERENCE CHANNEL PEAK
3110 GRAPH('S',256,,B(1))
3120 PRINT 'MOVE CURSOR UNTIL IT IS ON THE REFERENCE CHANNEL '
3130 B2=75 \ FIND_POINT(B2,B3)
3140 B2=INT(B2) \ PRINT USING 'THE PER. FILE REF.  IS ###',B2 \ RETURN
10000 END
```

All the following programmes i.e. B.3, B.4, B.5, B.6, and B.7 contain a subroutine to correct the streak rate non linearity in time and intensity.

B.3 ANSPN1.BAS + SNPLT1.BAS

These programmes analyze spin alignment and relaxation data obtained in chapter 4. It also plots the experimental data and theoretical fit. This requires two data files obtained with same laser shot and intensity correction ratio obtained for the windows as in B.2.

```
10 PRINT "&NSPN1-------POL. CURVE ON HP7225A    "
100 PRINT " THIS PROGRAM TAKES TWO INPUT FILES, CORRESPONDING TO LEFT AND"
110 PRINT "    RIGHT CIRCULAR POLARIZATIONS AND FITS TOTAL KINETIC DECAY AND"
120 PRINT "    SPIN RELAXATION KINETICS."
125 COMMON C(256),Z(256),R(256),S(256),I1,C2,C5,P2,B,A$,A$(19),R$,T2,P5
130 DIM R$(19)
140 DIM A(256),B(256)
150 GOSUB 2000 \ REM LOAD THE STREAK CAMERA FILE
160 GOSUB 2100 \ REM LOAD THE PARALLEL FILE AND CORRECT IT
170 GOSUB 2200 \ REM LOAD THE PERPENDICULAR FILE AND CORRECT IT.
180 PRINT "DO YOU WANT TO ENTER A CORRECTION FACTOR FOR A FILE? (Y OR N)"
190 LINPUT Q$ \ IF Q$="Y" THEN  GOSUB 2300
200 DISPLAY_CLEAR
210 REM ENTER REF CHANNEL PEAK, IF UNKNOWN THEN FIND IT.
220 REM
230 PRINT "ENTER REF. CH. PEAK FOR PARALLEL FILE. IF ? ENTER >256"
240 INPUT A2 \ IF A2>256 THEN  GOSUB 3000
250 PRINT "ENTER REF. CH PEAK FOR PERPENDICULAR FILE, IF ? ENTER >256"
260 INPUT B2 \ IF B2>256 THEN  GOSUB 3100
270 A4=A2-5 \ A5=251-A4 \ FOR I=A4 TO 251 \ J=I+B2-A2 \ P1=(A2+B2)/2
280 C(I)=A(I)+B(J) \ NEXT I
290 GOSUB 3200 \ REM FIND START POINT FOR FIT.
295 P2=C2
300 REM
310 REM PROPERLY SUM CURVES TO FIND K(T)
320 REM
330 A4=A2-5 \ A5=251-A4 \ FOR I=A4 TO 251 \ J=I+B2-A2
340 C(I)=A(I)+B(J) \ NEXT I
350 PRINT "WHAT TYPE OF PLOT? LOG=1, LIN=0,FOR SINGLE EXP RECOMB TIME" \ INPUT L9
360 IF L9=1 THEN  GOSUB 2700
370 GOSUB 2600 \ REM FIND MAX AND MIN VALUES OF C()
380 GOSUB 4000 \ REM GRAPH C(I)
390 GOSUB 5000 \ REM FIT AND GRAPH SINGLE EXPONENTIAL DECAY CURVE
400 PRINT "PLOT DIFFERENTLY? (Y OR N)" \ LINPUT Q$
410 IF Q$="Y" THEN DISPLAY_CLEAR \ GO TO 270
415 REM STORE LIFE TIME      \ T2=T1
420 REM
430 REM THIS SECTION FINDS THE SPIN RELAXATION TIME.
440 REM
450 FOR I=A4 TO 251 \ J=I+B2-A2
460 IF A(I)+B(J)=0 THEN C(I)=0 \ GO TO 475
470 C(I)=(A(I)-B(J))/(A(I)+B(J))
475 IF I=251 GO TO 490 \ NEXT I
490 PRINT "WHAT TYPE OF PLOT? LOG=1, LIN=0,FOR SINGLE EXP SPIN RELAX TIME" \ INPUT L9
492 DISPLAY_CLEAR \ GOSUB 3200 \ P3=C2 \ REM FIND START POINT
495 PRINT "BACKGROUND SUBSTRACTION(Y OR N)?" \ LINPUT Q$
496 IF Q$="Y" THEN PRINT "BACKGROUND?" \ INPUT B \ FOR I=C2 TO 251 \ C(I)=C(I)-B \ NEXT I
500 IF L9=1 THEN  GOSUB 2700
510 GOSUB 2600 \ REM FIND THE MAX AND MIN VALUES OF C(I)
520 D1=1 \ GOSUB 4000 \ POINT('B',S(P2),0,2) \ POINT('B',S(P3),0,2) \ REM GRAPH C(I)
530 GOSUB 5000 \ REM FIT AND GRAPH SINGLE EXPONENTIAL DIFFUSION LIFETIME.
540 D1=0
550 PRINT "PLOT DIFFERENTLY? (Y OR N)" \ LINPUT Q$
560 IF Q$="Y" THEN  GO TO 440
563 A$=A$+"/"+B$ \ PRINT " HARDCOPY OF POL FACTOR DATA(Y OR N)?" \ LINPUT Q$
565 IF Q$="Y" THEN CHAIN "SPNPLT" LINE 7000
570 PRINT "DO YOU WANT TO FIT MORE FILES? (Y OR N)"
580 LINPUT Q$ \ DISPLAY_CLEAR
582 PRINT USING "LAST FILES MAX.LUM AT PSEC  ####.#",S(P2)
583 PRINT USING "MAX POL FACTOR AT PSEC  ####.#",S(P3)
584 PRINT USING "TIME DIFF.IN MAXLUM & MAX POL IN PSEC ###.#",(S(P2)-S(P3))
585 PRINT USING "POL FACTOR OF ##.##",C(P3)
586 PRINT USING " RECOMB LIFE TIME OF #### & SPIN RELAX. TIME OF ####",T2,2*T1
587 IF Q$="Y" GO TO 160
590 GO TO 10000
```

```
2000 REM THIS SUBROUTINE LOADS THE STREAK CAMERA RATE FILE.
2010 PRINT "ENTER THE STREAK CAMERA RATE FILE." \ LINPUT R$
2020 OPEN R$ AS FILE #1
2030 FOR I=1 TO 256 \ INPUT #1,R(I) \ NEXT I
2040 S(1)=R(1) \ FOR I=2 TO 256 \ S(I)=S(I-1)+R(I) \ NEXT I
2050 CLOSE #1 \ RETURN
2100 REM
2105 REM THIS SUBROUTINE LOADS THE PARALLEL FILE
2107 REM
2110 PRINT "ENTER WINDOW 1 FILE NAME." \ LINPUT A$ \ A$="SY1:"+A$
2115 PRINT "ENTER WINDOW 2 FILE NAME" \ LINPUT B$ \ B$="SY1:"+B$
2120 OPEN A$ AS FILE #2 \ FOR I=1 TO 19 \ LINPUT #2,A$(I) \ NEXT I
2130 CLOSE #2 \ A1=POS(A$(2),"TA GAIN=",1) \ A0$=SEG$(A$(2),A1+8,A1+8)
2140 A(0)=VAL(A0$)
2150 FOR I=4 TO 19 \ FOR J=1 TO 16
2160 K=16*(I-4)+J \ C$=SEG$(A$(I),4*J-3,4*J-1) \ A(K)=VAL(C$)*R(1)/(A(0)*R(K))
2170 NEXT J \ NEXT I \ RETURN
2200 REM
2205 REM THIS SUBROUTINE LOADS THE PERPENDICULAR FILE
2207 REM
2220 OPEN B$ AS FILE #3 \ FOR I=1 TO 19 \ LINPUT #3,B$(I) \ NEXT I \ CLOSE #3
2230 A1=POS(B$(2),"TA GAIN=",1) \ A0$=SEG$(B$(2),A1+8,A1+8) \ B(0)=VAL(A0$)
2240 FOR I=4 TO 19 \ FOR J=1 TO 16 \ K=16*(I-4)+J
2250 C$=SEG$(B$(I),4*J-3,4*J-1) \ B(K)=VAL(C$)*R(1)/(B(0)*R(K))
2260 NEXT J \ NEXT I \ RETURN
2300 REM CORRECTION FACTOR ENTRY AND OPERATION
2310 PRINT "ENTER THE MULTIPLICATIVE FACTOR FOR WINDOW 1." \ INPUT C
2320 FOR I=1 TO 256 \ A(I)=A(I)*C \ NEXT I \ RETURN
2600 C3=0 \ C4=0 \ FOR I=A4 TO 251 \ IF C(I)>C3 THEN C3=C(I)
2610 IF C(I)<C4 THEN C4=C(I)
2620 NEXT I \ RETURN
2700 FOR I=1 TO 256
2710 IF C(I)<=0 THEN C(I)=-1 \ GO TO 2730
2720 C(I)=LOG10(C(I))
2730 NEXT I \ RETURN
3000 REM THIS SUBROUTINE FINDS THE REFERENCE CHANNEL PEAK
3010 GRAPH('S',256,,A(1))
3020 PRINT "MOVE CURSOR UNTIL IT IS ON THE REFERENCE CHANNEL PEAK"
3030 A2=75 \ FIND_POINT(A2,A3)
3040 A2=INT(A2) \ PRINT USING "PAR. FILE REFERENCE PEAK IS ###",A2 \ RETURN
3100 REM THIS SUBROUTINE FINDS THE REFERENCE CHANNEL PEAK
3110 GRAPH('S',256,,B(1))
3120 PRINT "MOVE CURSOR UNTIL IT IS ON THE REFERENCE CHANNEL PEAK"
3130 B2=75 \ FIND_POINT(B2,B3)
3140 B2=INT(B2) \ PRINT USING "THE PER. FILE REF. PEAK IS ###",B2 \ RETURN
3200 REM THIS SUBROUTINE FINDS THE BEGINNING POINT FOR CURVE FITTING
3210 GRAPH('S',256,,C(1))
3220 PRINT "MOVE CURSOR UNTIL IT IS AT THE STARTING POINT FOR CURVE FITTING"
3230 C2=100 \ FIND_POINT(C2,C3)
3240 C2=INT(C2) \ PRINT USING "REF. PEAK IS ###",C2 \ RETURN
4000 REM
4010 REM THIS SUBROUTINE GRAPHS C()ANDSETSWINDOWANDGRIDFORCURVEFITTING
4020 REM
4030 WINDOW('-E',S(A4),L4,S(251),C3,0)
4040 IF L9=1 THEN  GO TO 4060
4050 IF D1=1 THEN WINDOW(,S(A4),-1,S(251),1,0)
4060 GRAPH('-E,S',A5,S(A4),C(A4),,,1)
4070 E1=S(C2) \ E2=C(C2) \ GRAPH('-E,B',1,E1,E2,,0,2)
4080 RETURN
4200 REM
4210 REM THIS SECTION PLOTS THE EXPONENTIAL FIT AND CALCULATES THE SUM OF
4220 REM       SQUARES DEVIATION.
4230 C7=0 \ FOR I=C2 TO 251
4240 C6=C5*EXP(-(S(I)-S(C2))/T1) \ C7=C7+(C6-C(I))^2
4243 Z(I)=C6
4250 IF L9=0 THEN  GO TO 4270
4260 C6=LOG10(C6)
4270 POINT(,S(I),C6,2) \ NEXT I
4280 PRINT USING "FOR A TIME CONST. OF #### PS AND A CONST. OF #.##^^^^",T1,C5
4290 PRINT USING "   THE SUM OF THE SQUARES IS #.##^^^^",C7
4300 RETURN
```

```
5000 REM
5010 REM THIS SECTION CALCULATES A FIT FROM INPUTED TRIAL VALUES
5020 REM
5030 PRINT "ENTER A TRIAL TIME CONSTANT IN PICOSECONDS" \ INPUT T1
5040 IF L9=1 THEN C5=10^C(C2) \ GO TO 5060
5050 C5=C(C2)
5060 GOSUB 4200
5070 PRINT "DO YOU WANT TO TRY ANOTHER FIT? (Y OR N)"
5080 LINPUT Q$ \ IF Q$<>"Y" GO TO 5110
5090 PRINT "ENTER A NEW TIME CONSTANT AND MULTIPLICATIVE FACTOR."
5100 INPUT T1,C5 \ GOSUB 4200 \ GO TO 5070
5110 REM PRINT "DO YOU WANT A HARDCOPY OF THIS GRAPH? (YORN)"
5120 REM LINPUT Q$                              \ IF Q$="Y" THEN  GOSUB 6000
5130 RETURN
6000 RETURN
10000 END
```

```
7000 REM
7001 PRINT 'THIS PRG PLOTS DATA ON HP7225A PLOTER.( SPNPLT )'
7010 COMMON C(256),Z(256),R(256),S(256),T1,C2,C5,P3,B,A$,A$(19),R$
7020 REM
7030 REM THIS SUBROUTINE PLOTS THE EXPERIMENTAL FIT FILE ON HP7525A
7040 REM
7042 GOSUB 7070 \ GOSUB 8140
7043 PRINT 'THEORATICAL FIT (Y OR N )?' \ LINPUT Q$
7044 IF Q$='Y' THEN  GOSUB 7050 \ GOSUB 7170 \ CHAIN 'ANSPIN ' LINE 570
7070 V4=500
7080 IF R$='SF150' THEN V5=600
7090 IF R$='SF075' THEN V5=1800
7095 IF R$='SF030' THEN V5=3600
7100 IF R$='SF015' THEN V5=6000
7120 V6=-.1*V5 \ V7=-.1*V4
7130 V4=V4*5 \ V5=V5*5 \ V6=V6*5
7131 V7=-V4 \ REM MULT. BY 5 FOR BETTER PLOT RESOL.
7140 V4$=STR$(V4) \ V5$=STR$(V5) \ V6$=STR$(V6) \ V7$=STR$(V7)
7150 H1$='SC'+STR$(S(C2-10))+','+STR$(S(C2+40))+','+V7$+','+V4$+';' \ COUT(,H1$,,1)
      \ REM SCALING
7160 H2$='PU;PA'+STR$(S(C2-10))+',0;' \ COUT(,H2$,,1) \ RETURN \ REM MOVETOORIGIN
7161 H9$=CHR$(3) \ H1=POS(B$,'WL=',1)
7162 H3$=','+STR$(-.05*V4)+';LB'
7170 FOR I=C2-10 TO C2+40
7180 H1$='PA'+STR$(S(I))+','+STR$(Z(I)*2000)+';PD;' \ COUT(,H1$,,1)
7181 NEXT I \ REM PLOT CURVE
7184 B1$='SLOW TIME CONST. IN MSEC='
7185 B2$='SLOW AMPLITUDE = '
7186 B3$='FAST TIME CONST. IN MSEC='
7187 B4$='FAST AMPLITUDE = '
7188 B5$='TOTAL UNNORMALIZED AMPLITUDE = '
7189 W$=B1$ \ Y$=STR$(T1) \ H1$='IN;PA2000,5000;PD;' \ COUT(,H1$,,1) \ GOSUB 7210
7190 W$=B3$ \ Y$=STR$(T2) \ H1$='IN;PA2000,4000;PD;' \ COUT(,H1$,,1) \ GOSUB 7210
7191 W$=B4$ \ Y$=STR$(A9/C) \ H1$='IN;PA2000,3500;PD;' \ COUT(,H1$,,1) \ GOSUB 7210
7192 W$=B5$ \ Y$=STR$((A1+A9)/C) \ H1$='IN;PA2000,3000;PD;' \ COUT(,H1$,,1) \ GOSUB
      7210
7193 W$=B2$ \ Y$=STR$(A1/C) \ H1$='IN;PA2000,4500;PD;' \ COUT(,H1$,,1) \ GOSUB 7210
      \ GO TO 7211
7210 H1$='LB'+W$+Y$+H9$ \ COUT(,H1$,,1) \ RETURN
7211 RETURN
8000 REM
8010 RETURN
8140 H1$='PD;' \ FOR I=1 TO 12 \ H1$=H1$+'PA'+STR$(S(C2-10)+(S(C2+40)-S(C2-10))*I/12)
8150 COUT(,H1$,,1) \ REM PLOT AN X-AXIS                    +',0'+';XT;' \ NEXT I
8160 COUT(,'PU;PA'+STR$(S(C2-10))+',0;',,1) \ H1$='PD;'
8170 FOR I=1 TO 12 \ H1$=H1$+'PA'+STR$(S(C2-10))+','+STR$(V4*(I-6)/12)+';YT;' \ NEXT I
      \ H1$=H1$+'PU;'
8180 COUT(,H1$,,1) \ REM PLOT AN Y-AXIS
8190 FOR I=C2-10 TO C2+40
8200 H1$='PA'+STR$(S(I))+','+STR$(C(I)*2000)+';PD;PU;' \ COUT(,H1$,,1)
8210 NEXT I \ REM PLOT CURVE
8220 H1$='PU;PA'+STR$(.1*V5)+','+STR$(.9*V4)+';' \ COUT(,H1$,,1)
8225 H9$=CHR$(3) \ H3$=','+STR$(-.05*V4)+';LB'
8226 H1$='LB'+A$+H9$+'CP;' \ COUT(,H1$,,1)
8227 H1=POS(A$(1),'WL=',1)
8230 H1$='LB'+SEG$(A$(1),1,H1-1)+H9$+'CP;' \ COUT(,H1$,,1)
8235 H1$='CP4,0;LB'+SEG$(A$(1),H1,100)+H9$+'CP;' \ COUT(,H1$,,1)
8240 H1$='LB'+A$(2)+H9$+'CP;' \ COUT(,H1$,,1)
8242 REM H1$='LB'+A$(20)+H9$+'CP;' \ REM COUT(,H1$,,1)
8250 FOR I=1 TO 6 \ H1$='PU;PA'+STR$(V5*I/6)+H3$+STR$(V5*1/30)+H9$+'PU;'
8255 COUT(,H1$,,1)
8260 NEXT I \ REM NUMBERING THE X-AXIS
8270 CHAIN 'ANSPIN ' LINE
10000 END
```

B.4 ADDGNW.BAS

This program averages a number of data files taken under identical experimental conditions. Each data file must include a prepulse for better averaging.

```
318 PRINT 'PROGRAM   ADDG.BAS '
319 PRINT 'THIS PROGRAM ADDS MANY FILES OF DATA'
320 PRINT 'TA NORMALIZATION IS INCLUDED '
321 PRINT 'TAKE THE BEST FILE FIRST,IT IS TAKEN AS REFERENCE '
322 DIM A(256),B(256),R(256),S(256),A$(19),B$(20)
324 PRINT 'ENTER THE NAME OF FIRST FILE '
325 LINPUT A1$
326 B$(20)='FILES ADDED='+A1$ \ A1$='SY1:'+A1$
328 OPEN A1$ AS FILE #1
329 FOR I=1 TO 19 \ LINPUT #1,A$(I) \ NEXT I
332 CLOSE #1
333 FOR I=1 TO 3 \ B$(I)=A$(I) \ NEXT I
337 REM GOSUB 2000                  \ REM LOAD THE STREAK CAMERA FILE
347 GOSUB 2100 \ REM LOAD THE DATA FILE & CORRECT IT
357 DISPLAY_CLEAR
358 GOSUB 3200 \ REM FIND START POINT FOR FIT.
360 PRINT ' DO YOU WANT DIFFERENT FIRST FILE?(Y OR N)' \ LINPUT Q$
362 IF Q$='Y' GO TO 324
370 GOSUB 2600 \ REM FIND MAX & MIN VALUES OF A()
380 REM GOSUB 4000                  \ REM GRAPH A(I)
390 GO TO 5101
2000 REM THIS SUBROUTINE LOADS THE STREAK CAMERA RATE FILE.
2002 PRINT 'DO YOU WANT A NEW STREAK CAMERA RATE FILE? (Y OR N) LAST WAS',R$
2004 LINPUT Q$ \ IF Q$<>'Y' GO TO 2055
2010 PRINT 'ENTER THE STREAK CAMERA RATE FILE.' \ LINPUT R$
2020 OPEN R$ AS FILE #1
2030 FOR I=1 TO 256 \ INPUT #1,R(I) \ NEXT I
2040 S(1)=R(1) \ FOR I=2 TO 256 \ S(I)=S(I-1)+R(I) \ NEXT I
2050 CLOSE #1 \ RETURN
2055 RETURN
2100 REM
2105 REM THIS SUBROUTINE LOADS THE FILE
2107 REM
2130 A1=POS(A$(2),'TA GAIN=',1) \ A0$=SEG$(A$(2),A1+8,A1+8)
2140 A(0)=VAL(A0$)
2150 FOR I=4 TO 19 \ FOR J=1 TO 16
2160 K=16*(I-4)+J \ C$=SEG$(A$(I),4*J-3,4*J-1) \ A(K)=VAL(C$)/A(0)
2170 NEXT J \ NEXT I \ RETURN
2300 REM CORRECTION FACTOR ENTRY & OPERATION
2310 PRINT 'ENTER MULTIPLICATIVE FACTOR , IF NONE, ENTER 1' \ INPUT C
2320 FOR I=1 TO 256 \ A(I)=A(I)*C \ NEXT I \ RETURN
2600 A3=0 \ A4=0 \ FOR I=A4 TO 251 \ IF A(I)>A3 THEN A3=A(I)
2610 IF A(I)<A4 THEN A4=A(I)
2620 NEXT I \ RETURN
3200 REM THIS SUBROUTINE FINDS BIGINING POINT FOR CURVE FITTING'
3210 GRAPH('S',256,,A(1))
3220 PRINT 'MOVE CURSER UNTIL IT IS AT  POINT FOR CURVE MATCHING'
3230 A2=100 \ FIND_POINT(A2,A3)
3240 A2=INT(A2) \ PRINT USING 'START CHANNEL IS###',A2 \ RETURN
4000 REM
4010 REM THIS SUBR. GRAPHS A()&SETSWINDOWGRIDFORCURVEFITTING.
4020 REM
4030 WINDOW('-E',S(A4),A4,S(251),A3,0)
4050 IF D1=1 THEN WINDOW(,S(A4),-1,S(251),1,0)
4060 GRAPH('-E,S',256,S(A4),A(A4),,,1)
4070 E1=S(A2) \ E2=A(A2) \ GRAPH('-E,B',1,E1,E2,,,2)
4080 RETURN
5101 PRINT 'DO YOU WANT DIFFERENT START CHANNEL?(Y OR N)'
5102 LINPUT Q$ \ IF Q$='Y' THEN  GO TO 357
5120 FOR I=1 TO 256 \ B(I)=A(I) \ NEXT I
5125 A9=A2
5127 N=1
5128 B(0)=A(0)
5130 PRINT 'DO YOU HAVE ANOTHER FILE TO ADD(Y OR N ?)?LAST WAS ',A1$
5135 LINPUT Q$ \ IF Q$<>'Y' GO TO 5191
5136 PRINT 'TYPE ANOTHER FILE NAME TO ADD '
5140 LINPUT A1$
5141 A1$='SY1:'+A1$
5143 F1$=SEG$(A1$,5,15)
5145 OPEN A1$ AS FILE #1 \ FOR I=1 TO 19
5150 LINPUT #1,A$(I) \ NEXT I \ CLOSE #1
5153 REM GOSUB 2000                 \ REM LOAD THE STREAK CAMERA FILE
5154 GOSUB 2100 \ REM LOAD THE DATA FILE & CORRECT IT
5155 DISPLAY_CLEAR \ GOSUB 3200
```

```
5156 PRINT "LIKE IT?(Y OR N)" \ LINPUT Q$ \ IF Q$="Y" THEN B$(20)=B$(20)+"+"F1$
     \ IF Q$="N" GO TO 5130
5157 GOSUB 2600 \ REM FIND MAX & MIN POINT FOR FIT
5158 REM GOSUB4000                \ REM GRAPH A(I)
5159 PRINT "DO YOU WANT DIFFERENT START CHANNEL?(Y OR N)"
5160 LINPUT Q$ \ IF Q$="Y" THEN  GO TO 357
5161 IF N>1 THEN  GO TO 5177
5162 A=ABS(A9-A2) \ L=256-A \ IF SGN(A9-A2)>0 GO TO 5175
5165 E=L \ FOR I=1 TO L \ X=(A(A+I)+N*B(I))/(N+1) \ B(I)=X \ NEXT I
5170 FOR I=L+1 TO 256 \ B(I)=0 \ NEXT I \ GO TO 5184
5175 E=256 \ FOR I=1 TO L \ X=(N*B(I+A)+A(I))/(N+1) \ B(I+A)=X \ NEXT I \ GO TO 5184
5177 A=ABS(A9-A2) \ L=256-A \ IF (256-A2)>(E-A9) THEN  GO TO 5181
5178 FOR I=1 TO (256-A) \ X=(N*B(I)+A(I+A))/(N+1) \ B(I)=X \ NEXT I
5179 FOR I=(257-A) TO 256 \ B(I)=0 \ NEXT I \ E=256-A \ GO TO 5184
5181 IF A2>A9 THEN  GO TO 5183
5182 FOR I=1 TO (E-A) \ X=(N*B(I+A)+A(I))/(N+1) \ B(I+A)=X \ NEXT I \ GO TO 5184
5183 FOR I=1 TO E \ X=(N*B(I)+A(I+A))/(N+1) \ B(I)=X \ NEXT I
5184 B(0)=(A(0)+N*B(0))/(N+1)
5185 N=N+1
5190 GO TO 5130
5191 FOR I=1 TO 256 \ A(I)=B(I) \ NEXT I
5195 GOSUB 2600 \ REM FIND MAX & MIN VALUES OF A()
5196 GOSUB 3200 \ REM GRAPH A(I)
5200 FOR I=1 TO 256 \ A(I)=A(I)*B(0) \ NEXT I
5300 PRINT "ENTER  NAME OF FILE TO STORE DATA ,IF NOT TYPE N "
5310 LINPUT D$ \ IF D$="N" GO TO 5460
5320 IF SEG$(D$,1,4)="SY0:" GO TO 5340
5325 IF SEG$(D$,1,4)="SY1:" GO TO 5340
5330 D$="SY1:"+D$
5340 FOR I=4 TO 19 \ B$(I)="" \ FOR J=1 TO 16 \ K=16*(I-4)+J
5350 C$=STR$(INT(A(K)))
5360 IF SEG$(C$,2,2)=" " GO TO 5390
5370 IF SEG$(C$,3,3)=" " GO TO 5410
5375 GO TO 5430
5390 B$(I)=B$(I)+"0"+"0"+C$+" "
5400 GO TO 5440
5410 B$(I)=B$(I)+"0"+C$+" "
5420 GO TO 5440
5430 B$(I)=B$(I)+C$+" "
5440 NEXT J \ NEXT I
5442 H1=POS(A$(1),"SAMPLE",1)
5443 B$(1)=SEG$(A$(1),1,9)+SEG$(A$(1),H1,200)
5444 H2=POS(A$(2),"TA GAIN=",1)
5445 B$(2)=SEG$(A$(2),1,H2-1)+"TA GAIN="+STR$(B(0))+SEG$(A$(2),H2+9,200)
5450 OPEN D$ AS FILE #1 \ FOR I=1 TO 20 \ PRINT #1,B$(I) \ NEXT I \ CLOSE #1
5460 PRINT "DO YOU HAVE ANOTHER SET OF FILES TO ADD?(Y OR N) "
5470 LINPUT Q$ \ IF Q$<>"Y" GO TO 7000
5480 GO TO 324
7000 END
```

B.5 ANRISE.BAS

This program plots experimental data and a theoretical fit given by Eq. (3.4.2).

```
10 PRINT " FILE NAME:    ANRISE.BAS"
20 PRINT "  THIS PRG. FITS SINGLE EXP TO TAIL & RISE    "
30 PRINT "  FIRST TRY TO FIT THE TAIL OF THE LUM IN PURE    "
40 PRINT "  STARTING POINT OF RISE SHOULD BE KNOWN FROM 5300A SCATTERING FROM SAMPLE FILES."
130 DIM A$(19)
140 DIM A(256),R(256),S(256),L(100),Z(256)
150 GOSUB 2000 \ REM LOAD THE STREAK CAMERA FILE
160 GOSUB 2100 \ REM LOAD THE DATA FILE & CORRECT IT
200 DISPLAY_CLEAR
290 GOSUB 3200 \ REM FIND START POINT FOR FIT.
350 PRINT "WHAT TYPE OF PLOT? LOG=1,LIN=0" \ INPUT L9
360 IF L9=1 THEN  GOSUB 2700
370 GOSUB 2600 \ REM FIND MAX & MIN VALUES OF A()
380 GOSUB 4000 \ REM GRAPH A(I)
390 GOSUB 5000 \ REM FIT & GRAPH SINGLE EXP. DECAY CURVE
570 PRINT "DO YOU WANT TO FIT MORE FILES?(Y OR N)"
580 LINPUT Q$ \ IF Q$="Y" GO TO 160
590 GO TO 10000
2000 REM THIS SUBROUTINE LOADS THE STREAK CAMERA RATE FILE.
2010 PRINT "ENTER THE STREAK CAMERA RATE FILE." \ LINPUT R$
2020 OPEN R$ AS FILE #1
2030 FOR I=1 TO 256 \ INPUT #1,R(I) \ NEXT I
2040 S(1)=R(1) \ FOR I=2 TO 256 \ S(I)=S(I-1)+R(I) \ NEXT I
2050 CLOSE #1 \ RETURN
2100 REM
2105 REM THIS SUBROUTINE LOADS THE FILE
2107 REM
2110 PRINT "ENTER  FILE NAME ." \ LINPUT A$ \ A$="SY1:"+A$
2120 OPEN A$ AS FILE #2 \ FOR I=1 TO 19 \ LINPUT #2,A$(I) \ NEXT I
2130 CLOSE #2 \ A1=POS(A$(2),"TA GAIN=",1) \ A0$=SEG$(A$(2),A1+8,A1+8)
2140 A(0)=VAL(A0$)
2150 FOR I=4 TO 19 \ FOR J=1 TO 16
2160 K=16*(I-4)+J \ C$=SEG$(A$(I),4*J-3,4*J-1) \ A(K)=VAL(C$)*R(100)/R(K)
2170 NEXT J \ NEXT I \ RETURN
2300 REM CORRECTION FACTOR ENTRY & OPERATION
2310 PRINT "ENTER THE MULTIPLICATIVE FACTOR ." \ INPUT C
2320 FOR I=1 TO 256 \ A(I)=A(I)*C \ NEXT I \ RETURN
2600 A3=0 \ A4=0 \ FOR I=A4 TO 251 \ IF A(I)>A3 THEN A3=A(I)
2610 IF A(I)<A4 THEN A4=A(I)
2620 NEXT I \ RETURN
2700 FOR I=1 TO 256
2710 IF A(I)<=0 THEN A(I)=-1 \ GO TO 2730
2720 A(I)=LOG10(A(I))
2730 NEXT I \ RETURN
3000 REM THIS SUBROUTINE FINDS THE REFERENCE PEAK.
3010 GRAPH('S',256,,A(1))
3020 PRINT "MOVE THE CURSOR UNTIL IT IS ON THE REFERENCE CH."
3030 A2=75 \ FIND_POINT(A2,A3)
3040 A2=INT(A2) \ PRINT USING "FILE REF. CH. IS ###",A2 \ RETURN
3200 REM THIS SUBROUTINE FINDS BIGINING POINT FOR CURVE FITTING"
3210 GRAPH('S',256,,A(1))
3220 PRINT "MOVE CURSOR UNTIL IT IS AT THE STARTING POINT FOR CURVE FITTING"
3230 A2=100 \ FIND_POINT(A2,B3)
3240 A2=INT(A2) \ PRINT USING "START CHANEL IS###",A2 \ RETURN
4000 REM
4100 REM THIS SUBR IS FOR SETTING WINDOW & GRID FOR TOTAL FIT.
4105 F=256-A2
4110 WINDOW('-E',S(1),A4,S(251),A3,0)
4120 IF L9=1 THEN  GO TO 4140
4130 IF D1=1 THEN WINDOW(,S(A4),-1,S(251),1,0)
4140 GRAPH('-E,S',256,S(A4),A(A4),,,1)
4150 E1=S(A2) \ E2=A(A2) \ GRAPH('-E,B',1,E1,E2,,,2)
4160 RETURN
4170 REM
4200 REM
4210 REM      THIS SECTION PLOTS THE EXPONENTIAL FIT & CALCULATES THE SUM
4220 REM      OF SQUARES DEVIATION.
4230 A7=0 \ FOR I=A2 TO 251
4240 A6=A5*EXP(-(S(I)-S(A2))/T1) \ A7=A7+(A6-A(I))^2
4245 A1=A5
4250 IF L9=0 THEN  GO TO 4270
4260 Z(I)=A6
```

```
4270 POINT(,S(I),A6,2) \ NEXT I
4280 PRINT USING "FOR A TIME CONST. OF ####PS & A CONST. OF #.##^^^^",T1,A5
4290 PRINT USING " THE SUM OF THE SQAURES IS #.##^^^^",A7
4300 RETURN
5000 REM
5010 REM THIS SECTION CALCULATES A FIT FROM INPUTED TRIAL VALUES
5020 REM
5030 PRINT "ENTER A TRIAL TIME CONSTANT IN PICOSECOND" \ INPUT T1
5040 IF L9=1 THEN A5=10^A(A2) \ GO TO 5060
5050 A5=A(A2)
5055 G=S(A2)
5060 GOSUB 4200
5070 PRINT "DO YOU WANT TO TRY ANOTHER FIT?(Y OR N)"
5080 LINPUT Q$ \ IF Q$<>"Y" GO TO 5101
5090 PRINT " ENTER A NEW TIME CONST. & MULTIPLICATIVE FACTOR."
5100 INPUT T1,A5 \ GOSUB 4200 \ GO TO 5070
5101 PRINT "DO YOU WANT DIFFERENT START CHANEL?(Y OR N)"
5102 LINPUT Q$ \ IF Q$="Y" THEN  GO TO 200
5110 PRINT "IS THIS A RISE TIME EXP. FIT?(Y OR N)" \ LINPUT M$
5120 IF M$<>"Y" THEN  GOSUB 8999 \ T2=0 \ A9=0 \ IF M$<>"Y" GO TO 6175
5125 DISPLAY_CLEAR \ PRINT "GIVE LUMINESCENCE START POINT FROM PREPULSE IN PSEC"
5126 INPUT D \ PRINT "IN THE GRAPH PUT CURSOR AT PREPULSE"
5127 GOSUB 3200
5128 FOR I=1 TO 100 \ L(0)=0 \ L(I)=L(I-1)+R(A2+I-1) \ IF L(I)>D GO TO 5129 \ NEXT I
5129 PRINT "LUMSTART CHANEL #",A2+I \ A2=A2+I
5130 REM
5131 PRINT "MOVE CURSOR ON FLAT OF LUM" \ D2=100 \ FIND_POINT(D2,B3)
5133 PRINT " GIVE TIME CONST. OF RISE TIME IN PSEC" \ INPUT T2
5134 Z=(T2*T1/(T1-T2))*LOG(T1/T2)
5136 IF Z<(S(D2)-S(A2)) THEN T2=T2+3 \ GO TO 5134
5140 REM  THIS SUBROUTINE FINDS FAST COMPONENT.
5150 REM
5155 A1=A5*EXP((G-S(A2))/T1)
5165 GOSUB 4100
5175 A9=A(A2)-A1
5180 FOR I=A2 TO 256
5190 A8=A1*EXP(-(S(I)-S(A2))/T1)-A1*EXP(-(S(I)-S(A2))/T2)
6100 POINT(,S(I),A8,2) \ Z(I)=A8 \ NEXT I
6140 PRINT USING " SLOW TIME CONST. OF #### & COTRIBUTION #.##^^^^",T1,A1
6141 PRINT USING "RISE TIME CONST.OF ####",T2
6150 PRINT "DO YOU WANT ANOTHER RISE TIME COMP.?( Y OR N)"
6153 LINPUT Q$ \ IF Q$="N" GO TO 6157
6155 PRINT "GIVE T2 IN PSEC & A1" \ INPUT T2,A1 \ GO TO 5175
6157 PRINT "NEW START FOR RISE TIME (Y OR N)?" \ LINPUT Q$
6158 IF Q$="Y" THEN  GO TO 5125
6162 PRINT "SLOW COMP FIT?(Y OR N)" \ LINPUT Q$
6163 IF Q$="N" GO TO 6175
6164 PRINT " GIVE T1,A" \ PRINT USING "PREVIOUS T1 #### & A1 #.##^^^^",T1,A1
     \ INPUT T1,A1 \ GO TO 5175
6175 PRINT "HARDCOPY OF EXP. DATA?(Y OR N)" \ LINPUT Q$
6176 IF Q$="Y" THEN  GOSUB 8000 \ GOSUB 7020 \ GOSUB 8140
6177 PRINT "  HARDCOPY OF THOERITICAL FIT?(Y OR N)PLEASE WAIT FOR 30SEC" \ LINPUT Q$ \
     IF Q$="Y" THEN  GOSUB 7000
6178 IF Q$="N" THEN  GO TO 570
6179 GOSUB 7170 \ DISPLAY_CLEAR \ PRINT USING "T1 SLW #### & T2 ####",T1,T2
6185 PRINT USING "A1 SLW ###.# & A9 FST ###.#",A1,A9
6190 GO TO 570
7000 REM
7020 REM
7030 REM THIS SUBROUTINE PLOTS THE EXPERIMENTAL FIT FILE ON HP7525A
7040 REM
7050 C3=0 \ FOR I=1 TO 256 \ IF C(I)>C3 THEN C3=C(I) \ NEXT I
7060 IF I<100 THEN C4=100
7070 IF I>=100 THEN C4=300
7080 IF R$="SF150" THEN C5=600
7090 IF R$="SF075" THEN C5=1800
7095 IF R$="SF030" THEN C5=3600
7100 IF R$="SF015" THEN C5=6000
7110 C4=300
7120 C6=-.1*C5 \ C7=-.1*C4
7130 C4=C4*5 \ C5=C5*5 \ C6=C6*5
7131 C7=C7*5 \ REM MULT. BY 5 FOR BETTER PLOT RESOL.
7140 C4$=STR$(C4) \ C5$=STR$(C5) \ C6$=STR$(C6) \ C7$=STR$(C7)
7150 H1$="SC"+C6$+","+C5$+","+C7$+","+C4$+";" \ COUT(,H1$,,1) \ REM SCALING
```

```
7160 H2$="PU;PA0,0;" \ COUT(,H2$,,1) \ REM MOVE THE PEN TO 0,0
      \ RETURN
7161 H9$=CHR$(3) \ H1=POS(B$,"WL=",1)
7162 H3$=",",+STR$(-.05*C4)+";LB"
7170 FOR I=A2 TO 256
7180 H1$="PA"+STR$(S(I)*5)+","+STR$(Z(I)*5)+";PD;" \ COUT(,H1$,,1)
7181 NEXT I \ REM PLOT CURVE
7184 B1$="SLOW TIME CONST. IN PSEC="
7185 B2$=" AMPLITUDE $ ="
7186 B3$="RISE TIME CONST. IN PSEC="
7189 W$=B1$ \ Y$=STR$(T1) \ H1$="IN;PA2000,5000;PD;" \ COUT(,H1$,,1) \ GOSUB 7210
7190 W$=B3$ \ Y$=STR$(T2) \ H1$="IN;PA2000,4000;PD;" \ COUT(,H1$,,1) \ GOSUB 7210
7193 W$=B2$ \ Y$=STR$(A1) \ H1$="IN;PA2000,4500;PD;" \ COUT(,H1$,,1) \ GOSUB 7210 \ GO TO 7211
7210 H1$="LB"+W$+Y$+H9$ \ COUT(,H1$,,1) \ RETURN
7211 RETURN
8000 REM
8010 RETURN
8140 H1$="PD;" \ FOR I=1 TO 12 \ H1$=H1$+"PA"+STR$(C5*I/12)+",0"+";XT;" \ NEXT I
8150 COUT(,H1$,,1) \ REM PLOT AN X-AXIS
8160 COUT(,"PU;PA0,0;",,1) \ H1$="PD;"
8170 FOR I=1 TO 12 \ H1$=H1$+"PA0,"+STR$(C4*I/12)+";YT;" \ NEXT I \ H1$=H1$+"PU;"
8180 COUT(,H1$,,1) \ REM PLOT AN Y-AXIS
8190 FOR I=1 TO 256
8200 H1$="PA"+STR$(S(I)*5)+","+STR$(A(I)*5)+";PD;" \ COUT(,H1$,,1)
8210 NEXT I \ REM PLOT CURVE
8220 H1$="PU;PA"+STR$(.1*C5)+","+STR$(.9*C4)+";" \ COUT(,H1$,,1)
8225 H9$=CHR$(3) \ H3$=",",+STR$(-.05*C4)+";LB"
8226 H1$="LB"+A$+H9$+"CP;" \ COUT(,H1$,,1)
8227 H1=POS(A$(1),"WL=",1)
8230 H1$="LB"+SEG$(A$(1),1,H1-1)+H9$+"CP;" \ COUT(,H1$,,1)
8235 H1$="CP4,0;LB"+SEG$(A$(1),H1,100)+H9$+"CP;" \ COUT(,H1$,,1)
8240 H1$="LB"+A$(2)+H9$+"CP;" \ COUT(,H1$,,1)
8242 REM H1$="LB"+A$(20)+H9$+"CP;" \ REM COUT(,H1$,,1)
8250 FOR I=1 TO 6 \ H1$="PU;PA"+STR$(C5*I/6)+H3$+STR$(C5*I/30)+H9$+"PU;"
8255 COUT(,H1$,,1)
8260 NEXT I \ REM NUMBERING THE X-AXIS
8270 RETURN
8999 FOR I=A2 TO 256
9000 A8=A5*EXP(-(S(I)-S(A2))/T1)
9001 POINT(,S(I),A8,2) \ Z(I)=A8 \ NEXT I
9002 PRINT USING "SINGLE EXP TIME CONST. OF #### & CONTRB #.###^^^^",T1,A5 \ RETURN
10000 END
```

B.6 DEXPA.BAS

This program plots experimental data and a theoretical fit given by Eq. (3.5.26).

```
10 PRINT " FILE NAME:    DEXP.BAS"
20 PRINT "   THIS PRG. FITS DOUBLE EXP."
30 PRINT "  FIRST TRY TO FIT THE TAIL OF THE LUM IN PURE    "
130 DIM A$(20)
140 DIM A(256),R(256),S(256),Z(256)
150 GOSUB 2000 \ REM LOAD THE STREAK CAMERA FILE
160 GOSUB 2100 \ REM LOAD THE DATA FILE & CORRECT IT
200 DISPLAY_CLEAR
290 GOSUB 3200 \ REM FIND START POINT FOR FIT.
350 PRINT "WHAT TYPE OF PLOT? LOG=1,LIN=0" \ INPUT L9
360 IF L9=1 THEN  GOSUB 2700
370 GOSUB 2600 \ REM FIND MAX & MIN VALUES OF A()
380 GOSUB 4000 \ REM GRAPH A(I)
390 GOSUB 5000 \ REM FIT & GRAPH SINGLE EXP. DECAY CURVE
570 PRINT "DO YOU WANT TO FIT MORE FILES?(Y OR N)"
580 LINPUT Q$ \ IF Q$="Y" GO TO 160
590 GO TO 10000
2000 REM THIS SUBROUTINE LOADS THE STREAK CAMERA RATE FILE.
2010 PRINT "ENTER THE STREAK CAMERA RATE FILE." \ LINPUT R$
2020 OPEN R$ AS FILE #1
2030 FOR I=1 TO 256 \ INPUT #1,R(I) \ NEXT I
2040 S(1)=R(1) \ FOR I=2 TO 256 \ S(I)=S(I-1)+R(I) \ NEXT I
2050 CLOSE #1 \ RETURN
2100 REM
2105 REM THIS SUBROUTINE LOADS THE FILE
2107 REM
2110 PRINT "ENTER  FILE NAME ." \ LINPUT A$ \ A$="SY1:"+A$
2120 OPEN A$ AS FILE #2 \ FOR I=1 TO 20 \ LINPUT #2,A$(I) \ NEXT I
2130 CLOSE #2 \ A1=POS(A$(2),"TA GAIN=",1) \ A0$=SEG$(A$(2),A1+8,A1+8)
2140 A(0)=VAL(A0$)
2150 FOR I=4 TO 19 \ FOR J=1 TO 16
2160 K=16*(I-4)+J \ C$=SEG$(A$(I),4*J-3,4*J-1) \ A(K)=VAL(C$)*R(100)/R(K)
2170 NEXT J \ NEXT I \ RETURN
2300 REM CORRECTION FACTOR ENTRY & OPERATION
2310 PRINT "ENTER THE MULTIPLICATIVE FACTOR ." \ INPUT C
2320 FOR I=1 TO 256 \ A(I)=A(I)*C \ NEXT I \ RETURN
2600 A3=0 \ A4=0 \ FOR I=A4 TO 251 \ IF A(I)>A3 THEN A3=A(I)
2610 IF A(I)<A4 THEN A4=A(I)
2620 NEXT I \ RETURN
2700 FOR I=1 TO 256
2710 IF A(I)<=0 THEN A(I)=-1 \ GO TO 2730
2720 A(I)=LOG10(A(I))
2730 NEXT I \ RETURN
3000 REM THIS SUBROUTINE FINDS THE REFERENCE PEAK.
3010 GRAPH('S',256,,A(1))
3020 PRINT "MOVE THE CURSOR UNTIL IT IS ON THE REFERENCE CH."
3030 A2=75 \ FIND_POINT(A2,A3)
3040 A2=INT(A2) \ PRINT USING "FILE REF. CH. IS ###",A2 \ RETURN
3200 REM THIS SUBROUTINE FINDS BIGINING POINT FOR CURVE FITTING"
3210 GRAPH('S',256,,A(1))
3220 PRINT "MOVE CURSOR UNTIL IT IS AT THE STARTING POINT FOR CURVE FITTING"
3230 A2=100 \ FIND_POINT(A2,B3)
3240 A2=INT(A2) \ PRINT USING "START CHANEL IS###",A2 \ RETURN
4000 REM
4010 REM THIS SUBR. GRAPHS A()&SETSWINDOWGRIDFORCURVEFITTING.
4020 REM
4030 WINDOW('-E',S(A4),A4,S(251),A3,0)
4040 IF L9=1 THEN  GO TO 4060
4050 IF D1=1 THEN WINDOW(,S(A4),-1,S(251),1,0)
4060 GRAPH('-E,S',256,S(A4),A(A4),,,1)
4070 E1=S(A2) \ E2=A(A2) \ GRAPH('-E,B',1,E1,E2,,,2)
4080 RETURN
4100 REM THIS SUBR IS FOR SETTING WINDOW & GRID FOR TOTAL FIT.
4105 F=256-A2
4110 WINDOW('-E',S(A4),A4,S(251),A3,0)
4120 IF L9=1 THEN  GO TO 4140
```

```
4130 IF D1=1 THEN WINDOW(,S(A4),-1,S(251),1,0)
4140 GRAPH('-E,S',256,S(A4),A(A4),,,1)
4150 E1=S(A2) \ E2=A(A2) \ GRAPH('-E,R',1,E1,E2,,,2)
4160 RETURN
4170 REM
4200 REM
4210 REM      THIS SECTION PLOTS THE EXPONENTIAL FIT & CALCULATES THE SUM
4220 REM      OF SQUARES DEVIATION.
4230 A7=0 \ FOR I=A2 TO 251
4240 A6=A5*EXP(-(S(I)-S(A2))/T1) \ A7=A7+(A6-A(I))^2
4245 A1=A5
4250 IF L9=0 THEN  GO TO 4270
4260 Z(I)=A6
4270 POINT(,S(I),A6,2) \ NEXT I
4280 PRINT USING "FOR A TIME CONST. OF ####PS & A CONST. OF #.##^^^^",T1,A5
4290 PRINT USING " THE SUM OF THE SQAURES IS #.##^^^^",A7
4300 RETURN
5000 REM
5010 REM THIS SECTION CALCULATES A FIT FROM INPUTED TRIAL VALUES
5020 REM
5030 PRINT "ENTER A TRIAL TIME CONSTANT IN PICOSECOND" \ INPUT T1
5040 IF L9=1 THEN A5=10^A(A2) \ GO TO 5060
5050 A5=A(A2)
5055 G=S(A2)
5060 GOSUB 4200
5070 PRINT "DO YOU WANT TO TRY ANOTHER FIT?(Y OR N)"
5080 LINPUT Q$ \ IF Q$<>"Y" GO TO 5101
5090 PRINT " ENTER A NEW TIME CONST. & MULTIPLICATIVE FACTOR."
5100 INPUT T1,A5 \ GOSUB 4200 \ GO TO 5070
5101 PRINT "DO YOU WANT DIFFERENT START CHANEL?(Y OR N)"
5102 LINPUT Q$ \ IF Q$="Y" THEN  GO TO 200
5110 PRINT "IS THIS A DOUBLE EXP. FIT?(Y OR N)" \ LINPUT M$
5120 IF M$<>"Y" THEN  GOSUB 8999 \ T2=0 \ A9=0 \ IF M$<>"Y" GO TO 6175
5125 DISPLAY_CLEAR \ GOSUB 3200
5130 REM
5140 REM  THIS SUBROUTINE FINDS FAST COMPONENT.
5150 REM
5155 A1=A5*EXP((G-S(A2))/T1)
5165 GOSUB 4100
5170 PRINT " GIVE TIME CONST. OF FAST COMP. INPSECS" \ INPUT T2
5175 A9=A(A2)-A1
5180 FOR I=A2 TO 256
5190 A8=A1*EXP(-(S(I)-S(A2))/T1)+A9*EXP(-(S(I)-S(A2))/T2)
6100 POINT(,S(I),A8,2) \ Z(I)=A8 \ NEXT I
6140 PRINT USING " SLOW TIME CONST. OF #### & COTRIBUTION #.##^^^^",T1,A1
6141 PRINT USING " FAST TIME CONST. OF #### & CONTRIBUTION #.##^^^^",T2,A9
6150 PRINT "DO YOU WANT ANOTHER FAST COMP.?( Y OR N)"
6160 LINPUT Q$ \ IF Q$="N" GO TO 6162
6161 PRINT "GIVE T2 IN PSEC & A(A2)" \ INPUT T2,A(A2) \ GO TO 5175
6162 PRINT "SLOW COMP FIT?(Y OR N)" \ LINPUT Q$
6163 IF Q$="N" GO TO 6175
6164 PRINT " GIVE T1,A" \ PRINT USING "PREVIOUS T1 #### & A1 #.##^^^^",T1,A1
     \ INPUT T1,A1 \ GO TO 5175
6175 PRINT "HARDCOPY OF EXP. DATA?(Y OR N)" \ LINPUT Q$
6176 IF Q$="Y" THEN  GOSUB 8000 \ GOSUB 7020 \ GOSUB 8140
6177 PRINT "  HARDCOPY OF THOERITICAL FIT?(Y OR N)PLEASE WAIT FOR 30SEC"
     \ LINPUT Q$ \ IF Q$="Y" THEN  GOSUB 7000
6178 IF Q$="N" THEN  GO TO 570
```

```
6185 PRINT USING "A1 SLW ###.# & A9 FST ###.#",A1,A9
6190 GO TO 570
7000 REM
7020 REM
7030 REM THIS SUBROUTINE PLOTS THE EXPERIMENTAL FIT FILE ON HP7525A
7040 REM
7050 C3=0 \ FOR I=1 TO 256 \ IF C(I)>C3 THEN C3=C(I) \ NEXT I
7060 IF I<100 THEN C4=100
7070 IF I>=100 THEN C4=300
7080 IF R$="SF150" THEN C5=600
7090 IF R$="SF075" THEN C5=1800
7095 IF R$="SF030" THEN C5=3600
7100 IF R$="SF015" THEN C5=6000
7110 C4=300
7120 C6=-.1*C5 \ C7=-.1*C4
7130 C4=C4*5 \ C5=C5*5 \ C6=C6*5
7131 C7=C7*5 \ REM MULT. BY 5 FOR BETTER PLOT RESOL.
7140 C4$=STR$(C4) \ C5$=STR$(C5) \ C6$=STR$(C6) \ C7$=STR$(C7)
7150 H1$="SC"+C6$+","+C5$+","+C7$+","+C4$+";" \ COUT(,H1$,,1) \ REM SCALING
7160 H2$="PU;PA0,0;" \ COUT(,H2$,,1) \ REM MOVE THE PEN TO 0,0
     \ RETURN
7161 H9$=CHR$(3) \ H1=POS(B$,"WL=",1)
7162 H3$=",",+STR$(-.05*C4)+";LB"
7170 FOR I=A2 TO 256
7180 H1$="PA"+STR$(S(I)*5)+","+STR$(Z(I)*5)+";PD;" \ COUT(,H1$,,1)
7181 NEXT I \ REM PLOT CURVE
7184 B1$='SLOW TIME CONST. IN MSEC='
7185 B2$='SLOW AMPLITUDE # ='
7186 B3$='FAST TIME CONST. IN MSEC='
7187 B4$='FAST AMPITUDE # ='
7188 B5$='TOTAL UNNORMALIZED AMPLITUDE # ='
7189 W$=B1$ \ Y$=STR$(T1) \ H1$="IN;PA2000,5000;PD;" \ COUT(,H1$,,1) \ GOSUB 7210
7190 W$=B3$ \ Y$=STR$(T2) \ H1$="IN;PA2000,4000;PD;" \ COUT(,H1$,,1) \ GOSUB 7210
7191 W$=B4$ \ Y$=STR$(A9) \ H1$="IN;PA2000,3500;PD;" \ COUT(,H1$,,1) \ GOSUB 7210
7192 W$=B5$ \ Y$=STR$(A1+A9) \ H1$="IN;PA2000,3000;PD;" \ COUT(,H1$,,1) \ GOSUB 7210
7193 W$=B2$ \ Y$=STR$(A1) \ H1$="IN;PA2000,4500;PD;" \ COUT(,H1$,,1) \ GOSUB 7210 \
     GO TO 7211
7210 H1$="LB"+W$+Y$+H9$ \ COUT(,H1$,,1) \ RETURN
7211 RETURN
8000 REM
8010 RETURN
8140 H1$="PD;" \ FOR I=1 TO 12 \ H1$=H1$+"PA"+STR$(C5*I/12)+",0"+";XT;" \ NEXT I
8150 COUT(,H1$,,1) \ REM PLOT AN X-AXIS
8160 COUT(,"PU;PA0,0;",,1) \ H1$="PD;"
8170 FOR I=1 TO 12 \ H1$=H1$+"PA0,"+STR$(C4*I/12)+";YT;" \ NEXT I \ H1$=H1$+"PU;"
8180 COUT(,H1$,,1) \ REM PLOT AN Y-AXIS
8190 FOR I=1 TO 256
8200 H1$="PA"+STR$(S(I)*5)+","+STR$(A(I)*5)+";PD;PU;" \ COUT(,H1$,,1)
8210 NEXT I \ REM PLOT CURVE
8220 H1$="PU;PA"+STR$(.1*C5)+","+STR$(.9*C4)+";" \ COUT(,H1$,,1)
8225 H9$=CHR$(3) \ H3$=","+STR$(-.05*C4)+";LB"
8226 H1$="LB"+A$+H9$+"CP;" \ COUT(,H1$,,1)
8227 H1=POS(A$(1),"WL=",1)
8230 H1$="LB"+SEG$(A$(1),1,H1-1)+H9$+"CP;" \ COUT(,H1$,,1)
8235 H1$="CP4,0;LB"+SEG$(A$(1),H1,100)+H9$+"CP;" \ COUT(,H1$,,1)
8240 H1$="LB"+A$(2)+H9$+"CP;" \ COUT(,H1$,,1)
8245 H1$="LB"+A$(20)+H9$+"CP;" \ COUT(,H1$,,1)
8250 FOR I=1 TO 6 \ H1$="PU;PA"+STR$(C5*I/6)+H3$+STR$(C5*I/30)+H9$+"PU;"
8255 COUT(,H1$,,1)
8260 NEXT I \ REM NUMBERING THE X-AXIS
8270 RETURN
8999 FOR I=A2 TO 256
9000 A8=A5*EXP(-(S(I)-S(A2))/T1)
9001 POINT(,S(I),A8,2) \ Z(I)=A8 \ NEXT I
9002 PRINT USING "SINGLE EXP TIME CONST. OF #### & CONTRB #.###^^^^",T1,A5 \ RETURN
10000 END
```

B.7 PLASM2.BAS

This program plots experimental data and a theoretical fit given by Eq. (3.5.34).

```
10 PRINT ' FILE NAME:    PLASM2.BAS'
20 PRINT '  THIS PRG FITS IN SOL. OF EQ. DER N(T)=-A*N-B*N**2'
30 PRINT '  FIRST TRY TO FIT THE TAIL OF THE LUM IN PURE    '
40 PRINT '  EXP. CURVE WHICH GIVES A & THEN B.     '
130 DIM A$(20)
140 DIM A(256),R(256),S(256),Z(256)
150 GOSUB 2000 \ REM LOAD THE STREAK CAMERA FILE
160 GOSUB 2100 \ REM LOAD THE DATA FILE & CORRECT IT
200 DISPLAY_CLEAR
290 GOSUB 3200 \ REM FIND START POINT FOR FIT.
295 PRINT ' DO YOU LIKE (Y OR N)? ' \ LINPUT Q$
297 IF Q$='N' GO TO 570
350 PRINT 'WHAT TYPE OF PLOT? LOG=1,LIN=0' \ INPUT L9
360 IF L9=1 THEN  GOSUB 2700
370 GOSUB 2600 \ REM FIND MAX & MIN VALUES OF A()
380 GOSUB 4000 \ REM GRAPH A(I)
390 GOSUB 5000 \ REM FIT & GRAPH SINGLE EXP. DECAY CURVE
570 PRINT 'DO YOU WANT TO FIT MORE FILES?(Y OR N)'
580 LINPUT Q$ \ IF Q$='Y' GO TO 160
590 GO TO 10000
2000 REM THIS SUBROUTINE LOADS THE STREAK CAMERA RATE FILE.
2010 PRINT 'ENTER THE STREAK CAMERA RATE FILE.' \ LINPUT R$
2020 OPEN R$ AS FILE #1
2030 FOR I=1 TO 256 \ INPUT #1,R(I) \ NEXT I
2040 S(1)=R(1) \ FOR I=2 TO 256 \ S(I)=S(I-1)+R(I) \ NEXT I
2050 CLOSE #1 \ RETURN
2100 REM
2105 REM THIS SUBROUTINE LOADS THE FILE
2107 REM
2110 PRINT 'ENTER  FILE NAME .' \ LINPUT A$ \ A$='SY1:'+A$
2111 H1$=SEG$(A$,9,9) \ IF ASC(H1$)>57 THEN M=20 \ GO TO 2120
2113 M=19
2120 OPEN A$ AS FILE #2 \ FOR I=1 TO M \ LINPUT #2,A$(I) \ NEXT I
2130 CLOSE #2 \ A1=POS(A$(2),'TA GAIN=',1) \ A0$=SEG$(A$(2),A1+8,A1+8)
2140 A(0)=VAL(A0$)
2150 FOR I=4 TO 19 \ FOR J=1 TO 16
2160 K=16*(I-4)+J \ C$=SEG$(A$(I),4*J-3,4*J-1) \ A(K)=VAL(C$)*R(100)/R(K)
2170 NEXT J \ NEXT I \ RETURN
2300 REM CORRECTION FACTOR ENTRY & OPERATION
2310 PRINT 'ENTER THE MULTIPLICATIVE FACTOR .' \ INPUT C
2320 FOR I=1 TO 256 \ A(I)=A(I)*C \ NEXT I \ RETURN
2600 A3=0 \ A4=0 \ FOR I=A4 TO 251 \ IF A(I)>A3 THEN A3=A(I)
2610 IF A(I)<A4 THEN A4=A(I)
2620 NEXT I \ RETURN
2700 FOR I=1 TO 256
2710 IF A(I)<=0 THEN A(I)=-1 \ GO TO 2730
2720 A(I)=LOG10(A(I))
2730 NEXT I \ RETURN
3000 REM THIS SUBROUTINE FINDS THE REFERENCE PEAK.
3010 GRAPH('S',256,,A(1))
3020 PRINT 'MOVE THE CURSOR UNTIL IT IS ON THE REFERENCE CH.'
3030 A2=75 \ FIND_POINT(A2,A3)
3040 A2=INT(A2) \ PRINT USING 'FILE REF. CH. IS ###',A2 \ RETURN
3200 REM THIS SUBROUTINE FINDS BIGINING POINT FOR CURVE FITTING'
3210 GRAPH('S',256,,A(1))
3220 PRINT 'MOVE CURSOR UNTIL IT IS AT THE STARTING POINT FOR CURVE FITTING'
3230 A2=100 \ FIND_POINT(A2,A3)
3240 A2=INT(A2) \ PRINT USING 'START CHANEL IS###',A2 \ RETURN
4000 REM
4010 REM THIS SUBR. GRAPHS A()&SETSWINDOWGRIDFORCURVEFITTING.
4020 REM
4030 WINDOW('-E',S(A4),A4,S(251),A3,0)
4040 IF L9=1 THEN  GO TO 4060
4050 IF D1=1 THEN WINDOW(,S(A4),-1,S(251),1,0)
4060 GRAPH('-E,S',256,S(A4),A(A4),,,1)
4070 E1=S(A2) \ E2=A(A2) \ GRAPH('-E,B',1,E1,E2,,,2)
4080 RETURN
4100 REM THIS SUBR IS FOR SETTING WINDOW & GRID FOR TOTAL FIT.
4105 F=256-A2
4110 WINDOW('-E',S(A4),A4,S(251),A3,0)
4120 IF L9=1 THEN  GO TO 4140
```

```
4130 IF D1=1 THEN WINDOW(,S(A4),-1,S(251),1,0)
4140 GRAPH('-E,S',256,S(A4),A(A4),,,1)
4150 E1=S(A2) \ E2=A(A2) \ GRAPH('-E,B',1,E1,E2,,,2)
4160 RETURN
4170 REM
4200 REM
4210 REM      THIS SECTION PLOTS THE EXPONENTIAL FIT & CALCULATES THE SUM
4220 REM      OF SQUARES DEVIATION.
4230 A7=0 \ FOR I=A2 TO 251
4240 A6=A5*EXP(-(S(I)-S(A2))/T1) \ A7=A7+(A6-A(I))^2
4250 IF L9=0 THEN  GO TO 4270
4260 A6=LOG10(A6)
4270 POINT(,S(I),A6,2) \ NEXT I
4280 PRINT USING "FOR A TIME CONST. OF ####PS & A CONST. OF #.##^^^^",T1,A5
4290 PRINT USING " THE SUM OF THE SQAURES IS #.##^^^^",A7
4300 RETURN
5000 REM
5010 REM THIS SECTION CALCULATES A FIT FROM INPUTED TRIAL VALUES
5020 REM
5030 PRINT "ENTER A TRIAL TIME CONSTANT IN PICOSECOND" \ INPUT T1
5040 IF L9=1 THEN A5=10^A(A2) \ GO TO 5060
5050 A5=A(A2)
5055 G=S(A2)
5060 GOSUB 4200
5070 PRINT "DO YOU WANT TO TRY ANOTHER FIT?(Y OR N)"
5080 LINPUT Q$ \ IF Q$<>"Y" GO TO 5101
5090 PRINT " ENTER A NEW TIME CONST. & MULTIPLICATIVE FACTOR."
5100 INPUT T1,A5 \ GOSUB 4200 \ GO TO 5070
5101 PRINT "DO YOU WANT DIFFERENT START CHANEL?(Y OR N)"
5102 LINPUT Q$ \ IF Q$="Y" THEN  GO TO 200
5110 PRINT "IS THIS A SINGLE EXP. FIT?(Y OR N)" \ LINPUT M$
5120 IF M$="Y" THEN  GOSUB 8999 \ B=0 \ W=0 \ GOSUB 6175 \ B=0
5125 DISPLAY_CLEAR \ GOSUB 3200
5130 REM
5140 REM  THIS SUBROUTINE FINDS FAST COMPONENT.
5150 REM
5155 A1=A5*EXP((G-S(A2))/T1)
5160 B=(A(A2)/A1-1)/(T1*A(A2))
5165 GOSUB 4100
5170 B=(A(A2)/A1-1)/(T1*A(A2))
5180 FOR I=A2 TO 256
5190 A8=A(A2)/((1+B*A(A2)*T1)*EXP((S(I)-S(A2))/T1)-T1*B*A(A2))
6100 POINT(,S(I),A8,2) \ Z(I)=A8 \ NEXT I
6140 PRINT USING "BIMOLECULAR RECOMB.CONST.B  PER PSEC ##.###^^^^",B
6141 PRINT USING "TIME CONST. T1 IN PSEC ####",T1
6150 PRINT USING " DO YOU WANT TO GIVE A NEW VALUE TO B(Y OR N)?"
6160 LINPUT Q$ \ IF Q$="N" GO TO 6171
6170 PRINT "NEW B=" \ INPUT B \ GO TO 5180
6171 PRINT " DO YOU WANT ANOTHER TOTAL FIT?(Y OR N)"
6172 LINPUT Q$ \ IF Q$="N" THEN  GO TO 6175
6173 PRINT "GIVE T1,A1" \ INPUT T1,A1
6174 GO TO 5170
6175 PRINT "HARDCOPY OF EXP. DATA?(Y OR N)" \ LINPUT Q$
6176 IF Q$="Y" THEN  GOSUB 8000 \ GOSUB 7020 \ GOSUB 8140
6177 PRINT "  HARDCOPY OF THOERITICAL FIT?(Y OR N)PLEASE WAIT FOR 30SEC"
      \ LINPUT Q$ \ IF Q$="N" THEN  GO TO 6179 \ GOSUB 7000
6178 W=B*(A(A2))*1.00000E+12 \ GOSUB 7170 \ DISPLAY_CLEAR \ PRINT USING "T1
    IN PSEC####  &  B IS ##.###^^^^",T1,W \ GO TO 570
6179 W=B*(A(A2))*1.00000E+12 \ PRINT USING "T1 IN PSEC####  &  B IS
       ##.###^^^^",T1,W \ GO TO 570
7000 REM REGION('FULL')
7010 REM GRAPH('SHADE',256,S(1),Z(1))
7020 REM
7030 REM THIS SUBROUTINE PLOTS THE EXPERIMENTAL FIT FILE ON HP7525A
7040 REM
7050 C3=0 \ FOR I=1 TO 256 \ IF C(I)>C3 THEN C3=C(I) \ NEXT I
7060 IF I<100 THEN C4=100
7070 IF I>=100 THEN C4=300
7080 IF R$="SF150" THEN C5=600
7090 IF R$="SF075" THEN C5=1800
7095 IF R$="SF030" THEN C5=3600
7100 IF R$="SF015" THEN C5=6000
7110 C4=300
```

```
7120 C6=-.1*C5 \ C7=-.1*C4
7130 C4=C4*5 \ C5=C5*5 \ C6=C6*5
7131 C7=C7*5 \ REM MULT. BY 5 FOR BETTER PLOT RESOL.
7140 C4$=STR$(C4) \ C5$=STR$(C5) \ C6$=STR$(C6) \ C7$=STR$(C7)
7150 H1$="SC"+C6$+","+C5$+","+C7$+","+C4$+";" \ COUT(,H1$,,1) \ REM SCALING
7160 H2$="PU;PA0,0;" \ COUT(,H2$,,1) \ REM MOVE THE PEN TO 0,0                    \ RETURN
7161 H9$=CHR$(3) \ H1=POS(B$,"WL=",1)
7162 H3$=","+STR$(-.05*C4)+";LB"
7170 FOR I=A2 TO 256
7180 H1$="PA"+STR$(S(I)*5)+","+STR$(Z(I)*5)+";PD;" \ COUT(,H1$,,1)
7181 NEXT I \ REM PLOT CURVE
7183 B4$="BIMOLECULAR RECOMB. CONST. NORMALIZED TO A(A2)=" \ H=B*1.00000E+12
7184 B1$="SLOW TIME CONST. IN PSEC ="
7185 B2$="BIMOLECULAR RECOMBINATION RATE CONST. IN SEC="
7186 B3$="AMPLITUDE # ="
7188 W$=B4$ \ Y$=STR$(H) \ H1$="IN;PA2000,5500;PD;" \ COUT(,H1$,,1) \ GOSUB 7210
7189 W$=B1$ \ Y$=STR$(T1) \ H1$="IN;PA2000,5000;PD;" \ COUT(,H1$,,1) \ GOSUB 7210
7190 W$=B2$ \ Y$=STR$(W) \ H1$="IN;PA2000,4500;PD;" \ COUT(,H1$,,1) \ GOSUB 7210
7191 W$=B3$ \ Y$=STR$(A(A2)) \ H1$="IN;PA2000,4000;PD;" \ COUT(,H1$,,1)
      \ GOSUB 7210 \ GO TO 7220
7210 H1$="LB"+W$+Y$+H9$ \ COUT(,H1$,,1) \ RETURN
7220 RETURN
8000 REM REGION('FULL')
8010 REM GRAPH('SHADE',256,S(1),A(1)) \ RETURN
8140 H1$="PD;" \ FOR I=1 TO 12 \ H1$=H1$+"PA"+STR$(C5*I/12)+",0"+";XT;" \ NEXT I
8150 COUT(,H1$,,1) \ REM PLOT AN X-AXIS
8160 COUT(,"PU;PA0,0;",,1) \ H1$="PD;"
8170 FOR I=1 TO 12 \ H1$=H1$+"PA0,"+STR$(C4*I/12)+";YT;" \ NEXT I \ H1$=H1$+"PU;"
8180 COUT(,H1$,,1) \ REM PLOT AN Y-AXIS
8190 FOR I=1 TO 256
8200 H1$="PA"+STR$(S(I)*5)+","+STR$(A(I)*5)+";PD;PU;" \ COUT(,H1$,,1)
8210 NEXT I \ REM PLOT CURVE
8220 H1$="PU;PA"+STR$(.1*C5)+","+STR$(.9*C4)+";" \ COUT(,H1$,,1)
8225 H9$=CHR$(3) \ H3$=","+STR$(-.05*C4)+";LB"
8226 H1$="LB"+A$+H9$+"CP;" \ COUT(,H1$,,1)
8227 H1=POS(A$(1),"WL=",1)
8230 H1$="LB"+SEG$(A$(1),1,H1-1)+H9$+"CP;" \ COUT(,H1$,,1)
8235 H1$="CP4,0;LB"+SEG$(A$(1),H1,100)+H9$+"CP;" \ COUT(,H1$,,1)
8240 H1$="LB"+A$(2)+H9$+"CP;" \ COUT(,H1$,,1)
8242 H1$="LB"+A$(20)+H9$+"CP;" \ COUT(,H1$,,1)
8250 FOR I=1 TO 6 \ H1$="PU;PA"+STR$(C5*I/6)+H3$+STR$(C5*I/30)+H9$+"PU;"
8255 COUT(,H1$,,1)
8260 NEXT I \ REM NUMBERING THE X-AXIS
8270 RETURN
8999 FOR I=A2 TO 256
9000 A8=A5*EXP(-(S(I)-S(A2))/T1)
9001 POINT(,S(I),A8,2) \ Z(I)=A8 \ NEXT I
9002 PRINT USING "SINGLE EXP TIME CONST. OF #### & AMPLITUDE #.###^^^^",T1,A5 \ RETURN
10000 END
```

C.1 LUMIN.BAS

This program transfers stored data file consisting of 500 channels to the Digital 11-03 computer at 1200 baud. It also stores information concerning experimental condition.

```
90 PRINT '     LUMIN          '
100 REM THIS PROGRAM IS FOR RECIVING LUMIN. SPECTRA DATA FROM OMA2 1215
110 REM         NO PROVISION IS MADE FOR ONLINE ANALYSIS.
120 DIM A$(102)
140 PRINT 'ENTER FIRST FOUR DIGITS OF FILE CODE'
150 LINPUT W$ \ W$='SY1:'+W$
160 U$='Y' \ Z$=''
170 PRINT 'PRESS RETURN WHEN READY TO INPUT DATA'
180 INPUT T$
190 PRINT 'START OMA DIGITAL OUTPUT'
230 FOR I=1 TO 100
240 CIN(,A$(I),,1)
250 NEXT I
260 PRINT 'DATA INPUT COMPLETE'
270 FOR I=1 TO 100
280 A$(I)=SEG$(A$(I),1,100)
290 PRINT A$(I)
300 NEXT I
310 PRINT 'IS DATA TRANSFER GOOD? (Y OR N)'
320 LINPUT T$
330 IF T$<>U$ GO TO 170
340 C$=DAT$
350 PRINT 'ENTER PICTURE NUMBER'
360 LINPUT D$
370 PRINT 'WINDOW #'
380 LINPUT N$
410 PRINT 'OTHER INFO UNCHAGED? (Y OR N)' \ LINPUT T$ \ IF T$=U$ GO TO 570
420 PRINT 'ENTER SAMPLE TEMP.' \ LINPUT F$
430 PRINT 'OTHER INFO UNCHAGED? (Y OR N)' \ LINPUT T$ \ IF T$=U$ GO TO 570
440 PRINT 'ENTER EXCITATION WAVELENGTH AND FILTERS' \ LINPUT G$,H$
450 PRINT 'OTHER INFO UNCHAGED? (Y OR N)' \ LINPUT T$ \ IF T$=U$ GO TO 570
460 PRINT 'ENTER LUMINESCENT PATH FILTERS'
470 LINPUT O$
480 PRINT 'OTHER INFO UNCHAGED? (Y OR N)' \ LINPUT T$ \ IF T$=U$ GO TO 570
490 PRINT 'ENTER SAMPLE NAME'
500 LINPUT E$
510 PRINT 'ENTER WAVELENGTH RANGE'
520 LINPUT I$
530 PRINT 'ENTER SLIT WIDTH '
540 LINPUT J$
550 PRINT 'GRATING SPACIFICATIONS'
560 LINPUT L$
570 A$(101)=C$+' PICT#'+D$+' SAMPLE='+E$+' TEMP.='+F$+' WL='+G$+' ATTN. BY '
600 A$(101)=A$(101)+H$+' WAVELENTH='+I$
610 A$(102)='SLIT='+J$+'GRATING='+L$
620 A$(102)=A$(102)+' WINDOW#'+N$+' FILTERS='+O$
630 PRINT A$(101)
640 PRINT A$(102)
650 PRINT 'ENTER FILE NAME FOR THIS SHOT, LAST NAME WAS ',B$
660 INPUT B$
670 B$=W$+B$
680 OPEN B$ AS FILE #1
690 FOR I=1 TO 102
700 PRINT #1,A$(I)
710 NEXT I
720 CLOSE #1
730 PRINT 'DO YOU WANT ANOTHER SHOT? (Y OR N)'
740 LINPUT T$
750 IF T$=U$ GO TO 170
760 END
```

C.2 LUMFL4.BAS + OMAREG.BAS + LUMPLT4.BAS

These programs are 'chained' together for lack of sufficient (only 64K bytes) memory. The subroutines included correct the wavelength axis, plot data and a theoretical fit given by Eq.(3.5.22).

```
90 PRINT '  OMAREG    '
100 PRINT ' THIS PRG IS FOR RECIEVING OMA2 1215 REGISTERS FILE.'
120 DIM R$(8)
130 DIM S(500)
140 PRINT 'ENTER FIRST FOUR DIGITS OF FILE CODE'
150 LINPUT W$ \ W$='SY1:'+W$
160 U$='Y' \ Z$=''
170 PRINT 'PRESS RETURN WHEN READY TO INPUT DATA'
180 INPUT T$
190 PRINT 'START TA DIGITAL OUTPUT'
230 FOR I=1 TO 8
240 CIN(,R$(I),,1)
250 NEXT I
260 PRINT 'DATA INPUT COMPLETE'
270 FOR I=1 TO 8
280 R$(I)=SEG$(R$(I),1,100)
290 PRINT R$(I)
300 NEXT I
310 PRINT 'IS DATA TRANSFER GOOD? (Y OR N)'
320 LINPUT T$
330 IF T$<>U$ GO TO 170
340 C$=DAT$
350 V1$=SEG$(R$(8),9,18)
355 V2$=SEG$(R$(8),19,28)
360 V3$=SEG$(R$(8),29,38)
370 V4$=SEG$(R$(8),40,49)
380 V5$=SEG$(R$(8),50,59)
390 V1=VAL(V1$)
400 V2=VAL(V2$)
410 V3=VAL(V3$)
420 V4=VAL(V4$)
430 V5=VAL(V5$)
440 FOR I=0 TO 499
450 S(I)=V5*(I+V1)^3+V4*(I+V1)^2+V3*(I+V1)+V2
460 NEXT I
650 PRINT 'ENTER FILE NAME FOR THIS OMA REGESTERS, LAST NAME WAS ',B$
660 INPUT B$
670 B$=W$+B$
680 OPEN B$ AS FILE #1
690 FOR I=0 TO 499
700 PRINT #1,S(I)
710 NEXT I
720 CLOSE #1
730 PRINT 'WAVELENGTH RANGE IN ANGSTRM OF'
740 PRINT S(0),S(499)
760 END
```

```
10 PRINT " FILE NAME:    LUM4.BAS"
14 PRINT "E-H COMBINED DENSITY OF STATES (E-EG)^.5 "
15 PRINT "  BAND TO BAND W**2 TERM NOT PRESENT DIRECT TRANSITIONS"
16 Z$='DIRECT TRANSITIONS BAND-BAND W^2 TERM ABSENT.'
20 PRINT "THIS PRG FITS HIGH ENERGY TAIL SINGLE EXP TO FIND OUT TEMP."
30 PRINT "USING FERMI ENERGY AS A PARAMETER GET ENTIRE FIT.          "
40 PRINT " ENTER BANDGAP IN WAVELENGTH ANGSTRM " \ INPUT G1
43 PRINT "ENTER ELECTRON MASS RATIO. " \ INPUT M2
45 PRINT "ENTER RATIO OF ELECTRON/HOLE MASS OF SEMICONDUCTOR." \ INPUT M
50 PRINT "WAVELENGTH RANGE IN A >USED IN EXPERIMENT ." \ INPUT W5
51 PRINT "LONG WAVELENGTH LIMIT IN A " \ INPUT C0
80 COMMON S(250),A(250),L$(2),G1,A$,M,M2,Z(250),T1,G,S5,A5,E,W5,C0,F,Z$
82 DIM A$(102),B(500),X(500)
90 GOSUB 2000 \ REM LOAD OMA2 REGISTERS FILE AND GET WAVE LENTH CALIBRATION.
130 CHAIN 'LUMFL4'
200 DISPLAY_CLEAR
290 GOSUB 3200 \ REM FIND START POINT FOR FIT.
370 GOSUB 2600 \ REM FIND MAX & MIN VALUES OF A()
380 GOSUB 4000 \ REM GRAPH A(I)
390 GOSUB 5000 \ REM FIT & GRAPH SINGLE EXP. DECAY CURVE
570 PRINT "DO YOU WANT TO FIT MORE FILES?(Y OR N)"
580 LINPUT Q$ \ IF Q$="Y" GO TO 130
590 GO TO 10000
2000 REM THIS SUBROUTINE LOADS THE OMA2 PARAM.& GETS WAVE LENTH CALIBRATION.
2010 PRINT "ENTER THE OMA2 REGISTER FILE." \ LINPUT X$ \ X$="SY1:"+X$
2020 OPEN X$ AS FILE #1
2030 FOR I=0 TO 499 \ INPUT #1,X(I) \ NEXT I
2033 CLOSE #1
2034 FOR J=0 TO 249 \ S(J)=X(2*J) \ NEXT J \ RETURN
2600 A3=0 \ A4=0 \ FOR I=A4 TO 249 \ IF A(I)>A3 THEN A3=A(I)
2610 IF A(I)<A4 THEN A4=A(I)
2620 NEXT I \ RETURN
2700 FOR I=0 TO 499
2710 IF A(I)<=0 THEN A(I)=-1 \ GO TO 2730
2720 A(I)=LOG10(A(I))
2730 NEXT I \ RETURN
3000 REM THIS SUBROUTINE FINDS THE REFERENCE PEAK.
3010 GRAPH('S',249,,A(0))
3020 PRINT "MOVE THE CURSOR UNTIL IT IS ON THE REFERENCE CH."
3030 A2=250 \ FIND_POINT(A2,A3)
3040 A2=INT(A2) \ PRINT USING "FILE REF. CH. IS ###",A2 \ RETURN
3200 REM THIS SUBROUTINE FINDS BIGINING POINT FOR CURVE FITTING"
3210 GRAPH('S',249,,A(0))
3220 PRINT "MOVE CURSOR UNTIL IT IS AT THE STARTING POINT FOR CURVE FITTING"
3230 A2=150 \ FIND_POINT(A2,A3)
3240 A2=INT(A2) \ PRINT USING "START CHANEL IS###",A2 \ RETURN
4000 REM
4010 REM THIS SUBR. GRAPHS A()&SETSWINDOWGRIDFORCURVEFITTING.
4020 REM
4022 A3=A(A2)
4030 WINDOW('-E',S(0),A4,S(249),A3,0)
4060 GRAPH('-E,S',249,S(0),A(0),,,1)
4070 E1=S(A2) \ E2=A(A2) \ GRAPH('-E,B',1,E1,E2,,,2)
4080 RETURN
4100 REM THIS SUBR IS FOR SETTING WINDOW & GRID FOR TOTAL FIT.
4110 WINDOW('-E',S(249),0,S(0),A3,0)
4130 GRAPH('-E,S',249,S(0),A(0),,,1)
4150 E1=S(0) \ E2=A(0) \ GRAPH('-E,B',1,E1,E2,,,2)
4160 RETURN
4170 REM
4200 REM
4210 REM      THIS SECTION PLOTS THE EXPONENTIAL FIT & CALCULATES THE SUM
4220 REM      OF SQUARES DEVIATION.
4230 A7=0 \ FOR I=A2 TO 249
4240 A6=A5*EXP(((1/S(A2)-1/S(I))*Q)/T1) \ A7=A7+(A6-A(I))^2
4250 IF L9=0 THEN  GO TO 4270
4260 Z(I)=A6
4270 POINT(,S(I),A6,2) \ NEXT I
4280 PRINT USING "FOR A TEMPERATURE OF ##### K & PEAK LUM. OF #.##^^^^",T1,A5
4290 PRINT USING " THE SUM OF THE SQAURES IS #.##^^^^",A7
4300 RETURN
```

```
5000 REM
5010 REM THIS SECTION CALCULATES A FIT FROM INPUTED TRIAL VALUES
5020 REM
5030 PRINT 'ENTER A TRIAL TEMPERATURE IN KELVIN' \ INPUT T1
5050 A5=A(A2)
5051 S5=S(A2)
5054 Q=1.42450E+08
5055 W=1/G1-.5*T1/Q
5056 G=1/W
5060 GOSUB 4200
5070 PRINT 'DO YOU WANT TO TRY ANOTHER FIT?(Y OR N)'
5080 LINPUT Q$ \ IF Q$<>'Y' GO TO 5101
5090 PRINT ' CNTER A NEW TEMP. CONST. & MULTIPLICATIVE FACTOR.'
5100 INPUT T1,A5 \ GOSUB 4200 \ W=1/G1-.5*T1/Q \ G=1/W \ GO TO 5070
5101 PRINT 'DO YOU WANT DIFFERENT START CHANEL?(Y OR N)'
5102 LINPUT Q$ \ IF Q$='Y' THEN  GO TO 200
5110 PRINT 'DO YOU WANT ENTIRE CURVE FITTING USING FERMI DISTR.?(Y OR N)' \ LINPUT M$
5120 IF M$<>'Y' THEN  GO TO 6175
5125 DISPLAY_CLEAR \ PRINT 'STARTING POINT IS MAXIMA OF LUM.' \ GOSUB 3200
5130 REM
5140 REM     THIS SUBROUTINE FITS TOTAL LUMINESCENCE .
5150 REM
5155 A3=A(A2)
5165 GOSUB 4100
5166 PRINT 'GIVE FERMI ENERGY IN A  ' \ INPUT F
5167 E=6.34000E+27*(M2/F)^1.5*(1+5.87000E-17*(F*T1)^2)
5168 W=1/G1-.5*T1/Q \ G=1/W
5169 M1=1/(1+M)
5180 FOR I=0 TO 249
5184 K=10000*(1/S(I)-1/G) \ IF K<0 THEN  GO TO 5193
5185 X=A(A2)/(1/S(A2)-1/G)^.5*(EXP((M1*M*(1/S(A2)-1/G)-M/F)*Q/T1)+1)*(EXP((M1*(1/S(A2)
     -1/G)-1/F)*Q/T1)+1)
5190 A8=X*(1/(EXP((M1*M*(1/S(I)-1/G)-M/F)*Q/T1)+1))*(1/S(I)-1/G)^.5*(1/(EXP((M1*
     (1/S(I)-1/G)-1/F)*Q/T1)+1))
5191 GO TO 6100
5193 A8=0
6100 POINT(,S(I),A8,2) \ Z(I)=A8 \ NEXT I
6110 S5=S(A2) \ A5=A(A2)
6140 PRINT USING 'TEMP. OF #### & F ENERGY IN ANGSTRM OF ####',T1,F
6141 PRINT USING ' PEAK OF LUM IS #.##^^^^ & WAVE LENGTH #.##^^^^',A(A2),S(A2)
6150 PRINT 'DO YOU WANT ANOTHER FIT?( Y OR N)'
6151 LINPUT Q$ \ IF Q$='N' GO TO 6175
6158 PRINT 'NEW FERMI ENERGY(Y OR N)?' \ LINPUT Q$ \ IF Q$='Y' GO TO 5166
6164 PRINT ' GIVE T1,A(A2)' \ INPUT T1,A(A2) \ GO TO 5167
6175 PRINT 'HARDCOPY OF EXP. DATA?(Y OR N)' \ LINPUT Q$
6176 IF Q$='Y' THEN CHAIN 'LMPLT4' LINE 8000
6180 PRINT 'HARDCOPY OF THEORATICAL FIT?(Y OR N)'
6181 LINPUT Q$ \ IF Q$='Y' THEN CHAIN 'LMPLT4' LINE 8275
6190 GO TO 570
10000 END

 10 PRINT ' FILE NAME:    LUMFL4.BAS'
 20 PRINT '  THIS PRG. TAKES LUM.FILE & CONVERT INTO LINEAR FORMAT  '
 130 COMMON S(250),A(250),L$(2),G1,A$,M,M2
 132 DIM A$(102),B(500)
 2110 PRINT 'ENTER  FILE NAME .' \ LINPUT A$ \ A$='SY1:'+A$
 2120 OPEN A$ AS FILE #2 DOUBLE BUF, FILESIZE 20 \ FOR I=1 TO 102 \ LINPUT #2,A$(I)
      \ NEXT I
 2130 CLOSE #2
 2150 FOR I=1 TO 100 \ FOR L=1 TO 5
 2160 J=10*L-1
 2162 K=5*(I-1)+L-1
 2164 C$=SEG$(A$(I),J,J+6)
 2165 M5=LEN(C$)
 2166 N=POS(C$,'-',1) \ D$=SEG$(C$,N,M5) \ B(K)=VAL(D$)
 2170 NEXT L \ NEXT I
 2171 FOR J=0 TO 249 \ A(J)=B(2*J) \ NEXT J
 2175 L$(1)=A$(101) \ L$(2)=A$(102)
 2180 CHAIN 'LUM4' LINE 200.
```

```
6900 PRINT 'FILE NAME:  LMPLT4.BAS'
6910 PRINT 'THIS PRG.PLOTS LUMINESCENCE DATA ON HP7225A '
6920 COMMON S(250),A(250),L$(2),G1,A$,M,M2,Z(250),T1,G,S5,A5,E,W5,C0,F,Z$
7000 REM
7020 REM
7030 REM THIS SUBROUTINE PLOTS THE EXPERIMENTAL FIT FILE ON HP7525A
7040 REM
7050 C3=0 \ FOR I=0 TO 249 \ IF C(I)>C3 THEN C3=C(I) \ NEXT I
7060 IF I<100 THEN C4=100
7070 IF I>=100 THEN C4=300
7080 C5=W5
7110 C4=A5*2
7120 C6=-.1*C5 \ C7=-.1*C4
7130 C4=C4*5 \ C5=C5*5 \ C6=C6*5
7131 C7=C7*5 \ REM MULT. BY 5 FOR BETTER PLOT RESOL.
7140 C4$=STR$(C4) \ C5$=STR$(C5) \ C6$=STR$(C6) \ C7$=STR$(C7)
7150 H1$='SC'+C6$+',,'+C5$+',,'+C7$+',,'+C4$+';' \ COUT(,H1$,,1) \ REM SCALING
7160 H2$='PU;PA0,0;' \ COUT(,H2$,,1) \ REM MOVE THE PEN TO 0,0
      \ RETURN
7161 H9$=CHR$(3) \ H1=POS(B$,'WL=',1) \ H3$=',,'+STR$(-.05*C4)+';LB'
7162 FOR I=0 TO 249
7163 H1$='PA'+STR$((C0-S(0)-(S(249)-S(249-I)))*5)+',,'+STR$(Z(I)*5)+';PD;'
      \ COUT(,H1$,,1) \ NEXT I
7164 B0$='FERMI ENERGY IN EV FROM BOTTOM OF CONDUCTION BAND='
7165 B1$='ELECTRON TEMP. IN K='
7166 B2$='ELECTRON DENSITY IN CM-3='
7167 B3$='MAXIMUM OF LUM.='
7168 B4$='BAND GAP AT LATTICE TEMP IN A ='
7169 B5$='REDUCED BAND GAP AT ELECTRON TEMP. IN A ='
7170 B6$='MAX EMISSION WAVELENGTHIN A ='
7173 V=12500/F
7190 H1$='IN;PA2000,5500;PD;' \ COUT(,H1$,,1)
7191 H1$='LB'+Z$+H9$ \ COUT(,H1$,,1)
7195 W$=B0$ \ Y$=STR$(V) \ H1$='IN;PA2000,5000;PD;' \ COUT(,H1$,,1) \ GOSUB 7210
7196 W$=B1$ \ Y$=STR$(T1) \ H1$='IN;PA5000,4500;PD;' \ COUT(,H1$,,1) \ GOSUB 7210
7197 W$=B2$ \ Y$=STR$(E) \ H2$='IN;PA5000,4000;PD;' \ COUT(,H2$,,1) \ GOSUB 7210
7198 W$=B3$ \ Y$=STR$(A5) \ H3$='IN;PA5000,3500;PD;' \ COUT(,H3$,,1) \ GOSUB 7210
7199 W$=B4$ \ Y$=STR$(G1) \ H4$='IN;PA5000,3000;PD;' \ COUT(,H4$,,1) \ GOSUB 7210
7200 W$=B5$ \ Y$=STR$(G) \ H5$='IN;PA5000,2500;PD;' \ COUT(,H5$,,1) \ GOSUB 7210
7201 W$=B6$ \ Y$=STR$(S5) \ H6$='IN;PA5000,2000;PD' \ COUT(,H6$,,1) \ GOSUB 7210
7210 H1$='LB'+W$+Y$+H9$ \ COUT(,H1$,,1) \ RETURN
7220 RETURN
8000 REM
8010 GOSUB 6900 \ GOSUB 8140 \ GO TO 8275
8140 H1$='PD;' \ FOR I=1 TO 10 \ H1$=H1$+'PA'+STR$(C5*I/10)+',0'+';XT;' \ NEXT I
8150 COUT(,H1$,,1) \ REM PLOT AN X-AXIS
8160 COUT(,'PU;PA0,0;',,1) \ H1$='PD;'
8170 FOR I=1 TO 10 \ H1$=H1$+'PA0,'+STR$(C4*I/10)+';YT;' \ NEXT I \ H1$=H1$+'PU;'
8180 COUT(,H1$,,1) \ REM PLOT AN Y-AXIS
8185 H2$='PU;PAC0,0;' \ COUT(,H2$,,1)
8190 FOR I=0 TO 249
8200 H1$='PA'+STR$((C0-(S(249)-S(249-I))-S(0))*5)+',,'+STR$(A(I)*5)+';PD;PU;' \ COUT(,H1$,,1)
8210 NEXT I \ REM CURVE PLOT
8220 H1$='PU;PA'+STR$(.1*C5)+',,'+STR$(.9*C4)+';' \ COUT(,H1$,,1)
8225 H9$=CHR$(3) \ H3$=',,'+STR$(-.05*C4)+';LB'
8226 H1$='LB'+A$+H9$+'CP;' \ COUT(,H1$,,1)
8227 H1=POS(L$(1),'WL=',1)
8230 H1$='LB'+SEG$(L$(1),1,H1-1)+H9$+'CP;' \ COUT(,H1$,,1)
8235 H1$='CP4,0;LB'+SEG$(L$(1),H1,100)+H9$+'CP;' \ COUT(,H1$,,1)
8240 H1$='LB'+L$(2)+H9$+'CP;' \ COUT(,H1$,,1)
8250 FOR I=1 TO 10 \ H1$='PU;PA'+STR$(C5*I/10)+H3$+STR$(C0-C5*I/50)+H9$+'PU;'
8255 COUT(,H1$,,1)
8260 NEXT I \ REM NUMBERING THE X-AXIS
8270 RETURN
8275 PRINT 'HARDCOPY OF THEORATICAL FIT?(Y OR N)PLEASE WAIT FOR 30 SEC'
8280 LINPUT Q$ \ IF Q$='Y' THEN  GOSUB 7000 \ GOSUB 7161 \ CHAIN 'LUM4' LINE 570
8285 IF Q$='N' THEN  GOSUB 7164 \ CHAIN 'LUM4' LINE 570
```

BIBLIOGRAPHY

1. Alfano R. R.,'Semiconductors probed by ultrafast laser spectroscopy'Vol.2, Academic press (1985).

2. Auston D. H., Shank C. V. and LeFur P., Phys. Rev. Lett. 35, 1022 (1975).

3. Bardeen J. and Shockley W., Phys. Rev. 80, 72 (1950).

4. Beiser A., 'Perspectives of Modern Physics, McGraw-Hill, (1969).

5. Bell R. L., 'Negative Electron Affinity Devices', Oxford (1973).

6. Berlincourt D., Jaffe H. and Shiozawa L. R., Phys. Rev. 129, 1009 (1963).

7. Bir G. L., Aronov A. G. and Pikus G. E., Sov. Phys. JETP, 42, 705 (1975).

8. Birman J. L., Phys. Rev. Lett. 2, 157 (1959).

9. Birman J. L., J. Phys. Chem. solids, 8, 35 (1959).

10. Birman J. L., Phys. Rev. 114, 1490 (1959).

11. Blakemore J. S., 'Semiconductor Statistics', Pergammon, (1962).

12. Bloembergen N., American J. of Phys. 35, 989 (1967).

13. Blum H. and Orbach R., Phys. Rev. 127, 1587 (1962).

14. Bradley D. J., Higgins J. F. and Key M. H., Appl. Phys. Lett. 16, 53 (1970).

15. Camassel J. and Auvergne D., Phys. Rev. B, 12, 3258 (1975).

16. Cardona M., J. Phys. Chem. Sol. 24, 1543 (1963).

17. Cardona M. and Harbeeke G., Phys. Rev. A137, 1467 (1965).

18. Castro de A. R. B. and Tutelli R. S., Sol. State Comm. 32, 819 (1979).

19. Clark A. H., Burnham R. D., Chadi D. J. and White R. M., Sol. State Comm., 20, 385 (1976).

20. Cohen M. and Bergstresser T. K., Phys. Rev. 141, 789 (1966).

21. Cohen M. L. and Chadi D. J., 'Handbook on Semiconductors' Vol.2 Ed. M. Balkanski, North Holland (1980).

22. Collet J., Pugnet M., Cornet A., Brousseau M., Razbirin B. S., and Miknailov G. V., Phys. Stat. Sol.(b), 103, 367 (1981).

23. Combescot M., Sol. State Comm., 30, 81 (1979).

24. Conwell E., Sol. State Phys. Suppl. 9, (1967).

25. Cornet A., Pugnet M., Collet J., Amand T. and Brousseau, J. De Physique, C7 Suppl., 471 (1981).

26. Decker D. L. and Wild R. L., Phys. Rev.B, 4, 3425 (1971).

27. DeMaria A. J., Stetser D. A. and Gleen W. H., J. Science, 156, 1557 (1967).

28. Dietl T. and Spalek J., Phys. Rev. Lett., 48, 3551 (1982).

29. Dietl T. and Spalek J., Phys. Rev. B, 28, 1548 (1983).

30. Diouri J., Lascaray J. P. and Triboulet R., Sol. State Comm. 42, 231 (1982).

31. D'yakonov M. I. and Perel' V. I., Sov. Phys. JETP 33,1053 (1971).

32. D'yakonov M. I. and Perel' V. I., Sov. Phys. Solid State, 13, 3023 (1972).

33. D'yakonov M. I. and Perel' V. I., Sov. Phys. JETP, 38, 177 (1974).

34. Elci A., Smirl A. L., Leung C. Y. and Scully M. O., Sol. State Electr. 21, 151 (1978).

35. Elliot R. J., Phys. Rev. 96, 266 (1954).

36. Erninyam M. and Lampel G., XIth Intnl. Conf. on Phys. of electr. and atm. collisions., Kyoto (1979).

37. Fishman G. and Lampel G., Phys. Rev.B, 16, 820 (1977).

38. Fleury P. A. and Scott J. F., Phys. Rev. B, 3, 1979 (1971).

39. Forchel A., Schweizer H. and Mahler G., Phys. Rev. Lett. 51, 501 (1983).

40. Franken P. A., Hill A. E., Peters C. W. and Weinreich, Phys. Rev.

Lett. 7, 118 (1961).

41. Frigo N. J., Mahr H. and Erskine D. J., J. Quntm. Electr. 18, 192 (1982).

42. Frohlich H., Proc. Roy. Soc., A160, 230 (1937).

43. Furdyna J. K., J. Appl. Phys., 53, 7637 (1982).

44. Gaj J. A., Planel R. and Fishman G., Sol. State Comm. 29, 435 (1979).

45. Gaj J. A., Proc. 15th Int. Conf. on Phys. of Semicond. Kyoto J. Phys. Soc. Japan 49, 797 Suppl. (1980).

46. Galazka R. R., Nagata S. and Keesom P. H., Phys. Rev. B, 22, 3344 (1980).

47. Gennes de P. C., Phys. Rev. 118, 141 (1960).

48. Giebultowicz T., Minor W., Buras B., Lebech B. and Galazka R. R., Physica Scripta 25, Dec. (1981).

49. Giebultowicz T., Minor W., Kepa H. and Ginter J., J. Mag. and Mag. Mat. 30, 215 (1982).

50. Gobel E. O. and Hildebrand O., Phys. Stat. Sol.(b), 88, 645 (1978).

51. Goede O. and Thong D. D., Phys. Stat. Sol.(b), 124, 343 (1984).

52. Grancharova E. I., Lascaray J. P., Diouri J. and Allegne J., Phys. Stat. Sol. (b), 113, 503 (1982).

53. Grynberg M., Int. Conf. on Semicon. Phys. 7th Proc., Paris, Vol.1, Ed. Hulin M., Academic Press (1964).

54. Harris J. H. and Nurmikko A. V., Sol. State Comm., 48, 675 (1983).

55. Haug A., Sol. State Electr. 21, 1281 (1978).

56. Hayashi Masato, Saito H. and Shionoya S., Sol. State Comm. 24, 833 (1977).

57. Hearn C. J., Proc. Phys. Soc. 86, 881 (1965).

58. Heiman D., Appl. Phys. Lett. 42, 775 (1983).

59. Heiman D., Wolff P. A. and Warnock J., Phys. Rev. B, 27, 4848

(1983).

60. Hopfield J. J., J. Appl. Phys. 32, 2277 (1961).

61. Huber C. A. and Nurmikko A. V., Sol. State Comm. 48, 675 (1983).

62. Ito Takashi, Ito K. and Oka M., Jap. J. Appl. Phys. 17, 371 (1978).

63. Ivchenko E. L., Sov. Phys. Solid State 14, 2942 (1972).

64. Junnarkar M. R., Alfano R. R. and Furdyna J., (to be published).

65. Junnarkar M. R. and Alfano R. R., (to be Published in Phys. Rev.B).

66. Junnarkar M. R., Alfano R. R. and Furdyna J., (under process).

67. Kasuya T., Yanase A. and Takeda T., Sol. State Comm., 8, 1543 (1970).

68. Kittel C.,'Introduction to Solid State Physics' Wiley Eastern Univ. Ed. 5, (1977).

69. Kleinman D. A. and Miller R. C., Phys. Rev. Lett. 46, 68 (1981).

70. Lampel G., Phys. Rev. Lett. 20, 491 (1968).

71. Lampel G., Proc. of 12th Int. Conf. on the Phys. of Semicond. Ed. Pilkuhn M. H., Stuttgart (1974).

72. Leheny R. F., Shah J., Fork R. L., Shank C. V. and Migus A., Sol. State Comm. 809 (1979).

73. Long Donald,'Energy bands in semiconductors', Inter Science Publishers, (1968).

74. Lu P. Y., Ho P. P. and Alfano R. R., J. Quntm. Electr., QE-15, 406 (1979).

75. Mahan G. D. and Hopfield J. J., Phys. Rev. A, 135, 428 (1964).

76. Margulis A. D. and Margulis VI. A., Sov. Phys. Semicond., 18, 305 (1984).

77. Martinez Gerald,'Handbook on Semiconductors', Vol.2, Ed. Balkanski North-Holland Publication (1980).

78. Mauger A., Phys. Rev. B, 27, 2308 (1983).

79. Modesti S., Quaglino L. G., Frova A., Staehli J. L. and Guzzi M.

J. Lumin. 24/25, 581 (1981).

80. Moriwaki M., Ph.D. Thesis, Purdue Univ. (1983).

81. Mott M., Phil. Mag. 6, 287 (1961).

82. Nag B. R. 'Semiconductors probed by ultrafast laser spectroscopy Vol.1',Ed. Alfano R. R., Academic, (1984).

83. Nawrocki M., Planel R., Fishman G., Phys. Rev. Lett., 46, 735 (1981).

84. Nelson R. J. and Holonyak N. Jr., J. Phys. Chem. Solids, 37, 629 (1976).

85. Oelhafen P., Vecchi M. P., Freeouf J. L. and Maruzzi V. L., Sol. State Comm. 44, 1547 (1982).

86. Oseroff S. B., Phys. Rev. B, 25, 6584 (1982).

87. Pajaczkowska A., Prog. Crystal Growth Charact. 1, 289 (1978).

88. Pankove J. I.,'Optical processes in semiconductors, Dover Publ. (1971).

89. Parsons R. R., Wardzynski R. B. and Yoffe A. D., Proc. Roy. Soc. A262, 120 (1961).

90. Parsons R. R., Phys. Rev. Lett. 23, 1152 (1969).

91. Pendleton W. K. and Guenther A. H., Rev. Sci. Instr., 36, 1546 (1965).

92. Pierce D. I., Celotta R. J., Wang G. C., Unerti W. N., Galejs A. Kuyatt G. E. and Mielezareck S. R., Rev. Sci. Instr.,51 (1980).

93. Pikus G. E., Sov. Phys. Sol. State, 6, 261 (1964).

94. Planel R., Nhung Tran Hong, Fishman G. and Nawrocki M., J. Physique, 45, 1071 (1984).

95. Pugnet M., Collet J. and Cornet A., Sol. State Comm. 38, 531, (1981).

96. Romanek K. M., Nather H., Fischer J. and Gobel E. O., J. Lumin. 24/25, 585 (1981).

97. Romestain R., Geschwind S. and Devlin G., Phys Rev. Lett. 39, 1583 (1977).

98. Scott J. F., Damen T. C. and Fleury P.A., Phys. Rev.B, 6, 3856 (1972).

99. Seymour R. J. and Alfano R. R., Appl. Phys. Lett., 37, 231 (1980).

100. Seymour R. J. Thesis'Electron spin and energy relaxation in highly excited GaAs.' (unpublished) New York (1981).

101. Seymour R. J., Junnarkar M. R. and Alfano R. R., Phys. Rev. B, 24 3623 (1981).

102. Shah J., Phys. Rev. B, 9, 562 (1974).

103. Smirl A. L., Lindle J. R. and Moss S. C., Phys. Rev. B, 18, 5489 (1978).

104. Smith R. A., 'Semiconductors', Cambridge Univ. press, (1961).

105. Spalek J., Phys. Rev.B, 32, sept (1985).

106. Spalek J., Lewicki A., Tarnawski Z., Furdyna J. K., Galazka R. R. and Obuszko Z. (preprint).

107. Stankiewicz J., Phys Rev.B, 27, 3631 (1983).

108. Stewart A. F. and Bass M., Appl. Phys. lett. 37, 1040 (1980).

109. Takeshima M., Phys. Rev. B, 23, 6625 (1981).

110. Tanabe Y. and Sugano S., J. Phys. Soc. Japan, 9, 753 (1954).

111. Tao R. Y., Moriwaki M. M., Becker W. M. and Galazka R. R., J. Appl. Phys. 53, 3772 (1982).

112. Thong D. D., Heimbroelt W., Hommel D. and Goede O., Phys. Stat. Sol.(b) 81, 695 (1984).

113. Ulbrich R., Phys. Rev. B, 8, 5719 (1973).

114. Van Driel H. M., Phys. Rev. B, 19, 5928 (1979).

115. Vecchi M. P., Giriat W. and Videla L., Appl. Phys. Lett. 38, 99 (1981).

116. Vekua V. B., Dzhioev R. I., Zakharchenya B. P. and Fleisher V. G. Sov. Phys. Semicond. 10, 210 (1976).

117. Von der Linde D., Bernecker O. and Kaiser W., Opt. Comm. 2, 149 (1970).

118. Von der Linde D. and Lambrich, Phys. Rev. Lett. 42, 1090 (1979).

119. Von der Linde D., Kuhl J. and Klingenberg H., Phys. Rev. Lett. 44, 1505 (1980).

120. Warnock J., Kershaw R. N., Ridgley D., Dwight K., Wold A. and Galazka R. R., Sol. State Comm. 54, 215 (1985).

121. Yafet Y., Solid State Physics, Ed. Seitz F. and Turnbull D. Academic, Vol.14, (1963).

122. Yao S. S. and Alfano R. R., Phys. Rev. B, 27, 1180 (1983).

123. Yoffa E. J., Appl. Phys. Lett. 36, 37 (1980).

124. Yoffa E. J., Phys. Rev. B, 21, 2415 (1980).

125. Yoffa E. J., Phys. Rev. B, 23, 1909 (1981).

126. Yoshida H., Saito H. and Shionoya S., J. Phys. Soc. Japan, 50, 881 (1981).

127. Yoshikuni Yuzo, Saito H. and Shionoya S, Sol. state Comm. 32, 665 (1979).

128. Zimmerman R. and Rosler M., Phys. Stat. Sol.(b), 75, 633 (1976).